JOURNAL OF PETROLOGY

VOLUME 2 · NUMBER 1

FEBRUARY 1961

OXFORD · AT THE CLARENDON PRESS

PLYMOUTH COLLEGE

JOURNAL OF PETROLOGY

Editors

T. F. W. BARTH (Oslo); C. E. TILLEY (Cambridge)
L. R. WAGER (Oxford); H. S. YODER (Washington)

Managing Editors

G. M. BROWN (Oxford); S. R. NOCKOLDS (Cambridge)

Honorary Advisory Board

C. E. BURRI (Zürich)
C. W. CORRENS (Göttingen)
H. VON ECKERMANN (Stockholm)
P. ESKOLA (Helsinki)
L. HAWKES (London)
J. E. HAWLEY (Kingston, Ont.)
H. H. HESS (Princeton)
D. S. KORZHINSKY (Moscow)
H. KUNO (Tokyo)
W. T. PECORA (Washington)
E. RAGUIN (Paris)
H. H. READ (London)
A. RITTMANN (Catania)
F. J. TURNER (Berkeley, Calif.)

It is the aim of the editors to provide, in the *Journal of Petrology*, a place for the publication of original researches in the whole range of subjects which fall within a liberal definition of petrology. The subjects will thus include the physics and chemistry of rocks, their mineralogy and textures, and certain aspects of petrology which involve the dating of rocks by natural radioactivity. Quantitative studies of rock-forming minerals, experimental physical chemistry relevant to petrology, and parts of isotope geology, will appropriately find a place. Regional studies, unless they lead to results fundamental to the science of petrology, will not usually be considered suitable to the journal.

The journal is being published at first in 400-page volumes consisting of three numbers per year, in February, June, and October. The subscription price for three consecutive numbers is 80*s*. ($12 in the U.S.A. and Canada), post free. Single numbers cost 30*s*. net. Orders may be placed with any bookseller or sent direct to the publishers.

OXFORD UNIVERSITY PRESS

AMEN HOUSE · LONDON · E.C.4

Fusion of Torridonian Sandstone by a Picrite Sill in Soay (Hebrides)

by P. J. WYLLIE

Department of Geology, University of Leeds

WITH TWO PLATES

ABSTRACT

Up to 92 per cent of the original minerals were fused during progressive metamorphism of Torridonian sediment by a picrite sill. The liquid precipitated microlites of tridymite, cordierite, hypersthene, and magnetite until that remaining quenched to a glass. Stages of fusion were determined by petrographic methods. After decomposition of sericite and reduction of haematite, liquid developed by fusion of feldspar and quartz. The composition of liquid in a fused xenolith at various stages was calculated from chemical and modal analyses. The chemical analysis indicates that fusion occurred in the presence of excess water-vapour. The [illegible] closely with the behaviour of similar composi-

Journal of Petrology, volume 1, *number* 3

ERRATUM

pages 394 and 395. Figs. 10 and 11: Na+K at bottom left-hand corner of each figure should be $\frac{1}{2}$ (Na+K).

complex. According to Harker (p. 247): 'Clough has observed three clear instances of the vitrification of grits in Soay, besides others in which the effects seem to be obscured by subsequent alteration. Some of these are in connexion, not with basic but with ultrabasic sills. The vitrification is only locally produced in the case of any given sill.' The picritic minor intrusions have been numbered by Drever & Johnston (1958) for ease of reference. The subject of this study, Sill 1, is located on the SW. coast of the island, a quarter of a mile WSW. of the outlet of Loch Doir a'Chreamha.

Sill 1 belongs to the Hebridean group of non-alkaline picritic minor intrusions studied by Drever & Johnston (1958). It contains about 55 modal per cent of forsteritic olivine, 25 per cent of calcic plagioclase, 18 per cent of clinopyroxene, and 2 per cent of chromespinel; a detailed petrographic description will be presented elsewhere. This is one of the few ultrabasic sills where progressive metamorphism of the country rock has culminated in fusion. On cooling, the fused sediment precipitated microlites of tridymite (now inverted to quartz), hypersthene, cordierite, and magnetite, until the remaining liquid was quenched to a

[Journal of Petrology, Vol. 2, Part 1, pp. 1–37, 1961]
6233.1

Fusion of Torridonian Sandstone by a Picrite Sill in Soay (Hebrides)

by P. J. WYLLIE

Department of Geology, University of Leeds

WITH TWO PLATES

ABSTRACT

Up to 92 per cent of the original minerals were fused during progressive metamorphism of Torridonian sediment by a picrite sill. The liquid precipitated microlites of tridymite, cordierite, hypersthene, and magnetite until that remaining quenched to a glass. Stages of fusion were determined by petrographic methods. After decomposition of sericite and reduction of haematite, liquid developed by fusion of feldspar and quartz. The composition of liquid in a fused xenolith at various stages was calculated from chemical and modal analyses. The chemical analysis indicates that fusion occurred in the presence of excess water-vapour. The melting and crystallization processes compare closely with the behaviour of similar compositions in the system $NaAlSi_3O_8$–$KAlSi_3O_8$–SiO_2–H_2O. Liquidus temperatures corresponding to the calculated liquids provide temperature estimates. An upper pressure limit is given by the quartz–tridymite *PT* curve. It is estimated that the liquid crystallized between 1,025° C and 935° C at a water-vapour pressure of 430 kg/cm². Reaction between picrite and fused sediment indicates that maximum fusion occurred when crystallization of the picrite was almost completed. The estimated picrite intrusion temperature is at least 1,175° C.

INTRODUCTION

On the island of Soay, south of Skye, a number of basic and ultrabasic minor intrusions of Tertiary age have been emplaced in Torridonian sandstone. Detailed mapping was completed by Clough & Harker (1904), and Harker (1904) discussed the igneous rocks in his classic account of the Cuillin gabbroic complex. According to Harker (p. 247): 'Clough has observed three clear instances of the vitrification of grits in Soay, besides others in which the effects seem to be obscured by subsequent alteration. Some of these are in connexion, not with basic but with ultrabasic sills. The vitrification is only locally produced in the case of any given sill.' The picritic minor intrusions have been numbered by Drever & Johnston (1958) for ease of reference. The subject of this study, Sill 1, is located on the SW. coast of the island, a quarter of a mile WSW. of the outlet of Loch Doir a'Chreamha.

Sill 1 belongs to the Hebridean group of non-alkaline picritic minor intrusions studied by Drever & Johnston (1958). It contains about 55 modal per cent of forsteritic olivine, 25 per cent of calcic plagioclase, 18 per cent of clinopyroxene, and 2 per cent of chromespinel; a detailed petrographic description will be presented elsewhere. This is one of the few ultrabasic sills where progressive metamorphism of the country rock has culminated in fusion. On cooling, the fused sediment precipitated microlites of tridymite (now inverted to quartz), hypersthene, cordierite, and magnetite, until the remaining liquid was quenched to a

[Journal of Petrology, Vol. 2, Part 1, pp. 1–37, 1961]

glass. The highest degree of metamorphism is illustrated by black obsidian-like xenoliths in which up to 92 per cent of the original minerals were fused.

The stages of fusion and subsequent crystallization have been determined by petrographic methods, and these are compared with the behaviour of similar compositions in the system $NaAlSi_3O_8$–$KAlSi_3O_8$–SiO_2–H_2O. Agreement between the synthetic system and the more complex natural system is so close, that the measured liquidus temperatures in the synthetic system are used to estimate the temperature of the sediment at various stages of fusion and crystallization. This also permits an estimate of the temperature of the picrite at the time of intrusion.

FIELD RELATIONS

Torridonian sediments in the neighbourhood of Sill 1 belong to the Beinn Brheac group (Clough & Harker, 1904). The predominant country rock is feldspathic sandstone or grit, with varying grain size, dipping about 15° to the west. Sill 1, intersecting a thick dolerite dyke, was mapped by Clough, who recorded the presence of a fused grit xenolith at the place of intersection. Its field relations were illustrated by Drever & Johnston (1958, text-fig. 6). The contact of this outcrop with sediment was not found.

Another smaller outcrop of the sill, with upper and lower contacts against Torridonian sediment, was discovered by Drever just below high-tide level on the wave-cut platform about 30 metres from Sill 1. This outcrop, which will be referred to as Sill 1A, contains several black obsidian-like xenoliths, similar to that found in Sill 1, as well as xenoliths exhibiting lesser degrees of fusion. The sediment at the bottom contact is extensively fused. The relationship of the sill to the country rock is illustrated in Fig. 1. Its width is about 1 metre.

The upper margin has a narrow chilled selvage containing a few small olivine phenocrysts, and the upper 50 cm of picrite appears fresh and uniform. Below this, there extends a line of small, black, glassy xenoliths and xenoliths of coarser grit. The latter are surrounded by fine-grained rims of black vitrified sediment which is in contact with serpentinized picrite (Plate 1, fig. D). Below the sill, fine-grained sediment has been fused and converted into a tough black rock with the appearance of rapidly chilled basalt. Above the sill, the metamorphosed sediment forms a similar band, about 30 cm wide, which is somewhat fissile towards its edges. The black sediment is locally separated from the sill by narrow seams of coarse red grit which appear in hand specimen to be unaltered. Similar coarse red grit lies above the metamorphosed band.

The contact relations at the base of the sill are more irregular. The black sediment grades downwards, through 30 cm to 50 cm, into a fine-grained red feldspathic sandstone. Within the zone of fine-grained metamorphosed sediment there are several irregular bodies of coarser grit. These are injected by the finer, more mobile fused sediment (Plate 1, fig. B). The sediment below the sill extends seawards farther than the picrite, forming a prominent ledge. Within this ledge

the partially fused sediment is cut by a vertical 10-cm wide rheomorphic vein of black glassy sediment containing small fragments of picrite. The vein has sharply defined contacts (Plate 1, fig. A).

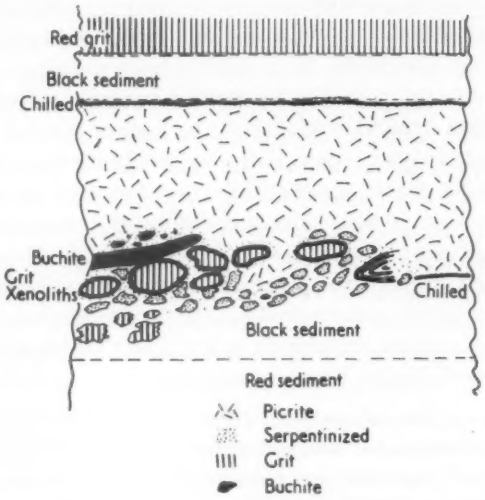

FIG. 1. Diagrammatic sketch of the field relations of Sill 1A just below high-tide level on the wave-cut platform below Sill 1.

The fused xenoliths and the rheomorphic vein may be called buchites. Buchite was first defined as a fused sandstone, but its connotation was subsequently extended to include all vitreous or semi-vitreous rocks produced by thermal metamorphism, regardless of their composition (Tomkeieff, 1940).

PROGRESSIVE METAMORPHISM OF ORIGINAL SEDIMENTS

The stages of fusion were traced by studying thin sections of specimens collected at various distances from Sill 1A, and the newly crystallized minerals were studied, in particular, in the glassy xenoliths. Between corroded grains the products of fusion form a glassy matrix which comprises the quenched liquid, the decomposition products of the original minerals, and the new phases which crystallized from the liquid. In the fine-grained sediments the matrix is so crowded with microscopic crystals that the stages of fusion were not readily discernible, but in the coarser grits a clear picture was obtained of the order and manner in which the minerals of the original sediment were fused and incorporated into the matrix. In the basal contact zone of Sill 1A there occurred hybridization between the picrite and the mobilized sediment with the result that resorbed olivine crystals are surrounded by the acid glass produced by fusion. Isolated olivine crystals and small picrite inclusions also occur in the rheomorphic vein.

Petrography

Only one specimen was collected from the unmetamorphosed sediment below Sill 1A. The red sediment is fine-grained and even-textured. Subrounded clastic fragments consist mainly of strained quartz grains, turbid crystals of potash feldspar (orthoclase and microcline) and a small amount of plagioclase feldspar. Turbidity of the feldspar results from minute haematite inclusions. Grain size varies from 0·1 mm to 0·2 mm. The quartz and feldspar grains are separated by sericite and siliceous cement containing much disseminated haematite dust. There are also larger flakes of muscovite, frequently curved. Magnetite, in very small and a few larger grains, tends to be arrayed in lines parallel to the length of the larger muscovite flakes. The red colour is produced mainly by the haematite, although the feldspar also contributes. This one specimen is not representative of the country rock, because even in the vicinity of the sill there are variations in grain size, and probably in the proportions and compositions of the clastic grains. A general description is given by Clough (Clough & Harker, 1904) who describes the Beinn Bhreac group as:

> Red and purplish-red false-bedded grits, most of them coarser than those in groups 1 and 3, and with abundant seams containing pebbles, from half an inch to two inches long, of quartzite felsite, andesite, and jasper. In most of the coarser grits the grains of feldspar and quartz are somewhat less than a small pea. Occasional thin bands of reddish and greenish sandy shale. Thickness about 2,200 ft. . . .
>
> The grits closely resemble those in the Applecross division on the mainland of Inverness-shire, but many of them are considerably coarser than most of those which are found in this division in the eastern part of Skye. . . .
>
> Specimens of grits from each of the groups have been examined by Dr. Flett, and each he finds to be highly feldspathic and to include orthoclase and microcline as well as, or in excess of, plagioclase.

The progressive fusion of the sediment with advancing metamorphism is illustrated by the approximate modal analyses listed in Table 1 (measured with

TABLE 1

Approximate modes of metamorphosed sediment

Specimen	87	85	83	90	129
Quartz	54·0	65·5	49·0	20·0	8·0
Alkali feldspar	7·5	3·0	5·0	—	—
Plagioclase feldspar	1·0	0·3	—	—	—
Magnetite	7·0	10·0	6·0	4·0	—
Sericite	22·5	—	—	—	—
Siliceous cement	8·0	—	—	—	—
Glassy matrix	—	21·2	40·0	76·0	91·3
Rest	—	—	—	—	0·7

Specimen 87: 60 cm below basal contact zone.
Specimen 85: 20 cm below basal contact zone.
Specimen 83: basal contact zone.
Specimen 90: rheomorphic vein.
Specimen 129: xenolith from Sill 1.

a Swift point-counter). The nature of the partially fused fine-grained sediment prohibited accurate determinations. Specimen 87, 60 cm below Sill 1A, is an unaltered feldspathic sandstone containing less feldspar than a normal arkose (Pettijohn, 1949). It grades evenly upwards into black metamorphosed sediment, the change in colour resulting from reduction of haematite to magnetite. Thirty centimetres below the basal contact zone the only haematite remaining is that preserved within feldspars. The sericite is replaced by a dense glassy matrix, crowded with magnetite, which merges into siliceous cement.

In specimen 85, 20 cm below the basal contact zone, the glassy matrix constitutes 21·2 per cent of the rock, which is approximately the percentage of sericite in the unaltered sediment. The matrix is crowded with magnetite and many microscopic crystals of which a few were tentatively identified as orthopyroxene and cordierite. Patches of the matrix are weakly birefringent. In this specimen there is 11·5 per cent more quartz than in the unaltered sediment. This could be due to variability of the sediment from one horizon to another, or to migration of some of the liquid from its place of formation. This would leave the residue relatively enriched in quartz. Mobility of the partially fused sediment is illustrated by the injection of fine-grained material into coarser-grained and more rigid grit (Plate 1, fig. B), and the movement of liquid from its place of formation is illustrated by the rheomorphic vein (Plate 1, fig. A). Table 1 also shows an increase in magnetite and a decrease in feldspar for specimen 85 compared with specimen 87. This may result in part from the variability of the sediment, but petrographic examination confirms that the feldspar has been partially fused at this level. Other specimens from above and below Sill 1A are similar in general appearance to specimen 87.

The basal contact zone of Sill 1A comprises a mixture of black glassy sediment and masses of serpentinized picrite (Plate 1, fig. C). Near the picrite the glassy matrix of the sediment is often coloured brown. Modes in this zone are extremely variable, and specimen 83 (Table 1) was selected as representative of the least-contaminated sediment. The glass was colourless and no inclusions of olivine or picrite were present in the thin section examined. The percentages of quartz, feldspar, and magnetite are smaller than in specimen 87, although the feldspar shows an increase over that in specimen 85. The glassy matrix, amounting to 40 per cent, is much increased.

The rheomorphic vein contains a higher proportion of glass, which is variable in amount from one specimen to another. Of the original minerals in specimen 90, only 20 per cent of rounded quartz grains remain. These are generally surrounded by secondary quartz rims. Seventy-six per cent of the specimen consists of clear glass containing numerous microlites of hypersthene and cordierite together with magnetite dust; and 4 per cent consists of larger magnetite grains. Small resorbed fragments of feldspar were found in another specimen. Inclusions of picrite and isolated olivine crystals, which are quite abundant, were omitted from the modal determinations. This vein probably represents a fluid fraction

separated from partially vitrified sediment near the basal contact zone or from a fused xenolith near the base of the sill. A process of filter-pressing is suggested by the variation in amount of glass along the vein.

A xenolith in Sill 1 exhibits the most extreme fusion discovered (specimen 129, Table 1). Glass containing microlites of cordierite, hypersthene, inverted tridymite, and magnetite amounts to 91·3 per cent. Of the original minerals, only 8 per cent of rounded quartz grains remain. These are surrounded by fringes of inverted tridymite (Plate 2, fig. B). In all sections examined, less than 1 per cent consists of isolated, serpentinized olivine crystals. An expanded modal analysis, giving in addition percentages of the microlites, is listed in Table 3. The xenolith probably illustrates almost complete fusion *in situ*.

The elongated buchite xenolith above the grit xenoliths (Fig. 1), is pale green, whereas others are black. It contains very little magnetite and the colour is imparted by green-tinted glass. Many of the remnant quartz grains have fringes of inverted tridymite, or secondary quartz rims, and some have colourless glassy borders around the quartz rims. The glassy borders are separated from the green-tinted glass by sharp boundaries. A few small resorbed feldspar grains remain. Grains of carbonate (sometimes surrounded by narrow, colourless glass rims) and veins containing rosettes of carbonate occur sporadically throughout the xenolith. Rare, perfect rhombs of carbonate, less than 0·03 mm in size, are set within the glass. Cordierite is present in small amounts and hypersthene is abundant. Some crystals, similar in morphology to hypersthene, exhibit green to yellowish-green pleochroism, and oblique extinction. These were tentatively identified as aegirine–augite. The rarity of magnetite, the colour of the glass, the relative abundance of carbonates, and the presence of aegirine-augite suggest that this buchite was derived from sediment with bulk composition different from that of the other xenoliths.

It is evident from the modal analyses that the development of liquid in the sediment resulted from decomposition of the sericite and the fusion of feldspar and quartz. This can also be illustrated in a qualitative way by X-ray powder diffraction patterns of rock specimens (Fig. 2). In the unaltered sediment, peaks representing quartz, feldspar, and muscovite are readily distinguished. Partial fusion of specimen 76 has resulted in disappearance of the muscovite peaks, a marked decrease in intensity of the feldspar peaks, and a decrease in intensity of the quartz peaks. In the fused xenolith, variation in the base of the diffraction pattern confirms the presence of much glass. No feldspar peaks remain, and the quartz peaks are much reduced in intensity. Small peaks representing cordierite and hypersthene can be distinguished, but peaks for magnetite occur outside the range of 2θ illustrated in the figure.

Examination of the modes and X-ray diffraction patterns of selected specimens establish the general behaviour of the sediment in response to progressive metamorphism. The detail was provided by petrographic study of coarse-grained sediments.

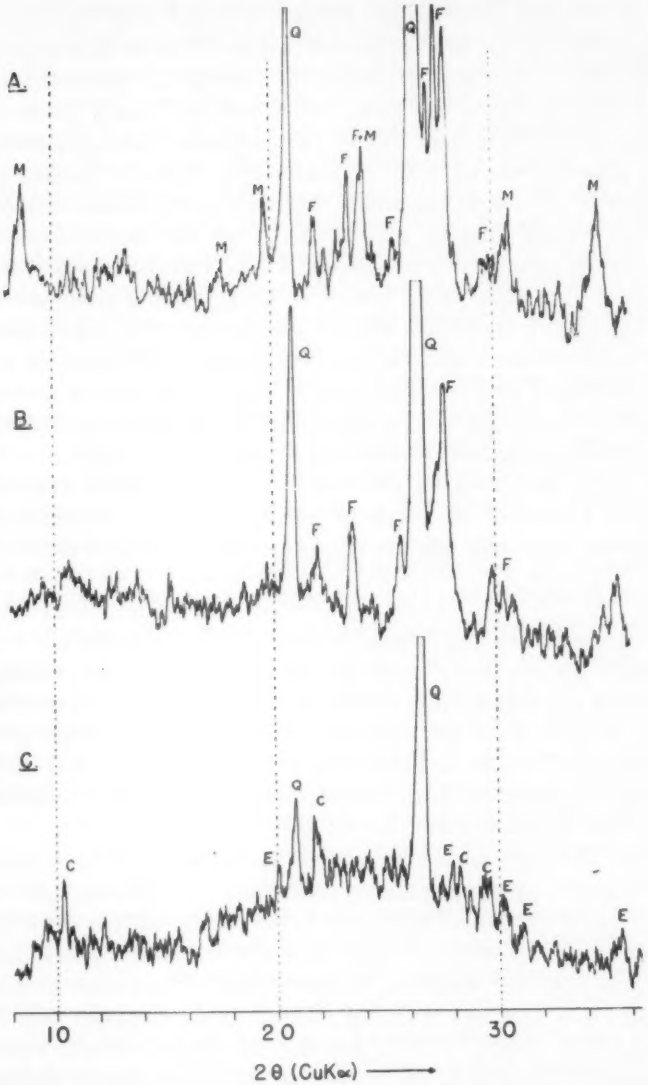

FIG. 2. X-ray powder diffraction patterns of crushed rock specimens (scanning speed 2° per second). A, specimen 87, unaltered sediment. B, specimen 76, buchite rim surrounding coarse-grained xenolith. C, specimen 129, fused xenolith (see Table 3). Peaks for the minerals present are denoted by: *Q*, quartz; *F*, feldspar; *M*, muscovite; *C*, cordierite; *E*, enstatite (or hypersthene).

Coarse-grained grits occur as irregular masses within the fine-grained sediment below the basal contact zone and as xenoliths within Sill 1A (Fig. 1; Plate 1, figs. B, D). They contain large feldspar grains, smaller quartz grains, and rounded pebbles of almost pure quartzite; these are enclosed by a glassy

matrix with irregular distribution. Magnetite is the only ore mineral in the matrix, but haematite has been preserved in many feldspar grains and in pebbles of quartzite. The component grains of the pebbles are cemented by siliceous material containing haematite dust, which outlines quartz grains and forms parallel lines within the cement. Between crossed nicols the composite fragments appear as granular quartz with no distinction between original grains and cement except where haematite occurs. Each grit xenolith is bordered by a band of black fine-grained buchite, separating it from the picrite (Plate 1, fig. D). The band may be variable in width. Some of the interstitial liquid was apparently squeezed out to the edges of the xenoliths. Larger quartz grains are sometimes fractured and slightly displaced, and the gap between the fragments is filled by glassy matrix containing angular splinters of quartz. The xenolith must therefore have been subjected to stress sufficient to fracture the quartz during cooling, otherwise the irregular edges of the quartz splinters would have become rounded. The same stresses could have squeezed out the interstitial liquid.

Narrow veins traversing all the coarse-grained xenoliths demonstrate the circulation of hydrothermal solutions which post-dated consolidation of the fused sediments. The veins contain siliceous material, or carbonates, or both.

Mineralogy

Sericite. Approaching the contact with Sill 1A, the first change noted in the sediment is the disappearance of sericite. Water-vapour released during decomposition would join that already present in the pores of the sediment and would hasten the formation of an interstitial melt. Many micas contain fluorine replacing hydroxyl (Yoder & Eugster, 1954; Correns, 1956) and the release of fluorine would enhance the fluxing properties of the interstitial material (Tuttle & Wyllie, 1957; Wyllie & Tuttle, 1957, 1960).

Haematite. The sediment's change in colour from red to black results partly from development of the glassy matrix containing finely disseminated magnetite, and partly from reduction of haematite to magnetite. This is not a function of temperature alone, because haematite is preserved within felspar crystals and quartzite pebbles in the xenoliths. The reduction of haematite to magnetite in contact rocks is a common result of thermal metamorphism (e.g. Walker & Poldervaart, 1949; Black, 1954*a*), but because of uncertainty regarding the partial pressure of oxygen in the circulating fluxes, the change cannot be used as a thermometer. The dependence of this reaction upon oxygen pressure is clearly displayed by Bastin's (1905) account of baked clays and natural slags in Wyoming. Widespread oxidation of iron in shales and sandstones has produced 'gaudy colours' in the sediments, but, in contact zones between argillite and slag, haematite has been reduced to magnetite. Elsewhere, sandstone passes into a glassy mass enclosing minute crystals of haematite.

Feldspar. Incipient fusion of the alkali feldspar is apparent in specimen 85, 20 cm below the basal contact zone, and the degree of fusion increases as the

base of the sill is approached. In the glassy xenoliths, feldspar is rare or absent. Incorporation of feldspar into the interstitial melt is a dual process, resulting from direct fusion and from mechanical disintegration. Not only is the feldspar marginally dissolved, but thin seams of liquid develop also along cleavage planes (Plate 1, fig. G). When the feldspar is traversed throughout by liquid veins it illustrates the 'finger-print' structure described by Guppy & Hawkes (1925), Tidmarsh (1932), Davidson (1935), and Allison (1936). At this stage, feldspars in plane polarized light are barely distinguishable from the glassy matrix (Plate 1, fig. F). Many crystals retain their integrity, but others are broken into fragments (Plate 2, fig. A) which become dispersed in the liquid (Lacroix, 1893; Knopf, 1938; Larsen & Switzer, 1939). The plagioclase feldspar undoubtedly behaved similarly (Allison, 1936), but its amount is too small for the stages of fusion to be traced. In the clear glass of the rheomorphic vein a few feldspar fragments are represented by small rounded aggregates of rectangular cleavage fragments, still in optical continuity. One of the aggregates retains polysynthetic twinning. Some of the larger feldspar grains in the coarse xenoliths are bordered by narrow colourless rims which may represent a new growth of feldspar (Richarz, 1924; Tidmarsh, 1932).

When feldspars are heated they undergo structural changes causing variations in optical and X-ray properties (Spencer, 1937; Mackenzie & Smith, 1956). Study of the feldspars in fused sediment might therefore yield information about the sediment's thermal history. At least three feldspars—microcline, orthoclase, and plagioclase—are present in the unaltered sediment, and their proportions and compositions probably vary from one stratigraphic horizon to another. Anorthoclase may occur as well (see below), but its presence was not confirmed. It is impossible, therefore, to relate studies of feldspars in the fused rocks to known starting materials. No microscopic unmixing of the feldspars was detected either in the unaltered sediment or in the fused sediment, and twinning persisted in the fused sediments.

The optical axial angle is the most useful optical property for the classification of alkali feldspars (Tuttle, 1952). Values of $2V$ for nine homogeneous feldspars within a coarse grit xenolith were therefore measured on the universal stage. The measured crystals are small compared to the large twinned crystals more characteristic of the partially fused grit. Limited conclusions may be reached by comparing the results with the diagram of Mackenzie & Smith (1955), modified after Tuttle (1952). The feldspars in the xenolith may include intermediate microcline, orthoclase, anorthoclase, sanidine, and high sanidine. Since microcline is present, the occurrence of high sanidine appears unlikely (high sanidines are rare in nature; Mackenzie & Smith, 1955). These feldspars could represent original microcline changed by heating, but the evidence is inconclusive.

Many of the large feldspar crystals within the xenolith show cross-hatch twinning, and one of these was prised from the specimen. Its X-ray powder pattern, covering the ranges of 2θ which provide information about the

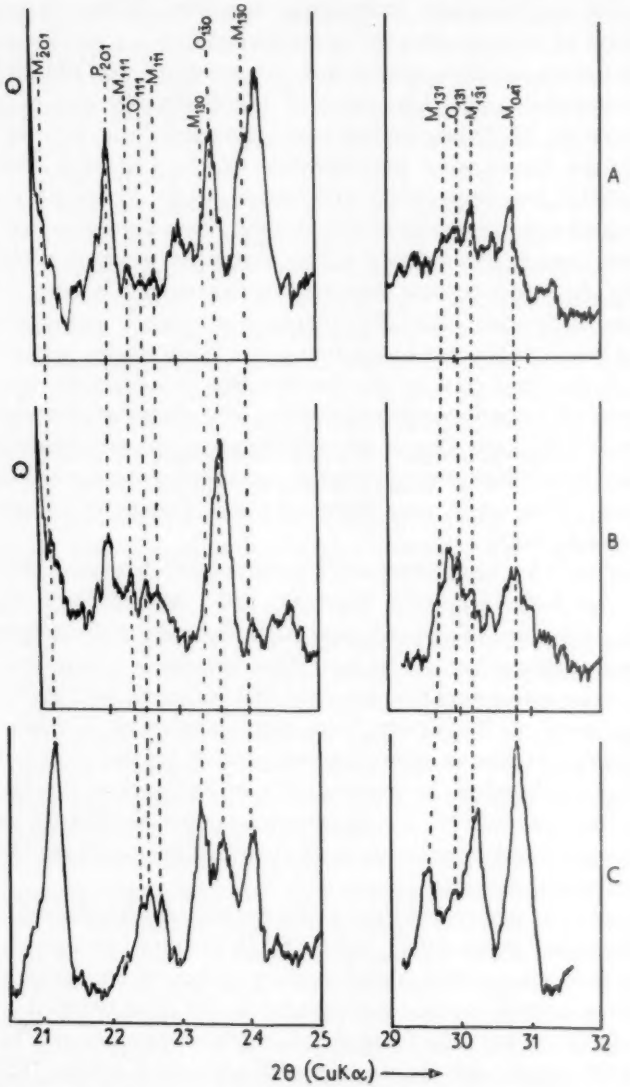

FIG. 3. X-ray powder diffraction patterns of crushed rock samples, and of a feldspar prised from sediment (scanning speed 0·25° per minute). A, specimen 87, unaltered sediment. B, specimen 76, buchite rim surrounding coarse-grained xenolith. C, feldspar prised from a grit xenolith, specimen 76. Feldspar peaks are indicated by: *P*, plagioclase feldspar; *M*, microcline; *O*, orthoclase (or possibly sanidine). *Q* is a quartz peak.

composition and structural state of feldspars, is given in Fig. 3C. The estimated composition is Or_{79} (estimated from the $\bar{2}01$ spacing, with Lake Toxaway quartz as an internal standard; Bowen & Tuttle, 1950). The pattern is almost identical

with one published by Mackenzie (1954, Fig. 5*a*), where orthoclase coexists with microcline in a single crystal. The spacing between the 130 and $1\bar{3}0$ peaks of the microcline indicates nearly maximum departure from monoclinic symmetry. The absence of structural states intermediate between maximum microcline and orthoclase suggests that the orthoclase was present before fusion of the sediment.

Portions of the X-ray powder diffraction patterns shown in Fig. 2 are reproduced in Figs. 3 A, B. The patterns are complicated because more than one feldspar is present in addition to other minerals. In the unaltered sediment (Fig. 3A), $\bar{2}01$ peaks for potassic feldspars are almost obliterated by the strong quartz peak. The peak near 22° is outside the range of $\bar{2}01$ for alkali feldspars (Bowen & Tuttle, 1950) and probably represents the $\bar{2}01$ peak for plagioclase feldspar. Its intensity suggests that the percentage of plagioclase feldspar in the sediment is greater than estimated by modal analysis, Table 1 (all untwinned feldspar was allocated to alkali feldspar in the modal determinations and some untwinned plagioclase could have been included. Alternatively, the proportion of plagioclase feldspar may vary within a single specimen, as well as from one horizon to another). The subsidiary peak just below $2\theta = 22°$ suggests the presence of anorthoclase. Several of the other feldspar peaks are superimposed on each other and further complicated by the presence of muscovite peaks.

No muscovite remains in specimen 76, the buchite rim surrounding a grit xenolith, so its pattern is simpler (Fig. 3B). The plagioclase $\bar{2}01$ peak is reduced in intensity relative to the alkali feldspar peaks. Microcline and possibly anorthoclase are present, but the 130 peak for orthoclase is dominant. This could indicate either that the proportion of orthoclase exceeded that of microcline in this buchite before fusion, or that original microcline was converted to orthoclase or sanidine. The 130, 131, and $1\bar{3}1$ peaks indicate intermediate states between maximum microcline and orthoclase, so it may be concluded, tentatively, that original microcline was partially converted to orthoclase or sanidine.

The buchite (specimen 76) surrounds the coarse grit xenolith in which the feldspar $2V$ measurements were made. Feldspars in the buchite may have responded structurally to the heating (X-ray), and some structural adjustment may also have occurred in the homogeneous feldspars within the coarse xenolith (optics), but one of the large twinned feldspars within the xenolith indicates no structural response to heating (X-ray). These results are inconclusive.

The smaller feldspars in the xenolith and in the buchite rim are more closely associated with the glassy matrix than are the larger feldspars, and the possible difference in response between them may have resulted from the fluxing action of the liquid (with its dissolved volatiles) on the smaller feldspars. Sanidinization of alkali feldspars in fused xenoliths enclosed by basic rocks has been recorded (Lacroix, 1893, 1908; Richarz, 1924), but the process of sanidinization is imperfectly understood. Some feldspars resist change even when heated for very long periods (Mackenzie & Smith, 1956). Failure of the feldspars to adjust

structurally might be due to rapid cooling with insufficient time at elevated temperatures. Studies by Mackenzie (1957) of changes in the lattice parameters of albite confirm that extremely long periods are required to produce structural changes either in natural low temperature albite or in synthetic (high) albite, except at temperatures near the melting-point. The presence of water-vapour under pressure promotes structural changes in albite at low temperatures, although a long time is still required for the attainment of equilibrium.

Quartz. Rounded and embayed quartz grains below the basal contact zone confirm that quartz began to fuse at an early stage of metamorphism. Fusion undoubtedly resulted from fluxing by the interstitial liquid and from mutual fluxing wherever quartz and feldspar grains were in contact (Thomas, 1922; Allison, 1936; Knopf, 1938). The quartzite pebbles in the coarser-grained sediments confirm the importance of interstitial fluxing material in the development of a liquid from minerals with high melting-points. Where no passageways were available for the transit of fluxes, no liquid developed. Boundaries between quartzite pebbles and the glassy matrix of grits are sharp and smoothly rounded, cutting across both original quartz grains and siliceous cement. The pebbles fused as if they were single crystals; there is no glass within them, and no evidence that tridymite ever developed. On cooling, tridymite crystallized from the interstitial melt forming fringes around resorbed quartz grains. This raises the question of why the quartz grains themselves did not change to tridymite. Although the transition from quartz to tridymite is sluggish, tridymite crystallizes readily from liquids in the presence of water-vapour under pressure (Tuttle & Bowen, 1958). Volatile materials dissolved in the interstitial liquid had access only to the margins of the quartz grains and quartzite pebbles, and therefore could not be very effective in promoting their inversion to tridymite.

Magnetite. The modal analyses of Table 1 confirm that iron oxide originally present in the sediment dissolved in the interstitial melt, and the presence of euhedral crystals in the buchites indicates that magnetite later recrystallized. No way of distinguishing with certainty between remnant and new crystallized magnetite was found. Clough & Harker (1904) concluded that all of the iron ore present in Torridonian sediments was dissolved during fusion by basic sills in Soay, and probably the same was true here.

PRODUCTS OF METAMORPHISM AND FUSION

Glass

Transition of the red fine-grained sediment into black metamorphosed sediment is accompanied by the appearance of a dense, extremely fine-grained matrix containing glass. Its proportion increases towards the basal contact zone, where it amounts to about 40 per cent. After decomposition of the sericite, the initial liquid probably developed by attack of the interstitial fluxes on feldspar and quartz. The fusion of quartz and feldspar at junctions between the two minerals, with the formation of a low-temperature liquid, has often been described

(Allison, 1936; Knopf, 1938), and the development of such liquids has also been explained by the selective fusion of feldspars followed by solution of quartz in the feldspathic melt (Thomas, 1922; Osborne, 1950). Consideration of phase-equilibrium studies confirms that both processes are applicable. Quartz and feldspar in contact would produce a low-temperature liquid by mutual fluxing and, once such a liquid is present, both quartz and feldspar would dissolve in it.

The coarse-grained xenoliths contain less glass than fine-grained xenoliths, but the ubiquitous presence of black glassy rims between the grit and the enclosing picrite suggests that much of the interstitial liquid was squeezed out from between the coarser grains. Marginal concentration of volatiles from the picrite may have increased the extent of fusion at the edges of the xenoliths.

The black obsidian-like xenoliths in both sills have been almost completely fused; they consist of clear, colourless glass containing resorbed grains of quartz, a few olivine pseudomorphs, and the new minerals which crystallized from the melt. The glass in one xenolith has a green tint. The percentage of glassy matrix in the rheomorphic vein is almost as high as in the fused xenoliths, but the preservation of a few small feldspar grains indicates an earlier stage of fusion. The glass is colourless and, although it encloses small discrete inclusions of picrite, it has suffered only slight contamination by solution of igneous material (Plate 2, figs. C, D).

A chemical analysis of the most highly fused xenolith found (specimen 129, Sill 1) and the calculated composition of glass within the xenolith, are listed in Table 2. Analyses of glasses in fused xenoliths from other localities are included for comparison. The relatively high MgO content of the fused xenolith (compare the other analyses, and analysis 5, Table 4) is probably due to the olivine xenocrysts. The norm and a modal analysis are given in Table 3 (compare Table 1). The modal percentages of cordierite, hypersthene, and magnetite have undoubtedly been overestimated, because many of these crystals are thinner than the slide containing them (0·03 mm). Some allowance has been made for this in calculating the composition of the glass. Inverted tridymite was similarly over-estimated but, since this mineral is densely packed around quartz grains, the error is smaller. The specific gravities of minerals involved in the calculations were obtained from Winchell & Winchell (1951), and that of the glass was assumed to be 2·38 (see Table 2). The method of calculation is given below, Table 2. Clearly, the calculated analysis of the glass is only an approximation, but the result agrees quite well with the analyses of similar glasses presented by Frankel (1950) and by Larsen & Switzer (1939), and, as shown later, the analysis probably represents the glass fairly accurately in its major constituents.

The fused xenolith contains a high proportion of water, and this is concentrated in the glass (cf. Harker, 1950, p. 71). The glass also contains 1·35 per cent of P_2O_5. The other analyses in Table 2 are characterized by high water-content, and there is little doubt that abundant volatile materials were available during the fusion of these rocks.

TABLE 2

Chemical analysis of a fused xenolith compared with other analyses of glasses produced by fusion

	1	2	3	4	5
SiO_2	71·04	71·90	69·72	72·57	71·29
Al_2O_3	10·92	12·45	14·80	13·08	12·69
Fe_2O_3	2·14	—	0·55	0·94	1·22
FeO	1·48	—	1·36	0·50	0·69
MgO	2·22	—	0·40	0·08	0·41
CaO	1·34	1·89	1·42	1·12	0·77
BaO	—	—	0·05	0·08	—
Na_2O	2·96	4·18	3·87	3·75	4·19
K_2O	1·35	1·91	2·75	2·33	3·54
H_2O+	4·48	6·32	4·33	5·21	4·57
H_2O-	0·52	—	0·15	0·17	—
TiO_2	0·68	—	0·48	0·18	0·29
MnO	0·07	—	0·13	0·02	—
P_2O_5	0·96	1·35	0·21	0·23	—
	100·16	100·00	100·22	100·26	99·66
Refractive index		1·502	1·505	1·501	1·497
Specific gravity		—	2·37	2·35	2·40

1. Fused xenolith, specimen 129, Sill 1A. Analyst: W. H. Herdsman (new series).

2. Calculated composition of the glass in the fused xenolith, specimen 129. Analysis 1, less remnant quartz and inverted tridymite, less 4 per cent normative enstatite, remaining MgO subtracted as cordierite and all iron and titania subtracted as normative ore minerals (see Table 3).

3. Calculated composition of glass in fused xenolith of feldspathic sandstone. Analyst: J. J. Frankel (from Frankel, 1950; Coldbrook glass).

4. Glass separated from fused xenolith of feldspathic sandstone. Analyst: J. J. Frankel (from Frankel, 1950; Ecca grit).

5. Glass separated from fused xenolith of tonalite. Analyst G. Switzer (from Larsen & Switzer, 1939).

TABLE 3

Comparison of the norm and mode of the analysed fused xenolith, specimen 129

Norm		*Mode*	
q	45·3	Quartz	8·0
or	7·8	Glass	66·5
ab	25·2	Cordierite	7·5
an	0·3	Hypersthene	5·8
co	4·5	Inverted tridymite	6·5
hy (en)	5·6	Magnetite	5·0
mt	3·0	Olivine	0·7
il	1·4		100·0
ap	2·4		
H_2O	5·0	Glass plus new minerals	91·3

The volatiles must have been derived either from the sediment or from the picrite. The average analysis of Torridonian sediment in south-eastern Skye (Table 4) contains only 1·06 per cent of water and 0·30 per cent of P_2O_5. The sediment in the neighbourhood of Sills 1 and 1A probably contains more mica than the average Torridonian sediment but, even so, the high proportion of volatile material contained by the fused xenolith, which is completely surrounded by picrite, could hardly have been present initially in the sediment. It thus appears certain that most of the volatiles emanated from the picrite. Larsen & Switzer (1939) similarly concluded that only the fluxing action of large quantities of water from olivine basalt magma made possible the fusion of a tonalite xenolith in the basalt. Walker & Poldervaart (1949) believed that the local fusion and mobilization of sediments in contact with the Karroo intrusions was caused by chloride and sulphate ions in the sediments, but the presence of such ions was not established. Later analyses of sediments fused by Karroo intrusions (Frankel, 1950, Table 2) revealed a high water-content, and the fluxing action of the water probably caused the fusion.

Samples of glass free from inclusions could not be obtained for specific gravity measurements, but refractive indices were determined in sodium light on crushed fragments ($\pm 0{\cdot}003$): (1) glass of the analysed xenolith (specimen 129): $n = 1{\cdot}502$; (2) glass in the rheomorphic vein: $n = 1{\cdot}500$; (3) glass in the green-tinted buchite: $n = 1{\cdot}482$.

Since silica is the most abundant oxide in natural glasses, it might be expected that the refractive indices and specific gravities of glasses should show some relationship to their silica contents. Stark (1904) and George (1924) attempted such correlations. George also correlated the percentages of other oxides in glasses with their refractive indices and specific gravities. He concluded boldly that his curves would provide rapid and fairly accurate estimates of the compositions of natural glasses. On the grounds that each constituent of a glass would contribute its effect, Tilley (1922) regarded such relationships, even for the dominant oxide silica, as no more than rough approximations. He demonstrated convincingly that the water-content of a glass has a significant effect on its refractive index.

Several glasses developed in xenoliths have been analysed since 1924 (Holmes, 1936; Larsen & Switzer, 1939; Frankel, 1950; analysis 2, Table 2) and, using George's curves, their chemical compositions were estimated from their determined refractive indices and specific gravities. Although Frankel's results showed fair agreement with George's curves, agreement of the estimated percentage of any particular oxide with the chemical analyses of the various glasses appeared to be quite fortuitous, and the errors were not consistent, the error in silica percentage varied from 1 to 10 per cent, and potash was constantly in error by $\pm$ 1 or 2 per cent. Mathews (1951) has demonstrated that the refractive indices of glasses produced by artificial fusion of samples from selected suites of igneous rocks do show a close correlation with their chemical composition.

The fusion eliminates water and converts all iron to the ferric state. In special circumstances, therefore, the refractive indices of glasses may give information concerning their compositions, but any estimate of the composition of glasses (2) and (3) above on the basis of their refractive indices is considered unjustifiable.

New minerals

Tridymite. Surrounding resorbed quartz grains in the fused xenoliths and the rheomorphic vein are fringes of small, colourless, prismatic crystals extending at all angles from the grains (Plate 2, fig. B). These are quartz in optical continuity with the grains to which they are attached. Similar fringes occur frequently in fused siliceous rocks, and descriptions have been given by Lacroix (1893), Thomas (1922), Campbell *et al* (1933), Holmes (1936), Tomkeieff (1940), Walker & Poldervaart (1949), Frankel (1950), and Osborne (1950). They are particularly well developed in xenoliths within the Tertiary igneous rocks of Scotland (Bailey & Wright, 1924). Reynolds (1940) described the development of similar fringes without the intervention of an interstitial melt, but noted that passageways for the movement of fluxes were necessary for their formation. Minute crystals with the same habit, associated also with hexagonal flakes, may be preserved within a glass or within feldspar crystals (Reynolds, 1908; Thomas, 1922; Holmes, 1936; Knopf, 1938; Harker, 1950; Osborne, 1950; Wells, 1951). Flett (1911) believed that the fringes were possibly due to penetration of the melt along rhombohedral cleavages of the quartz, and Tomkeieff (1940) thought that they might possibly represent inverted cristobalite. All other investigators are agreed that they represent inverted tridymite, and the preservation of tridymite in some of these occurrences confirms this conclusion (Lacroix, 1908; Knopf, 1938; Osborne, 1950).

Standard textbooks of mineralogy, e.g. Winchell & Winchell (1951), describe tridymite in wedge-shaped crystals or six-sided thin tabular crystals, commonly showing twinning, but no mention is made of prismatic crystals. From synthetic melts tridymite invariably crystallizes as thin six-sided plates (e.g. Bowen, 1914), and the development of a prismatic habit appears to be restricted to tridymite in natural melts.

Many quartz grains are surrounded by a secondary rim of quartz. The outer edge of the rim may be well defined or it may merge into the glassy matrix. In several examples from the buchites the fringes composed of distinct prismatic crystals grade into continuous rims of homogeneous quartz around a single quartz grain. The secondary rims thus result from the inversion and recrystallization of original tridymite fringes. Lacroix (1908) recorded the inversion of many small tridymite lamellae into a sponge of quartz in optical continuity, and Hawkes (1916) described examples where one or more tridymite plates inverted and recrystallized into a homogeneous quartz grain. Single tridymite crystals are also known to invert into an aggregate of smaller quartz crystals (Mallard, 1890; Hawkes, 1916; Wager *et al.*, 1953).

Cordierite. Minute, colourless, six-sided prisms of cordierite crystallized from the partially vitrified sediment. They are most plentiful in the glassy xenoliths and it is here that their form may be clearly distinguished. A few crystals attain lengths of 0·06 mm but most are much smaller. Some have short extensions to their prismatic faces indicating a tendency toward skeletal crystallization (Plate 2, fig. D). Their optical properties agree with those of the microscopic cordierites which characteristically occur in fused sandstones and shales. Refractive indices lie between 1·529 and 1·541, and $(-)2V$ is small. Sector twinning on (110) occurs frequently, and rare cruciform twins are also present (Plate 1, fig. E). The latter have (021) or (101) as the probable twin plane. Only (110) and (130) have been reported previously as cordierite twin planes. Minerals with cordierite composition exist in several structural modifications (Miyashiro *et al.*, 1955). Just as the structural state of feldspars may give some indication of their temperature of formation, so the structural state of minerals with cordierite composition in fused sediments may permit an estimate of the temperature of intrusion of the igneous body causing the fusion. A measure of the structural state is given by the distortion index Δ measured by X-ray powder diffraction methods (Miyashiro, 1957). Cordierite in the fused xenoliths has a small distortion index, 0·08. The possible use of such measurements in the development of a temperature scale has been described elsewhere (Wyllie, 1959). This paper also includes a more detailed account of the optical properties of the cordierite.

It is generally agreed that the formation of cordierite in fused siliceous rocks requires the mixing of basic magma with the fused material, or at least an accession of magnesia from the magma (Prohaska, 1885; Zirkel, 1891; Harker, 1904; Thomas, 1922; Bailey & Wright, 1924). Contamination of the fused products is often revealed by brown coloration of the glass (Harker, 1904; Frankel, 1950), but when cordierite occurs in colourless glass accession of magnesia is not necessarily indicated. If the growth of cordierite depended upon the transfer of magnesia from the igneous rock, it might be expected that its proportion would increase as the intensity of colour in the glass increased. This is not so near Sill 1A, nor in the examples described by Harker (1904). The greatest development of cordierite is not in the brown glass of the basal contact zone but in the colourless glass of the xenoliths and rheomorphic vein. Provided some magnesia were present in the original material cordierite would be expected to grow as a product of simple fusion and recrystallization (Richarz, 1924; Venkatesh, 1952). Tridymite, hypersthene, and cordierite constitute a stable metamorphic assemblage at high temperatures in rocks with appropriate bulk composition (Tilley, 1923).

Hypersthene. Small accicular crystals are developed wherever glass is plentiful. They are almost colourless, but sometimes exhibit weak yellowish-green pleochroism; rhombic cross-sections are brownish. All elongated sections show straight extinction, with the slow vibration direction parallel to the length. The accicular crystals projected from crushed fragments of glass and it was

established that the refractive indices α and γ lie between 1·670 and 1·680. $2V$ measured on the universal stage is near 90°. The optical properties accord with those of orthopyroxene and they indicate a composition in the range Fs_{18} to Fs_{20} (Kuno, 1954).

The most striking features of the crystals are their great elongation and skeletal form (Plate 2, fig. B). Rapid growth rate in the direction of elongation has produced deep funnel-shaped hollows in the prism terminations, which sometimes persist for half the length of a crystal. Locally developed are shorter crystals with well-defined funnels at each end (Plate 2, fig. C). Similar skeletal growths of microscopic hypersthene in buchites were described in detail by Rinne (1895). Orthopyroxene does not appear in buchites as often as clinopyroxene, but skeletal crystals of hypersthene have been reported also by Lacroix (1893), Richarz (1924), Knopf (1938), and Venkatesh (1952). Bastin (1905) described extremely elongated needles (50:1), probably clinopyroxene, and Tomkeieff (1940) recorded enstatite together with skeletal clinopyroxene in fused sediment.

Aegirine–augite. In one xenolith microlites similar in morphology to the hypersthene exhibited stronger pleochroism and oblique extinction. These were tentatively identified as aegirine–augite. Harker (1904) suspected the presence of aegirine in Torridonian sediment on Soay which was partially fused by a dolerite intrusion.

Magnetite. The glassy matrix of the partially fused sediments is crowded with magnetite dust and with larger magnetite grains. In buchites the clear glass contains large and small crystals of magnetite, both euhedral and irregular in shape. It is likely that all of the iron ore passed into the liquid phase during fusion (Harker, 1904) and in the buchites all the magnetite present probably recrystallized from the liquid.

REACTION BETWEEN PICRITE AND SEDIMENT

Reaction between picrite and fused sediment occurred on a microscopic scale in the fused xenoliths and rheomorphic vein, and on a macroscopic scale in the basal contact zone of Sill 1A. The reaction resulted in (1) the replacement of olivine by antigorite, (2) the development of orthopyroxene mantles around olivine, and (3) the isolation of olivine pseudomorphs and picrite inclusions within fused sediment.

(1) Where in contact with fused sediment, the olivine is usually pseudomorphed by antigorite, and sometimes the alteration affects olivine crystals within picrite masses enclosed by the sediment (e.g. in the basal contact zone, Plate 1, fig. C). Olivine xenocrysts within fused xenoliths and in the basal contact zone are invariably pseudomorphed, but similar crystals within the rheomorphic vein are usually fresh, although many exhibit marginal alteration.

The stages of alteration were observed at the junction between a buchite inclusion and the main picrite above the grit xenoliths of Sill 1A (Fig. 1). Passing

from the buchite to the picrite there are narrow zones characterized by (*a*) a mixture of quartz grains and olivine pseudomorphs set in brown glass, (*b*) brown glass enclosing olivine pseudomorphs and plagioclase laths with only a few quartz grains; abundant prismatic crystals of clinopyroxene are locally developed, (*c*) normal picrite, with some brown glass extending through the matrix. The junction between the hybrid rock (*b*) and the unaltered picrite (*c*) is sharp (seen in thin section), and just below the junction many of the olivine pseudomorphs retain cores of olivine. Some of them straddle the junction, and in these the upper portions are unaltered and the portions below the junctions are altered to antigorite. The sharp boundary between fresh and altered olivine is broken in one place, where the brown glassy matrix extends upwards between the olivine crystals in the picrite. Contact of the matrix with olivine results in marginal serpentinization. Similar effects were observed near the contacts of other fused xenoliths.

(2) Mantles of small, weakly pleochroic crystals surround olivines in contact with fused sediment. The prismatic crystals are usually normal and rarely parallel to the olivine pseudomorphs (Plate 2, fig. C). The crystals are too small for the measurement of $2V$ but they were identified as orthopyroxene by their pleochroism, straight extinction, positive elongation, and by their similarity to hypersthene crystals in the neighbouring glass.

(3) Isolated olivine crystals are dispersed throughout the buchite xenoliths and the rheomorphic vein, and they may be highly concentrated in the basal contact zone (Plate 1, fig. C). They are usually somewhat rounded and corroded (Drever & Johnston, 1957, Plate II, fig. 1). Inclusions of picrite were found only in the rheomorphic vein and the basal contact zone. Solution of olivine in the rheomorphic vein is indicated by a concentration of hypersthene microlites in the glass around olivine xenocrysts and picrite inclusions (Plate 2, fig. C). The inclusions have fairly sharp contacts with glass and normally there is a narrow zone where the olivines are marginally altered to antigorite. Within these zones, the inclusions consist of normal picrite. Hybridization between picrite inclusions and the fused sediment in the rheomorphic vein was thus very slight, but reaction was more extensive at contacts between xenoliths and the picrite. The nature of the junction between a fused xenolith and the picrite has been described above. Junctions between picrite and the buchite rims surrounding grit xenoliths are more abrupt (Plate 1, fig. D), but alteration of the olivines extends farther into the enclosing picrite. Only a few olivine xenocrysts are enclosed by the buchite rims.

In the basal contact zone the fused sediment and the picrite may be intimately mixed (Plate 1, fig. C). The glass is pale or colourless in places, but normally it is brown. A more intense, almost opaque brown matrix, often weakly birefringent, extends through discrete picrite inclusions, and olivine crystals in contact with it are altered. The alteration does not always extend throughout the inclusions. The nature of the brown matrix made it difficult to distinguish

minerals present in addition to olivine pseudomorphs, but plagioclase laths were detected both within the picrite and in the brown glass surrounding the inclusions. Rare quartz grains were also found within the inclusions. Quartz and olivine pseudomorphs are abundant in the brown glass enclosing the picrite inclusions. Differences in colour of the fused sediment as seen in polished specimens appear to be related to the concentration of olivine pseudomorphs. Such concentrations may represent original inclusions which have disintegrated. The olivine pseudomorphs at the edges of the picrite inclusion shown in Plate 1, fig. C look as if they had been drifting away from the inclusion before the liquid was quenched to a glass. Other picrite inclusions in the basal contact zone are similar to those found in the rheomorphic vein; i.e. they consist of fresh picrite with only a narrow border of marginally altered olivine.

Contacts between the fused sediment and the picrite are thus very variable, and they provide conflicting evidence about the nature of the picrite when hybridization occurred. The sharp junctions with narrow altered borders imply that the picrite had crystallized completely by the time it was enclosed by the mobilized sediment, and the discrete nature of many inclusions points to the same conclusion. On the other hand, the presence of so many isolated olivine pseudomorphs in the sediment suggests that consolidation of the picrite was not complete at the time of mixing, and quartz grains could not have penetrated the inclusions unless there was some liquid present within them. Since most of the inclusions appear to have remained fairly rigid, crystallization must have been quite well advanced. Forcible mixing of fused sediment with picrite inclusions containing olivine, plagioclase, and some liquid could result in marginal disintegration of the inclusions, and the dispersion of olivine crystals through the acid liquid. Mixing of acid and basic liquids is indicated by the brown coloration of the glass in the basal contact zone. Liquid and quartz grains from the fused sediment could have penetrated the picrite inclusions, and quenching of the mixed liquid would have trapped quartz grains and volatiles within them.

Reaction between fused sediment and picrite would be expected whenever sufficient liquid developed in the sediment for it to become mobile, and the variety of reaction phenomena exhibited suggests that this did not always occur at the same stage of consolidation of the picrite. In most instances it occurred when the picrite consisted largely or completely of crystals. A xenolith enclosed by the sill would reach the temperature of the enclosing picrite, but the maximum temperature reached by the xenolith would be less than the intrusion temperature of the picrite. The development of large amounts of liquid within a xenolith would depend not only upon its temperature and volatile content, but also upon the diffusion of volatiles from the picrite. Concentration of volatiles within the xenolith would not occur instantaneously; there would be a distinct time-lag between the conduction of heat to the xenolith and the development of liquid within it. Fig. 4 illustrates diagrammatically the cooling and heating curves of the picrite and a xenolith, respectively, and the time-lag is represented

by the space between the heating curve and the curve showing the development of the equilibrium liquid for each temperature.

If the temperature of a xenolith were maintained at T_1, reached after a time t_1, the equilibrium liquid for this temperature would develop at a later time t_2. However, after a time t_2, the temperature of the xenolith would have increased to T_2. The equilibrium liquid for this temperature would develop at a time t_4, but

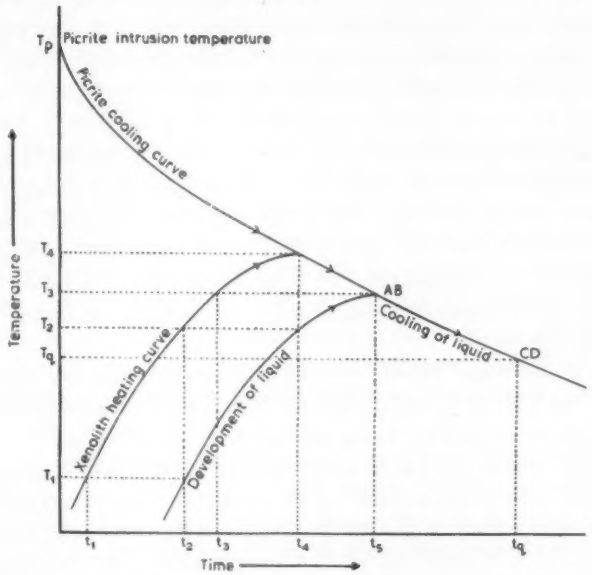

FIG. 4. Schematic representation of the cooling curve and heating curve of the picrite and a xenolith respectively. The third curve represents the stage at which an 'equilibrium' liquid develops within the xenolith, and horizontal lines between this curve and the heating curve represent the time-lag between the attainment of a given temperature and the development of a liquid which can exist in equilibrium at this temperature.

by this time the temperature of the xenolith (and the liquid it contains) would have reached the temperature of the cooling picrite T_4. By the time t_5, both picrite and xenolith would have cooled to the temperature T_3, and the composition of the liquid within the xenolith would correspond to that which would have developed if the xenolith had been maintained at the temperature T_3 throughout the time interval t_3–t_5. While the liquid was cooling from T_4 to T_3 the xenolith continued to melt. At the temperature T_3 the xenolith would reach its maximum stage of fusion. After time t_5 the picrite and the liquid would continue to cool together, with crystallization of minerals from the liquid developed by fusion, and the remaining liquid would be quenched to a glass after a time t_q when the temperature reached T_q. Equilibrium conditions would probably be approached quite closely during the time t_5–t_q.

The intrusion temperature of the picrite T_p was therefore greater than the

maximum temperature reached by the xenolith T_4. The interval between T_p and T_4 would depend upon the rates of cooling and heating of the picrite and xenolith respectively. The initial cooling rate of the picrite would be greater for higher temperatures of intrusion, which would probably result in a greater temperature interval T_p–T_4. This would also be greater for sediments farther away from the picrite because their heating rates would be slower. The temperature interval T_4–T_3 will depend upon the time-lag between the heating curve and the development of an 'equilibrium' liquid within the xenolith. The high viscosity of liquids of granite composition is well known (Schairer, 1950), and without the action of volatile components a rock of granitic composition would have to be maintained above its fusion temperature for a very long time before an equilibrium assemblage of liquid and crystals could develop. The temperature interval T_4–T_3 will therefore depend mainly upon the rate of diffusion of volatiles from the picrite, which will depend in turn upon the amount of volatiles present in the picrite and the ease with which they could enter the sediment. It would clearly be greater for sediments farther away from the sill than for those in contact with the picrite, but with so many unknown variable factors it is impossible to estimate its magnitude.

Walker & Poldervaart (1949) investigated the transfusion and melting of sediments by the Karroo dolerites and the injection of rheomorphic veins. They concluded from petrographic evidence that the maximum activity of partially fused sediments, which probably corresponded to the maximum development of liquid, occurred well below 1,000° C after solidification of most of the dolerite. From other evidence they estimated that the dolerites were intruded at temperatures between 1,100° C and 1,150° C. The maximum development of liquid therefore occurred more than 100° C to 150° C below the dolerite intrusion temperature.

Sills 1 and 1A are small intrusions, and their textures suggest that they cooled more rapidly than many of the larger Karroo dolerite intrusions. By analogy with the evidence presented by Walker & Poldervaart, the stage of maximum fusion in the xenoliths and fused sediments probably occurred more than 150° C below the intrusion temperature of the picrite, i.e. the temperature interval T_p–T_3 was greater than 150° C.

This means that before hybridization occurred between the picrite and fused sediment, the picrite had cooled through at least 150° C. Almost complete crystallization would be expected in such a large temperature interval. If the last liquid in the picrite crystallized near the temperature T_3 (Fig. 4), the fused sediments in contact with the picrite during the time t_4–t_5 would have reacted with picrite containing some residual liquid, and the fused sediments in contact with the picrite during the time t_5–t_q would have reacted with crystallized picrite. In order to account for the diversity of observed reaction phenomena, it can be concluded that the temperature of final crystallization of the picrite was near to the temperature of maximum activity of the sediments.

Role of volatiles. The fusion of sedimentary xenoliths enclosed by basic magmas may be more dependent upon special conditions, especially the amount and nature of the volatile ingredients in the sediment and magma, than upon the temperature. There is evidence that the widespread fusion of sediments below Sill 1A was caused predominantly by volatiles released from the picrite, although chemical analyses of the picrite provide little evidence that volatiles were present when the sill was emplaced. The olivine is remarkably fresh except in the chilled margins and where in contact with fused sediment. Water in the fused sediment was undoubtedly responsible for the alteration of nearby olivines, and serpentinization of olivines near the margins of the sills was possibly effected by original water trapped in rapidly chilled magma.

Fusion of the sediment was initiated by the release of fluxes resulting from decomposition of sericite. Volatile ingredients from the magma (particularly H_2O and P_2O_5) were subsequently concentrated in the interstitial melt, enhancing its fluxing power and facilitating the development of large quantities of liquid. The degree of fusion varies even near Sill 1A suggesting that volatiles in the picrite magma became concentrated in favourable localities after intrusion. Development of an initial melt was perhaps necessary for the later migration of volatiles from the picrite. Decomposition of sericite near Sill 1A may have provided avenues of escape for volatiles in the picrite magma by forming passageways between the grains of the sediment.

No evidence of metamorphism was found in two specimens collected from the dolerite dyke intersected by Sill 1, and fusion of sediments by other picritic intrusions of the group is, on the whole, rare (Drever & Johnson, 1958). Muscovite is not an abundant constituent of the Beinn Brheac sediments, and it would be interesting to see if fusion occurred only in the mica-rich sediments.

The flux initially developed in the sediment was strongly reducing as shown by the reduction of haematite to magnetite, but the fused xenolith in Sill 1 has a ratio of ferric to ferrous iron greater than 1 (Table 2). The partial pressure of oxygen in water increases with the partial pressure of water and with temperature (Kennedy, 1948), and the increase in temperature and in the amount of water dissolved in the melt as fusion progressed must have reversed the reducing conditions prevalent at lower temperatures. Larsen & Switzer (1939) found that oxidation occurred during fusion of a tonalite xenolith enclosed by olivine basalt.

Most of the volatiles must have escaped from the picrite during crystallization with the exception of those trapped in the chilled margin, otherwise the olivine would have been altered to serpentine. In their study of the system MgO–SiO_2–H_2O, Bowen & Tuttle (1949) proved that only below 430° C at a water-vapour pressure of 15,000 p.s.i. does forsterite decompose to serpentine and brucite. Serpentinization of olivine therefore occurred at a low temperature when movement and hybridization of picrite and fused sediment had ceased. The virtual absence of serpentinization in the olivines and picrite inclusions of the

rheomorphic vein indicates that diffusion of water from the glass at low temperatures was not effective, so the extent of serpentinization in the basal contact zone and at junctions between xenoliths and picrite may be regarded as a measure of the extent of hybridization which occurred at higher temperatures.

EXPERIMENTAL EVIDENCE RELATED TO MELTING TEMPERATURES OF THE SEDIMENT

Introduction

The first change noted with progressive metamorphism was the decomposition of sericite, about 40 cm below the basal contact zone of Sill 1A. Breakdown of the muscovite structure in air has been described and interpreted by several mineralogists. Yoder & Eugster (1955), after a brief review of earlier studies, concluded that the different results reported suggest that observed decomposition products were not equilibrium assemblages. They published detailed studies of the stability ranges of synthetic and natural muscovites in the presence of water-vapour under pressure.

Reduction of haematite to magnetite occurred at about the same level as the decomposition of muscovite. The reaction haematite $\rightleftharpoons$ magnetite is dependent upon both temperature and the partial pressure of oxygen (Muan, 1955). A temperature estimate is available from the experimental studies on muscovite, and this provides some information about the fluxes present during the initial stages of fusion.

The former presence of tridymite in the fused sediments provides fairly well-defined lower temperature and upper pressure limits for the metamorphism. Wager *et al.* (1953) doubt the usefulness of tridymite as a geological thermometer, because the inversion from quartz to tridymite is sluggish (Larsen, 1929) and it is known from experimental studies that tridymite may crystallize metastably outside its stability field (Fenner, 1913). Other petrologists have not hesitated to use the presence or absence of tridymite in a rock to provide an indication of temperature (Thomas, 1922; Davidson, 1935; Black, 1954*b*). There is now reason to believe that in the presence of water-vapour under pressure the inversion quartz $\rightleftharpoons$ tridymite proceeds quite readily, and that tridymite crystallizes rapidly from melts only within its stability field (Tuttle & England, 1955; Tuttle & Bowen, 1958).

The sediment is a feldspathic sandstone. Such sediments result from the weathering and transportation of granitic rocks, and much of the original feldspar is decomposed during transportation (Williams *et al.*, 1955). Selective fusion produces first the lowest melting or 'granitic' fraction and, with increasing temperature, the more refractory minerals are fused (Bowen, 1928, pp. 175–223; Allison, 1936; Knopf, 1938). The chemical analysis of the fused sediment (specimen 129, Tables 2 and 4) is too low in alumina and alkalis to correspond to a granitic rock (compare the average compositions of granitic rocks in Nockolds, 1954), but the liquids produced by fusion would be granitic in

composition until the excess quartz had also dissolved. The most useful diagram for the comparison of granitic rocks is Petrogeny's Residua System, $NaAlSiO_4$–$KAlSiO_4$–SiO_2 (Bowen, 1937). Liquidus temperatures in this system provide an estimate of the temperature at which a given composition would be completely liquid. However, the sediments were fused in the presence of volatiles, and temperatures estimated from the 'dry' system would be too high.

Tuttle & Bowen (1958) determined liquidus temperatures for the system $NaAlSi_3O_8$–$KAlSi_3O_8$–SiO_2–H_2O, and they compared results obtained in this system with results obtained from experiments on natural granites in the presence of water-vapour under pressure. Agreement between the synthetic system and the complex 'magmatic' system is remarkably good. The effect of other volatile components in addition to water on the melting temperatures of natural granites have also been investigated (Wyllie & Tuttle, 1957, 1960; Tuttle & Wyllie, 1957). Some volatiles, when added to water, lower the temperature of beginning of melting of granite more than water alone, and the addition of others to water raises the temperature of beginning of melting. What the combined effect of several volatile components would be is not yet known. The effect of volatile materials in addition to water on liquidus temperatures is much less marked.

Some equilibrium data are available on the solubility of water in silicate melts (Goranson, 1931, 1938; Tuttle & Bowen, 1958); the percentage of water-vapour dissolved in a melt depends upon the pressure, temperature, and composition of the liquid. It is to be expected that volatiles from a hot magma would become concentrated in cooler areas, such as contact rocks and xenoliths, and Shepherd (1938) therefore believes that the volatile content of these rocks will be a chance figure depending upon their past histories. Later hydration of a glass may increase its volatile content (Ross & Smith, 1955). It is impossible, therefore, to make a reliable estimate of the temperature attained by the fused sediment on the basis of its present volatile content, because there are too many variable factors. However, from the high proportion of water in the analysed xenolith (Table 4) it seems reasonable to conclude that the fusion occurred in the presence of excess water-vapour.

Early stages of fusion

The univariant equilibrium curve for the reaction: muscovite $\rightleftharpoons$ sanidine + corundum + vapour was determined by Yoder & Eugster (1955). At a pressure of 5,000 p.s.i. of water-vapour, synthetic muscovite decomposes at 635° C, and at 30,000 p.s.i. the decomposition temperature is 715° C. Some water-vapour would be present in pores of the original sediment, and decomposition of sericite would therefore occur in the presence of water-vapour under pressure. The maximum pressure on the rock during metamorphism was probably 430 kg/cm^2 (6,230 p.s.i., estimated below), so decomposition of the sericite probably occurred near 635° C. None of the decomposition products was recognized in the matrix

replacing the original sericite. Decomposition of the sericite occurred about 40 cm below the base of Sill 1A, so the rocks at this level probably reached a temperature of 635° C. This estimate is not too reliable because the composition of the sericite is not known. Other micas, for instance, phlogopite, remain stable to much higher temperatures (Yoder & Eugster, 1954).

According to Osborn (1956) haematite is stable in air between 500° C and 1,390° C; at 1,390° C it is reduced to magnetite. This reaction occurs at lower temperatures with lower oxygen pressure and at higher temperatures with higher oxygen pressure. Haematite in the sediment was reduced to magnetite at about the same level as the sericite decomposition. Since this occurred near 635° C, it can be concluded that the fluxes present were strongly reducing. The preservation of haematite in feldspar crystals and composite quartz grains is undoubtedly due to its effective isolation from the interstitial flux.

System $NaAlSi_3O_8$–$KAlSi_3O_8$–SiO_2–H_2O

Fig. 5 compares the compositions of fused rocks and the glasses contained within them. Experimentally determined projections of isobaric field boundaries in the system $NaAlSi_3O_8$–$KAlSi_3O_8$–SiO_2–H_2O (Tuttle & Bowen, 1958)

TABLE 4

Calculated compositions of original liquids in the analysed fused xenolith, specimen 129

	1	2	3	4	5
SiO_2	71·04	68·72	66·29	71·90	75·57
Al_2O_3	10·92	11·94	12·87	12·45	11·38
Fe_2O_3	2·14	2·34	2·52	—	0·82
FeO	1·48	1·62	1·74	—	1·63
MgO	2·22	2·43	2·62	—	0·72
CaO	1·34	1·47	1·58	1·89	1·69
Na_2O	2·96	3·24	3·49	4·18	2·45
K_2O	1·35	1·48	1·59	1·91	3·35
H_2O+	4·48	4·90	5·28	6·32	1·06
H_2O-	0·52	—	—	—	0·05
TiO_2	0·68	0·74	0·80	—	0·42
MnO	0·07	0·08	0·08	—	0·05
P_2O_5	0·96	1·05	1·13	1·35	0·30
	100·16	100·01	99·99	100·00	99·49

1. Fused xenolith, specimen 129. See Table 2.

2. Calculated composition of the liquid existing in the xenolith at the maximum stage of fusion. Analysis 1, less remnant quartz (see Table 3).

3. Calculated composition of the liquid which would have existed in the xenolith if only tridymite had crystallized from the original liquid. Analysis 2, less inverted tridymite (see Table 3).

4. Calculated composition of the liquid in the xenolith which was quenched to a glass, i.e. the composition of the glass. See Table 2, Analysis 2.

5. Average Torridonian arkose in south-eastern Skye. (Average of three analyses by M. H. Kerr in Kennedy, 1951).

are also shown. The boundaries separate the primary crystallization fields of feldspar and a silica mineral (cristobalite, tridymite, or quartz, depending upon the composition and the pressure), and the points M_1, M_2, and M_3 mark positions of the temperature minima on the boundaries for water-vapour pressures of 500, 1,000, and 2,000 kg/cm². Liquidus isotherms in the silica field are approximately parallel to the field boundaries. The temperature required to completely

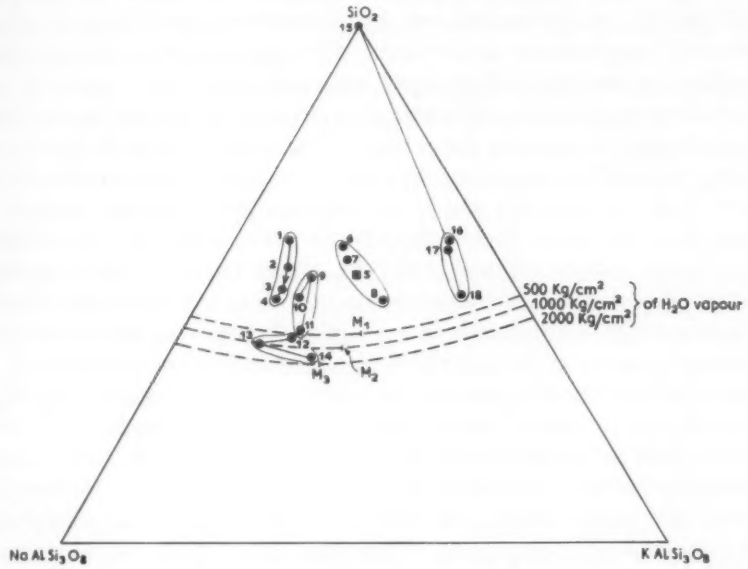

FIG. 5. The compositions of fused rocks and their glasses plotted in terms of normative albite, orthoclase, and quartz. Points 1–4, Soay rocks, Table 4. Points 6–8, analyses of Torridonian arkoses, and point 5 the average of 6–8, Kennedy (1951) (see Table 4). Points 9–11, Frankel, 1950. Points 12–14, Larsen & Switzer, 1939. Points 15–18, Holmes, 1936. See Table 2 for points 10, 11, and 14. The dotted lines are the projected isobaric quartz-feldspar field boundaries for pressures 500, 1,000, and 2,000 kg/cm² in the system $NaAlSi_3O_8$–$KAlSi_3O_8$–SiO_2–H_2O, Tuttle & Bowen (1958). M_1, M_2, and M_3 are the minimum temperatures on these boundaries.

melt a given composition is lowered with increasing water-vapour pressure. The temperature trough existing near the minimum in the dry system (Schairer, 1950) persists under pressure. Orthoclase melts incongruently to leucite, but this does not affect the present discussion.

Points 1–4 represent the composition of the analysed fused xenolith from Sill 1 and the calculated compositions of liquids which existed within the xenolith at different stages of cooling (Table 4). The specific gravities of minerals involved in the calculations were obtained from Winchell & Winchell (1951) and the specific gravity of the glass was estimated (Table 2). For each analysis, normative albite, orthoclase, and quartz were recalculated to 100 per cent, and plotted.

Point 1 represents the bulk composition of the fused xenolith and point 2 represents the calculated composition of the liquid in the xenolith at the stage of maximum fusion (the modal amount of quartz was subtracted from the bulk composition). This calculated analysis is believed to be accurate because the percentage of remnant quartz was easily measured (Table 3). The liquid 2 changed in composition as it cooled, precipitating crystals of tridymite, hypersthene, cordierite, and magnetite. Point 3 represents the bulk composition of the xenolith less the remnant quartz and the inverted tridymite fringes, and point 4 represents the approximate composition of the glass within the xenolith, i.e. the composition of the liquid when it was quenched (Table 4). Points 6, 7, and 8 represent three analysed Torridonian arkoses from south-eastern Skye (Kennedy, 1951), and point 5 represents the average of these three (Table 4). According to Kennedy 'the analyses are thoroughly representative of the formation', a fact apparent from the analyses and from a regional study of thin sections. The analyses have distinctly higher K_2O/Na_2O ratios than the fused xenolith (point 1) and, although point 5 may be representative of the Torridonian sediments in Skye, the Soay rocks are known to vary in composition. The bulk composition of the fused xenolith is regarded as the best available estimate of the original composition of the sediment before metamorphism and fusion.

If a synthetic mixture of feldspar and quartz with bulk composition 1 (Fig. 5) were heated at a constant pressure of water-vapour, the first liquid developed would be close to the minimum on the appropriate isobaric field boundary. Its exact composition would depend on the arrangement of the isobaric three-phase triangles liquid+quartz+feldspar, i.e. on the composition of the feldspar in the sediment. With increasing temperature, the liquid would increase in amount and change in composition along the field boundary, while the quartz and feldspar dissolved. When all the feldspar had dissolved, the tie-line connecting the liquid to the remaining solid phase, quartz, would pass through the bulk composition 1. With further heating, more quartz would dissolve and the composition would change along the tie-line, becoming progressively richer in silica until the charge consisted of liquid of composition 1. Petrographic study of the partially fused sediments confirms that this is the manner in which the sediment was selectively fused but fusion was not completed. At the stage of maximum fusion, the sediment consisted of quartz and liquid of composition 2.

In the synthetic system, a liquid 2, on cooling, would change in composition along the tie-line through SiO_2 and point 2, with the precipitation of tridymite (or cristobalite or quartz, depending upon the composition of the remaining liquid and the pressure) until it reached the isobaric field boundary. Tridymite would then be joined by feldspar, and feldspar and tridymite would crystallize together while the liquid composition changed along the field boundary toward the minimum. The last trace of liquid would disappear when the side of the three-phase triangle connecting the feldspar composition and SiO_2 passed through point 2 (assuming equilibrium crystallization).

In the fused xenolith, considering only the precipitation of tridymite, the liquid 2 would change in composition as far as point 3. In fact, the natural sample contained also minor amounts of magnesia, iron, and lime, which resulted in the precipitation of cordierite, hypersthene, and magnetite in addition to tridymite. This caused the liquid to change to composition 4 (instead of 3) where it was quenched to a glass. Points 3 and 4 are not far apart, confirming that the influence of small amounts of cafemic oxides on liquidus temperatures is very slight. Points 2, 3, and 4 lie close to the extended tie-line connecting SiO_2 and composition 1.

The behaviour of the sediments with progressive metamorphism, fusion, and crystallization, is very similar to that expected from consideration of the synthetic system. This justifies use of the system for comparison of the metamorphosed products with similar rocks. Analyses of glass in xenoliths of quartzose rocks enclosed in basic or ultrabasic igneous rocks from three other localities are plotted for comparison.

Frankel (1950) described the fusion of feldspathic sandstones by dolerite intrusions. Point 9 represents the composition of a glassy xenolith and point 10 represents a calculated analysis of the glass within the xenolith. The composition of the glass separated from a fused inclusion in a different intrusion is represented by point 11. No analysis of the original sediment is available, and the composition of the fused xenolith (9) must be taken as the best estimate of the original composition. The relative positions of the fused xenolith (9) and the quenched liquids (10 and 11) are similar to those determined for Sill 1. The tie-line through SiO_2 and point 9 is almost parallel to lines connecting the bulk composition of the fused xenolith (9) to the glasses produced by fusion (10 and 11), and the presence of inverted tridymite fringes confirms that the liquid present in the xenolith at the stage of maximum fusion changed in composition down the liquidus surface of the silica field.

Larsen & Switzer (1939) analysed the glass (point 14) formed by fusion of a tonalite inclusion enclosed by olivine basalt. The K_2O/Na_2O ratio is lower in the fused xenolith (point 13) than in the parent tonalite (point 12) but the authors ascribe this to differences in the original tonalite. Selective fusion of a synthetic mixture of composition 13 would produce first a liquid near the minimum on the appropriate isobaric field boundary, and this would change in composition along the field boundary approaching the bulk composition as feldspar and silica pass into the liquid phase. The line joining the glass (point 14) to the fused xenolith (point 13) is directed approximately along the field boundaries, as expected from consideration of the synthetic system. Cooling and crystallization of the liquid produced at the stage of maximum fusion would cause the liquid to change in composition down the field boundary towards the minimum, with the crystallization of feldspar and a silica phase, until it was quenched in a glass. Tridymite was not recognized (temperature below 870° C, Larsen & Switzer, 1939), but microlites of plagioclase feldspar are present.

Holmes (1936) described the development of glass around and within pure quartzite xenoliths immersed in ultrabasic potassic lavas. Point 15 represents the quartzite xenoliths, and points 16, 17, and 18 represent the compositions of analysed glasses. It is clear from the compositions of the xenoliths and glasses that the process was not direct melting, but involved also the migration of material from the lava to the xenoliths. The metasomatic process was described in detail by Holmes.

Estimate of fusion temperatures

The calculated compositions of the original liquid and the quenched liquid in the fused xenolith of Sill 1 (analyses 2, 4, and 1 respectively, Table 4, and Fig. 5) permit an estimate of the temperature of the xenolith between the stages of maximum fusion and quenching (the interval *AB–CD* in Fig. 4). The temperature at which any mixture in the system $NaAlSi_3O_8$–$KAlSi_3O_8$–SiO_2–H_2O would be completely liquid will depend upon the composition of the mixture and the pressure of water-vapour. Normative albite, orthoclase, and silica for the fused xenolith and calculated glasses of Sill 1 amount to more than 80 per cent of the rocks (omitting water). The combined effect of the remaining oxides on the liquidus temperature of the original sediment cannot be estimated from available experimental evidence, but there is evidence that their effect would be small.

Schairer (1957) recently published a useful summary of the phase relations in ternary systems combining one of the early crystallizing minerals in rocks with the late crystallizing alkali aluminosilicates of the Residua System. The addition of, for example, diopside to the Residua System would produce the quaternary system nepheline–kaliophilite–diopside–silica which can be represented as a tetrahedron. The silica field in the ternary Residua System would extend upwards into the quaternary tetrahedron as a silica space, partially bounded by the silica fields of the Residua System and of the systems leucite–diopside–silica (Schairer & Bowen, 1938) and nepheline–diopside–silica (Schairer, 1957). Liquidus isotherms in the silica fields of the latter two systems, if extended from the joins leucite–silica and nepheline–silica respectively, would pass very close to the composition diopside. This means that the addition of diopside to the binary systems leucite–silica or nepheline–silica would cause very little change in the liquidus temperatures of mixtures for which a silica mineral was the primary phase.

The other diagrams reproduced by Schairer show that the effects of anorthite and forsterite are similar to that of diopside, and it seems reasonable to assume that similar relations pertain within the quaternary silica spaces bounded by silica fields of the several ternary systems. It may be concluded that the addition of minor amounts of diopside, anorthite, and forsterite to synthetic mixtures represented by points 1–4 in Fig. 5 would change the liquidus temperatures only slightly.

Confirmation is available from the study of more complex 'magmatic' systems. Tuttle & Bowen (1958) showed that in the presence of water-vapour under pressure, the temperatures of beginning of melting of natural granites, containing an excess of cafemic oxides compared to the synthetic system $NaAlSi_3O_8$–$KAlSi_3O_8$–SiO_2–H_2O, are almost identical with the minimum melting temperature in the synthetic system. It is unlikely that the excess oxides, in moderate amounts, would have a much greater effect on liquidus temperatures. It has been shown above that when the fusion and subsequent crystallization of the sediments is considered only in terms of normative albite, orthoclase, and silica, the sequence of events is only slightly different from the observed sequence in the presence of additional cafemic oxides.

The analysis of the fused xenolith confirms that fusion occurred in the presence of abundant water-vapour. P_2O_5 was also present (Tables 2 and 4) but its effect on liquidus temperatures is apparently negligible (unpublished data, Wyllie & Tuttle). Since no independent estimate of pressure is available, no definite estimate of liquidus temperatures for the calculated liquid compositions can be made. However, the 'equilibrium' temperatures at which the calculated compositions 2 and 4 would be completely liquid at different pressures of water-vapour can be estimated from the determined isotherms in the isobaric projections of the system $NaAlSi_3O_8$–$KAlSi_3O_8$–SiO_2–H_2O (Tuttle & Bowen, 1958).

The liquidus temperature of the quenched glass, composition 4 (Fig. 5), was estimated in this way for the pressures 500, 1,000, and 2,000 kg/cm^2, and the dry liquidus temperature was estimated from isotherms in the system $NaAlSi_3O_8$–$KAlSi_3O_8$–SiO_2 (Schairer, 1950). A *PT* curve drawn through the four estimated points gives a projection of the liquidus for this composition. Part of the *PT* projection, *DC*, is shown in Fig. 6, and this represents the possible range of conditions at which the liquid in the xenolith would have been quenched to a glass (compare the point *CD* in Fig. 4). If the pressure were known, the temperature could be estimated from the curve. The calculated composition of the original liquid in the fused xenolith (composition 2, Fig. 5) is beyond the range of determined liquidus isotherms in the hydrothermal system, but its liquidus temperature may be estimated in the dry system. The temperature interval on the liquidus of the dry system between the compositions 2 and 4 is 90° C. Assuming that the shape of the liquidus surface for this composition range does not change significantly with increasing water-vapour pressure, the curve *BA* extended in Fig. 6, 90° C higher than the curve *DC* at each pressure, is the *PT* projection for the liquidus of composition 2. This corresponds to the stage of maximum development of liquid within the xenolith, as represented by the point *AB* in Fig. 4. At a fixed pressure the temperature interval between the curves *AB* and *CD* in Fig. 6 corresponds to the temperature interval *AB–CD* in Fig. 4.

Tridymite, cordierite, hypersthene, and magnetite crystallized from the liquid

as it cooled from the *PT* conditions represented by the curve *AB* to those represented by the curve *CD*. Crystallization of tridymite implies that the liquid was within the stability field of tridymite when it started to cool, and the relatively high proportion of inverted tridymite present in the fused xenolith suggests that it remained there during most of its cooling interval. The experimentally determined *PT* projection of the quartz–tridymite inversion (in the presence of excess

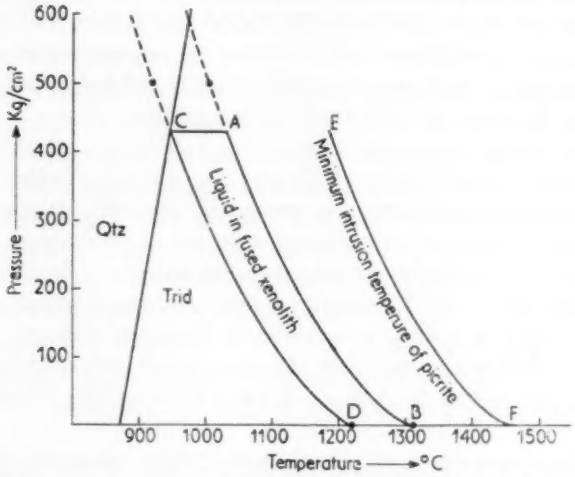

FIG. 6. Estimated *PT* curves: *CD*, for the liquid present in the fused xenolith (specimen 129, Table 3) when it was quenched to a glass; *AB*, for the liquid present in the xenolith at the stage of maximum fusion; *EF*, for the picrite when it was intruded. The experimentally determined *PT* curve for the inversion quartz ⇌ tridymite in the presence of water-vapour is also shown. The *PT* curves *AB* and *CD* correspond to the points *AB* and *CD* in Fig. 4. *Qtz*, quartz; *Trid*, tridymite.

water-vapour) is plotted in Fig. 6 (Tuttle & England, 1955; Tuttle & Bowen, 1958), and its intersection with the curve *CD* gives the maximum pressure on the xenolith during fusion, 430 kg/cm². If the pressure were greater than this, tridymite would not have crystallized from the liquid throughout its cooling interval and, if the pressure had been greater than 600 kg/cm² (the intersection of the curve *AB* extended with the quartz–tridymite inversion curve), tridymite would not have crystallized from the liquid at all.

The area *ABCD* in Fig. 6 thus represents the probable range of pressures and temperatures from the stage of maximum development of liquid in the xenolith to the stage when the remaining liquid was quenched to a glass. The maximum pressure corresponds to a depth of intrusion of about 1·7 km, assuming a superincumbent load of sediments with average density 2·5. If the sill was emplaced at this depth, the maximum 'equilibrium' temperature reached by the liquid in the xenolith would be about 1,025° C, represented by the point *A*, Fig. 6. (Before the stage of maximum fusion, the liquid could have reached a higher temperature, but the liquid present would not have been an equilibrium

liquid for this temperature, and therefore cannot be considered in relation to the synthetic system. See description of Fig. 4.)

It should be emphasized that this estimate of the *PT* conditions accompanying fusion of the xenolith is based only upon the available phase equilibrium data for the dominant constituents of the natural system, namely, orthoclase, albite, silica, and water. It has been shown that the effect of other silicate components is unlikely to change the conditions greatly, and it is probable that the effect of other volatile components on the liquidus temperatures is slight. Use of the quartz–tridymite *PT* projection is believed justifiable, but the tridymite could have crystallized metastably.

It was concluded earlier that the maximum activity of the fused sediments, i.e. the stage of maximum development of liquid, probably occurred at least 150° C below the intrusion temperature of the picrite. The *PT* curve *EF* in Fig. 6 is 150° C higher in temperature, at a given pressure, than the curve *AB* which represents the conditions of maximum fusion in the xenolith. The curve *EF* therefore represents the estimated range of minimum intrusion temperatures of the picrite, the actual temperature depending upon the depth of intrusion.

If the picrite was emplaced at a depth of 1·7 km, its estimated intrusion temperature was at least 1,175° C (*E*) and if it was emplaced at shallower levels the minimum intrusion temperatures would be between 1,175° C and 1,460° C (*F*). It seems unlikely that the picrite was emplaced much nearer to the surface than 1·7 km, and the intrusion temperature was probably in the range 1,175° C to 1,200° C. This is slightly higher than temperatures estimated for the Karroo dolerites, 1,100° C to 1,150° C (Walker & Poldervaart, 1949), but it corresponds to experimentally determined liquidus temperatures of natural basalts in the presence of water-vapour under pressure (Yoder & Tilley, 1956).

CONCLUDING REMARKS

As Mackenzie (1960) has pointed out, 'It is rarely possible to apply the results of phase equilibrium studies directly to a petrological problem because the artificial systems are of necessity very much simpler than the natural systems, both from the point of view of their chemistry and also the physical conditions of crystallization. For this reason there has been a tendency for some geologists to treat the results of experimental studies as of very doubtful value in the interpretation of the origin of rocks.' The latter statement is particularly true for granitic rocks.

Tuttle & Bowen (1958) have discussed the origin of granite in the light of experimental data from the system $NaAlSi_3O_8$–$KAlSi_3O_8$–SiO_2–H_2O. The compositions of granites, when expressed in terms of normative or modal albite, orthoclase, and quartz, are concentrated near the minima on the isobaric cotectic boundaries illustrated in Fig. 5. Moreover, granites which are genetically related lie on the same side of the low-temperature trough along the boundaries

(Chayes, 1952). This is strong evidence that their evolution was dominated by crystal ⇌ liquid equilibria.

Field evidence may often be interpreted in several ways, and field geologists who conclude that crystal ⇌ liquid equilibria were not involved in the emplacement of granites may dismiss the experimental evidence on the grounds that the extrapolation to natural systems is too great. Experimental data are obtained at fixed temperatures and pressures, using charges of known bulk composition; whereas pressure, temperature, and composition may all vary in natural systems.

Although the fusion of Torridonian sediment described in this paper occurred on a small scale, the scale was nevertheless much greater than that of laboratory experiments. The fusion occurred in a natural environment, in the presence of components additional to those of the synthetic system, and under varying physical conditions. From the synthetic to this natural system is quite a long extrapolation, yet the fusion and crystallization of the sediment proceeded in a manner which could have been predicted from consideration of the synthetic system. The components present were similar to those involved in the emplacement of large granitic masses (whatever their mode of formation), and the components additional to those of the system $NaAlSi_3O_8$–$KAlSi_3O_8$–SiO_2–H_2O have modified the predicted sequence of events only slightly.

The rocks in this small natural system may be regarded as stepping stones between the synthetic system and the large, complex natural systems which include plutonic granites. The fact that they follow so closely the synthetic system is evidence that direct comparison of chemically related natural systems with the synthetic system is justified. The present study thus supports the conclusions reached by Tuttle & Bowen (1958) after their comparison of natural granites with compositions in the system $NaAlSi_3O_8$–$KAlSi_3O_8$–SiO_2–H_2O.

ACKNOWLEDGEMENTS

The writer wishes to thank Dr. H. I. Drever and Mr. R. Johnston for their co-operation and assistance. Drever discovered the fused sediments and suggested this detailed study, and Johnston was a stimulating companion on Soay. Both provided critical comments which have led to improvements in the paper. The laboratory work was completed in the Geology Department, University of St. Andrews, and in the Department of Geophysics and Geochemistry, The Pennsylvania State University. The field work was partly financed by the Shell Petroleum Company.

REFERENCES

ALLISON, A., 1936. The tertiary dykes of the Craignish area, Argyll. *Geol. Mag. Lond.* **73**, 73–87.

BAILEY, E. B., WRIGHT, W. B., *et al.* 1924. The tertiary and post-tertiary geology of Mull, Loch Aline, and Oban. *Mem. geol. Surv. U.K.*

BASTIN, E. S., 1905. Note on baked clays and natural slags in eastern Wyoming. *J. Geol.* **13**, 408–12.

BLACK, G. P., 1954*a*. The acid rocks of western Rhum. *Geol. Mag. Lond.* **91**, 257–72.

—— 1954*b*. The significance of tridymite in igneous and metamorphic petrogenesis. *Miner. Mag.* **30**, 518–24.

BOWEN, N. L., 1914. The ternary system diopside–forsterite–silica. *Amer. J. Sci.* **38,** 207–64.
—— 1928. *The evolution of the igneous rocks.* Princeton University Press (reprinted by Dover Press 1956).
—— 1937. Recent high-temperature research on silicates and its significance in igneous geology. *Amer. J. Sci.* **33,** 1–21.
—— & TUTTLE, O. F., 1949. The system MgO–SiO_2–H_2O. *Bull. geol. Soc. Amer.* **60,** 439–60.
—— —— 1950. The system $NaAlSi_3O_8$–$KAlSi_3O_8$–H_2O. *J. Geol.* **58,** 489–511.
CAMPBELL, R., DAY, T. C., & STENHOUSE, A. G., 1933. The Braefoot outer sill, Fife. Part II. *Trans. geol. Soc. Edinb.* **13,** 148–73.
CHAYES, F., 1952. The finer-grained calcalkaline granites of New England. *J. Geol.* **60,** 207–54.
CLOUGH, C. T., & HARKER, A., 1904. The geology of west central Skye with Soay. *Mem. geol. Surv. U.K.*
CORRENS, C. W., 1956. The geochemistry of the halogens. Chapter 7 in *Physics and chemistry of the earth,* I. London: Pergamon Press, 181–233.
DAVIDSON, C. F., 1935. The tertiary geology of Raasay, Inner Hebrides. *Trans. roy. Soc. Edinb.* **58,** 375–407.
DREVER, H. I., & JOHNSTON, R., 1957. Crystal growth of forsteritic olivine in magmas and melts. Ibid. **63,** 289–315.
—— —— 1958. The petrology of picritic rocks in minor intrusions—a Hebridean group. Ibid. 459–99.
FENNER, G. N., 1913. The stability relations of the silica minerals. *Amer. J. Sci.* **36,** 331–84.
FLETT, J. S., 1911. Notes in: The geology of Colonsay and Oronsay, with part of the Ross of Mull. *Mem. geol. Surv. U.K.* 95.
FRANKEL, J. J., 1950. A note on the vitrification of Karroo sediment by dolerite intrusions. *Trans. roy. Soc. S. Afr.* **32,** 287–93.
GEORGE, W. O., 1924. The relation of the physical properties of natural glasses to their chemical composition. *J. Geol.* **32,** 353–72.
GORANSON, R. W., 1931. The solubility of water in granite magmas. *Amer. J. Sci.* **22,** 481–502.
—— 1938. Silicate-water systems: phase equilibria in the $NaAlSi_3O_8$–H_2O and $KAlSi_3O_8$–H_2O systems at high temperatures and pressures. *Amer. J. Sci.* **35,** 71–91.
GUPPY, E. M., and HAWKES, L., 1925. A composite dyke from eastern Iceland. *Quart. J. geol. Soc. Lond.* **81,** 325–43.
HARKER, A., 1904. The tertiary igneous rocks of Skye. *Mem. geol. Surv. U.K.*
—— 1950. *Metamorphism,* 3rd ed. London: Methuen & Co.
HAWKES,, L., 1916. On tridymite and quartz after tridymite in Icelandic rocks. *Geol. Mag. Lond.* 6th Ser. **3,** 205–9.
HOLMES, A., 1936. Transfusion of quartz xenoliths in alkali, basic and ultrabasic lavas, south-west Uganda. *Miner. Mag.* **24,** 408–21.
KENNEDY, G. C., 1948. Equilibrium between volatiles and iron oxides in igneous rocks. *Amer. J. Sci.* **246,** 529–49.
KENNEDY, W. Q., 1951. Sedimentary differentiation as a factor in the Moine-Torridonian correlation. *Geol. Mag. Lond.* **88,** 257–66.
KNOPF, A., 1938. Partial fusion of granodiorite by intrusive basalt, Owens Valley, California. *Amer. J. Sci.* **36,** 373–6.
KUNO, H., 1954. Study of orthopyroxenes from volcanic rocks. *Amer. Min.* **39,** 30–46.
LACROIX, A., 1893. Les Enclaves des roches volcaniques. *Ann. Acad. Mâcon,* **10,** 697.
—— 1908. Sur la tridymite de Vesuve et sur la genèse de ce mineral par fusion. *Bull. Soc. franç. Minér.* **31,** 323.
LARSEN, E. S., 1929. The temperatures of magmas. *Amer. Min.* **14,** 81–94.
—— & SWITZER, G., 1939. An obsidian-like rock formed from the melting of a granodiorite. *Amer. J. Sci.* **237,** 562–8.
MACKENZIE, W. S., 1954. The orthoclase–microcline inversion. *Miner. Mag.* **30,** 354–66.
—— 1957. The crystalline modifications of $NaAlSi_3O_8$. *Amer. J. Sci.* **255,** 481–516.
—— 1960. Review of some contributions of experimental studies to petrology. *Lpool. Manchr. geol. J.* **2,** 369–88.
—— & SMITH, J. V., 1955. The alkali feldspars. I. Orthoclase microperthites. *Amer. Min.* **40,** 707–32.

MACKENZIE, W. S., & SMITH, J. V., 1956. The alkali feldspars. III. An optical and X-ray study of high temperature feldspars. *Amer. Min.* **41,** 405–27.

MALLARD, E., 1890. Sur la tridymite et la christobalite. *Bull. Soc. franç. Minér.* **13,** 161–81.

MATHEWS, W. H., 1951. A useful method for determining approximate composition of fine-grained igneous rocks. *Amer. Min.* **36,** 92–101.

MIYASHIRO, A., 1957. Cordierite–indialite relations. *Amer. J. Sci.* **255,** 43–62.

—— IIYAMA, T., YAMASAKI, M., & MIYASHIRO, T., 1955. The polymorphism of cordierite and indialite. Ibid. **253,** 185–208.

MUAN, A., 1955. Phase equilibria in the system FeO–Fe_2O_3–SiO_2. *Trans. Amer. Inst. Min.* (*Metall.*) *Engrs.* **203,** 965–76.

NOCKOLDS, S. R., 1954. Average chemical compositions of some igneous rocks. *Bull. geol. Soc. Amer.* **65,** 1007–32.

OSBORN, E. F., 1956. Importance of the spinel phase in the steel industry. *Regional technical meetings: addresses presented at series of five meetings.* Published by America Iron and Steel Institute, New York, 135–50.

OSBORNE, G. D., 1950. Note on the occurrence of tridymite in metamorphosed Hawkesbury sandstone at Bundeena and West Pymble, Sidney district, New South Wales. *J. roy. Soc. N.S.W.* **82,** 309–11.

PETTIJOHN, F. J., 1949. *Sedimentary rocks.* New York: Harper Bros.

PROHASKA, C., 1885. Über den Basalt von Kollnitz im Lavanttale und dessen glassige cordierit-führende Einschlüsse. *S.B. Akad. Wiss. Wien.*, Math.-naturw. Kl. **92,** 20–32.

REYNOLDS, D. L., 1940. Contact metamorphism by a tertiary dyke at Waterfoot, Co. Antrim. *Geol. Mag. Lond.* **77,** 461–9.

REYNOLDS, S. H., 1908. The basic intrusions of Bartestree, near Hereford. *Quart J. geol. Soc. Lond.* **64,** 501–11.

RICHARZ, S., 1924. Some inclusions in basalts. *J. Geol.* **32,** 685–9.

RINNE, F., 1895. Ueber rhombischen Augit als Kontaktproduct. *N. Jb. Min. Geol. Paläont*, **2,** 229.

ROSS, C. S., & SMITH, R. L., 1955. Water and other volatiles in volcanic glasses. *Amer. Min.* **40,** 1071–89.

SCHAIRER, J. F., 1950. The alkali–feldspar join in the system $NaAlSiO_4$–$KAlSiO_4$–SiO_2. *J. Geol.* **58,** 512–17.

—— 1957. Melting relations of the common rock-forming oxides. *J. Amer. ceram. Soc.* **40,** 215–35.

—— & BOWEN, N. L., 1938. The system leucite–diopside–silica. *Amer. J. Sci.* **35A,** 289–309.

SHEPHERD, E. S., 1938. The gases in rocks and some related problems. Ibid. **35A,** 311–51.

SPENCER, E., 1937. The potash-soda-feldspars. I. Thermal stability. *Miner. Mag.* **24,** 453–94.

STARK, M., 1904. Zusammenhang des Brechungsexponenten natürlicher Gläser mit ihrem Chemismus. *Tscherm. Mitt.*, **23,** 536.

THOMAS, H. H., 1922. On certain xenolithic tertiary minor intrusions in the island of Mull (Argyllshire). *Quart J. geol. Soc. Lond.* **78,** 229–60.

TIDMARSH, W. G., 1932. The permian lavas of Devon. Ibid. **88,** 712–75.

TILLEY, C. E., 1922. Density, refractivity, and composition relations of some natural glasses. *Miner. Mag.* **19,** 275–94.

—— 1923. Paragenesis of the minerals of the three component system MgO–Al_2O_3–SiO_2 in thermal metamorphism. *Geol. Mag. Lond.* **60,** 101–7.

TOMKEIEFF, S. I., 1940. The dolerite plugs of Tiveragh and Tievebulliagh near Cushendall, Co. Antrim, with a note on buchite. Ibid. **77,** 54–64.

TUTTLE, O. F., 1952. Optical studies on alkali feldspars. *Amer. J. Sci.*, Bowen volume, 553–67.

—— & BOWEN, N. L., 1958. Origin of granite in the light of experimental studies in the system $NaAlSi_3O_8$–$KAlSi_3O_8$–SiO_2–H_2O. *Mem. geol. Soc. Amer.* **74.**

—— & ENGLAND, J. L., 1955. A preliminary report on the system SiO_2–H_2O. *Bull. geol. Soc. Amer.* **66,** 149–52.

—— & WYLLIE, P. J., 1957. Hydrothermal studies in the systems $NaAlSi_3O_8$ (albite)–H_2O–HF and granite–H_2O–HF. (Abstract.) Ibid. **68,** 1087.

VENKATESH, V., 1952. Development and growth of cordierite in paralavas. *Amer. Min.* **37,** 831–48.

WAGER, L. R., WEEDON, D. S., & VINCENT, E. A., 1953. A granophyre from Coire Uaigneich, Isle of Skye, containing quartz paramorphs after tridymite. *Miner. Mag.* **30,** 263–76.

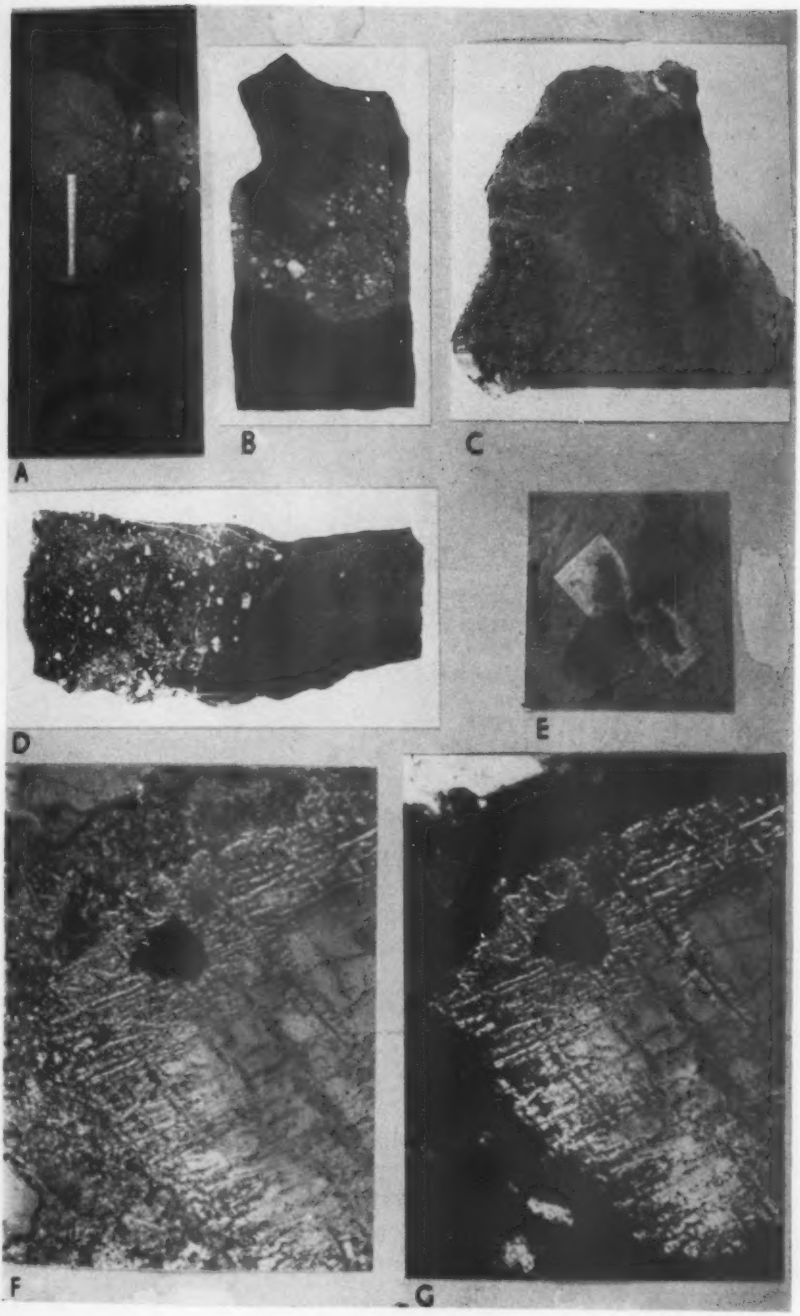

P. J. WYLLIE

Plate 1

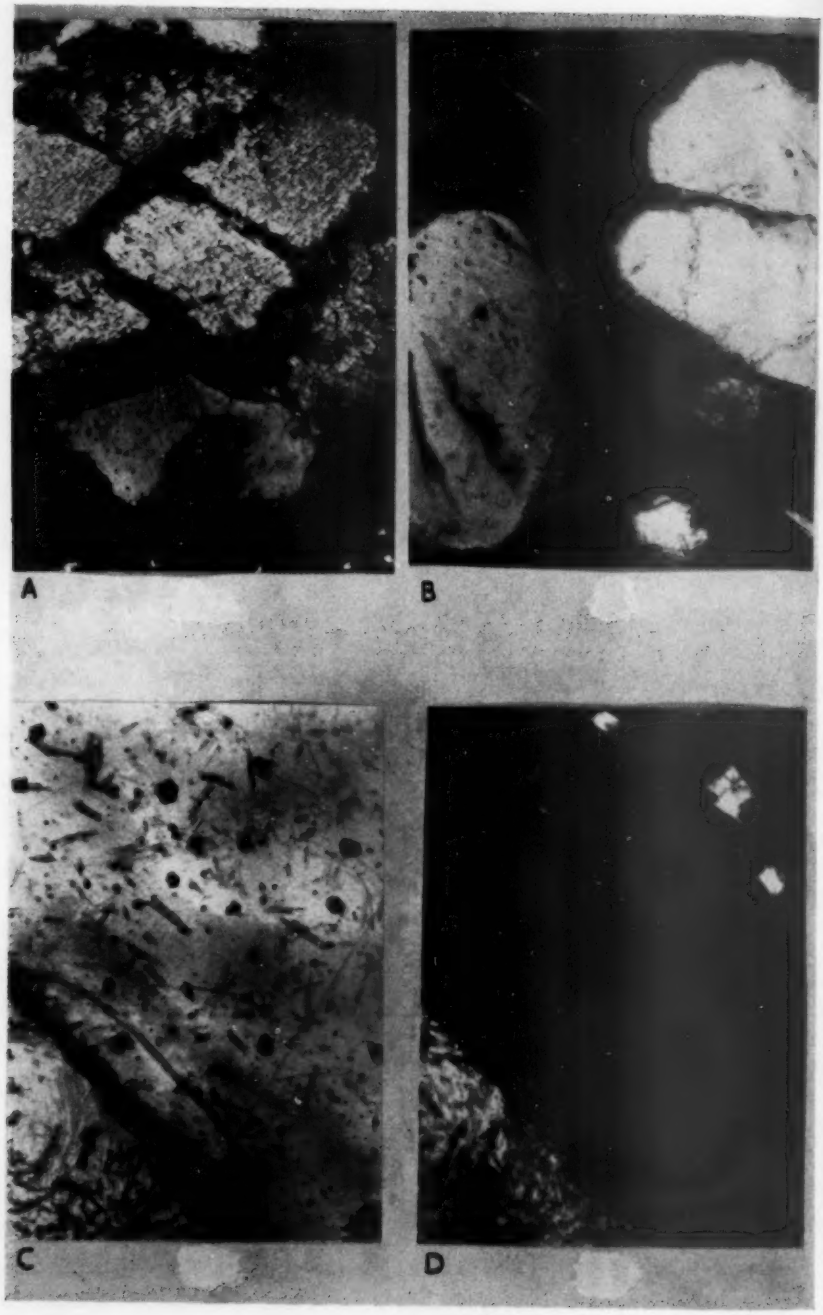

P. J. WYLLIE

Plate 2

WALKER, F., & POLDERVAART, A., 1949. Karroo dolerites of the Union of South Africa. *Bull. geol. Soc. Amer.* **60,** 591–706.

WELLS, M. K., 1951. Sedimentary inclusions in the hypersthene–gabbro, Ardnamurchan, Argyllshire. *Amer. Min.* **29,** 715–36.

WILLIAMS, H., TURNER, F. J., & GILBERT, C. M., 1955. *Petrography*. San Francisco: Freeman & Co.

WINCHELL, A. N., & WINCHELL, H., 1951. *Elements of optical mineralogy*. Part II. Descriptions of Minerals. New York: J. Wiley & Sons, Inc.

WYLLIE, P. J., 1959. Microscopic cordierite in fused Torridonian arkose. *Amer. Min.* **44,** 1039–46.

—— & TUTTLE, O. F., 1957. The effect of volatile materials on the melting temperatures of silicates. (Abstract.) *Trans. Amer. geophys. Un.* **38,** 413–14.

—— —— 1960. Experimental investigation of silicate systems containing two volatile components. Part II. The effects of NH_3 and HF on the melting temperatures of albite and granite. *Amer. J. Sci.* In press.

YODER, H. S., & EUGSTER, H. P., 1954. Phlogopite synthesis and stability range. *Geochim. et Cosmochim. Acta.* **6,** 157–85.

—— 1955. Synthetic and natural muscovites. Ibid. **8,** 225–80.

—— & TILLEY, C. E. 1956. Natural tholeiite basalt-water system, *Ann. Rep. geophys. Lab., Yearb. Carneg. Instn.*, No. **55,** 169–71.

ZIRKEL, F., 1891. Cordieritbildung in verglasten sandstein. *N. Jb. Min. Geol. Palaont.* **1,** 109–13.

EXPLANATION OF PLATES

PLATE 1

FIG. A. Rheomorphic vein of fused sediment cutting Torridonian sandstone. The vein extends approximately parallel to, and to the right of, the hammer, whose shaft is marked in inches. The view is looking vertically downwards.

FIG. B. Partially fused sediment below the basal contact zone of Sill 1A. The dark fine-grained sediment has apparently been intruded into the coarser-grained sediment. Scale: $\times\frac{3}{4}$.

FIG. C. Specimen from the basal contact zone of Sill 1A. The light and dark-grey areas are fused sediment containing isolated olivine pseudomorphs (black). Picrite occurs as discrete inclusions (left); concentrations of olivine pseudomorphs in the glassy matrix (bottom, right of centre) show that other inclusions have disintegrated. Scale: $\times 1$.

FIG. D. Fused grit xenolith (left) surrounded by fine-grained buchite (right) in Sill 1A. The black olivine pseudomorphs (right) indicate the junction between the buchite and the picrite. Scale: $\times\frac{3}{4}$.

FIG. E. Cruciform twin of cordierite from the fused xenolith (specimen 129) in Sill 1. The cordierite, containing inclusions of ore, is surrounded by glass. Stepped edges to the prism faces indicate parallel growth. Small cracks in the glass surround the crystal. Scale: $\times 400$, crossed nicols, with a one wavelength retardation plate inserted in the 45° position.

FIG. F. Feldspar crystal in fused grit xenolith, Sill 1A. The crystal appears to merge into the glassy matrix. Plane polarized light. Scale: $\times 200$.

FIG. G. The same as F, between crossed nicols. This shows the development of glass along the cleavages.

PLATE 2

FIG. A. Feldspar crystal from a grit xenolith. The crystal has separated into several fragments which retain optical continuity. Below the feldspar is a corroded quartz grain. The glassy matrix is crowded with small feldspar cleavage fragments. Crossed nicols. Scale: $\times 200$.

FIG. B. Remnant quartz grains in the fused xenolith from Sill 1 (specimen 129). The rounded quartz grains are surrounded by fringes of inverted tridymite. Accicular hypersthene crystals occur in the glass. Crossed nicols. Scale: $\times 200$.

FIG. C. Olivine pseudomorph in the glass of the rheomorphic vein. A mantle of hypersthene borders the olivine. Skeletal hypersthene crystals are scattered through the glass. Plane polarized light. Scale: $\times 200$.

FIG. D. The same as C, between crossed nicols. This shows short prismatic cordierite crystals, with a tendency toward skeletal crystallization.

Igneous nepheline-bearing rocks of the Haliburton–Bancroft province of Ontario

by C. E. TILLEY *and* J. GITTINS *with chemical analyses by* J. H. SCOON

Department of Mineralogy and Petrology, Cambridge, England, and Division of Earth Sciences, College of Mineral Industries, The Pennsylvania State University.

WITH TWO PLATES

ABSTRACT

Assemblages of magmatic origin—hypersolvus nepheline syenites, theralites, and theralitic canadites—developed in a belt of nepheline rocks extending through Monmouth and Glamorgan townships of Haliburton County, Ontario, are described and their significance in the problems of origin of the Haliburton–Bancroft alkali province briefly discussed.

SINCE the classic studies of Adams & Barlow (1910) on the nepheline rocks of the Haliburton–Bancroft province of Ontario, the magmatic interpretation of these assemblages has been critically re-examined and especially within the last two decades radical revisions of genesis have been proposed. Gummer & Burr (1943, 1946) in particular have appealed to a process of regional metasomatism—nephelinization—employing this term for their concept of a process of alkalization of the lime-bearing paragneisses of the Grenville Series by solutions enriched in soda and alumina, and tentatively traced to a granitic parentage. The history of the later stages of investigation on these alkali rocks as revealed in published papers has been summarized by Tilley (1957) in a discussion of the metasomatic problems of the York River nepheline belt in the Bancroft region for which a nephelinization process was accepted. The status of nephelinization was then reviewed and it was concluded that the solutions responsible for the metasomatism were in the main nepheline-bearing and that it was reasonable to suppose for the York River area a magmatic source at depth. It was further observed that the wider investigations of the Haliburton–Bancroft province which had for some years been undertaken by the officers of the Ontario Department of Mines had revealed that genuine feldspathoidal assemblages of magmatic origin were developed in neighbouring townships. 'Igneous textured feldspathoidal rocks including hypersolvus nepheline syenites are known from the townships of Monmouth and Glamorgan, and give conclusive evidence of their origin from magma. Thus a magmatic source is readily available in the province to provide metasomatic solutions capable of transforming the limestone belt of the York River area' (Tilley, 1957, p. 356).

It is the purpose of the present communication to set out some of the evidence presented by the feldspathoidal assemblages in Monmouth and Glamorgan referred to in the preceding paragraph. The rocks in question are developed in

[Journal of Petrology, Vol. 2, Part 1, pp. 38–48, 1961]

a belt of nepheline rocks which fringe the northern outcrop of the Glamorgan gabbro, south of Gooderham from a point north of Trooper Lake, north-eastward for a distance of 6 miles to the vicinity of Tory Hill (Fig. 1). This belt of feldspathoid rocks is associated with a broad zone of syenites and syenite gneisses, the whole flanked by Grenville limestone. The igneous rock types recognized range from theralites through theralitic canadites to nepheline

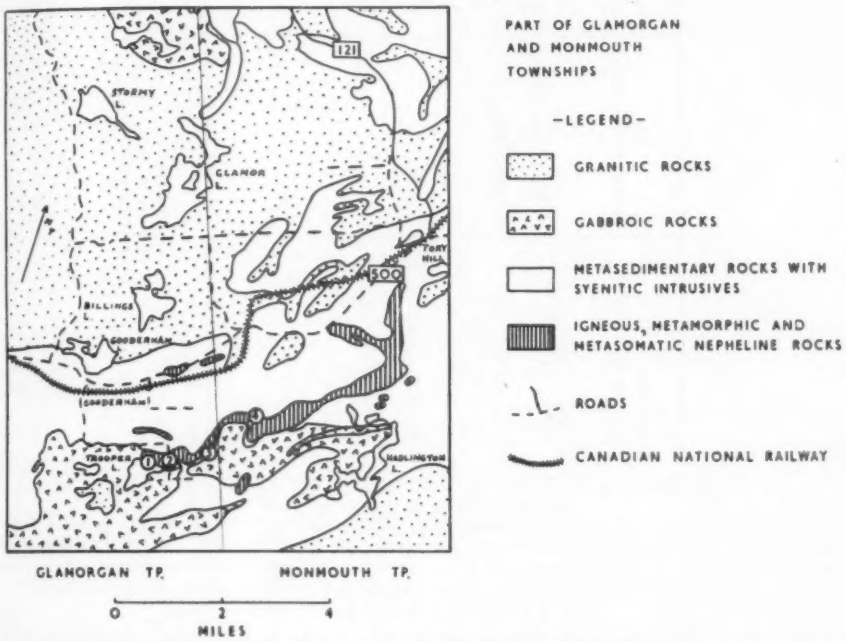

FIG. 1. Geological map of part of Glamorgan and Monmouth Townships, Haliburton Co., Ontario, based on Map 1957-b of the Ontario Department of Mines. The positions 1–4 marked on the nepheline belt shown on the map refer to localities of igneous assemblages discussed in the text. Theralites and theralitic canadites: 1. Lot 30, con. IV; 2. Lot 31, con. IV; 3. Lot 35, con. III, Glamorgan Township. Nepheline syenites: 4. Lot 4, con. IV, Monmouth Township.

syenites and are now reported in the following localities (Fig. 1). Theralites and theralitic canadites—lots 30, 31, con. IV, Glamorgan Township (north shore of Trooper Lake); lot 35, con. III, Glamorgan Township. Nepheline syenites—lot 4, con. IV, Monmouth Township.

1. *Hypersolvus nepheline syenites*

In lot 4, con. IV, Monmouth Township, there is a rapid alternation in outcrop between a fine- and a coarse-grained nepheline syenite in rather poorly exposed ground bordering a beaver swamp. In the coarse-grained variety the feldspar laths, often more than a centimetre in length, show a rude flow orientation with nepheline and clinopyroxene, variable in grain size but reaching 3 mm

TABLE 1

	1	2	3	4	*Norm of* 1		*2a Metal atoms to 32 oxygens in nepheline (anal. 2)*		*3a Microperthite (anal. 3)*	*4a Metal atoms to 6 oxygens in clinopyroxene (anal. 4)*		
SiO_2	52·23	43·61	65·38	46·83								
Al_2O_3	19·50	33·05	19·73	2·65	Or	31·69	Si 8·466	16·01		Si 1·898	2·000	
Fe_2O_3	4·44	0·85	0·08	5·88	Ab	21·48	Al 7·546		$Or_{48·4}Ab_{49·1}An_{2·5}$	Al 0·102		
FeO	5·78			21·02	Ne	23·28				Al 0·019		
MnO	0·21	0·01	nil	0·84	An	3·06	Ca 0·116	ΣR	$(Or_{49·7}Ab_{50·3})$	Fe^{+3} 0·180		
TiO_2	0·42	nil	nil	0·52	Di	11·28	Na 6·055	7·50		Fe^{+2} 0·710	1·047	
MgO	0·20	0·05	0·08	1·57	Ol	0·99	K 1·211			Mn 0·029		2·013
CaO	3·52	0·53	0·49	18·87	Il	0·76				Ti 0·014		
Na_2O	7·59	16·09	5·77	1·86	Mt	6·50	$Ne_{75·2}Ks_{16·8}An_{2·8}Qz_{5·1}$			Mg 0·095		
K_2O	5·41	4·92	8·16	0·05	Ap	0·34				Ca 0·820	0·966	
H_2O+	0·57	0·70	0·28*		Ct	0·27	$(Ne_{77·5}Ks_{17·5}Qz_{5·2})$			Na 0·146		
H_2O-	0·03	0·01	0·03	nil	Rest	0·79						
P_2O_5	0·14					100·44						
CO_2	0·12											
C	0·19				$Ne_{45·8}Ks_{22·8}Qz_{30·7}$							
	100·35	99·82	100·00	100·09								

* Loss on ignition.

1. Nepheline syenite with clinopyroxene (65270), coarse grained facies, lot 4, con. IV, Monmouth Township, Haliburton Co., Ontario.
2. Nepheline from 1.
3. Microperthite from 1.
4. Clinopyroxene from 1.

Analyses by J. H. Scoon.

or more in section. The remaining constituents are amphibole, olivine, magnetite, and apatite. An approximate mode in weight per cent is alkali feldspar 55, nepheline 24, clinopyroxene with subordinate amphibole 16, magnetite 4, olivine 1. The dominant alkali feldspar is a fine microperthite with Carlsbad twinning (Plate 1, fig. 1) often showing a very fine rim of the albite component

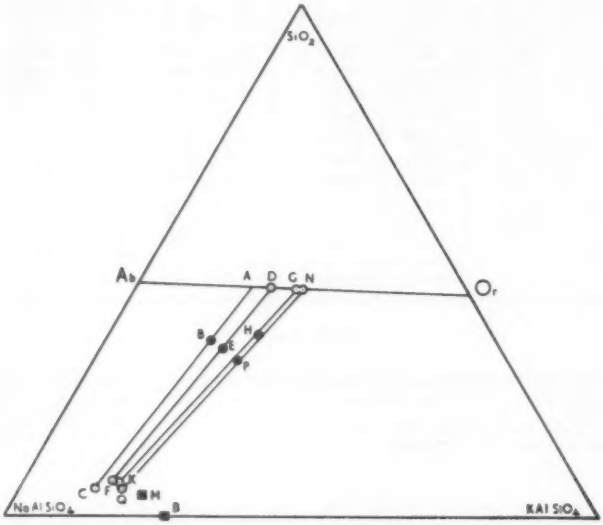

FIG. 2. Tie lines of Dunedin phonolite and hypersolvus nepheline syenites of Norway and Ontario in the system $NaAlSiO_4$–$KAlSiO_4$–SiO_2. *ABC*, phonolite, Dunedin (Tilley 1954, p. 66); *DEF*, coarse lardalite, Laagendal, Norway (Table 3*a*, Nos. 1–3); *GHK*, ditroite, Bratholmen, Norway (Table 3*b*, Nos. 1–3); *NPQ*, pyroxene nepheline syenite, east of Gooderham, Ontario (Table 1, Nos. 1–3).

of the perthite. The composition of this microperthite is set out in Table 1, analysis 3, and can be expressed as $Or_{48\cdot4}Ab_{49\cdot1}An_{2\cdot5}$. X-ray study confirms that the triclinic soda phase is twinned according to the albite law and is a low albite. The subidiomorphic nepheline has a considerable range in grain size; it is usually unaltered but is characterized by an abundance of acicular inclusions of pale green clinopyroxene, a dominant set lying along the *c*-axis, but other orientations may also be present. The composition of this nepheline is shown in Table 1, analysis 2, corresponding to $Ne_{75\cdot3}Ks_{16\cdot8}An_{2\cdot8}Qz_{5\cdot1}$. The green clinopyroxene is a sodic hedenbergite (Table 1, analysis 4) pleochroic, yellow green to dark green, and unzoned, β 1·719, γ 1·739, $\gamma \wedge c$ 46°. Within the grains hair-like inclusions of iron ore, in places abundant enough to make the grain almost opaque, are characteristic. The amphibole, hastingsite in type, is associated principally with the clinopyroxene fringing these grains or mantling magnetite. Olivine, an accessory usually rimmed by clinopyroxene, is a pale straw-brown fayalitic variety.

A photomicrograph of this coarse-grained nepheline syenite is shown in Plate 1,

TABLE 2

	1	2	3	*Norm of* 1		*Metal atoms to 32 oxygens in* 2	
SiO_2	51·72	43·35	65·72				
Al_2O_3	19·38	33·03	19·65	Or	30·58	Si 8·41	15·96
Fe_2O_3	4·22	1·12	0·14	Ab	22·14	Al 7·55	
FeO	6·70			Ne	20·38		
MnO	0·17	nil	nil	An	5·84	Ca 0·15	ΣR 7·69
MgO	0·45	0·11	nil	Di	9·06	Na 6·06	
CaO	3·45	0·71	0·36	Ol	3·56	K 1·33	
Na_2O	7·06	16·15	5·60	Il	0·61		
K_2O	5·17	5·38	8·33	Mt	6·03	$(Ne_{77\cdot3}Ks_{18\cdot8}Qz_{3\cdot9})$	
H_2O+	0·75	0·60	0·29*	Ap	0·34		
H_2O-	0·06	0·03	nil	Ct	0·07		
P_2O_5	0·16			Rest	0·81		
CO_2	0·03				99·42		
TiO_2	0·32		nil				
	99·64	100·48	100·09	$(Ne_{44\cdot3}Ks_{23\cdot8}Qz_{31\cdot9})$			

* Loss on ignition.

1. Nepheline syenite with clinopyroxene (82464), fine-grained facies, lot 4, con. IV, Monmouth Township, Haliburton Co., Ontario.
2. Nepheline from 1.
3. Microperthite from 1 = $Ab_{68\cdot1}$ $Or_{16\cdot2}$ $An_{1\cdot7}$ ($Ab_{68\cdot9}$ $Or_{31\cdot1}$).
Analyses 1, 2 by J. Gittins: 3 by J. H. Scoon.

fig. 1; with this we may compare the photograph (fig. 2) of the finer-grained facies of nepheline syenite from the same locality. The latter rock is somewhat more mafic, olivine being more conspicuous. Analyses of both rocks, their constituent nephelines and microperthites, are set out in Tables 1 and 2 which also provide interpretation of the formulae of these minerals and of the hedenbergitic pyroxene of the coarse-grained facies. The rocks are typical hypersolvus assemblages, single feldspar rocks in which unmixing is limited to the intimate intergrowth within the original feldspar (Tuttle & Bowen, 1958). Furthermore, the compositions of the nepheline lying on the soda side of the Morozewicz–Buerger concentration field give further confirmation that these assemblages consolidated from a magmatic state. The compositions of the coarse-grained nepheline syenite and the component nepheline and microperthite are shown graphically in the system $NaAlSiO_4$–$KAlSiO_4$–SiO_2 in Fig. 2 by *NPQ* (*P* = rock). In this diagram are also portrayed tie lines of a Dunedin phonolite (*ABC*), the microperthite and nepheline (*DF*) of a coarse lardalite, and of a ditroite (*GHK*) both from the Oslo alkali province, a remarkable parallelism of magmatic tie lines (Tilley 1957, fig. 4, p. 328). The chemical data for the Norwegian lardalite and ditroite minerals are set out in Tables 3*a* and 3*b*. The analysis of the Ontario rock (*P* in Fig. 2) falls in the low melting trough of the nepheline syenites in the alkali alumina silicate system (petrogeny's residua system (Tilley, 1957, fig. 1, p. 326)).

TABLE 3*a*

	1	2	3	*Metal atoms to 32 oxygens in* 3			
SiO_2	54·54	65·85	45·17	Si	8·61		
Al_2O_3	19·90	19·76	32·60	Al	7·31	7·38	15·99
Fe_2O_3	2·59	0·12	0·47	Fe^{+3}	0·07		
FeO	2·81			Ca	0·10	ΣR	
MnO	0·15	nil	< 0·01	Na	6·13	7·39	
MgO	1·59	0·07	0·05	K	1·06		
CaO	2·79	0·48	0·52				
Na_2O	8·39	7·05	16·62				
K_2O	4·98	6·63	4·36	$Ne_{76\cdot3}Ks_{14\cdot8}An_{2\cdot5}Qz_{6\cdot4}$			
H_2O-	nil	nil	nil	$(Ne_{78\cdot2}Ks_{15\cdot2}Qz_{6\cdot6})$			
H_2O+	0·63	0·04*	0·38*				
TiO_2	1·24	0·06	0·03				
P_2O_5	0·64	—	—				
Rest	0·16						
	100·41	100·06	100·20				

* Loss on ignition.

1. Average of 4 lardalites (Brögger 1933, p. 74). Coordinates in system Ne–Ks–Qz ($Ne_{45\cdot5}Ks_{20\cdot4}Qz_{34\cdot1}$).
2. Orthoclase microperthite of coarse lardalite (65936), Laagendal, South Norway ($Or_{34\cdot7}Ab_{59\cdot9}An_{2\cdot3}$).
3. Nepheline of same rock.

Analyses by J. H. Scoon.

TABLE 3*b*

	1	2	3	*Metal atoms to 32 oxygens in* 3				*Norm of* 1	
SiO_2	57·07	66·16	45·02	Si	8·58			Or	37·53
Al_2O_3	19·48	19·17	32·72	Al	7·35	16·00		Ab	30·92
Fe_2O_3	1·10	0·12	0·52	Fe^{+3}	0·07			Ne	17·04
FeO	3·46			Ca	0·12	ΣR		An	1·25
MnO	0·15			Na	6·04	7·43		Di	5·74
MgO	0·85	0·07	0·06	K	1·15			Ol	2·13
CaO	1·91	0·12	0·60					Il	2·28
Na_2O	7·41	6·16	16·36	$Ne_{75\cdot1}Ks_{15\cdot6}An_{3\cdot1}Qz_{6\cdot0}$				Mt	1·62
K_2O	6·35	7·90	4·70					Ap	0·34
H_2O+	0·37	0·12*	0·44*	$(Ne_{77\cdot8}Ks_{16\cdot3}Qz_{6\cdot2})$				Ct	0·25
H_2O-	nil	nil	nil					Z	0·55
TiO_2	1·22	0·04	0·04					Rest	0·37
P_2O_5	0·23	—	—						100·02
CO_2	0·11	—	—						
ZrO_2	0·42	—	—					$Ne_{39\cdot5}Ks_{24\cdot9}Qz_{35\cdot6}$	
	100·13	99·86	100·46						

* Loss on ignition.

1. Ditroite (Brögger) Bratholmen, Langesundsfjord, Norway.
2. Microperthite ($Or_{47\cdot1}Ab_{51\cdot9}An_{0\cdot4}$) of ditroite (1).
3. Nepheline of the same rock.

Analyses by J. H. Scoon.

2. *Theralites and theralitic canadites*

In their early studies Adams & Barlow (1910) described from lots 9, 10, and 11 of concessions VII and VIII, Monmouth Township, nepheline assemblages which they regarded as examples of extreme differentiation. Analytical data were provided on two rocks described as 'nepheline syenites' (essexose and vulturose) from lot 11, con. VIII. Subsequently (1913) a description and further analysis of a 'nepheline syenite' (lujavrose) was given in the *International Congress Guide Book*, No. 2, pp. 76, 96, from lot 32, con. III of Glamorgan Township. These rocks are dark-coloured mafic types carrying nepheline and albite along with much hornblende (40 per cent) of hastingsite type (No. 1), a second variety having 18 per cent of green clinopyroxene and a higher content of nepheline, while the third from lot 32 con. III, Glamorgan, had preponderant nepheline and hornblende, albite being subordinate.

In 1913 Quensel, in describing the alkali rocks of Almunge, Sweden, drew attention to the similarity of the rocks described by Adams & Barlow from Monmouth Township with the Almunge types, the distinctive features of which were the occurrence of albite or sodic plagioclase in the mode, but with significant anorthite in the norm. He proposed to call such rocks canadites, and described as theralitic canadites those assemblages—richer in mafic minerals—which still retained the singular feature of contrast of modal and normative plagioclase which characterized the canadites. Quensel made a direct chemical comparison of a theralitic canadite from near Sågen in Almunge (p. 182) with the rocks described by Adams & Barlow (1910, p. 270). Before giving further consideration to the particular rocks examined by Adams & Barlow we will discuss examples both from Monmouth and Glamorgan which give clear evidence of a magmatic origin.

It has already been noted that mafic rocks of theralite and theralitic canadite type have been recognized from three localities in Glamorgan north of Trooper Lake and on the eastern border of the township in lot 35, con. III. Good examples of igneous textured assemblages are met with 2 miles east-south-east of Gooderham in the fields north of Trooper Lake and on the road to Mintz Farm. The first rock (64870) from the field west of the Mintz Farm road is a mafic type showing idiomorphic nepheline and long laths of acid plagioclase set in a matrix of hedenbergite and hastingsite. The photograph of Plate 2 brings out clearly the textural character of the two felsic minerals and in Plate 1, figs. 3, 4, the microscopic characters of the rock are revealed. As in the hypersolvus nepheline syenite of Monmouth the nephelines show the oriented acicular inclusions of green clinopyroxene. The plagioclase is an acid oligoclase sometimes showing the intergrowth with nepheline characteristic of the essexite of Ditro (Tilley, 1957, Plate XXIX, fig. 3). The clinopyroxene is fringed with a green hornblende and this mineral may appear also as part of a corona with oligoclase (Plate I, fig. 4).

The rock (64872) from the road leading to Mintz Farm is a somewhat different type, with albite, nepheline, and hastingsite as the principal constituents but also carrying subordinate biotite. The coarse-grained nepheline holds green acicular inclusions, many noticeably pleochroic and clearly amphibole. The analyses of the two rocks are set down in Table 4 together with an analysis of

TABLE 4

	1	2	2*a*	*Norms*	1	2	*Metal atoms to 32 oxygens in 2a*			
SiO_2	41·79	42·40	44·40							
Al_2O_3	18·07	18·48	33·14	Or	9·45	9·45	Si	8·52		
Fe_2O_3	3·94	5·31	0·18	Lc	1·74	—	Al	7·48	7·50	16·02
FeO	13·54	12·94		Ab	—	14·67	Fe^{+3}	0·02		
MnO	0·24	0·41	< 0·01	Ne	30·39	27·83				
MgO	1·19	0·98	0·05	An	13·62	10·56	Ca	0·07	ΣR	
CaO	9·84	6·43	0·36	Di	28·63	13·38	Na	6·37	7·41	
Na_2O	6·61	7·79	17·17	Ol	5·80	10·71	K	0·90		
K_2O	1·93	1·62	3·72	Mt	5·80	7·66				
H_2O+	1·16	1·35	0·94*	Il	2·74	1·82	$Ne_{79\cdot9}Ks_{12\cdot5}An_{1\cdot7}Qz_{4\cdot9}$			
H_2O-	0·14	0·10	0·02	Ap	0·67	1·34	$(Ne_{81\cdot2}Ks_{12\cdot7}Qz_{6\cdot1})$			
TiO_2	1·48	0·95	nil	Ct	0·34	1·00				
P_2O_5	0·34	0·51		Rest	1·30	1·45				
CO_2	0·15	0·44			100·48	99·87				
	100·42	99·71	99·98							
				Ne	73·0	68·9				
				Ks	16·1	10·3				
				Qz	10·9	20·8				

* Loss on ignition.

1. Theralitic Canadite (64870) (hedenbergite, hastingsite, oligoclase, nepheline), field west of road to Mintz Farm.
2. Theralitic Canadite (64872) (hastingsite, biotite, albite, nepheline), road to Mintz Farm.

} 2 miles east-south-east of Gooderham and north of Trooper Lake, Glamorgan Township, Haliburton Co., Ontario.

2*a*. Nepheline of rock 2.
Analyses by J. H Scoon..

the nepheline of the hastingsite-bearing assemblage. The compositions of the two assemblages in the system $NaAlSiO_4$–$KAlSiO_4$–SiO_2 are indicated in Fig. 3 in relation to the data for the hypersolvus nepheline syenite of Fig. 2. Table 5 contains the analytical data (1–3) of three additional theralitic canadites, one (82471) from the locality north of Trooper Lake and two others (82505, 82508) from lot 35 con. III on the eastern edge of Glamorgan Township. The contained nepheline of the first rock (82471) has been separated and analysed (Table 5, analysis 2*a*). The clinopyroxenes of these theralitic canadites (analyses 2*b* and 3*a* of Table 5) are distinguished from the hedenbergite pyroxene of the nepheline syenite (Table 1) by their alumina content and lower lime values. Optically they show distinctive pleochroism with *X* purplish green, *Y* apple green, *Z* yellow green, β 1·721. In zoned crystals a purplish core may grade out to a pale green as the titanium content decreases and exsolved iron ore is frequently observed. The plagioclase of these rocks is an oligoclase–andesine and shows the

TABLE 5

	1	2	3	2*a*	2*b*	3*a*
SiO_2	42·66	41·66	37·40	42·39	42·02	40·21
Al_2O_3	22·00	18·63	21·19	34·00	6·56	10·43
Fe_2O_3	4·45	7·51	7·22	1·28	8·77	5·55
FeO	9·16	9·86	10·95		18·73	20·66
MnO	0·18	0·23	0·17	nil	0·67	0·62
MgO	1·60	1·74	2·50	0·08	3·91	4·56
CaO	8·05	9·79	11·31	1·15	15·24	13·30
Na_2O	6·87	5·84	4·68	15·63	1·52	2·17
K_2O	1·60	1·51	1·16	4·36	0·46	0·53
H_2O+	1·42	1·38	1·51	0·85	0·76	n.d.
H_2O-	0·09	0·58	0·02	0·02	0·28	nil
TiO_2	1·25	1·02	1·56	—	1·03	1·68
P_2O_5	0·39	0·35	0·18	—	—	—
CO_2	0·18	0·12	0·04	—	—	—
	99·90	100·22	99·89	99·76	99·95	99·71

Norms	1	2	3
Or	9·45	8·90	1·81
Ab	11·92	8·64	—
Ne	24·92	22·01	21·58
Ks	—	—	2·92
An	24·50	20·02	33·22
Di	9·14	21·79	18·42
Ol	7·94	2·81	6·59
Il	2·43	1·98	2·96
Mt	6·50	10·90	10·44
Ap	1·01	0·84	0·34
Ct	0·40	0·27	0·09
$H_2O\pm$	1·51	1·96	1·53
	99·72	100·12	99·90

Metal atoms to 32 oxygens in nepheline (anal. 2a)

Si	8·414	15·97	ΣR 7·69
Al	7·552		
Ca	0·151		
Na	6·060		
K	1·328		

$Ne_{74\cdot5}Ks_{18\cdot2}An_{3\cdot6}Qz_{3\cdot7}$
$(Ne_{77\cdot2}Ks_{18\cdot8}Qz_{3\cdot9})$

Metal atoms to six oxygens in clinopyroxenes (2b and 3a) of rocks 2 and 3 respectively

(2*b*)					(3*a*)			
Si	1·713	2·000			1·622	2·000		
Al	0·287				0·378			
Al	0·026				0·116			
Fe^{+3}	0·269				0·165			
Fe^{+2}	0·636		1·225		0·695		1·325	
Mn	0·022				0·022			
Ti	0·032				0·051			
Mg	0·240			2·032	0·276			2·094
Ca	0·666		0·807		0·576		0·769	
Na	0·117				0·169			
K	0·024				0·024			

1. Theralitic Canadite (82505), Lot 35, con. III, Glamorgan Township, Haliburton Co., Ontario.
2. Theralitic Canadite (82471), Lot 30, con. IV, Glamorgan Township, Haliburton Co., Ontario.
3. Theralitic Canadite (82508), Lot 35, con. III, Glamorgan Township, Haliburton Co., Ontario.

2*a*. Nepheline in 2; 2*b*. Clinopyroxene in 2; 3*a*. Clinopyroxene in 3.

Analyses by J. Gittins.

effects of thermal metamorphism by the fine dusty clouding which is prevalent. The nepheline contains the characteristic acicular inclusions of pyroxene, and hornblende appears both as the ubiquitous corona around clinopyroxene and as separate grains.

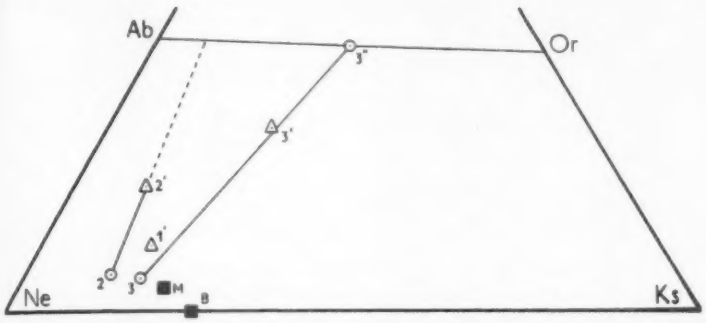

FIG. 3. Tie lines of nepheline rocks (igneous paragenesis) of Haliburton–Bancroft province, Ontario. 3–3^{I}–3^{II}, pyroxene nepheline syenite east of Gooderham, Ontario (Table 1, Nos. 1–3). 2–2^{I}, theralitic canadite, Glamorgan Township, Ontario (Table 4, Nos. 2–2*a*). 1^{I}, theralitic canadite, Glamorgan Township, Ontario (Table 4, No. 1).

Of the rocks described by Adams & Barlow and styled theralitic canadites by Quensel, we have been able to study only the example from lot 32, con. III, Glamorgan (Adams & Barlow, 1913, pp. 76, 96). It bears so close a comparison with the mafic type (64872) already described from the road leading to the Mintz Farm that a similar magmatic origin may be ascribed to it.

The assemblages that have now been described and assigned a magmatic origin have in their present environment a unique significance transcending their interest as petrographic rock types, for they are to be interpreted not only as relics of igneous rocks which in the same nepheline belt and elsewhere in the Haliburton–Bancroft province have been transmuted into foliated metamorphic gneisses, but also as indicators of the ultimate source of those agents of nephelinization which have converted Grenville sediments of the province into nepheline gneisses of the type characteristic of the York River nepheline belt of the Bancroft region. To some of these problems it is hoped to return in a later contribution.

ACKNOWLEDGEMENT

Grateful acknowledgement for permission to publish this paper is made to the Provincial Geologist of the Ontario Department of Mines under whose auspices the field work was conducted.

REFERENCES

ADAMS, F. D., & BARLOW, A. E., 1910. Geology of the Haliburton and Bancroft areas, Province of Ontario. *Mem. geol. Surv. Can.* **6.**

—— —— 1913. Excursion A2. Haliburton–Bancroft area of Central Ontario. *XII Int. geol. Congr.* (*Canada*), *Guide Book*, **2.**

BRÖGGER, W. C., 1933. Die Eruptivgesteine des Oslogebietes VII. *Skr. norske Vidensk. Akad.*, Mat.-nat. Kl., No. 1, p. 74.

GUMMER, W. K., & BURR, S. V., 1943. The nephelinized paragneisses of the Bancroft region, Ontario. *Science*, **97**, 286–7.

—— 1946. Nephelinized paragneisses in the Bancroft area, Ontario. *J. Geol.* **54**, 137–68.

QUENSEL, P., 1913. The alkaline rocks of Almunge. *Bull. geol. Instn. Univ. Upsala*, **12**, 129–200.

TILLEY, C. E., 1954. Nepheline–alkali feldspar parageneses. *Amer. J. Sci.* **252**, 65–75.

—— 1957. Problems of alkali rock genesis. *Quart. J. geol. Soc. Lond.*, **113**, 323–60.

TUTTLE, O. F., & BOWEN, N. L., 1958. Origin of granite in the light of experimental studies in the system $NaAlSi_3O_8$–$KAlSi_3O_8$–SiO_2–H_2O. *Mem. geol. Soc. Amer.*, **74**, 129.

EXPLANATION OF PLATES

PLATE 1

FIG. 1. Clinopyroxene nepheline syenite (65270), lot 4, con. IV, east of Gooderham, Monmouth Township, Haliburton Co., Ontario; 34 diameters. Nepheline enclosed in twinned microperthite; *bottom right*, some green hedenbergite. Acicular inclusions of clinopyroxene are seen in the nepheline on the lower right.

FIG. 2. Clinopyroxene nepheline syenite (82464), finer grained facies, same locality as fig. 1; 48 diameters. Microperthite, nepheline with acicular inclusions; fayalite olivine rimmed by clinopyroxene; clinopyroxene and magnetite.

FIG. 3. Theralitic canadite (64870), north of Trooper Lake, Glamorgan Township, Haliburton Co., Ontario; 19 diameters. Nepheline with acicular pyroxene inclusions; oligoclase and green augite.

FIG. 4. Theralitic canadite (64870), same locality as fig. 3; 26 diameters. Green augite in part with corona of plagioclase and hornblende (centre); nepheline and oligoclase.

PLATE 2

Theralitic canadite (64870), north of Trooper Lake, Glamorgan Township, Haliburton Co., Ontario. Photograph of weathered face showing idiomorphic nepheline (squarish sections) and plagioclase (lath-shaped sections) associated with mafic minerals, clinopyroxene, and subordinate amphibole.

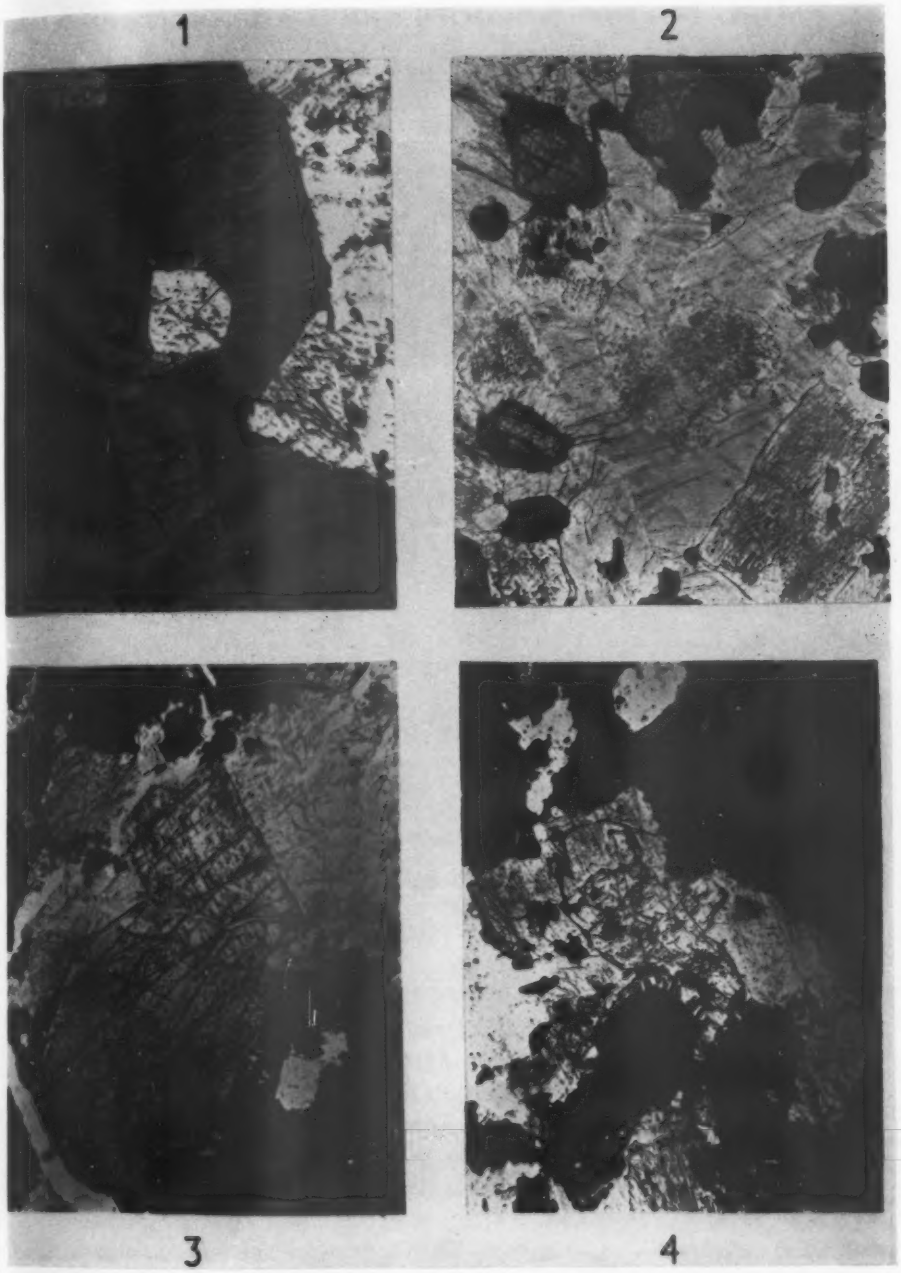

C. E. TILLEY *and* J. GITTINS

Plate 1

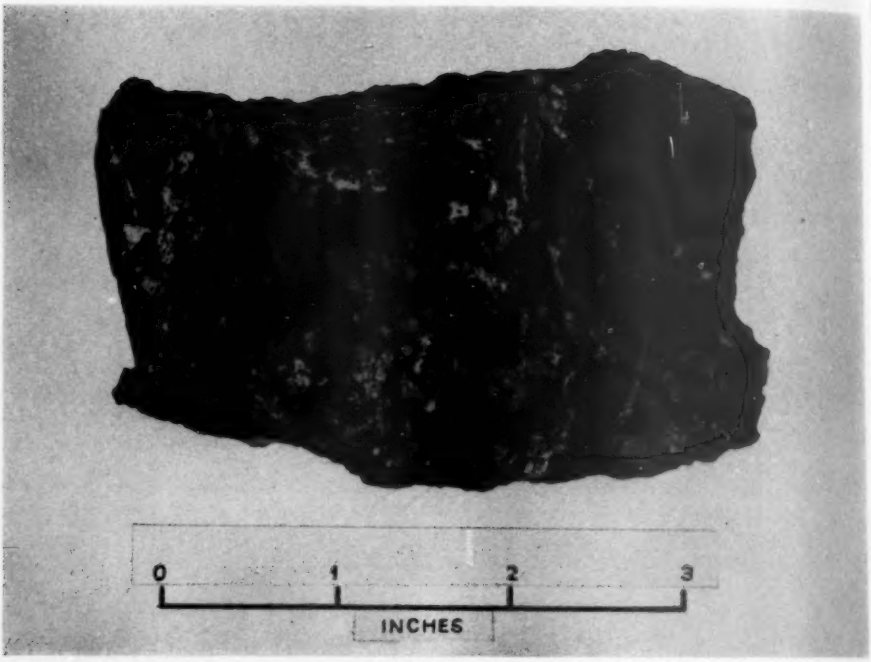

C. E. TILLEY *and* J. GITTINS

Plate 2

Chloritoid: Its Composition, X-ray and Optical Properties, Stability, and Occurrence

by L. B. HALFERDAHL[1]

The Johns Hopkins University, Baltimore, Md., and Geophysical Laboratory, Carnegie Institution of Washington, Washington, D.C., U.S.A.

WITH TWO PLATES

ABSTRACT

The nomenclature of the chloritoid group, which includes ottrelite, is reviewed. Five new chemical analyses, and all published analyses that are considered reliable, indicate that the chloritoid group can be represented by the general formula $H_2FeAl_2SiO_7$ with up to two-fifths of the ferrous iron replaced by magnesium, up to one-sixth by manganese, and up to one-seventh of the aluminium replaced by ferric iron. Chloritoid crystallizes in both monoclinic and triclinic polymorphs. The triclinic unit cell is one-half the monoclinic unit cell. Both polymorphs are widely distributed; they may be distinguished by their X-ray diffraction powder patterns. In most monoclinic chloritoids the optic plane is normal to (010), whereas in most triclinic chloritoids it is nearly parallel to (010). Replacement of iron by magnesium lowers the indices of refraction.

With increasing temperatures chloritoid breaks down to iron cordierite + hercynite + vapour at low pressures and to staurolite + almandine + hercynite + vapour at high pressures. Chloritoid was synthesized only at pressures of about 10,000 bars, but natural chloritoids were stable at higher pressures. At lower pressures chloritoid was not synthesized because of the persistence of a metastable chamosite with a 7 Å basal spacing. Natural chloritoids did not decompose below about 600° C at these lower pressures. Stress as defined by Harker is not necessary for the growth of chloritoid.

Chloritoid-bearing rocks have a high content of alumina relative to potash, soda, lime, and mafic components, and have more ferrous oxide than magnesium oxide. In pelitic and lateritic sediments having these characteristics, chloritoid is one of the first new minerals to form during regional or contact metamorphism. In higher metamorphic grades it is accompanied by cordierite, andalusite, kyanite, or staurolite. It also grows in hydrothermal veins. Various reactions in which chloritoid is produced or consumed are presented.

INTRODUCTION

CHLORITOID is a critical mineral which has been described from worldwide occurrences under many names, and yet its properties and composition are still disputed among mineralogists. Some petrologists have suggested that it can form only under restricted conditions, notably those in which stress plays a part, despite the fact that its growth has been recorded in other geological environments. It is the purpose of this investigation to obtain new data on the composition, the optical and X-ray properties, the stability, and the nature of the occurrences of chloritoid and to apply these along with previously published data to the many problems concerning this geologically significant mineral.

[1] Present address: Research Council of Alberta, Edmonton, Alberta, Canada.

[Journal of Petrology, Vol. 2, Part 1, pp. 49-135, Feb. 1961]

NOMENCLATURE

The name chloritoid was first applied, apparently, by Breithaupt to material discovered by Fiedler (1832, p. 327) in a vein near an emery quarry several kilometres from the village of Kossoibrod in the Ural Mountains. Fiedler described it as occurring in blackish green, curved scaly flakes which one might suppose were chlorite at first glance. He proposed the name chloritespar. Rose (1837, p. 252) later visited the Kossoibrod area and wrote that Breithaupt chose the name chloritoid for this mineral. Von Bonsdorff's analysis (42, Table 5) published in 1837 shows that its composition approaches the simple formula $FeO \cdot Al_2O_3 \cdot SiO_2 \cdot H_2O$, corresponding to FeO 28·5 per cent, Al_2O_3 40·5 per cent, SiO_2 23·8 per cent, and H_2O 7·2 per cent by weight.

TABLE 1

Names previously proposed for minerals of the chloritoid group

Name	*Proposed by (in honour of)*	*Reference*	*Type locality*
Ottrelite	Dethier	Dethier, 1819	Ottré, Belgium
Otrélite	Leonhard	Haüy, 1822	Otrélite,* Saxony
Phyllite	Thomson	Thomson, 1828	Sterling, Massachusetts, U.S.A.
Chloritespar	Fiedler	Fiedler, 1832	Kossoibrod, Ural Mts., U.S.S.R.
Chloritoid	Breithaupt	Rose, 1837	Kossoibrod, Ural Mts., U.S.S.R.
Barytophyllite	Glocker	Glocker, 1839	
Masonite	Jackson (Owen Mason)	Jackson, 1840	Natick, Rhode Island, U.S.A.
Sismondine	Bertrand de Lom (A. de Sismonda)	Delesse, 1843	St. Marcel, Piedmont, Italy
Newportite	Totten	Shepard, 1852	Newport, Rhode Island, U.S.A.
Venasquite	Boubée	Boubée, 1857	Vénasque, Pyrénées Mts., France
Strueverite	Brezina (Giovanni Struever)	Brezina, 1876	St. Marcel, Piedmont, Italy
Salmite	Dumont	Prost, 1883–4	Vielsalm, Belgium
Bliabergsite	Igelström	Igelström, 1896*a*	Mt. Blia, Sweden

Many other names have been proposed for minerals once regarded as possible new species but later found to have physical properties similar to chloritoid, and which may, therefore, be grouped with it. These names are listed chronologically in Table 1. The realization that these minerals belong to the same species is the result of work by Hermann (1851, p. 13), von Kobell (1853), Des Cloizeaux (1862, pp. 372, 463), Dana (1868, p. 504), Tschermak & Sipöcz (1879, p. 506), Weibull (1896), Manasse (1911), and Simpson (1915). Of the names listed only ottrelite in addition to chloritoid is used frequently in the current literature; sismondine and salmite are found occasionally. The usage of these three names will be reviewed, and then recommendations concerning the nomenclature of the chloritoid group will be presented.

The name sismondine was proposed by Bertrand de Lom (Delesse, 1843,

p. 388) in honour of Prof. A. de Sismonda, of the University of Turin, for a mineral from St. Marcel, Piedmont, Italy. Delesse's analyses (91, 92, 93; Table 7) show that this mineral is chloritoid. Delesse (1846*a*) realized this but retained the name sismondine because he could not compare the St. Marcel mineral with the Kossoibrod chloritoid. Later, more complete analyses (4, Table 2; 44, Table 5) showed that some Piedmont chloritoids contained about 6 per cent MgO. Thus Simpson (1915) suggested that the name sismondine be applied to magnesium-bearing chloritoids. However, he failed to specify a minimum content of MgO, and apparently overlooked the fact that von Bondorff's analysis (42, Table 5) shows that the Kossoibrod chloritoid contains 4·29 per cent MgO.

Haüy (1822, p. 455) cited K. C. von Leonhard (1821) as being the first author to use the name 'otrélite' for a variety of diallage which occurs in a 'talc schistoïde' in the vicinity of Spa near the village of Otrélite[1] in Saxony. Haüy called it 'une diallage lamelliforme noire' and remarked that he also had a specimen from Newport, Rhode Island. In several old mineralogies Haüy is given the honour of having named ottrelite (see Hintze, 1897, p. 666; Naumann & Zirkel, 1901, p. 678). Davreaux (1833, p. 237), however, gave the credit to Dethier, who discovered it in a 'stéaschiste diallagic' at Ottré, Belgium, in 1809, and named it ottrelite. Buttgenbach (1947, p. 359) agreed with Davreaux and cited Dethier (1819) as having given the name ottrelite to the diallage from a talc schist that he had found at Ottré, Belgium, a few years before 1819.

The first analyses of ottrelite (50, 51; Table 6) showed that it was evidently a hydrous ferrous aluminium silicate containing about 8 per cent MnO and that it was distinctly different from diallage. Some later analyses of ottrelite from the Ardennes of Belgium and France (52–56, Table 6) showed varying and lesser amounts of MnO, but always 39 to 43 per cent SiO_2. Even before these later analyses had been made, the similarity of physical properties between ottrelite and chloritoid led some mineralogists to suspect their identity and to ascribe the higher silica content of ottrelite to quartz inclusions in the analysed material (Dana, 1868, p. 504; Tschermak & Sipöcz, 1879, p. 509). Thus ottrelite came to be known as manganiferous chloritoid (Lacroix, 1893, p. 364) but no minimum content of manganese has ever been specified. A comparatively modern analysis (56, Table 6) led Koch (1935, p. 462) to propose a substitution scheme which the writer interprets to be $2Fe^{2+}+2Al \rightarrow Mn^{2+}+2Si$ in order to make ottrelite from chloritoid. Some geologists have observed tiny black disks containing numerous quartz and other inclusions in schists and slates, and have called them ottrelite because of their similarity in gross appearance to the ottrelite in the Salmian phyllites of the Ardennes, but without chemical evidence. Rosenbusch (1889, p. 266) and Mügge (1927, p. 614) have used ottrelite as a synonym for chloritoid. Thus confusion has arisen because of the following four uses for the name ottrelite: (1) manganese-bearing variety of chloritoid, (2) high-silica variety of

[1] This is apparently a misspelling of Ottré, a village not far from Liège, Belgium.

chloritoid with or without manganese, (3) fine-grained chloritoid containing numerous inclusions, (4) synonym for chloritoid.

Prost (1883–4) studied a mineral labelled salmite found near Vielsalm, Belgium, from a collection assembled by Dumont at the University of Liège. A chemical analysis (17, Table 3) showed it to be chloritoid in which manganese partly replaced ferrous iron. Prost suggested that the name salmite be retained for manganese-bearing chloritoids. This was prior to the use of ottrelite in this sense.

In a review of the chloritoid–ottrelite–salmite problem, Mélon (1938) realized that chemical distinctions between ottrelite and salmite (manganiferous chloritoid) were doubtful. However, he did note from the work of Corin (1929) that chloritoid and ottrelite could be distinguished optically. The normal to (001) lies in a plane of optic symmetry in chloritoid, but is inclined at least 15° to such a plane in ottrelite. He concluded that ottrelite is clearly triclinic, whereas chloritoid is nearly if not exactly monoclinic.

On the basis of data to be presented in this investigation the writer proposes that all names for this mineral group except chloritoid and ottrelite be dropped. Ottrelite (even though salmite has priority) is to be retained because it is so widely used, but will be defined more rigorously. The usage recommended and followed throughout this paper follows.

Chloritoid is the name for the group of minerals represented by the formula $FeO \cdot Al_2O_3 \cdot SiO_2 \cdot H_2O$ where Fe^{2+} may be replaced by Mg or Mn, Al by Fe^{3+}, and OH by F.

Chloritoid is also the name for the ferrous iron end-member,

$$FeO \cdot (Al, Fe)_2O_3 \cdot SiO_2 \cdot H_2O.$$

Ottrelite is the name for the manganese end-member, $MnO \cdot (Al, Fe)_2O_3 \cdot SiO_2 \cdot H_2O$.

Magnesium chloritoid or Mg chloritoid is the name for the magnesium end-member, $MgO \cdot (Al, Fe)_2O_3 \cdot SiO_2 \cdot H_2O$.

Binary and ternary members of the group may be designated as mol percentages of the end-members (e.g., $Ctd_{90}Ott_2Mg\text{-}Ctd_8$), or simply as magnesian or manganiferous chloritoids.

CHEMICAL COMPOSITION

Friedlaender (1929), in a discussion of the chemical composition of chloritoid, divided 28 analyses into four groups corresponding to the ratios of $RO:R_2O_3:SiO_2:H_2O$ :: 1:1:1:1, 1:1:2:1, 1:1:3:1, 2:3:3:2. He realized that many of these analyses had been made on impure chloritoid, and hence that the chief differences between the groups are not real. Nevertheless, he questioned Manasse's procedure (1911) of subtracting the required amount of quartz from some of his analyses in order to achieve the molecular ratios of approximately 1:1:1:1. Surely, however, the attainment of such ratios simply by subtracting quartz from several analyses made on impure chloritoid is significant. Simpson

(1915, 1930) obtained the same result on two different analyses by the same procedure. Milne (1949) selected, on an unspecified basis, 20 analyses from the literature including some previously listed by Friedlaender. From these he concluded that its composition can be represented by the formula $(Fe^{2+}, Mg)_2(Al, Fe^{3+})_2(Al_2Si_2)O_{10}(OH)_4$.[1] However, he did not consider the manganiferous chloritoids from the Ardennes or elsewhere. More recent chemical analyses and the crystal structure determined by Harrison & Brindley (1957) indicate that the number of silicon atoms per formula is exactly 2 and that no aluminium atoms have tetrahedral coordination in the chloritoid structure. Because of these difficulties it is clear that further critical review of the available chemical analyses is necessary.

All the chemical analyses of chloritoid (including those given under the names in Table 1) that could be found in the literature are listed in Tables 2–7. These analyses have been divided into six tables for convenience in discussion and plotting. The bases of this division are the purity of the analysed chloritoid, as specified by the authors, and the number of components determined. Table 2 contains those analyses which are considered to have been made on chloritoid free, or almost free, from impurities (except as noted) and in which at least SiO_2, Al_2O_3, Fe_2O_3, FeO, MnO, MgO, and H_2O or loss on ignition (l.o.i.) have been determined. Table 3 contains those analyses which have been adjusted, as noted, to account for quartz and other minerals present in the analysed material and in which at least the seven oxides above have been determined. In Table 4 are those analyses in which at least one of CaO, Na_2O, and K_2O was determined and is greater than 0·50 per cent, and in which at least the seven oxides mentioned previously have been determined. As noted, some of the chloritoid prepared for these analyses contained impurities. In Table 5 are those analyses which are considered to have been made on pure or fairly pure material as noted, and in which not all of the seven oxides, SiO_2, Al_2O_3, Fe_2O_3, FeO, MnO, MgO, and H_2O, have been determined. These analyses are listed separately because, although they are incomplete and hence less reliable than those in the previous tables, some information can be obtained from them (see Figs. 2 and 3). Table 6 contains analyses made on chloritoid which is stated, or suspected, to contain significant amounts of quartz or other impurities or both, as noted. Table 7 contains those analyses in which too few components were determined for much use to be made of them except to show that they were made on chloritoid. The analyses have been numbered consecutively throughout Tables 2–7. The notes accompanying these tables give first the locality, second the reference, then the analyst if different from the specified author, and last, remarks by the present author pertaining to the purity of the analysed chloritoid, and other information.

Five new analyses of chloritoid made in the Rock Analysis Laboratory,

[1] Milne wrote a structural formula similar to the micas, following Machatschki & Mussgnug (1942).

TABLE 2

Previously published analyses of chloritoid which are considered reliable

	1	2	3	4	5	6	7	8	9	10	11	12	13	14
SiO_2	24·90	25·18	24·56	25·36	26·13	25·03	24·47	24·0	24·37	26·07	25·36	23·40	25·24	26·05
TiO_2	0·63	0·40	—	—	—	—	—	1·0	tr.	tr.	tr.	1·19	0·16	0·11
Al_2O_3	39·93	39·48	34·57	42·58	40·11	39·75	41·34	40·0	37·03	37·01	38·99	39·31	39·00	37·65
Fe_2O_3	3·20	2·00	5·93	0·72	3·44	0·00	0·38	1·8	5·36	3·97	2·54	5·14	1·47	1·69
FeO	19·44	22·26	27·20	18·02	23·01	22·92	18·52	23·3	21·91	24·76	23·06	21·94	24·43	25·04
MnO	1·04	1·32	1·14	0·53	tr.	1·30	0·91	0·3	0·52	tr.	tr.	tr.	0·01	0·05
MgO	3·85	1·25	0·36	5·96	0·94	3·32	6·80	2·6	4·32	1·90	3·16	2·18	2·42	1·96
CaO	0·00	0·06	—	0·18	—	0·21	0·30	0·1	0·16	0·12	0·24	tr.	0·25	0·33
Na_2O	0·00	0·15	—	—	—	0·07	—	—	—	—	—	0·20	0·18	0·14
K_2O	0·09	0·43	—	—	—	0·07	—	—	—	—	—	0·20	0·10	0·02
H_2O^+	6·70	7·30	6·64	7·50	—	—	6·98	7·0	7·16	7·03	7·28	6·81	6·90	7·05
H_2O^-	0·14	0·06	—	—	—	—	—	—	—	—	—	—	0·02	0·05
L.O.I.	—	—	—	—	6·91	6·64	—	—	—	—	—	—	—	—
Rem.								0·1				tr.		
	99·92	99·89	100·40	100·85	100·54	99·31	99·70	100·2	100·83	100·86	100·63	100·37	100·18	100·25
G	3·517–3·522	—	3·54	3·45	3·353	3·614	3·313–3·462	—	3·44	3·51	3·56	—	—	—
	Atomic proportions													
Si	2·03	2·10	2·09	2·01	2·12	2·06	1·96	1·99	2·01	2·15	2·08	1·95	2·09	2·17
Al	3·85	3·88	3·46	3·98	3·84	3·86	3·93	3·92	3·60	3·60	3·76	3·87	3·80	3·68
Fe^{3+}	0·20	0·13	0·38	0·04	0·21	0·00	0·02	0·11	0·33	0·25	0·16	0·32	0·09	0·11
Fe^{2+}	1·33	1·55	1·93	1·20	1·56	1·58	1·25	1·62	1·51	1·71	1·58	1·53	1·69	1·74
Mn	0·07	0·09	0·08	0·04	0·00	0·09	0·06	0·02	0·04	0·00	0·00	0·00	0·00	0·00
Mg	0·47	0·16	0·05	0·70	0·11	0·41	0·82	0·32	0·53	0·23	0·39	0·27	0·30	0·24
OH	3·65	4·06	3·76	3·97	3·75	3·65	3·75	3·88	3·94	3·87	3·98	3·79	3·81	3·90
O	10·00	10·00	10·00	10·00	10·00	10·00	10·00	10·00	10·00	10·00	10·00	10·00	10·00	10·00

1. Rawlinsville, Lancaster County, Pennsylvania, U.S.A. Hietanen (1951, p. 867). Analyst: Ståhlberg. Chloritoid was separated from the enclosing schist by means of Clerici solutions of specific gravities 3·517 and 3·522. This chloritoid was pure except for some rutile inclusions which Heitanen thinks account for all the TiO_2 determined. The small amount of K_2O is probably due to muscovite in the analysed material. Both TiO_2 and K_2O have been omitted from the calculations.
2. Mt. Herrick, Ira Township, Vermont, U.S.A. Zen (1955). Analyst: Byler. The analysed chloritoid contained 0·1 per cent quartz, and sericite and rutile inclusions. X-rays by the writer showed a small amount of chlorite as well. In the calculations, Na_2O and K_2O have been omitted along with enough SiO_2, Al_2O_3, and H_2O to make paragonite and muscovite. TiO_2 has been omitted to account for the rutile. CaO has also been omitted.
3. Natick, Rhode Island, U.S.A. Manasse (1911, pp. 29–42). Only pieces of chloritoid completely pure or containing minute traces of biotite were selected from crushed material for analysis.
4. Vallone di Champ de Praz, Val d'Aosta, Piedmont, Italy. Manasse (1911, p. 32). The material analysed was pure chloritoid from which the accompanying chlorite had been completely removed. CaO has been omitted from the calculations.
5. Chatham County, North Carolina, U.S.A. Genth (1873, p. 399). Although great pains were taken to obtain pure chloritoid, which was examined under a powerful magnifying glass, that analysed may have contained minute quantities of pyrophyllite.
6. Indian Grave Mountain near Bull Mountain, Patrick County, Virginia, U.S.A. Genth (1890, pp. 49–50). Pure chloritoid contained no Fe_2O_3. CaO, Na_2O, and K_2O were omitted from the calculations as they are probably due to margarite, paragonite, and muscovite, all of which are reported present with the chloritoid at this locality.
7. Vanlup, Shetland Islands, Scotland. Heddle (1879, pp. 28–29). Fresh dark green chloritoid containing inclusions of sphene was analysed.
8. Dale of Oddsta, Fetlar, Shetland Islands, Scotland. Guppy & Sabine (1956, pp. 63–64). Analysts: Wilson and Coombs. Rem. is rarer oxides which were determined spectrochemically by Harvey and Murray. They are ZrO_2, 0·03; Cr_2O_3, 0·02; V_2O_3, 0·03; NiO, 0·01; CoO, 0·01; BaO, 0·002; SrO, 0·002; Ga_2O_3, 0·01; Sc_2O_3, 0·004.
9. Stazzenia, Apuane Alps, Tuscany, Italy. Manasse (1910, p. 127). For the analysis chloritoid containing few or no inclusions was hand-picked under a lens from the crushed rock. This chloritoid was washed with water and then with dilute HCl. CaO has been omitted from the calculations as it is probably due to either calcite or epidote in the analysed material. Both of these minerals were present in the marble breccia from which this chloritoid was obtained.
10. Camporaghena, Apuane Alps, Tuscany, Italy. Manasse (1910, p. 128). The material for analysis was obtained in the same manner as that for analysis 9. CaO has been omitted from the calculations as it is probably due to inclusions of sphene or feldspar in the analysed material. Both occur with the chloritoid at this locality.
11. Monte Corchia, Apuane Alps, Tuscany, Italy. Manasse (1910, p. 128). The material for analysis was obtained in the same way as that for analysis 9. CaO has been omitted from the calculations as it is probably due to calcite in the analysed material.
12. Liberty, Frederick County, Maryland, U.S.A. *U.S. Geol. Surv. Bull.*, No. 113 (1893, p. 111). Analyst: Eakins. The material for analysis was prepared by G. H. Williams. Rem. is P_2O_5.
13. Frunze Mine, Krivoy–Rog, Ukraine, U.S.S.R. Istshenko (1957, p. 291). The chloritoids in analyses 13 and 14 were associated with quartz, chlorite, rutile, and black dusty particles.
14. Severnaia Mine, Krivoy–Rog, Ukraine, U.S.S.R. Istshenko (1957, p. 291).

TABLE 3. *Previously published analyses of chloritoid which have been adjusted to account for impurities in the analysed material*

	15	16	17	18	19	20	21	22	23	24	25
SiO_2	24·31	23·38	19·14	24·44	24·4	22·78	23·98	23·74	26·00	23·48	23·85
TiO_2	0·00	–	–	–	1·3	0·00	–	0·00	–	2·55	0·56
Al_2O_3	39·18	33·57	33·66	39·08	39·6	37·98	37·72	39·01	40·05	39·71	35·83
Fe_2O_3	3·56	2·01	3·38	1·14	2·4	2·32	3·94	3·04	5·05	3·79	9·00
FeO	22·64	9·16	13·05	20·36	23·0	21·97	24·82	23·98	19·50	20·73	20·33
MnO	1·51	16·63	7·14	4·95	0·2	0·29	0·76	0·49	0·02	0·66	0·99
MgO	2·70	4·40	1·79	2·80	1·8	1·28	1·74	1·61	2·88	2·00	1·94
CaO	tr.	0·91	0·30	–	tr.	tr.	tr.	1·02	0·00	0·31	0·34
H_2O	6·65	6·96	6·32	7·23	7·3	6·04	7·04	7·72	6·00	6·77	7·16
Rem.	–	2·77	15·10	–	–	–	–	–	–	–	–
	100·55	99·79	99·88	100·00	100·0	92·66	100·00	100·61	99·50	100·00	100·00
G	3·55	3·47	> 3·38	3·44	–	–	3·56	3·54	–	–	–
	Atomic proportions										
Si	2·00	2·05	1·89	2·03	2·04	2·01	2·01	2·00	2·09	1·98	2·02
Al	3·79	3·47	3·93	3·82	3·90	3·96	3·73	3·87	3·80	3·95	3·57
Fe^{3+}	0·22	0·13	0·25	0·07	0·15	0·15	0·25	0·19	0·31	0·24	0·57
Fe^{2+}	1·55	0·67	1·08	1·41	1·61	1·62	1·74	1·69	1·31	1·46	1·44
Mn	0·11	1·24	0·60	0·35	0·01	0·02	0·05	0·03	0·00	0·05	0·07
Mg	0·33	0·58	0·26	0·35	0·22	0·17	0·22	0·20	0·35	0·25	0·24
OH	3·64	4·08	4·17	4·00	4·07	3·56	3·94	4·33	3·22	3·81	4·04
O	10·00	10·00	10·00	10·00	10·00	10·00	10·00	10·00	10·00	10·00	10·00

15. Collier Bay, Yampi Sound, Western Australia. Simpson (1915, p. 76). This analysis and specific gravity is a recalculation by Simpson of analysis 49, Table 6, after omitting 9·50 per cent SiO_2 and 0·54 per cent TiO_2. These amounts were estimated to be present as quartz and rutile inclusions.
16. Ottré, Belgium. de Rauw (1912). Analysts: de Rauw and Joassart. The chloritoid for analysis was separated from the rock using Thoulet solution ($G = 3·3$). SiO_2 present as quartz was determined by treating the chloritoid concentrate with H_2SO_4, igniting, and boiling with a concentrated solution of Na_2CO_3. The analysis given is an average of fifty. Rem. is SiO_2 as free quartz, 2·12; P_2O_5, 0·65. The calculations have been made omitting SiO_2 as free quartz, and CaO and P_2O_5, both of which were probably present as apatite.
17. Vielsalm, Belgium. Prost (1883–4). Analyst: de Koninck. This chloritoid contained quartz and other inclusions. SiO_2 present as free quartz was determined in the same manner as described for analysis 16. *G* was determined on material with quartz inclusions and is, therefore, a minimum. Rem. is SiO_2 as free quartz, 15·06; CoO, 0·04. CaO was omitted from the calculations because it is probably present in inclusions such as apatite. The writer believes that the deficiency of Si atoms is probably due partly to opaque iron, titanium, and manganese-bearing minerals in the analysed material and partly to the procedure for determining SiO_2 as free quartz.
18. Ottré, Belgium. Manasse (1911, p. 34). This analysis and specific gravity is a recalculation of analysis 55, Table 6, by Manasse to 100 per cent after subtracting 24·38 per cent SiO_2 to account for quartz inclusions.
19. Dutchess County, New York, U.S.A. Barth & Balk (1934, p. 348). Analyst: Barth. This analysis was made on that part of some inclusion-filled chloritoid which was soluble in H_2SO_4. H_2O was obtained by difference. TiO_2 probably is present as ilmenite, and hence has been omitted from the calculations.
20. Womble Mine, Deep River Region, North Carolina, U.S.A. Stuckey (1926). This is analysis 58, Table 6, after subtracting 6·5 per cent SiO_2 and 0·86 per cent TiO_2 to account for quartz and leucoxene impurities (see Plate 1, fig. B).
21. Vénasque, Pyrénées, France. Manasse (1911, p. 41). This analysis and specific gravity is a recalculation of analysis 62, Table 6, by Manasse to 100 per cent after subtracting 17·98 per cent SiO_2 to account for quartz inclusions.
22. Kalgoorlie, Western Australia. Simpson (1930). The material for analysis was concentrated from the crushed rock by means of methylene iodide. It contained inclusions of quartz and rutile. SiO_2 present as free quartz was determined by repeated fuming with H_2SO_4 and then treatment of the residue with Lunge's solution. The analysis given here was recalculated by Simpson after subtracting 7·35 per cent SiO_2, which was present as free quartz, and 1·46 per cent TiO_2, which was the quantity of rutile estimated to be present. *G* was adjusted by Simpson from 3·46 for these inclusions. CaO was omitted from the calculations as it is probably present in the carbonate which is associated with the chloritoid at this locality (see Plate 1, fig. C).
23. Stonehaven, Kincardineshire, Scotland. Barrow (1898). A chloritoid concentrate was separated from the crushed rock by means of an electromagnet and heavy liquids. This concentrate was treated with hot dilute HCl and analysed at intervals until no alkalis remained. H_2O was determined as loss on ignition.
24. Ritten Hamar, Unst, Shetland Islands, Scotland. Snelling (1957, p. 472). This analysis is a recalculation of analysis 77, Table 6, by Snelling to 100 per cent based on the partial analysis of the residue remaining after solution of the chloritoid in concentrated H_2SO_4. The residue contained 0·05 per cent TiO_2, 1·78 per cent Al_2O_3, 1·09 per cent Fe_2O_3. In the recalculation it is assumed that the Al_2O_3 in the residue was present as muscovite and the Fe_2O_3 as magnetite. CaO has been omitted from the calculations because it probably is present in an impurity in the chloritoid.
25. Red Man, near Stonehaven, Kincardineshire, Scotland. Snelling (1957, p. 472). This analysis is a recalculation of analysis 78, Table 6, by Snelling to 100 per cent after subtracting 6·61 per cent SiO_2 to account for quartz inclusions. CaO has been omitted from the calculations because it probably is present in an impurity such as a carbonate in the chloritoid.

TABLE 4

Previously published analyses of chloritoid which are considered unreliable

	26	27	28	29	30	31	32	33	34	35	36
SiO_2	26·62	25·30	26·42	23·37	23·77	24·98	25·36	24·29	23·89	26·64	23·92
TiO_2	0·21	0·00	0·68	0·00	0·00	–	–	0·28	–	0·37	tr.
Al_2O_3	37·65	41·24	35·20	39·43	39·09	35·07	41·74	34·00	37·19	36·31	39·13
Fe_2O_3	11·91	2·39	16·80	19·71	15·71	4·81	3·90	10·55	5·10	2·19	6·01
FeO	13·70	18·02	9·91	9·30	13·88	26·84	13·93	20·51	22·01	25·57	20·38
MnO	0·04	0·09	0·02	0·03	0·02	0·79	0·92	tr.	1·53	0·07	0·16
MgO	2·67	3·60	2·09	2·36	1·42	0·67	6·82	1·29	1·83	1·80	1·33
CaO	0·00	0·00	1·90	0·00	0·00	0·58	0·90	0·61	1·26	0·70	0·20
Na_2O	1·21	2·53	1·65	1·78	0·92	–	–	0·35	–	0·21	2·08
K_2O	0·46	0·76	0·02	0·03	0·02	–	–	0·97	–	0·03	0·15
H_2O^+	5·59	6·15	5·42	4·08	5·16	6·34	6·57	6·75	7·19	6·45	6·92
H_2O^-	0·00	0·00	–	0·00	0·00	–	–	–	–	0·04	–
	100·06	100·08	100·11	100·09	100·02	100·08	100·14	99·60	100·00	100·38	100·28
G	3·358	3·371	–	–	–	3·516	3·356	3·552	3·68	–	3·57

26. Crestlianderstobel, Graubünden, Switzerland. Friedlaender (1929, p. 256). Analyst: Jakob. Coarse chloritoid flakes, entirely free from inclusions as seen under a microscope, were separated for chemical analysis.
27. Saas Valley, Wallis, Switzerland. Friedlaender (1929, p. 260). Analyst: Jakob.
28. Ernen Power Station, Wallis, Switzerland. Oberholzer (1955, p. 388). Analyst: Jakob. The analysed chloritoid contained extremely few inclusions.
29. Çatalçam, Turkey. Önay (1949, p. 383). Analyst: Jakob.
30. Üstüaçiksarinç, Turkey. Önay (1949, p. 383). Analyst: Jakob.
31. Natick, Rhode Island, U.S.A. Koch (1935, pp. 460–1). The chloritoid for analysis was obtained by centrifuging in Clerici solution. It was checked under a microscope. *G* was determined with Clerici solution.
32. Vanlup, Shetland Islands, Scotland. Heddle (1879). The chloritoid analysed was a clove or chocolate-brown colour and was partly altered.
33. Champion Mine, Michigan, U.S.A. Keller & Lane (1891). The chloritoid analysed was slightly impure. It contained inclusions of magnetite, ilmenite, rutile, quartz, and sericite.
34. Monte Fenouillet, Var, France. Manasse (1911). This analysis and specific gravity is a recalculation of analysis 73, Table 6, by Manasse to 100 per cent after subtracting 7·65 per cent SiO_2 to account for quartz inclusions.
35. Valiavko-Skipovaia Mine, Krivoy-Rog, Ukraine, U.S.S.R. Istshenko (1957, p. 291). This chloritoid was associated with quartz, chlorite, rutile, and black dusty particles.
36. Hennensädel, südlich Vals, Graubünden, Switzerland. van der Plas *et al.* (1958, p. 239). Analyst: Th. Hügi. The analysed chloritoid was separated from the enclosing rock with Clerici solution and by a magnetic separator. It was as clean as possible.

Department of Geology, University of Minnesota, on material carefully purified by the writer are presented in Table 8. Pure chloritoid was separated from the rock by crushing to at least −100 mesh, sieving, washing, drying, and then obtaining a chloritoid concentrate with the aid of a Frantz Isodynamic Magnetic Separator. At this point all the concentrates except that from Chibougamau, Quebec, were treated with a hot concentrated solution of ammonium citrate in order to remove hydrated iron oxide coatings.[1] These concentrates were then repeatedly centrifuged with Clerici solution. The specific gravity of the Clerici solution was changed by small amounts until a fraction as free from inclusions as possible was obtained, material both heavier and lighter than the chloritoid being eliminated. In order to detect transparent inclusions such as quartz it was necessary at almost every stage to mount samples of the concentrates in oil whose index of refraction was about 1·72 and to examine them with transmitted

[1] This part of the procedure was suggested by Dr. E. G. Zies. Throughout the separation procedure some oxidation of ferrous to ferric iron might be expected. The analyses (Table 8) show, however, that such oxidation is not a serious problem, the highest Fe_2O_3 content in the five analyses being only 2·52 per cent.

TABLE 5

Previously published analyses of chloritoid which are somewhat incomplete

	37	38	39	40	41	42	43	44	45	46	47	48
SiO_2	26·30	26·19	24·90	22·67	23·94	27·48	24·54	26·03	28·48	27·30	24·79	26·43
Al_2O_3	37·10	38·30	40·99	38·86	39·52	35·57	30·72	42·33	36·86	37·80	40·37	39·06
Fe_2O_3	–	6·00	0·55	2·98	–	–	17·28	4·09	–	6·85	–	–
FeO	25·92	21·11	24·28	25·46	28·05	27·05	17·30	14·32	21·88	20·82	25·87	19·58
MnO	0·93	–	–	–	0·52	0·30	–	–	0·97	–	tr.	1·70
MgO	3·66	3·30	3·33	1·96	0·80	4·29	3·75	7·30	2·80	0·93	0·17	4·26
CaO	–	–	–	0·93	0·45	–	–	0·35	0·59	–	0·43	–
H_2O	6·10	5·50	7·82	7·14	7·08	6·95	6·38	6·56	8·09	6·19	8·63	9·94
Rem.	–	–	–	–	tr.	–	–	tr.	0·69	–	–	–
	100·01	100·40	101·87	100·00	100·36	101·64	99·97	100·98	100·36	99·89	100·26	100·97
G	3·513	–	3·538	–	3·52	3·557	3·52	3·42	–	–	–	
	Atomic proportions											
Si	2·16	2·10	2·02	1·92	2·01	2·24	2·06	2·02	2·35	2·21	2·08	2·17
Al	3·59	3·63	3·91	3·88	3·91	3·42	3·04	3·88	3·59	3·61	4·00	3·78
Fe^{3+}	–	0·36	0·03	0·19	–	–	1·09	0·24	–	0·42	–	–
Fe^{2+}	1·78	1·42	1·64	1·81	1·97	1·85	1·21	0·93	1·52	1·41	1·82	1·35
Mn	0·06	–	–	–	0·04	0·02	–	–	0·07	–	0·00	0·12
Mg	0·45	0·40	0·40	0·25	0·10	0·52	0·47	0·85	0·35	0·11	0·02	0·52
OH	3·34	2·95	4·22	4·03	3·93	3·78	3·57	3·40	4·45	3·35	4·84	5·45
O	10·00	10·00	10·00	10·00	10·00	10·00	10·00	10·00	10·00	10·00	10·00	10·00

37. Leeds, Megantic County, Quebec, Canada. Hunt (1861). Milne (1949) gives 3·528 as the measured specific gravity of chloritoid from the Harvey Hill Mine, Megantic County, Quebec.
38. Pregratten, Tirol, Austria. von Kobell (1854). Von Kobell attributes the high SiO_2 content to fine quartz inclusions.
39. Pregratten, Tirol, Austria. Tschermak & Sipöcz (1879, p. 508). Analyst: Sipöcz. In spite of performing the analysis in triplicate the high total could not be reduced.
40. Blackbird District, Lemhi County, Idaho, U.S.A. Shannon (1926). The analysis was corrected for 3 per cent cobaltiferous arsenopyrite and recalculated to 100 per cent by Shannon. CaO has been omitted from the calculations.
41. Gumuch-dagh, Turkey. Smith (1851). The analysed chloritoid was obtained without much difficulty from a well-crystallized specimen and was perfectly pure. For the analysis the chloritoid was decomposed by means of Na_2CO_3. Rem. is TiO_2. CaO has been omitted from the calculations.
42. Kossoibrod, Ural Mountains, U.S.S.R. Rose (1837). Analyst: von Bonsdorff. Fiedler (1832) gives 3·55 as the measured specific gravity of chloritoid from Kossoibrod.
43. Kossoibrod, Ural Mountains, U.S.S.R. Hermann (1851).
44. St. Marcel, Piedmont, Italy. Tschermak & Sipöcz (1879, p. 511). Analyst: Suida. Rem. is Na_2O+K_2O. CaO has been omitted from the calculations.
45. Kaisersberg, Steiermark, Austria. von Foullon (1883, p. 226). Thoulet's solution (G = 3·165) was used to separate the chloritoid from the rock which had previously been treated with HF for several hours at 40° to 50° C and sieved through 1-mm openings. Zircon was removed from this chloritoid by stirring and decanting the more slowly settling chloritoid. Ignition of a sample of the chloritoid concentrate revealed that it contained a colourless mineral in addition to chloritoid. This analysis is the average of two. Alkalis were absent. Rem. is organic substance. CaO and the organic substance have been omitted from the calculations.
46. Tarapaka, Krivoy–Rog, Ukraine, U.S.S.R. Tarasenko (1925).
47. Kitakami Area, Japan. Seki (1954, p. 234). Analyst: Kido. H_2O was determined as loss on ignition. CaO has been omitted from the calculations.
48. Taunus Mountains, Germany: von der Marck (1878, p. 260). The analysis was performed on the part of a mixture of chloritoid and albite soluble in H_2SO_4. The soluble part contained no alkalis.

light. Such inclusions cannot be distinguished from chloritoid in reflected light under a stereomicroscope. After the heavy liquid separation the Frantz separator was again used to remove some remaining impurities. Photomicrographs of samples of the analysed material for each of the five chloritoids are given in Fig. 1 A–E in order to demonstrate the character of the inclusions remaining. Comparison of these figures with those of some analysed plagioclases (Emmons *et al.*, 1953, plates 1 and 2) shows that these five chloritoids are of acceptable purity.

TABLE 6

Previously published analyses of chloritoid which were made on impure material

	49	50	51	52	53	54	55	56	57	58	59	60	61	62	63
SiO_2	31·40	43·52	43·34	42·48	41·65	40·55	42·93	39·40	29·5	29·28	32·27	25·50	44·79	37·87	33·200
TiO_2	0·54	—	—	—	—	—	—	—	1·2	0·86	0·89	1·88	—	—	—
Al_2O_3	35·29	23·89	24·63	29·29	29·47	30·80	29·60	29·61	38·1	37·98	33·87	38·69	29·71	31·12	29·000
Fe_2O_3	3·21	—	—	3·30	4·02	3·82	0·86	4·43	2·3	2·32	5·14	—	—	3·25	—
FeO	20·39	16·81	16·72	12·11	17·87	12·46	15·43	15·36	21·5	21·97	19·82	27·19	20·75	20·48	25·938
MnO	1·36	8·03	8·18	6·10	0·93	6·51	3·75	3·67	0·2	0·29	—	—	—	0·62	6·000
MgO	2·43	—	—	2·05	1·57	0·45	2·12	1·71	1·6	1·28	1·16	0·08	0·62	1·44	0·240
CaO	tr.	—	—	tr.	—	1·29	—	0·12	tr.	tr.	0·28	0·40	—	tr.	—
H_2O	5·99	5·63	5·66	5·07	5·84	—	5·48	5·86	5·6	6·04	6·36	6·67	4·93	5·80	4·000
Rem.	—	—	—	—	—	—	—	—	—	—	0·78	—	—	—	—
	100·61	97·88	98·53	100·40	101·35	95·88	100·17	100·16	100·0	100·02	100·57	100·41	100·80	100·58	98·374
G	3·40–3·47	4·40	4·40	—	3·266	3·266	3·25	3·318	—	3·45	3·5	—	3·26	3·40	3·450

	64	65	66	67	68	69	70	71	72	73	74	75	76	77	78
SiO_2	32·68	38·40	39·13	41·67	42·1	37·47	39·79	35·52	30·61	30·02	31·75	28·49	33·21	24·36	28·96
TiO_2	—	—	—	—	—	—	0·85	—	0·00	tr.	—	1·02	0·80	2·47	0·53
Al_2O_3	26·38	23·68	27·60	23·81	32·39	33·00	31·62	29·53	36·06	34·70	36·20	40·51	40·81	38·43	33·56
Fe_2O_3	18·95	17·52	—	27·38	—	—	5·49	5·85	—	4·76	3·03	3·06	1·56	4·13	8·43
FeO	16·17		26·74	—	21·60	23·45	13·07	22·38	23·82	20·54	22·38	17·56	12·48	20·14	19·05
MnO	0·00	—	4·45	—	tr.	—	—	—	0·37	1·42	0·24	0·45	0·32	0·63	0·93
MgO	1·32	8·96	0·43	—	1·20	0·52	2·09	0·76	1·21	1·71	0·06	2·56	3·72	1·90	1·82
CaO	—	—	—	—	—	—	0·78	1·38	0·22	1·17	tr.	0·49	tr.	0·29	0·32
H_2O	4·50	4·80	3·26	7·14	4·6	5·58	5·94	5·94	6·66	6·71	4·47	6·26	5·78	6·63	6·70
Rem.	—	6·80	—	—	—	—	0·25	tr.	1·05	—	1·30	0·21	0·11	0·03	0·08
	100·00	100·16	101·61	100·00	101·89	100·02	99·88	101·36	100·00	101·03	99·43	100·61	98·79	99·01	100·38
G	3·46	2·889	—	—	3·6	3·6	3·387	—	3·561	3·60	—	3·48	3·39	—	—

49. Collier Bay, Yampi Sound, Western Australia. Simpson (1915, p. 76). The chloritoid analysed contained quartz and rutile inclusions.
50 and 51. Ottré, Belgium. Des Cloizeaux & Damour (1842). Analyst: Damour. The chloritoid crystals were separated from the enclosing schist even though they were held with great adherence. Renard and de la Vallée Poussin (1879) doubted the reliability of Damour's analyses because of the difficulty of freeing the chloritoid crystals from their high content of microscopical inclusions. Hunt (1861) believed the values given for *G* to be typographical errors.
52. Ottré, Belgium. Renard (1882). Analyst: Klement.
53. Serpont, Belgium. Renard (1882). Analyst: Klement. The analysed chloritoid contained quartz inclusions.
54. Lierneux, Belgium. Renard (1882). The analysed chloritoid contained quartz inclusions. An accident prevented the determination of H_2O.
55. Ottré, Belgium. Manasse (1911, p. 34). A thin section showed that the chloritoid was filled with inclusions of quartz, magnetite, and ilmenite.
56. Ottré, Belgium. Koch (1935). The analysed chloritoid was concentrated by means of Clerici solution and examined under the microscope. *G* was determined with Clerici solution.
57. Dutchess County, New York, U.S.A. Barth & Balk (1934, p. 346). Analyst: Barth. The analysed chloritoid contained inclusions of quartz, muscovite, garnet, and opaque dust-like particles. H_2O was determined by difference.
58. Womble Mine, North Carolina, U.S.A. Stuckey (1926). A chloritoid concentrate was obtained by crushing the rock to −70 mesh and using Thoulet solution. This concentrate is stated to contain less than 1 per cent impurities. Chloritoid from the same locality and stated to be typical of that analysed was collected for the writer by Dr. J. L. Stuckey. A chloritoid concentrate of this material obtained by a procedure similar to that used by Stuckey would contain at least 5 per cent quartz and opaque inclusions (Plate 1, fig. B).
59. Alp de Nadèls, Graubünden, Switzerland. Niggli (1912, p. 20). Chloritoid was separated from the pulverized rock by means of a magnet and with both Thoulet and Rohrbach solutions ($G = 3{\cdot}5$). The chloritoid obtained was checked with a magnifying glass and found to have adhering fragments of sericite and quartz. Rem. is $Na_2O + K_2O$, 0·60; H_2O^-, 0·18. Niggli was uncertain about the reliability and meaning of his analysis because of the impurities.
60. Grossarl, Pongau, Austria. Cathrein (1887). This analysis is of the part soluble after the following treatment. A chloritoid concentrate was treated in H_2SO_4, evaporated to dryness, treated with HCl and filtered. The residue was treated with NaOH, thereby rendering the combined SiO_2 soluble. The remaining residue amounted to 33·06 per cent of the original concentrate and consisted of scales, quartz, rutile, and leucoxene.
61. Vénasque, Pyrénées, France. Damour (1879). The analysed chloritoid was too opaque for optical study.
62. Vénasque, Pyrénées, France. Manasse (1911, p. 40). The analysed chloritoid contained inclusions of quartz, magnetite, and tourmaline.
63. Natick, Rhode Island, U.S.A. Jackson (1840). Jackson's total is 99·974.
64. Natick, Rhode Island, U.S.A. Hermann (1851). *G* was determined by Kenngott and is given by Des Cloizeaux (1862, p. 465).
65. Sterling, Massachusetts, U.S.A. Thomson (1828, p. 47). The analysed material is bluish-grey, like plumbago, can be scratched with the fingernail, is sectile and occurs in thin bent plates. The iron content is given as 'peroxide of iron'. Thomson states that K_2O and MgO are

The atomic proportions were calculated according to a method of equivalents suggested by Stevens (1942) for the micas. The analyses in Tables 2, 3, 4, 5, 7, and 8 show that chloritoid contains about 24 per cent SiO_2 or 2 atoms of silicon per formula, $Fe_2Al_4Si_2O_{10}(OH)_4$. Only the analyses in Table 6 differ much from this amount. Most of these analyses were stated by the analysts to have been made on chloritoid that contained quartz and other inclusions. All the other analyses in Table 6 are suspected of having been made on impure chloritoid. Even analyses 56 and 75, which are stated to have been made on material that was checked for purity under the microscope, are suspect because the method of microscopic checking is not specified. As previously noted, in order to detect quartz inclusions in chloritoid, transmitted light is required. Inclusion-bearing chloritoid similar to that in Fig. 1 F and Plate 1, figs. A–D is almost certainly responsible for the analyses in Table 6. Some of the analyses approach the molecular ratios of $RO:R_2O_3:SiO_2:H_2O::1:1:2:1–2$. These ratios are, in fact, found in ferrocarpholite, a mineral described by de Roever (1951) from eastern central Celebes. Hence, one might suspect that some of the 'high-silica chloritoids' of Table 6 are really not chloritoid, but ferrocarpholite. However, the optical properties of ferrocarpholite are distinct from those of chloritoid. Furthermore, all those 'high-silica chloritoids' which were X-rayed (Table 16) were found to be mixtures of chloritoid and quartz.

The amount of TiO_2 which can be present in the chloritoid structure is uncertain. Chloritoid is generally associated with rutile, leucoxene, ilmenite, or sphene. As the complete separation of these minerals from chloritoid is very difficult, they account for most or all of the TiO_2 reported in chemical analyses of chloritoid. If titanium is actually present in the chloritoid structure, it will probably

---

extraneous. Hunt (1861) suspected the reliability of the analysis. Rem. is K_2O.

66. Mt. Blia, Wermland, Sweden. Igelström (1896*b*). The analysed material was dark, almost black and came from the cores of reddish-brown knots.
67. Mt. Blia, Wermland, Sweden. Igelström (1896*b*). The analysed material was light brownish red and occurred as rims on black cores. Fe_2O_3 includes Mn_2O_3.
68. Mt. Blia, Wermland, Sweden. Weibull (1896, p. 519). The analysed chloritoid was obtained by grinding the rock to −0·2 mm and treating with hot dilute HCl for 2 h. The concentrate so obtained contained 15 to 20 per cent kyanite and traces of dark material.
69. Mt. Blia, Wermland, Sweden. Weibull (1896, p. 520). The analysed chloritoid contained 20 per cent kyanite.
70. Gleinalp, Steiermark, Austria. Machatschki (1923). The analysed chloritoid contained inclusions of quartz, ilmenite, iron oxide, and carbonaceous material. *G* was adjusted from 3·387 to 3·571 by Machatschki to account for 19·62 per cent quartz, an amount obtained by various assumptions. H_2O includes C. Rem. is H_2O^-.
71. Michigamme Lake, Michigan, U.S.A. Hobbs (1895). Analyst: Kahlenberg. The analysed chloritoid contained inclusions of quartz and magnetite. Rem. is P_2O_5.
72. Mt. Maré, Transvaal, South Africa. Götz (1886, p. 145). The analysed chloritoid was separated from the rock by means of Thoulet solution. It contained rutile inclusions. This analysis was recalculated to 100 per cent by Götz after subtracting 2·66 per cent TiO_2. *G* was adjusted from 2·574 to account for the rutile inclusions. Rem. is Na_2O, 0·78; K_2O, 0·27.
73. Monte Fenouillet, Var, France. Manasse (1911, p. 37). The analysed chloritoid contained inclusions of quartz, iron oxide, rutile, and carbonaceous material.
74. Southern Jenissei District, Siberia, U.S.S.R. Meister (1910). The analysed chloritoid contained muscovite inclusions. H_2O was determined as l.o.i. Rem. is Na_2O, 0·32; K_2O, 0·98.
75. Crown Mines, Witwatersrand, South Africa. Frankel (1944). The analysed chloritoid was separated from the rock with a superpanner, heavy liquids, and an electromagnet. It was checked frequently for purity under the microscope. Rem. is Cr_2O_3.
76. Crown Mines, Witwatersrand, South Africa. Frankel (1944). The analysed chloritoid was separated in the same manner as that for analysis 75. It contained minute inclusions. Rem. is Cr_2O_3.
77. Ritten Hamar, Unst, Shetland Islands, Scotland. Snelling (1957, p. 472). Chloritoid was separated with some difficulty from the Saxa Vord schists. The analysed material contained a few magnetite and quartz inclusions, and some fine muscovite. Rem. is H_2O^-.
78. Red Man, near Stonehaven, Kincardineshire, Scotland. Snelling (1957, p. 472). Numerous quartz inclusions made the separation of a pure sample of this chloritoid impossible. Rem. is H_2O^-.

TABLE 7

Previously published analyses of chloritoid which are incomplete

	79	80	81	82	83	84	85	86	87	88	89	90	91	92	93	94	95	96	97	98
SiO_2	24·90	24	24·40	25·07	24·10	23·20	24·20	24·900	24·963	24·40	23·01	28·27	24·1	24·10	24·10	25·75	25·50	28·04	25·70	25·17
Al_2O_3	40·36	26	42·80	38·69	39·8	40·21	40·46	46·200	43·833	45·17	40·26	32·16	43·2	40·71	41·56	37·50	38·13	36·19	36·95	34·70
FeO	26·17	26	19·17	25·30	27·55	27·25	24·24	28·890	31·204	30·29	27·40	33·72	23·8	27·10	27·10	21·00	23·58	29·79	23·44	34·04
MgO	2·54	20	6·17	0·08	—	0·95	2·60	—	—	—	3·97	0·13	—	—	—	6·20	5·19	1·25	6·12	0·57
H_2O	6·23	4	6·90	6·67	6·5	6·97	7·30	0·004	—	—	6·34	5·00	7·6	7·24	7·24	7·80	6·90	5·88	6·31	4·30
Rem.	—	—	—	—	0·30	0·83	—	tr.	tr.	—	—	—	tr.	—	—	0·50	—	0·20	0·59	0·14
	100·20	100	99·44	95·81	98·25	99·41	98·80	99·994	100·000	99·86	100·98	99·28	98·7	99·15	100·00	98·75	99·30	101·35	99·11	98·92
G	—	—	3·32–3·40	—	3·52	3·52	3·46	—	—	—	—	—	3·565	—	—	3·5	3·49	3·45	—	3·5

79. Ile de Groix, Morbihan, France. Barrois (1884*a*). Analyst: Renard. Barrois (1884*b*) noted that Renard analysed large chloritoid crystals from veins.
80. Ottré, Belgium. Davreaux (1833). Analyst: Vauquelin. This analysis was performed in 1812. The results have been doubled to bring the total to 100 instead of 50 as given. Iron and manganese oxides were given as 13; loss on ignition as 2.
81. Zermatt, Wallis, Switzerland. Des Cloizeaux (1884). Analyst: Damour.
82. Grossarl, Pongau, Austria. Cathrein (1887). This is analysis 60, Table 6, after Cathrein subtracted 0·40 per cent CaO, 0·59 per cent TiO_2, 0·43 per cent SiO_2 for titanite, and 1·89 per cent FeO, 1·29 per cent TiO_2 for iron oxides and rutile, all of which were present as inclusions.
83. Gumuch-dagh, Turkey. Smith (1851). Pure chloritoid, obtained without much difficulty from a well-crystallized specimen, was prepared for analysis by decomposing it with H_2SO_4. Rem. is $Na_2O + K_2O$.
84. Gumuch-dagh, Turkey. Smith (1851). Pure chloritoid, obtained without much difficulty from a well-crystallized specimen, was prepared for analysis by decomposing it with Na_2CO_3. Rem. is TiO_2, trace; CaO, 0·83.
85. El Cardoso, Spain. Recarte (1951). *G* was determined by Quiroga (1879).
86. Kossoibrod, Ural Mountains, U.S.S.R. Erdmann (1835). Hermann (1851) noted that it was customary at the Kossoibrod emery mines to burn the emery before shipment. Diaspore and chloritoid were sorted out after burning and left in dumps at the mines. He suggested that this treatment may have accounted for the absence of water in analyses 86, 87, and 88. The chloritoid was decomposed by fusing with K_2CO_3. Rem. is MnO.
87. Kossoibrod, Ural Mountains, U.S.S.R. Erdmann (1835). The chloritoid for analysis was dried and fused with Na_2CO_3. Al_2O_3 was obtained by difference. Rem. is MnO.
88. Kossoibrod, Ural Mountains, U.S.S.R. Erdmann (1845, p. 456). Analyst: Gerathewohl. Insignificant traces of water were given off during the analysis.
89. Kossoibrod, Ural Mountains, U.S.S.R. von Kobell (1853). Rusty stains were removed from the analysed material with HCl.
90. Natick, Rhode Island, U.S.A. Whitney (1849).
91. St. Marcel, Piedmont, Italy. Delesse (1843). The separation of chloritoid from the gangue was difficult. Rem. is TiO_2.
92. St. Marcel, Piedmont, Italy. Delesse (1846*a*). The analysed chloritoid was very pure.
93. St. Marcel, Piedmont, Italy. Delesse (1846*b*). The analysed chloritoid was very pure. Al_2O_3 was obtained by difference.
94. St. Marcel, Piedmont, Italy. von Kobell (1853). Rem. is undecomposed material.
95. St. Marcel, Piedmont, Italy. Des Cloizeaux (1884). Analyst: Damour.
96. Hetzschen, Vogtland, Germany. Schröder (1884). Rem. is CaO. FeO includes some TiO_2.
97. Murlo Canal, Apuane Alps, Tuscany, Italy. Manasse (1906, p. 28). The analysed chloritoid contained a few inclusions of quartz, magnetite, ilmenite, and rutile. Only 0·1920 g was available for analysis. All the iron was calculated as FeO. H_2O was determined as loss on ignition. Rem. is TiO_2.
98. Lainiciu, Juil Valley, District of Gorjiu, Rumania. Duparc & Mrazec (1893). The analysed chloritoid was separated from the rock using a magnet and methylene iodide. It contained some haematite. Rem. is CaO.

TABLE 8

New analyses of chloritoid

	99	100	101	102	103
SiO_2	24·84	24·00	24·30	23·91	24·49
TiO_2	0·61	0·05	0·18	0·20	0·30
Al_2O_3	38·71	40·30	39·92	40·12	39·18
Fe_2O_3	2·42	2·52	1·80	1·23	1·99
FeO	20·51	25·13	25·63	27·06	25·75
MnO	4·50	0·09	0·41	0·16	0·17
MgO	1·41	1·23	0·77	0·51	1·13
CaO	0·06	0·10	0·09	0·04	0·10
Na_2O	0·02	0·00	0·01	0·00	tr.
K_2O	0·04	0·00	0·06	tr.	tr.
H_2O^+	6·87	6·90	6·86	7·03	6·84
H_2O^-	0·03	0·00	0·07	0·01	0·00
F	0·04	0·01	0·05	0·01	0·01
	100·06	100·33	100·15	100·28	99·96
Less O ≡ F	0·02		0·02		
	100·04		100·13		
	Atomic proportions				
Si	2·07	1·99	2·02	2·00	2·04
Al	3·80	3·93	3·92	3·95	3·85
Fe^{3+}	0·15	0·16	0·11	0·08	0·12
Fe^{2+}	1·43	1·74	1·78	1·89	1·80
Mn	0·32	0·01	0·03	0·01	0·01
Mg	0·18	0·15	0·10	0·06	0·14
OH	3·82	3·81	3·81	3·92	3·81
F	0·01	0·00	0·01	0·00	0·00
O	10·00	10·00	10·00	10·00	10·00

99. Salm-Château, Belgium. Analyst: C. O. Ingamells. Collected by Dr. Jean Michot. The rock from which this chloritoid came is in the northerly B formation shown in Fig. 2 of Michot (1954–5, p. M6). Sample No. 19*M*.

100. Üstüaçiksarinç, Turkey. Analyst: Eileen H. Oslund. Given to the writer by Dr. Hans P. Eugster who had obtained it from Dr. Togan S. Önay. See Önay (1949, p. 383). Sample No. 11.

101. Siderite Hill Showing, Chibougamau, Quebec, Canada. Analyst: Eileen H. Oslund. Collected by Dr. Gilles Allard, a few inches away from a siderite vein in meta-anorthosite. Sample No. 12.

102. Natick, Rhode Island, U.S.A. Analyst: Eileen H. Oslund. From the mineralogical collection of The Johns Hopkins University, No. 466R. Sample No. 21*a*.

103. Michipicoten District, Ontario, Canada. Analyst: Eileen H. Oslund. Collected by Dr. William A. Jarvis from altered acidic volcanic rocks which form the hanging wall of the Helen Mine. Sample No. 42.

have octahedral coordination and occur by substitutions such as $Ti \rightarrow 2Fe^{2+}$ or $3Ti \rightarrow 4Al$. These substitutions result in vacant sites in the octahedrally coordinated layers of the chloritoid structure. Vacancies may exist, but many vacancies of this type will cause the chloritoid structure to be distorted. The new chemical analyses indicate that the maximum amount of TiO_2 in chloritoid is less than 0·6 per cent and probably less than 0·2 per cent or about 0·01 Ti atoms per formula. The actual amount in any chloritoid depends on the conditions under which that chloritoid was formed. Because TiO_2 enters the chloritoid structure to such a small extent, if at all, it has been omitted in calculating the atomic proportions from the analyses. Such omissions cause no significant changes in the calculated atomic proportions.

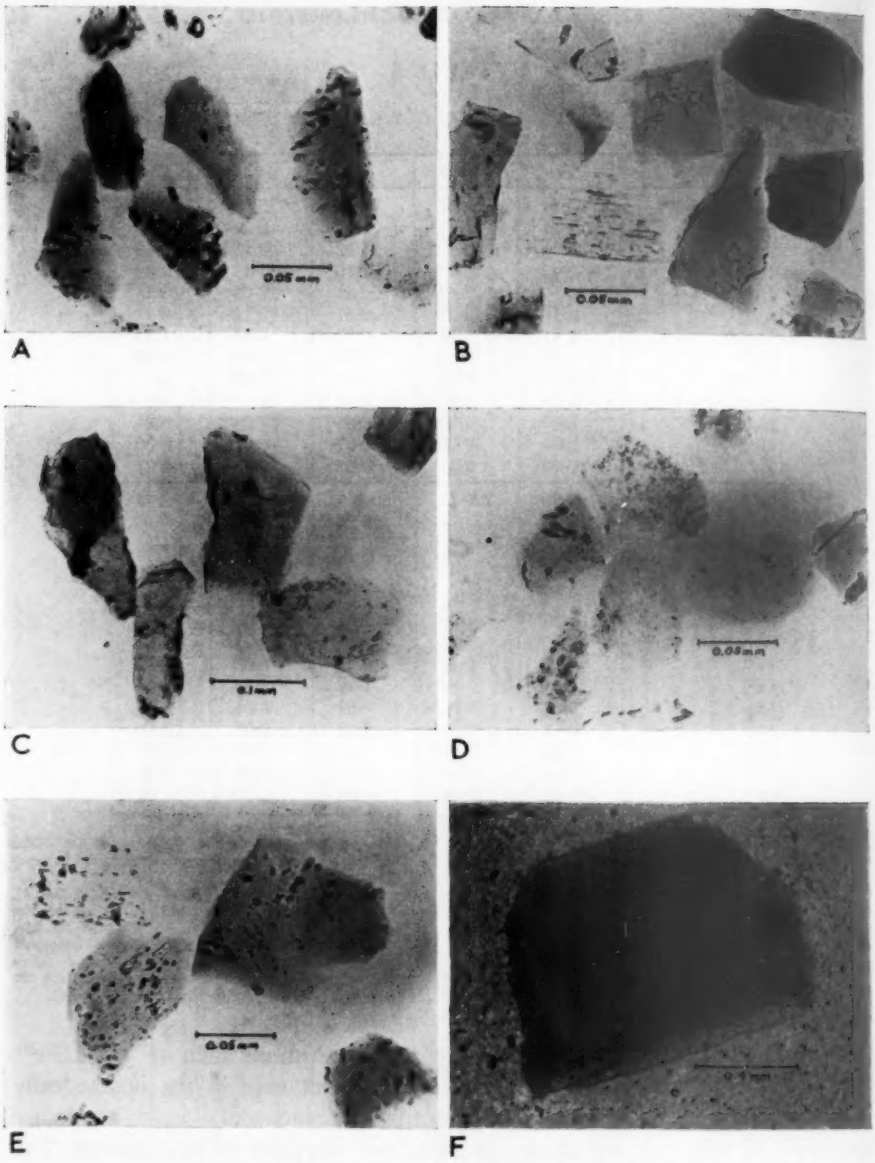

FIG. 1. A–E. Grain samples of chemically analysed chloritoids mounted in oil, whose index of refraction is 1·73. Transmitted plane polarized light. A, Salm-Château, Belgium (anal. 99, Table 8). Grains are 270–325 mesh. Impurities are quartz, haematite, and rutile. B, Üstüaçiksarinç, Turkey (anal. 100, Table 8). Grains are 200–325 mesh. Impurity is rutile. C, Chibougamau, Quebec, Canada (anal. 101, Table 8). Grains are 100–200 mesh. Impurities are quartz, ilmenite, and leucoxene. D, Natick, Rhode Island, U.S.A. (anal. 102, Table 8). Grains are 200–325 mesh. Impurities are ilmenite and muscovite. E, Michipicoten District, Ontario, Canada (anal. 103, Table 8). Grains are 200–270 mesh. Impurities are quartz, magnetite, and leucoxene.

FIG. 1. F. Inclusion-bearing chloritoid crystal in a groundmass of quartz, chlorite, muscovite, and haematite from Ottré, Belgium. Two sides of the crystal are relatively free from inclusions, whereas the central part is crowded with them, particularly within the hour-glass which is faintly visible. The inclusions are mostly quartz and haematite. Transmitted plane polarized light.

Solid solution in natural chloritoids occurs chiefly by the following substitutions: $Fe^{3+} \rightarrow Al$, $Mg \rightarrow Fe^{2+}$, $Mn \rightarrow Fe^{2+}$. In addition, partial oxidation of Fe^{2+} can take place probably by $2Fe^{3+} \rightarrow 3Fe^{2+}$ or $Fe^{3+} \rightarrow Fe^{2+}H$ as suggested by Yoder (1957). The extents of some of these substitutions are shown in Figs. 2 and 3. In Fig. 2 each triangle represents one chemical analysis. The corners of these triangles are the number of atoms in the mixed octahedral layer, $[(Fe^{2+}, Mg, Mn)_2(Al, Fe^{3+})]$, of the structure determined by Harrison & Brindley (1957), $[(Fe^{2+}, Mg, Mn)_2(Al, Fe^{3+})](OH)_4Al_3[O_2(SiO_4)_2]$ (see section on polymorphism). The size of each triangle indicates the difference between the ideal number of atoms per formula in the mixed layer and the number obtained from the corresponding chemical analysis. Hence, the size of each triangle provides an inverse measure of the reliability of each analysis. Ideally each analysis should plot as a point on the dashed line in Fig. 2. Deviations from this line can be explained as due partly to impurities in the analysed material and partly to partial oxidation of ferrous iron. In Fig. 3 the two analyses showing the highest MnO contents, 16·63 and 7·14 per cent (anal. 16, 17; Table 3) were made on impure chloritoid. In these analyses, allowance was made for quartz impurities but not for other impurities, such as pyrolusite, manganese-bearing carbonate, or manganiferous ilmenite. These minerals are known to occur with chloritoid in the Ardennes of Belgium and France (De Dycker, 1938–9, pp. M55–62; Renard, 1882–4, p. 265). Hence, it is uncertain if any natural chloritoid approaches the Mn end-member (i.e. ottrelite) in composition.

The small amounts of CaO shown in many analyses are probably due to inclusions such as apatite, sphene, or lime-bearing carbonate; an example of the last is analysis 22, Table 3 (see Plate 1, fig. C).

The small amounts of alkalis determined by some analysts are most likely present in inclusions of muscovite or paragonite, or both. These minerals are commonly associated with chloritoid. Some of the analyses in Table 4, however, show amounts of CaO, Na_2O, or K_2O which cannot easily be explained by the presence of impurities in the analysed material. New chemical data from two of these specimens have been obtained. Chloritoid was carefully separated from a specimen from Crestlianderstobel, Switzerland, by means of the Frantz magnetic separator and Clerici solution in the manner described previously. This specimen was sent by Professor C. Burri and was part of the original material described by Friedlaender (1929). The alkali content of this chloritoid was kindly determined by Dr. P. M. Orville with a flame photometer. The results showed less than 0·02 per cent Na_2O and less than 0·05 per cent K_2O. Analysis 26, Table 4, however, shows 1·21 per cent Na_2O and 0·46 per cent K_2O. Friedlaender, when referring to this chloritoid, wrote (p. 259): 'Das Material war mikroskopisch rein, frei von Einschlüssen und konnte leicht isoliert werden.' Analysis 100, Table 8, was made during this study on chloritoid from Üstüaçiksarinç, Turkey. A sample of chloritoid broken from the material described by Önay (1949, p. 383) was given to the writer by Dr. H. P. Eugster. This sample consists of coarse chloritoid

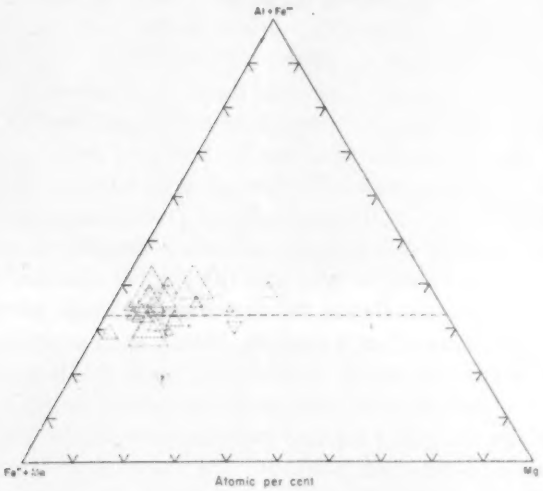

FIG. 2. Chemical composition of natural chloritoids showing variations in the mixed octahedral layer, $[(Fe^{2+}, Mg, Mn)_2(Al, Fe^{3+})]$, of the structure. Chemical analyses from Table 2 are shown with dashed lines, from Table 3 with alternate dashes and dots, from Table 5 with dots, and from Table 8 with full lines.

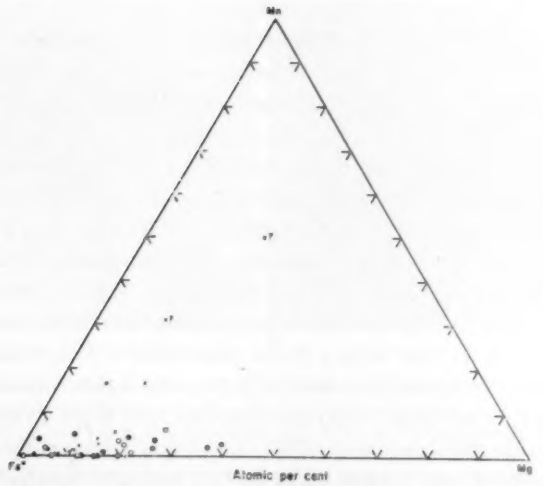

FIG. 3. Chemical composition of natural chloritoids showing variations in Fe^{2+}, Mg, and Mn. Chemical analyses from Table 2 are indicated by crosses in circles, from Table 3 by crosses, from Table 5 by open circles, and from Table 8 by filled-in circles.

intergrown with fine kaolinite and haematite, all adhering to massive brown calcite. The results of this new analysis indicate that analysis 30, Table 4, was probably made on an impure sample of chloritoid from this locality. There appears to be no convincing evidence that chloritoid actually contains more than traces of CaO, Na_2O, or K_2O.

Ideally, chloritoid contains 4 OH groups per formula, corresponding to about 7 per cent H_2O. The water content in many of the analyses in Tables 2, 3, 5, and 8 is less than, but approaches, this amount. This deficiency may be explained by the oxidation of part of the ferrous iron according to the substitution $Fe^{3+} \rightarrow Fe^{2+}H$. The analyses in Table 8 show that the substitution $F \rightarrow OH$ occurs only to a very small extent in chloritoid.

The preceding data indicate that the simple chemical formula for chloritoid may be written $FeO \cdot Al_2O_3 \cdot SiO_2 \cdot H_2O$ with the following ranges in the amounts of substitution.

Substitution	*Range in per cent*
$Mg \rightarrow Fe^{2+}$	0–42
$Mn \rightarrow Fe^{2+}$	0–17
$Fe^{3+} \rightarrow Al$	0–14
$F \rightarrow OH$	0–0·25

The upper limits for these substitutions have been calculated from the atomic proportions in Tables 2, 3, 5, and 8. That for the substitution $Fe^{3+} \rightarrow Al$ has been obtained by assuming that all the ferric iron is replacing aluminium. Too many assumptions are required to allocate the ferric iron among other substitutions such as $Fe^{3+} \rightarrow Fe^{2+}H$ and $2Fe^{3+} \rightarrow 3Fe^{2+}$. These limits may not represent the maximum possible amounts of substitutions, as chloritoids with greater amounts of substitutions may yet be found.

POLYMORPHISM

Previous observations

The platy habit of chloritoid was noted by Fiedler (1832, p. 327) in the type locality near Kossoibrod. The plane of the plates has long been designated (001) in accord with the setting generally adopted for platy minerals. Chloritoid has perfect cleavage parallel to (001). Plates resulting from this cleavage are irregular in shape or are bounded by poor cleavages whose traces on (001) form rhombs, hexagons, or triangles with angles of about 60° and 120°. These polygons have been observed and their angles measured by many mineralogists including Tschermak & Sipöcz (1879, p. 506), von Foullon (1883, p. 207), von Lasaulx (1883, p. 270), Barrois (1884*a*), Des Cloizeaux (1884), Lane & Keller (1891), Hobbs (1895), Manasse (1906), de Rauw (1912), Souza-Brandão (1914), Tschopp (1923–4, p. 118), and Recarte (1951). This hexagonal character has been clearly shown by Rosenbusch by means of etch figures (Mügge, 1927, p. 615). Most of these investigators followed Tschermak & Sipöcz (1879) and chose an $a:b$ ratio similar to that in muscovite, and hence concluded that these cleavages were

(110), (010), and ($\bar{1}$10). Milne (1949), however, found from single-crystal X-ray studies that the $a:b$ ratio was the reciprocal of that in muscovite, and that two of these poor cleavages are of the type (*hhl*). The third cleavage is then of the type (*h*0*l*) and not (010) as previously thought. Renard & de la Vallée Poussin (1879) noted two other cleavages, intersecting at 129° to 133°, and a third normal to one of these.

Chloritoid has been considered monoclinic by some mineralogists and triclinic by others on the bases of goniometric measurements,[1] the angles between the traces of cleavages measured in basal sections, and extinction angles measured in various known orientations (see, for example, Delesse, 1846*a*; Des Cloizeaux, 1862, p. 463, and 1884; Tschermak & Sipöcz, 1879; Renard & de la Vallée Poussin, 1879; Lacroix, 1886; Lane & Keller, 1891; Weibull, 1896). These methods are generally not very satisfactory because of the high dispersion of most chloritoids, the poor quality of cleavages other than (001), the almost ubiquitous presence of polysynthetic twinning (whose composition plane is parallel to (001)), and the tendency for the basal plates of some chloritoids to curve. Nevertheless, studies by Barrois (1884*a*), Corin (1929), and van der Plas (van der Plas *et al.*, 1958) on the orientation of the optical indicatrix support the conclusion that chloritoid exists in both monoclinic and triclinic polymorphs.

Barrois (1884*a*) in a study of the chloritoid from Ile de Groix, France, found that when changing from blue to red light, Y and Z varied from 8° to 28° in a plane that bisected the acute angle between the traces of the 120° cleavages, whereas X was always contained in (001) and the plane bisecting the obtuse angle between the traces of the 120° cleavages. From this he concluded that X must be fixed by symmetry and, hence, that this chloritoid was monoclinic with $X = b$.

Corin (1929) measured the optic orientation of eight chloritoids from unspecified localities and of two from the Ardennes of Belgium. He found that X lies in (001) for the eight unspecified chloritoids, whereas no optic direction lies in (001) for the two from the Ardennes. He concluded that the eight unspecified chloritoids may well be monoclinic with $X = b$, but that the two from the Ardennes are triclinic.

Van der Plas (van der Plas *et al.*, 1958) used a universal stage to measure the optic orientation in chloritoid from Hennensädel, Switzerland. He found that in some twin lamellae X lies in (001), but in others no optic direction lies in (001). He considered the former monoclinic and the latter triclinic, and confirmed these conclusions by X-rays.

Other optical studies concerning the polymorphism of chloritoid are summarized with the optical properties in Table 19.

[1] See Milne (1949, p. 424) for an attempt to correlate early measurements of interfacial angles with those calculated from X-ray data. Naha (1955*a*) recently reported (001)$\wedge(1\bar{1}0) = 84°\ 20'$. No chloritoid specimen studied by the writer had faces or cleavages except (001) suitable for optical goniometry.

Previous X-ray studies

Single-crystal methods. Barth (1936, p. 796) made the first X-ray study of chloritoid. He confirmed his earlier contention (Barth & Balk, 1934) that chloritoid from Dutchess County, New York, was monoclinic but gave no details on the methods used nor any of the data.

Machatschki & Mussgnug (1942) chose a unit cell for chloritoid from an unspecified locality with *a*- and *b*-axes similar in length to those in muscovite (see Table 9). They did not, however, completely define the unit cell, nor did they make any statement about the symmetry. Nevertheless, they proposed a crystal structure similar to that of muscovite.

Milne (1949) established a monoclinic unit cell (Table 9) for a chloritoid crystal from Megantic County, Quebec. Systematically absent reflections restricted the possible space groups to $C2/c$ and Cc.

TABLE 9

Unit cells of monoclinic chloritoid

Cell dimensions are in Å

	Machatschki & Mussgnug, 1942	*Milne, 1949*	*Harrison & Brindley, 1957*	*Halferdahl, this study*
Locality	not specified	Harvey Hill Mine, Quebec	Ile de Groix, France	Natick, Rhode Island
Space group	—	*C2/c* or *Cc*	*C2/c*	*C2/c* or *Cc*
a	5·4	9·45	9·52±0·02	9·50±0·03
b	9·4	5·48	5·47±0·01	5·50±0·02
c	—	18·16	18·19±0·04	18·22±0·05
d (001)	17·85	—	—	—
β	—	101° 30′	101° 39′±25′	101° 57′±5′
Technique	not specified	Rotation and Weissenberg	Rotation and Weissenberg	Precession

Brindley & Harrison (1952) in a paper presenting preliminary data on the crystal structure of chloritoid from Ile de Groix, France, confirmed Milne's unit cell and established the space group $C2/c$. These authors (Harrison & Brindley, 1957) have since refined their earlier structure. Briefly their structure consists of two close-packed layers in which the metal atoms have octahedral coordination. One of these layers is similar to the layers in corundum and contains aluminium atoms. The other is similar to the layers in brucite and contains aluminium, ferrous iron, and magnesium atoms. These layers are joined by SiO_4 tetrahedra and by hydrogen bonds. The SiO_4 tetrahedra do not share any corners with each other as in the micas but are present as individual groups. An additional oxygen atom lies in the centre of the hexagons formed by the oxygen atoms of the SiO_4 tetrahedra. The structural formula is written

TABLE 10

Possible unit cells of triclinic chloritoid

Cell dimensions are in Å. Cells 1, 2, 3, and 5 refer to chloritoid from Chibougamau, Quebec, Canada; cell 4, to chloritoid from Ile de Groix, France

	C-centred cells				*Delaunay primitive cell*
	1	2	3	4	5
a	9·50±0·03	9·49	9·50	9·52	5·48
b	5·48±0·02	5·48	5·48	5·47	9·16
c	9·16±0·03	9·16	9·16	9·15	5·48
α	96° 54′±5′	96° 44′	103° 44′	96° 21′	96° 44′
β	101° 49′±5′	101° 55′	89° 55′	101° 35′	120° 2′
γ	90° 2′±5′	90° 3′	90° 1′	90° 0′	96° 54′
Transformation matrix to obtain cell from cell 1	1 0 0 0 1 0 0 0 1	$\frac{1}{2}$ $\frac{3}{2}$ 0 $\frac{1}{2}$ $\frac{1}{2}$ 0 0 0 $\bar{1}$	$\frac{1}{2}$ $\frac{3}{2}$ 0 $\frac{1}{2}$ $\frac{1}{2}$ 0 0 0 1	— — —	0 0 1 $\frac{1}{2}$ $\frac{1}{2}$ 0 0 1 0

TABLE 11

Coordinates of atoms in decimal fractions of the axial lengths of monoclinic chloritoid from Ile de Groix, France (after Harrison & Brindley, 1957), and those of triclinic chloritoid derived from them by means of the transformation matrix $100/01\frac{2}{3}/002$. *For the triclinic coordinates the origin has been shifted to* $0, -\frac{1}{10}, \frac{1}{4}$ *of the monoclinic cell, and* $\frac{1}{2}$ *has been added to* z_T

Chemical analyses show that the OH positions are 85 per cent filled in this monoclinic chloritoid (anal. 79, Table 7), and 95 per cent filled in this triclinic chloritoid (anal. 101, Table 8)

	Monoclinic chloritoid C2/c (Harrison & Brindley, 1957) Coordinates of equivalent positions $(0, 0, 0; \frac{1}{2}, \frac{1}{2}, 0)\pm\|x, y, z; \bar{x}, y, \frac{1}{2}-z\|$				*Triclinic chloritoid C$\bar{1}$ Coordinates of equivalent positions* $(0, 0, 0; \frac{1}{2}, \frac{1}{2}, 0)\pm\|x, y, z\|$			
Atom	*No. of atoms*	x_M	y_M	z_M	*No. of atoms*	x_T	y_T	z_T
O_1	8	$0{\cdot}069_5$	$0{\cdot}085_3$	$-0{\cdot}065_9$	4	$0{\cdot}069_5$	$0{\cdot}058_9$	$0{\cdot}368_2$
O_{2a}	8	$0{\cdot}105_0$	$0{\cdot}347_5$	$-0{\cdot}186_1$	4	$0{\cdot}105_0$	$0{\cdot}273_1$	$0{\cdot}127_5$
O_{2b}	8	$0{\cdot}105_0$	$0{\cdot}847_5$	$-0{\cdot}186_1$	4	$0{\cdot}105_0$	$0{\cdot}773_1$	$0{\cdot}127_5$
O_{3a}	8	$-0{\cdot}143_2$	$0{\cdot}098_1$	$-0{\cdot}196_6$	4	$-0{\cdot}143_2$	$0{\cdot}019_5$	$0{\cdot}106_9$
O_{3b}	8	$-0{\cdot}143_2$	$0{\cdot}598_1$	$-0{\cdot}196_6$	4	$-0{\cdot}143_2$	$0{\cdot}519_5$	$0{\cdot}106_9$
OH_1	8	$0{\cdot}105_5$	$0{\cdot}585_3$	$-0{\cdot}050_0$	4	$0{\cdot}105_5$	$0{\cdot}565_3$	$0{\cdot}400_0$
OH_2	8	$0{\cdot}233_0$	$0{\cdot}585_3$	$-0{\cdot}052_5$	4	$0{\cdot}233_0$	$0{\cdot}564_6$	$0{\cdot}396_0$
Si	8	$0{\cdot}033_9$	$0{\cdot}090_3$	$-0{\cdot}156_0$	4	$0{\cdot}033_9$	$0{\cdot}027_9$	$0{\cdot}188_9$
Al_a	4	0·0	$0{\cdot}403_6$	0·25	2	0·0	$0{\cdot}503_6$*	0·0
Al_b	8	$0{\cdot}250_0$	$0{\cdot}342_1$	$-0{\cdot}250_0$	4	$0{\cdot}250_0$	$0{\cdot}242_1$	$0{\cdot}000_0$
Ia	4	0·25	0·25	0·0	2	0·25	0·25	0·5
Ib	8	$0{\cdot}085_7$	$0{\cdot}750_0$	$0{\cdot}000_6$	4	$0{\cdot}085_7$	$0{\cdot}750_3$	$0{\cdot}501_2$
	$Ia = 0{\cdot}75\ Al+0{\cdot}25\ Fe^{2+}$ $Ib = 0{\cdot}5\ (1{\cdot}5\ Fe^{2+}+0{\cdot}3\ Mg)$				$Ia = 0{\cdot}92\ Al+0{\cdot}08\ Fe^{3+}$ $Ib = 0{\cdot}5\ (1{\cdot}78\ Fe^{2+}+0{\cdot}03\ Mn+$ $0{\cdot}10\ Mg+0{\cdot}03\ Fe^{3+})$			

* This value is not 0·5 as required by symmetry. The discrepancy may arise from the incompleteness of the chemical analysis (79, Table 7) used by Harrison & Brindley (1957). Only five constituents were determined (see section on chemical composition, p. 53). A value of 0·5 has been used in calculating the structure factors in Table 13.

$[(Fe^{2+},Mg)_2Al](OH)_4Al_3[O_2(SiO_4)_2]$. The atomic coordinates determined by Harrison & Brindley are given in Table 11.

TABLE 12

Calculation of c_T, α_T, and β_T from the y atomic parameters of monoclinic chloritoid

Atoms	*y*	$\frac{c_M \tan(\alpha_T-90)}{2b_M}$			*No. of atoms*	
O_1	$0{\cdot}085_3$	$2y$	$0{\cdot}170_6$	×	8	= 1·3648
Si	$0{\cdot}090_3$	$2y$	$0{\cdot}180_6$	×	8	= 1·4448
O_{2a}	$0{\cdot}098_1$	$2y$	$0{\cdot}196_2$	×	8	= 1·5696
Al_b	$0{\cdot}342_1$	$2y-\frac{1}{2}$	$0{\cdot}184_2$	×	8	= 1·4736
O_{2a}	$0{\cdot}347_5$	$2y-\frac{1}{2}$	$0{\cdot}195_0$	×	8	= 1·5600
Al_a	$0{\cdot}403_6$	$1-2y$	0·1928	×	4	= 0·7712
OH_1	$0{\cdot}585_3$	$2y-1$	0·1706	×	8	= 1·3648
OH_2	$0{\cdot}585_3$	$2y-1$	0·1706	×	8	= 1·3648
O_{2b}	$0{\cdot}598_1$	$2y-1$	$0{\cdot}196_2$	×	8	= 1·5696
O_{2b}	$0{\cdot}847_5$	$2y-1\frac{1}{2}$	$0{\cdot}195_0$	×	8	= 1·5600
TOTAL					76	14·0432

Weighted average of $\frac{c_M \tan(\alpha_T-90)}{2b_M} = \frac{14{\cdot}0432}{76} = 0{\cdot}1848$

$$\tan(\alpha_T-90) = \frac{2b_M}{c_M}\times 0{\cdot}1848 = \frac{2\times 5{\cdot}47}{18{\cdot}19}\times 0{\cdot}1848 = 0{\cdot}1111$$

$\alpha_T = 96° 21'$

$$c_T = \frac{c_M}{2\sin\alpha_T} = \frac{18{\cdot}19}{2\sin 96° 21'} = 9{\cdot}15\ \text{Å}$$

$\cos\beta_T = \cos\beta_M \sin\alpha_T = \cos 101° 39' \sin 96° 21' = -0{\cdot}2007$

$\beta_T = 101° 35'$

Mladeck (van der Plas *et al.*, 1958) compared some parameters of the reciprocal unit cells of both monoclinic and triclinic chloritoids from Hennensädel, Switzerland, with those determined in this study and found excellent agreement.

Powder data. Milne (1949) satisfactorily indexed 24 reflections for a monoclinic chloritoid from Megantic County, Quebec. Hietanen (1951) listed 47 interplanar spacings for chloritoid from Rawlinsville, Pennsylvania, but did not index them. Some of these spacings cannot be indexed using the established monoclinic unit cell, but all can be indexed using both the monoclinic cell and a new triclinic cell which will be described. Bachmann (1956) listed interplanar spacings for chloritoids from Pregratten, Tirol; Lake Superior Iron Region, Michigan; and Natick, Rhode Island. He indexed only the (00*l*) reflections including those with *l* odd which are prohibited by the space group $C2/c$. He listed several spacings which cannot be indexed by means of either the previously established monoclinic cell or the new triclinic cell. He proposed a mixed-layer structure consisting of chloritoid and sericite to account for some of the interplanar spacings listed for the Natick chloritoid. Such a structure may exist, but is apparently rare because two chloritoids from Natick, Rhode Island, as well

TABLE 13. *Comparison of observed intensities with calculated structure factors for triclinic chloritoid*

Observed intensities were estimated visually from precession pictures taken with MoK_α radiation ($\lambda = 0{\cdot}7107$ Å): vs, very strong; s, strong; ms, medium strong; m, medium; mw, medium weak; w, weak; vw, very weak. Calculated structure factors have not been corrected for polarization, Lorentz, or other factors

hkl	I_{obs}	F_{calc}	*hkl*	I_{obs}	F_{calc}	*hkl*	I_{obs}	F_{calc}
001	vw	35	0.2.$\bar{1}\bar{1}$	mw	81	800	w	54
002	vs	158	0.2.$\bar{1}\bar{2}$	w	−24	801	w	88
003	s	−55	04$\bar{1}$	m	101	802	vw	33
004	—	10	04$\bar{2}$	ms	100	803	w	96
005	—	23	04$\bar{3}$	vw	−2	804	vw	31
006	ms	108	04$\bar{4}$	w	46	805	—	35
007	vw	5	04$\bar{5}$	mw	−33	806	—	−17
008	ms	115	04$\bar{6}$	m	115	807	—	14
009	vw	1	04$\bar{7}$	—	−15	808	w	33
0.0.10	m	118	04$\bar{8}$	mw	93	20$\bar{1}$	—	37
020	mw	13	04$\bar{9}$	—	5	20$\bar{2}$	vw	−32
021	vw	17	0.4.$\bar{1}\bar{0}$	mw	83	20$\bar{3}$	s	−45
022	ms	−38	06$\bar{1}$	mw	87	20$\bar{4}$	—	−12
023	w	36	06$\bar{2}$	w	−50	20$\bar{5}$	w	−38
024	m	−64	06$\bar{3}$	vw	34	20$\bar{6}$	w	86
025	m	103	06$\bar{4}$	mw	−42	20$\bar{7}$	—	−36
026	m	−80	06$\bar{5}$	—	27	20$\bar{8}$	—	31
027	vw	29	06$\bar{6}$	vw	−4	40$\bar{1}$	ms	133
028	mw	−65	06$\bar{7}$	w	30	40$\bar{2}$	m	46
029	vw	41	06$\bar{8}$	mw	−55	40$\bar{3}$	ms	147
0.2.10	—	11	200	mw	76	40$\bar{4}$	m	72
0.2.11	w	55	201	mw	−73	40$\bar{5}$	m	118
040	s	174	202	mw	36	40$\bar{6}$	mw	64
041	w	−13	203	w	−74	40$\bar{7}$	vw	57
042	mw	88	204	—	67	40$\bar{8}$	vw	−25
043	m	−69	205	—	30	40$\bar{9}$	—	30
044	m	88	206	—	33	4.0.$\bar{1}\bar{0}$	—	14
045	—	17	207	w	−35	4.0.$\bar{1}\bar{1}$	w	87
046	mw	76	400	w	−19	4.0.$\bar{1}\bar{2}$	w	49
047	—	19	401	vw	4	60$\bar{1}$	s	118
048	w	71	402	vw	−22	60$\bar{2}$	ms	−45
049	—	17	403	mw	85	60$\bar{3}$	mw	35
0.4.10	m	84	404	m	91	60$\bar{4}$	m	−42
060	w	−42	405	ms	162	60$\bar{5}$	vw	27
061	—	35	406	vw	37	60$\bar{6}$	vw	−17
062	w	−42	407	vw	55	60$\bar{7}$	w	55
063	—	20	408	—	−14	60$\bar{8}$	mw	−82
064	—	−8	409	—	41	60$\bar{9}$	—	29
065	mw	34	4.0.10	vw	18	6.0.$\bar{1}\bar{0}$	mw	−54
066	—	−51	4.0.11	w	50	6.0.$\bar{1}\bar{1}$	mw	68
067	—	25	600	ms	−79	6.0.$\bar{1}\bar{2}$	—	8
02$\bar{1}$	vs	96	601	w	52	80$\bar{1}$	w	76
02$\bar{2}$	vs	−111	602	m	−75	80$\bar{2}$	vw	46
02$\bar{3}$	s	97	603	vw	40	80$\bar{3}$	—	5
02$\bar{4}$	vs	−106	604	—	−8	80$\bar{4}$	vw	−16
02$\bar{5}$	ms	93	605	vw	40	80$\bar{5}$	vw	62
02$\bar{6}$	mw	−30	606	mw	−61	80$\bar{6}$	vw	40
027	—	10	607	—	20	80$\bar{7}$	m	134
02$\bar{8}$	m	−59	608	mw	−43	80$\bar{8}$	w	33
02$\bar{9}$	—	17	609	mw	70	80$\bar{9}$	—	41
0.2$\bar{1}\bar{0}$.	vw	−15	6.0.10	vw	−6	8.0.$\bar{1}\bar{0}$	—	7

as those from more than thirty other localities which were X-rayed by the writer fail to show mixed layering. Istshenko (1957) listed interplanar spacings for two samples of chloritoid from Krivoy–Rog, Ukraine, but did not index them. He noted that his spacings differed somewhat from those given by Hietanen (1951), and attributed these differences to other phases beside chloritoid in his samples. Most of his spacings are characteristic of chloritoid but do not identify his samples as either the monoclinic or the triclinic polymorph on the bases of the diagnostic reflections listed in Table 17. Van der Plas (van der Plas *et al.*, 1958) listed interplanar spacings for chloritoid from Hennensädel, Switzerland. He concluded, from monoclinic and triclinic chloritoid samples supplied by the writer, that his chloritoid consists of both polymorphs. He also identified other Swiss chloritoids: two as triclinic and one as monoclinic.

New X-ray studies

Single-crystal investigation. Data obtained from a chloritoid crystal from Natick, Rhode Island (anal. 102, Table 8), are given in Table 9 for comparison with the previously determined unit-cell data on other samples.

Chloritoid from Chibougamau, Quebec (anal. 101, Table 8), was examined on the precession camera. Precession pictures of the zero level of the b^*c^* net and the zero and first levels of the a^*c^* nets were taken with MoK_α radiation ($\lambda = 0{\cdot}7107$ Å). These yielded the following data: $a^* = 0{\cdot}1077$ Å^{-1}, $b^* = 0{\cdot}1838$ Å^{-1}, $c^* = 0{\cdot}1124$ Å^{-1}, $\alpha^* = 82°\ 57'$, $\beta^* = 78°\ 5'$, $\gamma = 90°\ 2'$, with the only systematic absences being of the type $h+k$ odd for (hkl) reflections. Because of systematic absences the value given for b^* is half that measured on the zero level of the b^*c^* net. These measurements lead to a triclinic C-centred cell whose dimensions are given in Table 10, cell 1.

In order to choose the most convenient cell for triclinic chloritoid a primitive cell was obtained from cell 1 by the transformation matrix $\frac{1}{2}\bar{\frac{1}{2}}0/010/001$. In this primitive cell the b- and c-axes, and α are the same as in the C-centred cell, $\gamma = 120°\ 2'$, $\beta = 96°\ 44'$, and $a = b$; the ab net is hexagonal within 5 min. of arc. Thus in addition to cell 1 two other C-centred cells (2 and 3, Table 10) can be obtained from cell 1 by the transformation matrices $\bar{\frac{1}{2}}\bar{\frac{3}{2}}0/\bar{\frac{1}{2}}\frac{1}{2}0/00\bar{1}$ and $\frac{1}{2}\bar{\frac{3}{2}}0/\frac{1}{2}\frac{1}{2}0/001$, respectively. Comparison of the lattice parameters of monoclinic chloritoid (Table 9) with those of cells 1 and 2 shows that within experimental error a, b, and $\gamma = 90°\ 0'$ are the same; and hence[1] $\cos\beta_T = \cos\beta_M \sin\alpha_T$. Furthermore, $2c_T \sin\alpha_T = c_M$. Figs. 4 A and 4 B show that the length of the c-axis in triclinic chloritoid is approximately half that in monoclinic chloritoid. Measurements show that $5c_T \cos(180-\alpha_T) = b_T = b_M$, and hence the transformation matrix from triclinic to monoclinic axes is $100/010/0\frac{5}{2}2$. The dimensional relation between the cells of triclinic and monoclinic chloritoids is shown in Fig. 5. Either cell 1 or cell 2 can be chosen as the most convenient for triclinic chloritoid. Cell 3, Table 10, approaches monoclinic geometry, but the optical

[1] The subscripts T and M refer to triclinic and monoclinic chloritoid respectively.

data presented in another section confirm the triclinic symmetry. The lattice parameters of the Delaunay primitive cell (Donnay, Nowacki, & Donnay, 1954, pp. 139–41) are also listed in Table 10.

The atomic coordinates for monoclinic chloritoid (Table 11) reveal a relation similar to that shown in Fig. 5, but with the lower triclinic cell on top of the upper. In the monoclinic and triclinic cells, a, b, and $\gamma = 90°$ are the same. The remaining lattice parameters of triclinic chloritoid can be obtained from the y atomic coordinates of Harrison & Brindley (1957) as shown in Table 12. The atomic coordinates for cations Ia and Ib cannot be used, for in space group $C2/c$ they lie on the n-glide planes at $y = \frac{1}{4}, \frac{3}{4}$, midway between the c-glide planes. The triclinic lattice parameters are listed under cell 4, Table 10. They are very close to those for cells 1 and 2, and thus confirm the choice of cell 1 or cell 2 for triclinic chloritoid.

Calculation of the triclinic lattice parameters from the monoclinic by means of the monoclinic atomic coordinates implies that the atomic structure of triclinic chloritoid is the same as that of one-half the unit cell of monoclinic chloritoid. In order to test this implication, some of the observed intensities are compared with calculated structure factors in Table 13. The atomic coordinates used for these calculations have been obtained by transforming monoclinic atomic coordinates to triclinic by the matrix $100/01\frac{2}{5}/002$, and shifting the origin to 0, $-\frac{1}{10}, \frac{1}{4}$, monoclinic; they are listed in Table 11. This rough comparison between observed intensities and calculated structure factors shows sufficient agreement to confirm the implied relation between monoclinic and triclinic chloritoids. Coordinations and interatomic distances in triclinic chloritoid are the same as those in monoclinic chloritoid; they have been discussed by Harrison & Brindley (1957). The relation between monoclinic and triclinic chloritoids accounts for the parallel growth of both types in some rocks.

The relation between monoclinic and triclinic chloritoids is similar to that between monoclinic and triclinic wollastonites. Peacock (1935) proved the existence of both monoclinic and triclinic wollastonites, and noted further that in the triclinic form $\alpha = 90°\ 0'$ and that the plane $(1\bar{4}0)$ is normal to the b-axis. Ito (1950, p. 94) gave data from which the relations $2a_T \sin \gamma_T = a_M$, $b_T = b_M$, $c_T = c_M$, $\cos \beta_T = \cos \beta_M \sin \gamma_T$, $4a_T \cos (180-\gamma_T) = b_T$ can be derived. He also showed (pp. 95–96) how monoclinic wollastonite can be obtained from triclinic by twinning of the triclinic space group $P\bar{1}$. The twinning operation—twofold screw axes parallel to the b-axis—produces the monoclinic space group $P2_1/a$. In triclinic chloritoid $\gamma = 90°$, and the plane $(0\bar{5}1)$ is normal to the b-axis. The geometrical relations between monoclinic and triclinic chloritoids indicate that the monoclinic space group $C2/c$ may be obtained from the triclinic space group $C\bar{1}$, by twinning. According to Ito (1950, p. 6) reflection, rotation, and gliding are the three twinning operations by which twinned space groups may be derived. Only twofold rotation or screw axes parallel to the b-axis will produce the cell of monoclinic chloritoid from two triclinic cells. Both kinds of axes

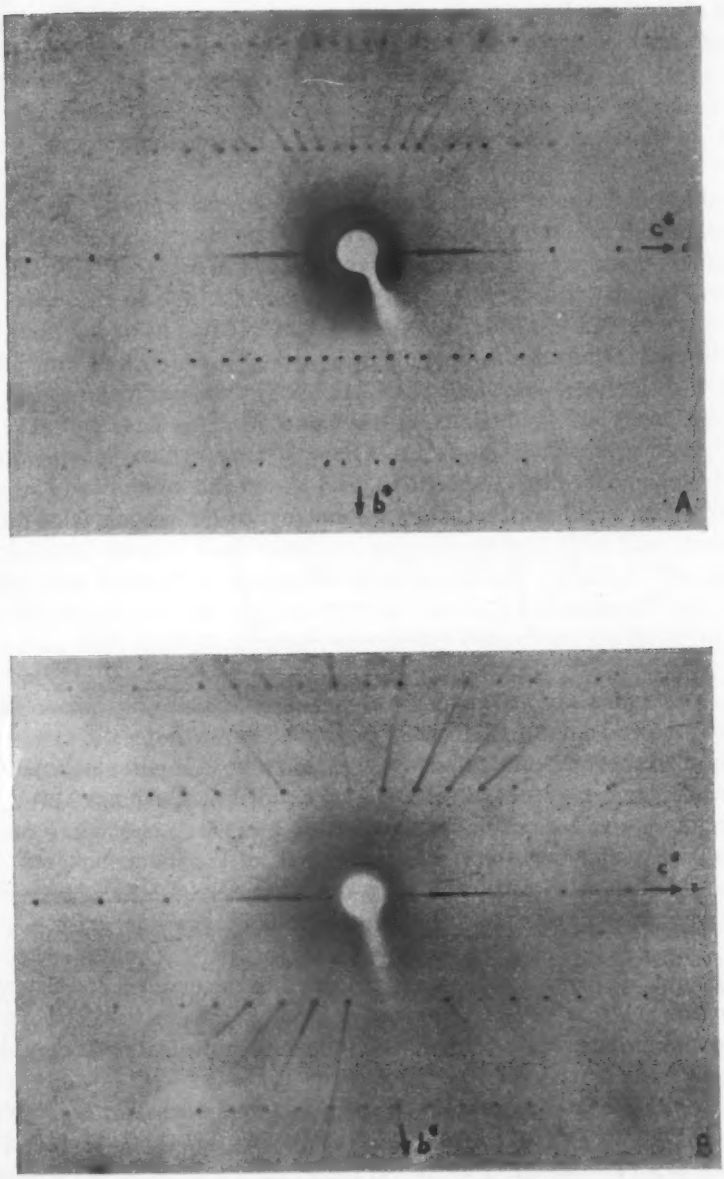

FIG. 4. Precession photographs of the zero level b^*c^* nets of chloritoid polymorphs. MoK_α radiation. A, monoclinic chloritoid from Natick, Rhode Island, U.S.A. B, triclinic chloritoid from Chibougamau, Quebec, Canada.

are present in space group $C2/c$. Mirrors or glide-planes parallel to (001), or simple gliding parallel to (010) will not produce a monoclinic cell with lattice parameters which agree with those measured for monoclinic chloritoid.

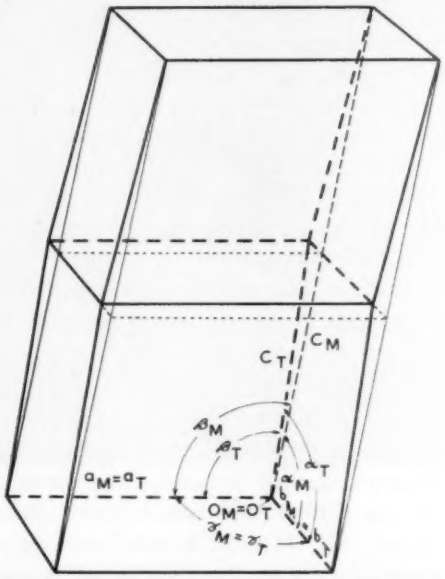

FIG. 5. Dimensional relation between the cells of triclinic and monoclinic chloritoid. Heavy lines outline two triclinic cells. Light lines outline one monoclinic cell. The subscripts T and M refer to triclinic and monoclinic cells respectively. O is the origin.

In order to show that the twinning group, a twofold rotation axis parallel to the b-axis, operating on the space group $C\bar{1}$ is equivalent to the space group $C2/c$, consider the equivalent positions, x, y, z; $\bar{x}, \bar{y}, 1-z$; $\frac{1}{2}+x, \frac{1}{2}+y, z$; $\frac{1}{2}-x, \frac{1}{2}-y, 1-z$; of the triclinic cell, representing one-half of the monoclinic cell. When these coordinates are transformed by the matrix $100/01\frac{1}{5}/00\frac{1}{2}$, they can be located with respect to the monoclinic axes as follows: $x, y-\frac{1}{5}z, \frac{1}{2}z$; $\bar{x}, -(y-\frac{1}{5}z), \frac{1}{2}-\frac{1}{2}z$; $\frac{1}{2}+x, \frac{1}{2}+(y-\frac{1}{5}z), \frac{1}{2}z$; $\frac{1}{2}-x, \frac{1}{2}-(y-\frac{1}{5}z), \frac{1}{2}-\frac{1}{2}z$. It is convenient to place the origin at $0, \frac{1}{10}, \frac{1}{2}$ of the triclinic cell or $0, 0, \frac{1}{4}$ of the new cell and the twofold rotation axis at $0, y, 1$ in the triclinic cell or $0, y, \frac{1}{2}$ in the new cell. The operation of the twofold rotation axis doubles the number of equivalent positions, making eight in all. They are $x, y-\frac{1}{5}z, \frac{1}{2}z-\frac{1}{4}$; $\bar{x}, -(y-\frac{1}{5}z), -(\frac{1}{2}z-\frac{1}{4})$; $\frac{1}{2}+x, \frac{1}{2}+(y-\frac{1}{5}z), \frac{1}{2}z-\frac{1}{4}$; $\frac{1}{2}-x, \frac{1}{2}-(y-\frac{1}{5}z), -(\frac{1}{2}z-\frac{1}{4})$; $\bar{x}, y-\frac{1}{5}z, \frac{1}{2}-(\frac{1}{2}z-\frac{1}{4})$; $x, -(y-\frac{1}{5}z), \frac{1}{2}+(\frac{1}{2}z-\frac{1}{4})$; $\frac{1}{2}-x, \frac{1}{2}+(y-\frac{1}{5}z), \frac{1}{2}-(\frac{1}{2}z-\frac{1}{4})$; $\frac{1}{2}+x, \frac{1}{2}-(y-\frac{1}{5}z), \frac{1}{2}+(\frac{1}{2}z-\frac{1}{4})$. By putting $X = x$, $Y = y-\frac{1}{5}z$, $Z = \frac{1}{2}z-\frac{1}{4}$, these become X, Y, Z; $\bar{X}, \bar{Y}, \bar{Z}$; $\frac{1}{2}+X, \frac{1}{2}+Y, Z$; $\frac{1}{2}-X, \frac{1}{2}-Y, \bar{Z}$; $\bar{X}, Y, \frac{1}{2}-Z$; $X, \bar{Y}, \frac{1}{2}+Z$; $\frac{1}{2}-X, \frac{1}{2}+Y, \frac{1}{2}-Z$; $\frac{1}{2}+X, \frac{1}{2}-Y, \frac{1}{2}+Z$, which are the equivalent positions of space group $C2/c$.

In a similar manner a twofold screw axis parallel to the b-axis, operating on the space group $C\bar{1}$ can be shown to yield the space group $C2/c$. The origin is

the same as before but the twofold screw axis is placed at $\frac{1}{4}$, y, $\frac{1}{2}$ in the new cell. The eight positions then are x, $y-\frac{1}{8}z$, $\frac{1}{2}z-\frac{1}{4}$; $\bar{x}$, $-(y-\frac{1}{8}z)$, $-(\frac{1}{2}z-\frac{1}{4})$; $\frac{1}{2}+x$, $\frac{1}{2}+(y-\frac{1}{8}z)$, $\frac{1}{2}z-\frac{1}{4}$; $\frac{1}{2}-x$, $\frac{1}{2}-(y-\frac{1}{8}z)$, $-(\frac{1}{2}z-\frac{1}{4})$; $\frac{1}{2}-x$, $\frac{1}{2}+(y-\frac{1}{8}z)$, $\frac{1}{2}-(\frac{1}{2}z-\frac{1}{4})$; $\frac{1}{2}+x$, $\frac{1}{2}-(y-\frac{1}{8}z)$, $\frac{1}{2}+(\frac{1}{2}z-\frac{1}{4})$; $\bar{x}$, $1+(y-\frac{1}{8}z)$, $\frac{1}{2}-(\frac{1}{2}z-\frac{1}{4})$; x, $1-(y-\frac{1}{8}z)$, $\frac{1}{2}+(\frac{1}{2}z-\frac{1}{4})$. These can be simplied by the same substitutions as before, and subtracting one where necessary, to yield the equivalent positions of space group $C2/c$.

Powder data. X-ray powder films of monoclinic and triclinic chloritoids from several samples are compared in Fig. 6. Indexed powder data for the monoclinic Natick chloritoid are given in Table 14, and for the triclinic Chibougamau chloritoid in Table 15. The weak diffuse lines in the back reflection region have been omitted from Tables 14 and 15. Only those lines above $2\theta = 120°$ in which both the Fe$K_{\alpha 1}$ and Fe$K_{\alpha 2}$ lines could be distinguished are included. Even though several manganese filters were tried, and FeK_β line corresponding to the very strong FeK_α line at $2\theta = 25{\cdot}15°$ could not be eliminated. The films, mounted in the Straumanis manner, were exposed in a Debye–Scherrer type camera with a radius of 114·59 mm made by the North American Philips Company. The 2θ values are an average of measurements from at least three films, each obtained with a different spindle. Each measurement was corrected for film shrinkage, and many were checked by using quartz as an internal standard. The powder camera was chosen for this work in place of the Geiger-counter diffractometer because even with slowest scanning speeds the diffractometer failed to yield intense peaks suitable for precise measurements for many reflections.

The chloritoid polymorphs occurring at various localities are given in Table 16. They were distinguished by comparing their photographic powder patterns. The diffractometer can be used, however, to distinguish between the two polymorphs of chloritoid provided pure enough chloritoid is examined. The reflections used to distinguish the two polymorphs are in Table 17.

Specific gravity and cell content

Cell dimensions, cell volumes, and calculated and measured specific gravities for six chloritoids are given in Table 18. The cell dimensions of the monoclinic chloritoids were obtained from samples consisting entirely or mostly of monoclinic chloritoid by solving simultaneous equations of the type

$$h^2a^{*2}+k^2b^{*2}+l^2c^{*2}+2lhc^*a^*\cos\beta^* = Q = 1/d^2,$$

by the method of least squares using the following fifteen reflections: (110), (202), (113), (11$\bar{4}$), (114), (006), (20$\bar{6}$), (311), (31$\bar{4}$), (023), (312), (223), (22$\bar{5}$), (40$\bar{6}$), (026). The 2θ angles and, hence, the d and Q values for these solutions were obtained in the same way as the 2θ angles in Tables 14 and 15. The cell dimensions for the triclinic Chibougamau chloritoid are those obtained by means of the precession camera. A least-squares method using powder data to determine the cell dimensions of triclinic chloritoid was not attempted because too

TABLE 14. *X-ray diffraction powder data for monoclinic chloritoid from Natick, Rhode Island, U.S.A.*

$2\theta_{obs}$	d	$Q_{obs} \times 10^5$	$\Delta Q \times 10^5$	hkl	I
22·80	4·443	5,065	−12	004	1
23·58	4·741	4,450	33	110	1
24·08	4·644	4,637	9	200	1
b 24·87	4·498	4,942	−33	$20\bar{2}$	
b 25·15	4·449	5,052	−3	111	>10
			1	004	
25·70	4·355	5,272	−25	$11\bar{2}$	1
29·47	3·808	6,895	15	202	2
31·18	3·604	7,698	0	$20\bar{4}$	1
31·95	3·520	8,073	2	113	3
32·90	3·421	8,547	−12	$11\bar{4}$	3
36·66	3·080	10,541	−5	114	4
37·62	3·004	11,080	47	115	1
38·16	2·963	11,389	−20	006	9
38·66	2·926	11,678	22	204	1
40·89	2·773	13,004	10	$20\bar{6}$	3
41·39	2·741	13,311	−27	020	1
			30	$31\bar{1}$	
b 41·90	2·709	13,625	−25	021	1
			3	115	
43·06	2·639	14,355	−4	$11\bar{6}$	5
			12	$31\bar{3}$	
43·82	2·596	14,840	2	311	2
45·32	2·514	15,820	7	$31\bar{4}$	2
45·81	2·489	16,144	−18	023	2
46·42	2·458	16,554	−15	312	3
47·55	2·403	17,322	30	116	1
48·31	2·367	17,847	1	$40\bar{2}$	7
48·98	2·337	18,314	23	024	2
49·68	2·306	18,809	−63	221	7
			60	313	
50·85	2·256	19,645	−8	$40\bar{4}$	1
51·59	2·226	20,187	7	222	2
52·68	2·183	20,982	0	$22\bar{4}$	1
53·65	2·146	21,706	2	117	1
54·41	2·119	22,277	−4	223	4
55·78	2·071	23,318	6	$22\bar{5}$	1
56·63	2·042	23,977	−25	$40\bar{6}$	3
			21	317	
57·53	2·013	24,680	−27	026	1
58·44	1·984	25,397	25	315	2
60·08	1·935	26,708	−13	118	1
62·04	1·880	28,305	21	225	3
62·63	1·864	28,790	− 32	027	1
63·69	1·836	29,669	−23	316	1
65·04	1·802	30,803	−9	$40\bar{8}$	1
67·16	1·751	32,605	−2	$31\bar{9}$	2
68·24	1·727	33,536	−41	028	1
			26	$1.1.\overline{10}$	
69·39	1·702	34,533	−31	317	2
71·26	1·6628	36,168	−43	512	1
			59	$51\bar{6}$	
72·07	1·6466	36,883	23	227	2
73·01	1·6284	37,712	−17	$13\bar{5}$	1
			1	423	

TABLE 14 (*cont.*)

$2\theta_{obs}$	d	$Q_{obs} \times 10^5$	$\Delta Q \times 10^5$	hkl	I
74·48	1·6007	39,028	−20 54	229 517	1
75·55	1·5813	39,992	−49 −3	1.1.$\bar{11}$ 318	8
76·56	1·5636	40,902	−34 17 22 33	604 136 424 333	3
77·10	1·5543	41,393	17	331	2
79·72	1·5114	43,777	−43	3.1.$\bar{11}$	1
80·80	1·4945	44,772	−5 2	425 137	2
81·55	1·4832	45,457	−20 −11 18	333 1.1.11 0.0.12	4
82·25	1·4728	46,101	−19 7	602 319	1
82·89	1·4634	46,695	−9	51$\bar{9}$	2
84·27	1·4438	47,972	40	229	1
86·50	1·4137	50,036	−12	60$\bar{8}$	1
87·16	1·4051	50,651	−11	2.2.$\bar{11}$	4
88·67	1·3861	52,049	−59 7	335 4.0.$\bar{12}$	2
b 90·15	1·3681	53,427	15 19 25	62$\bar{3}$ 4.2.$\bar{10}$ 041	
b		54,090	−73 62	62$\bar{1}$ 62$\bar{4}$	3
b 91·20	1·3557	54,409	−62 −29 −10	427 13$\bar{9}$ 024	
97·51	1·2883	60,251	−12 −10	710 3.1.11	2
101·02	1·2551	63,481	−22	71$\bar{7}$	1
102·56	1·2415	64,879	−43	244	2
106·31	1·2104	68,256	−2	3.1.12	1
112·34	1·1661	73,541	−16 5 35	1.3.$\bar{12}$ 2.0.14 3.1.$\bar{15}$	1
121·00	1·1122	80,841	4	0.0.16	4
139·77	1·0309	94,095	−44 −40 −24 34	91$\bar{5}$ 15$\bar{6}$ 35$\bar{3}$ 0.2.16	2
150·65	1·0006	99,880	44 56	64$\bar{7}$ 448	1

$2\theta_{obs}$ in degrees Fe$K\beta$ 0°–23° λ = 1·75654 Å.
FeK_α 23°–120° λ = 1·9373 Å.
Fe$K_{\alpha 1}$ 120°–160° λ = 1·93597 Å.
d = interplanar spacing in Å.

$Q = 1/d^2$.
$\Delta Q = Q_{calc} - Q_{obs}$.
b = broad line or band.
I = relative intensity based on visual comparison.

TABLE 15. *X-ray diffraction powder data for triclinic chloritoid from Chibougamau, Quebec, Canada*

$2\theta_{obs}$	d	$Q_{obs}\times10^5$	$\Delta Q\times10^5$	hkl	I
22·77	4·449	5,052	3	002	1
23·55	4·747	4,438	3	$\bar{1}10$	1
24·10	4·640	4,645	−11 −5	200 110	1
b 24·87	4·498	4,942	−45 −43	$11\bar{1}$ $20\bar{1}$	>10
b 25·15	4·449	5,052	3	002	
29·49	3·806	6,904	−6 7	201 111	3
31·15	3·608	7,683	−2 7	$11\bar{2}$ $20\bar{2}$	1
34·71	3·247	9,483	−8 22	$1\bar{1}2$ $\bar{1}12$	6
38·14	2·965	11,377	−3	003	8
38·69	2·924	11,695	−6 14	202 112	2
40·92	2·771	13,022	−12	$20\bar{3}$	4
42·12	2·696	13,762	2 9	$02\bar{1}$ $\bar{3}11$	7
42·69	2·661	14,120	−7	310	3
45·32	2·514	15,820	−27 11	021 $\bar{1}13$	1
46·45	2·456	16,574	−34 −4	$02\bar{2}$ $\bar{3}12$	9
47·63	2·399	17,377	7	311	5
48·28	2·369	17,818	−16 −10	$40\bar{1}$ $22\bar{1}$	3
49·31	2·322	18,545	−8 14	400 220	1
49·94	2·295	18,993	−5 14 25 42	$22\bar{1}$ 203 $\bar{2}21$ 113	5
50·78	2·259	19,596	−11 −2	$22\bar{2}$ $40\bar{2}$	3
52·10	2·206	20,555	−17 44	$3\bar{1}2$ $02\bar{2}$	3
53·85	2·139	21,854	−53 −17 −9 43	401 221 $02\bar{3}$ $\bar{3}13$	6
55·07	2·095	22,775	−11 49	$22\bar{2}$ $\bar{2}22$	2
55·57	2·078	23,161	21	312	1
56·59	2·044	23,935	−45 −21	$22\bar{3}$ $40\bar{3}$	2
57·44	2·016	24,610	15	$1\bar{1}4$	1
b 59·74	1·945	26,437	−62	$31\bar{4}$	1
b 61·15	1·904	27,576	15 66	402 222	2
b 61·46	1·896	27,830	19	$3\bar{1}3$	
63·02	1·853	29,111	−43 47	$22\bar{3}$ $\bar{2}23$	2
63·77	1·834	29,737	−60 14	$02\bar{4}$ $\bar{3}14$	7
65·84	1·782	31,491	10 21	$1\bar{3}1$ $42\bar{1}$	3
68·23	1·727	33,529	−48 16	$42\bar{1}$ $\bar{1}31$	1
70·18	1·6850	35,221	−17	$42\bar{3}$	1
70·96	1·6688	35,908	1	403	3

TABLE 15 (*cont.*)

$2\theta_{obs}$	d	$Q_{obs}\times 10^5$	$\Delta Q\times 10^5$	hkl	I
72·43	1·6395	37,203	−21	$13\bar{3}$	1
73·00	1·6285	37,707	−19	$3\bar{1}4$	2
75·60	1·5804	40,037	−37	$33\bar{1}$	8
			−1	$0\bar{2}5$	
			45	$22\bar{5}$	
76·45	1·5655	40,803	−36	$60\bar{2}$	
			−33	$33\bar{2}$	
			69	$5\bar{1}2$	
b		41,010	−39	$13\bar{2}$	3
			27	$42\bar{4}$	
			42	$51\bar{4}$	
76·91	1·5575	41,223	−69	$33\bar{1}$	
			−24	$3\bar{3}1$	
			4	$20\bar{5}$	
77·45	1·5484	41,709	1	600	2
			48	$33\bar{0}$	
78·10	1·5375	42,303	58	$31\bar{4}$	1
79·98	1·5072	44,021	−14	$13\bar{4}$	1
81·59	1·4826	45,494	3	006	4
82·98	1·4620	46,785	−30	$40\bar{4}$	2
			51	$22\bar{4}$	
83·90	1·4490	47,628	−58	$31\bar{6}$	1
85·76	1·4235	49,350	−38	$13\bar{3}$	2
			47	$42\bar{5}$	
86·46	1·4142	50,001	−66	$60\bar{4}$	4
			−25	$\bar{1}16$	
			53	$3\bar{1}5$	
87·81	1·3968	51,254	−35	$33\bar{3}$	1
88·69	1·3858	52,071	−32	$40\bar{6}$	1
90·25	1·3669	53,521	−53	$51\bar{5}$	
			−38	$62\bar{2}$	
b		53,705	0	$62\bar{1}$	3
90·81	1·3605	54,042	−48	$\bar{6}20$	
			16	040	
91·90	1·3477	55,057	−3	$04\bar{2}$	2
93·38	1·3312	56,430	24	620	1
97·41	1·2892	60,167	−38	$40\bar{5}$	2
			−1	$24\bar{1}$	
			14	$13\bar{4}$	
			54	$53\bar{3}$	
			56	$33\bar{4}$	
			58	225	
			58	$71\bar{3}$	
99·51	1·2690	62,098	−18	603	1
100·82	1·2569	63,299	27	$22\bar{6}$	2
102·70	1·2403	65,005	−57	$3\bar{1}6$	2
			−18	$24\bar{2}$	
			60	$71\bar{4}$	
104·23	1·2273	66,389	−4	$22\bar{7}$	1
			24	$\bar{1}17$	
109·88	1·1833	71,418	−23	$33\bar{5}$	2
			−2	$80\bar{1}$	
			52	$44\bar{1}$	
119·79	1·1197	79,762	8	$22\bar{7}$	1
			18	$7\bar{1}3$	
			53	$3\bar{1}7$	
121·07	1·1118	80,900	−17	008	3
137·61	1·0382	92,776	−47	624	1
156·70	0·98835	102,372	−4	009	2
			29	$44\bar{5}$	

Column headings explained at foot of Table 14.

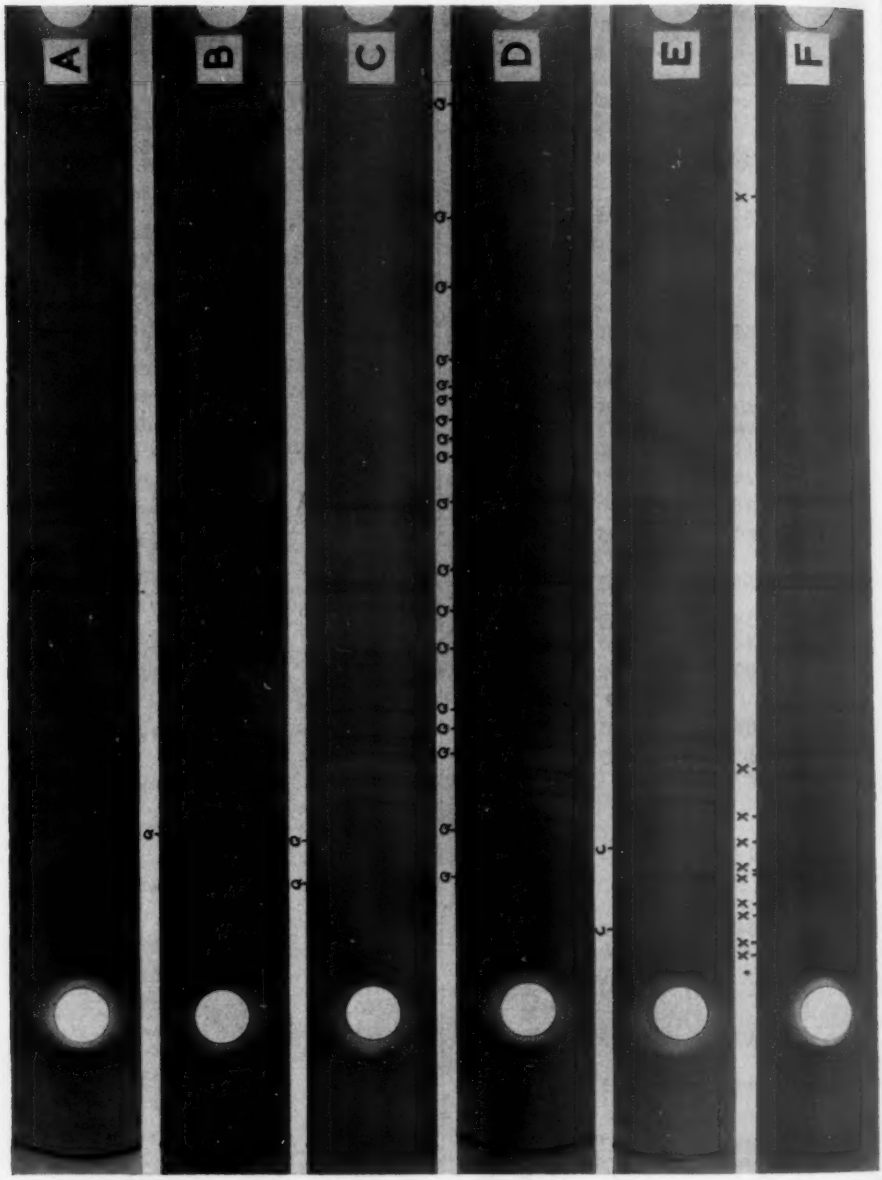

FIG. 6. X-ray powder photographs of various chloritoids. Fe radiation with Mn filter. *Q*, quartz lines; *C*, chlorite lines; *X*, lines of unidentified phases. A, Natick, Rhode Island, U.S.A. Monoclinic (No. 21*a*). B, Chibougamau, Quebec, Canada. Triclinic (No. 12). C, Salm-Château, Belgium. Monoclinic and triclinic (No. 19*M*). D, Ottré, Belgium, Triclinic (No. 3*GHW*). E, St. Marcel, Piedmont, Italy. Monoclinic (No. 22, U.S. National Museum R4502). F, synthetic chloritoid and other phases made from a mixture of siderite, γ-alumina, and kaolinite at 600° C and 10,000 bars.

TABLE 16. *Distribution of chloritoid polymorphs*

Sample No.	*Locality*	*Source*	*Remarks*
		Monoclinic	
2	Ile de Groix, France	Muséum National d'Histoire Naturelle, Paris, No. 101.302	
11	Üstüaçiksarinç, Turkey	Dr. H. P. Eugster from Dr. T. S. Önay	
13	Pregratten, Tirol, Austria	U.S. National Museum, R4496	
18	Gumuchdagh, Turkey	U.S. National Museum, 79909	
20	Techen, Chelyabinsk, Ural Mts, U.S.S.R.	Dr. P. N. Varfolomeev, Director, F. N. Chernsheva Geological Museum, Leningrad	
21	Natick, Rhode Island, U.S.A.	U.S. National Museum, 93568	
21*a*	Natick, Rhode Island, U.S.A.	The Johns Hopkins University	
22	St. Marcel, Piedmont, Italy	U.S. National Museum, R4502	
27	Leoben, Austria	U.S. National Museum, R4495	
52	Winnemucca, Nevada, U.S.A.	Dr. R. R. Compton, No. 17–19–9	
53	Mesquite Canyon, Kern County, Calif., U.S.A.	Mr. C. W. Chesterman	
58	Summit of Mt. Leconte, Tennessee, U.S.A.	Dr. C. A. Hopson	
59	Ellijay, Georgia, U.S.A.	Dr. V. J. Hurst	
		Triclinic	
3	Ottré, Belgium	U.S. National Museum, 47022	with quartz
3 *GHW*	Ottré, Belgium	The Johns Hopkins University	with quartz
5	Womble Mine, North Carolina, U.S.A.	Dr. J. L. Stuckey	
8	Crestlianderstobel, Switzerland	Prof. C. Burri	
12	Chibougamau, Quebec, Canada	Dr. Gilles Allard	
19	Vielsalm, Belgium	U.S. National Museum, R4498	
23	St. Gilles, Quebec, Canada	U.S. National Museum, 79008	
25	Lebanon, Massachusetts, U.S.A.	U.S. National Museum, 79007	
26	Mt. Blia, Sweden	U.S. National Museum, R4508	with quartz
33*A*	Kalgoorlie, Western Australia	Prof. R. T. Prider	
42	Michipicoten District, Ontario, Canada	Dr. W. A. Jarvis	
47*B*	Yukizawa, Kitakami Area, Japan	Dr. Yôtarô Seki, No. YS 53081502	
49*a*	Hollinger Mine, Ontario, Canada	Dr. W. A. Jones	
60	Barvue Mine, Quebec, Canada	Dr. Robert Assad	
		Monoclinic and triclinic	
1	Collier Bay, Western Australia	Government Chemical Laboratory, Western Australia, through Prof. R. T. Prider	
6	Rawlinsville, Pennsylvania, U.S.A.	Collected by the writer	mostly monoclinic
7*A*	Harvey Hill Mine, Quebec, Canada	Dr. Paul E. Grenier	very minor monoclinic
17	Vénasque, France	U.S. National Museum, R4506	
19*M*	Salm-Château, Belgium	Dr. Jean Michot	mostly monoclinic
51	Mt. Herrick, Vermont, U.S.A.	Dr. E-an Zen	mostly triclinic
55	Ernen Power Station, Switzerland	Prof. C. Burri	mostly monoclinic
66	Newfound Gap, Swain County, North Carolina, U.S.A.	Dr. J. B. Hadley, No. MG250	mostly monoclinic

TABLE 17

Reflections used to distinguish monoclinic from triclinic chloritoid

Monoclinic				*Triclinic*			
2θ	*d*	*hkl*	*I*	2θ	*d*	*hkl*	*I*
31·95	3·520	113	3	34·71	3·247	$\begin{pmatrix}1\bar{1}2\\ \bar{1}12\end{pmatrix}$	6
36·66	3·080	114	4				
43·06	2·639	$\begin{pmatrix}11\bar{6}\\ 31\bar{3}\end{pmatrix}$	5	42·69	2·661	310	3
43·82	2·596	311	2	49·94	2·295	$\begin{pmatrix}2\bar{2}1\\ 20\bar{3}\\ \bar{2}21\\ 113\end{pmatrix}$	5
45·81	2·489	023	2				
49·68	2·306	$\begin{pmatrix}221\\ 313\end{pmatrix}$	7				
54·41	2·119	223	4	52·10	2·206	$\begin{pmatrix}3\bar{1}2\\ 022\end{pmatrix}$	3
				55·07	2·095	$\begin{pmatrix}2\bar{2}2\\ \bar{2}22\end{pmatrix}$	2

2θ in degrees FeK_α $\lambda = 1{\cdot}9373$ Å.
d = interplanar spacing in Å.
I = relative intensity based on visual comparison with the strong reflection at $2\theta = 25{\cdot}15° > 10$.

TABLE 18

Unit cell parameters, volumes, and specific gravities of six chloritoids

Cell dimensions are in Å; cell volumes are in Å^3
M, monoclinic; T, triclinic. *Z* is number of formula units, $H_2FeAl_2SiO_7$, in the cell

Specimen No.:	2	6	11	12	19*M*	21*a*
a. . .	$9{\cdot}48_3$	$9{\cdot}47_4$	$9{\cdot}48_3$	9·50	$9{\cdot}48_0$	$9{\cdot}48_2$
b. . .	$5{\cdot}47_7$	$5{\cdot}47_9$	$5{\cdot}48_4$	5·48	$5{\cdot}49_2$	$5{\cdot}48_7$
c. . .	$18{\cdot}17_8$	$18{\cdot}18_0$	$18{\cdot}18_5$	9·16	$18{\cdot}20_0$	$18{\cdot}18_7$
α. . .	—	—	—	96° 53′	—	—
β. . .	101° 38′	101° 43′	101° 46′	101° 49′	101° 54′	101° 55′
γ. . .	—	—	—	90° 2′	—	—
Cell volume .	924·73	924·03	925·42	462·99	928·00	925·30
Z . .	8	8	8	4	8	8
Calculated *G*	3·50	3·48	3·57	3·56	3·55	3·60
Measured *G* .	3·54±0·02	3·52±0·03	3·58±0·02	3·58±0·02	3·53±0·03	3·61±0·01
Polymorph .	M	M, small amount T	M	T	M, small amount T	M

2. Ile de Groix, France. No. 101.302, Muséum National d'Histoire Naturelle, Paris (anal. 79, Table 7).
6. Rawlinsville, Pennsylvania, U.S.A. (anal. 1, Table 2).
11. Üstüaçiksarinç, Turkey (anal. 100, Table 8).
12. Chibougamau, Quebec, Canada (anal. 101, Table 8).
19*M*. Salm-Château, Belgium (anal. 99, Table 8).
21*a*. Natick, Rhode Island, U.S.A. (anal. 102, Table 8).

Additional data:
42. Michipicoten District, Ontario, Canada (anal. 103, Table 8). Calculated $G = 3{\cdot}57$ (the cell volume of the Chibougamau chloritoid was used in calculating *G* for nos. 42 and 51]; measured $G = 3{\cdot}58 \pm 0{\cdot}04$, triclinic.
51. Mt. Herrick, Vermont, U.S.A. (anal. 2, Table 2). Calculated $G = 3{\cdot}55$ triclinic, small amount monoclinic.

few reflections could be unambiguously indexed. Specific gravities were measured by means of a pycnometer. The given value is an average of three determinations. The calculated and measured specific gravities are in good agreement for determinations made with samples of 1 g or less and with material whose grain size was 200 mesh or less. These calculated and measured specific gravities agree

well with those measured by previous investigators (see Tables 2–7). The cell dimensions in Table 18 are in good agreement with those previously determined (Table 9). No large changes in cell dimensions occur throughout the composition range of the chloritoids measured.

OPTICAL PROPERTIES

Some of the optical properties of chloritoid are summarized in Table 19 (previously determined data) and Table 20 (new data). All the new measurements were made in sodium light because of the high dispersion characteristic of most chloritoids. The optic angles and the orientations of the optical indicatrices were measured on the universal stage in thin sections or grain mounts, or both. The optic orientations were measured with respect to the poles to (001). For grains in which an optic axis was not reached, the distinction between the optic directions was made by means of the pleochroic formula which had been previously determined for other grains of the same sample. All measurements of $2V$ were made by direct rotation from one optic axis to the other. The optical orientations of six of the samples recorded in Table 20 are shown in Fig. 7. In this figure the signs have been chosen so that all the poles to (001) are plotted in one quadrant of the stereographic projection. The indices of refraction were measured to $\pm 0{\cdot}001$ by the oil-immersion method, in grains lying on the (001) cleavage. They are designated α' and β' in Table 20. The average direction angles and the average optic angles were used with the Fresnel–Biot theorem to determine the orientations in the optical indicatrix of the rays whose indices of refraction were measured. Then two equations of the type

$$\frac{x^2}{\alpha^2}+\frac{y^2}{\beta^2}+\frac{z^2}{\gamma^2}=1$$

and the equation

$$\tan^2 V_Z=\frac{\gamma^2(\beta^2-\alpha^2)}{\alpha^2(\gamma^2-\beta^2)}$$

were solved simultaneously for the three principal refractive indices, α, β, and γ.

The data in Table 20 indicate that Z makes angles varying from 2° to 30° with the normal to (001). X varies from 65° to 90° with this direction and Y, 60° to 90°. Much of the variation in individual samples was found to be outside the limits of error. In all the monoclinic chloritoids measured only X lies in (001); therefore, $X = b$ and the optic plane is normal to (010). In the triclinic polymorphs X and Y make angles from 0° to 30° with (001), but in many Y is closer to (001) than X. The orientations of X and Y with respect to the a- and b-axes in triclinic chloritoids were not determined because no crystallographic directions other than the (001) cleavage were identified with certainty in the thin sections and grain mounts of the specimens studied.

Before attempting to reconcile these results with those obtained by other investigators (Table 19) two points must be considered. Most chloritoids have dispersion so high that in most orientations they fail to extinguish between

crossed nicols in white light. Hence, many studies made with light other than monochromatic are of dubious value. Unfortunately, some authors do not specify whether or not they used monochromatic light, and thus it is uncertain how much of the reported variation in optical properties is the result of dispersion. The second point concerns the orientation of the indicatrix with respect

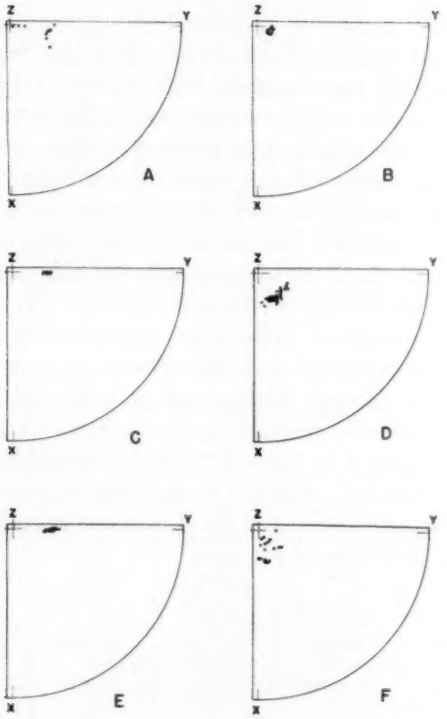

FIG. 7. One quadrant of stereograms showing the orientation of the optic directions, *X*, *Y*, and *Z* with respect to the pole of the (001) cleavage of chloritoid. Measurements made in thin sections designated by crosses, in grain mounts by filled-in circles. Each symbol represents one measured crystal. A, Salm-Château, Belgium (No. 19*M*). B, Rawlinsville, Pennsylvania, U.S.A. (No. 6). C, Üstüaçiksarinç, Turkey (No. 11). D, Chibougamau, Quebec, Canada (No. 12). E, Natick, Rhode Island, U.S.A. (No. 21*a*). F, Michipicoten District, Ontario, Canada (No. 42).

to crystallographic directions. Before the work of Milne (1949) the indices of the crystallographic planes forming the 60° cleavages were not known. Hence, before 1949, anyone who assumed axial ratios similar to those of muscovite obtained an incorrect position for the optic plane (see for example, Tschermak & Sipöcz, 1879, p. 506). In addition to this difficulty the *X*- and *Y*-directions vary with respect to the (001) cleavage in some triclinic chloritoids (Fig. 7 D, F). One is, therefore, not at liberty to conclude from a few measurements,

TABLE 19

Previously determined optical data of chloritoid

	1	2	3	4	5	6	7	8
$\perp(001)\wedge X$	68–85	—	—	—	90	—	90	90
$\perp(001)\wedge Z$	5–22	—	15	30	15	24–25 r* 21 y 18–20 g	18–21	—
Optic plane	∥ (010)	∥ one secondary cleavage	—	—	⊥(010)	—	⊥(010)	⊥(010)
Polymorph†	M	—	—	—	M	—	M	M and T
Indices α	1·722 ±0·002	1·714	> 1·723	1·724	1·716 y ±0·001	1·724 y ±0·002	1·720	1·716 ±0·003
Indices β	1·725 ±0·002	1·717	1·728 ±0·005	1·726	1·719 y ±0·001	1·726 y ±0·002	1·722	1·719 ±0·003
Indices γ	1·728 ±0·002	1·730	< 1·732	1·730	1·725 y ±0·001	1·737 y ±0·003	1·731	1·724 ±0·003
$2V_g$	variable average ~ 60	50–60	—	68	66±2 y	63±2 y	small-medium	56±2
Dispersion	anomalous	r > v	of bisectrices	r > v	r > v	r > v	r > v cross	—

	9	10	11	12		13	14	15	16	17
$\perp(001)\wedge X$	80–90	90	77–87	90 y	78–87 y	—	—	—	—	—
$\perp(001)\wedge Z$	13	—	10½–14	6–12 y	20 y	~ 20	12½ y	13½ y	~ 11	20
Optic plane	⊥(010) ~⊥(010)	⊥(010)	~⊥(010)	⊥(010)	~ ∥(010)	—	—	—	—	—
Polymorph	M and T	M and T	T	M	T	—	—	—	—	—
Indices α	1·719 ±0·003	1·721 ±0·001	—	1·720 y ±0·002		1·725	1·723 y	1·723 y	—	1·721
Indices β	1·721 ±0·001	1·725 ±0·003	1·714 ±0·003	1·723 y ±0·002		1·731	1·727 y	1·725 y	1·708 ±0·005	1·725
Indices γ	1·725 ±0·001	1·728 ±0·003	—	1·727 y ±0·002		—	1·734 y	1·732 y	—	1·728
$2V_g$	56±2	55±2	37–60	54–69 y		~ 45	—	—	45–70	~ 50

	18	19	20	21	22	23	24	25	26
$\perp(001)\wedge X$	—	—	69–78	≠90	90	90	90	—	—
$\perp(001)\wedge Z$	~ 11	~20	12–21	—	9 b 25 r	12–19	~ 12	small	~ 25 3–4 > for r than v
Optic plane	—	—	∥(010)	∥(010)	⊥(010)	⊥(010)	—	~⊥(010)‡	⊥(010)
Polymorph	—	—	M	M	M	M	—	T	M
Indices α	1·713 ±0·003	1·720 ±0·002	—	—	—	—	—	—	—
Indices β	1·719 ±0·003	1·722 ±0·002	—	—	—	—	—	—	—
Indices γ	1·723 ±0·003	1·725 ±0·002	—	—	—	—	—	—	—
$2V$	~ 55–65	—	60	65–70	45–55	58	< 48	69±2½ r 63½±2 v	—
Dispersion	—	—	—	—	r > v horizontal	—	—	r > v horizontal	r > v of bisectrices

TABLE 19 (*cont.*)

	27	28	29	30	31	32	33	34	35	36
$\perp(001) \wedge Z$	—	—	—	10–13	21	12	12	10	12–23	20
Optic plane	∥(010)	∼⊥(010)‡	∼⊥(010)‡	—	—	∥(010)	∥(010)	∥(010)	∥(010)	⊥(010)‡
Polymorph	—	T	T	—	T	M	M	M	M and T	M or T
$2V_Z$	small	70±5 r 62±5 v	64½ r 58 v	∼40	—	—	—	—	> 90	—
Dispersion	r > v	r > v horizontal	r > v horizontal	r > v	r > v horizontal	—	—	—	—	—

	37	38	39	40	41	42	43	44	45
$\perp(001) \wedge Z$	small	—	—	—	—	—	—	—	—
Optic plane	∥ one prismatic cleavage	—	—	—	—	—	—	—	—
Indices α	—	1·716 y	1·722 ±0·001	1·715 y ±0·002	1·730 y	1·721 y	1·721 ±0·002	1·718	1·714 ±0·003
Indices β	—	1·718 y	1·724 ±0·001	1·719 y ±0·002	1·734 y	1·723 y −1·724	1·725 ±0·002	1·727	1·720 ±0·003
Indices γ		1·724 y	1·731 ±0·001	1·737 y ±0·005 52½ r	1·740 y	1·729 y	1·729 ±0·002	1·730	1·724 ±0·003
$2V_Z$	—	—	40–45	50½ y 49 g	—	68	56	65	—
Dispersion	—	—	—	r > v	—	r > v	—	—	—

* r, y, g, b, and v indicate determinations made with red, yellow, green, blue, and violet light, respectively.
† Polymorph reported by the author. M, monoclinic; T, triclinic.
‡ Deduction made from the data given according to the unit cell parameters presented in an earlier section.

1. Dutchess County, New York, U.S.A. Barth & Balk (1934). Analysis 19, Table 3.
2. Ardennes, Belgium. Mélon (1938).
3. Womble Mine, North Carolina, U.S.A. Stuckey (1926). Analysis 20, Table 3. $\gamma-\alpha = 0{\cdot}007$.
4. Champion Mine, Michigan, U.S.A. Milne (1949).
5. Harvey Hill Mine, Quebec, Canada. Milne (1949). $Z \wedge c\text{-axis} = +26\frac{1}{2}°$.
6. Crestlianderstobel, Switzerland. Friedlaender (1929). Analysis 26, Table 4.
7. Blackbird District, Idaho, U.S.A. Shannon (1926). Analysis 40, Table 5.
8. Saxa Vord schists, Ritten Hamar, Unst, Shetland Islands, Scotland. Snelling (1957). Analysis 24, Table 3.
9. Rawlinsville, Pennsylvania, U.S.A. Hietanen (1951). Analysis 1, Table 2.
10. Red Man, Stonehaven, Scotland. Snelling (1957). Analysis 25, Table 3.
11. Mayurbhanj, India. Naha (1955*a*). $\gamma-\alpha = 0{\cdot}0077$. $Z \wedge c\text{-axis} = 13\frac{1}{2}°$. $\perp(001) \wedge Y = 79°–88\frac{1}{2}°$.
12. Hennensädel, Switzerland. van der Plas *et al.* (1958). Analysis 36, Table 4.
13. South-eastern Pennsylvania, U.S.A. Agron (1950, p. 1273).
14. Çatalçam, Turkey. Önay (1949, p. 383). Analysis 29, Table 4.
15. Üstüaçiksarinç, Turkey. Önay (1949, p. 383). Analysis 30, Table 4.
16. Michipicoten District, Ontario, Canada. Collins *et al.* (1926, p. 29).
17. Stonehaven, Scotland. Williamson (1953).
18. From quartz–ankerite vein, Hollinger Mine, Ontario, Canada. Gustafson (1946).
19. Mt. Herrick, Vermont, U.S.A. Zen (1955). Analysis 2, Table 2.
20. Collier Bay, Yampi Sound, Western Australia. Simpson (1915). Analysis 15, Table 3.
21. Ile de Groix, Morbihan, France. von Lasaulx (1883).
22. Ile de Groix, Morbihan, France. Barrois (1884*a*). Analysis 79, Table 7.
23. Alcapedrinka, Portugal. Souza-Brandão (1914). $\gamma-\alpha = 0{\cdot}009$. $\gamma-\beta = 0{\cdot}0065$. $\beta-\alpha = 0{\cdot}0027$.
24. From erratic boulder near Geneva, Switzerland. Duparc & Loup (1903). $\gamma-\alpha = 0{\cdot}015$. $\gamma-\beta = 0{\cdot}010$. $\beta-\alpha = 0{\cdot}002$.
25. Zermatt, Wallis, Switzerland. Des Cloizeaux (1884). Analysis 81, Table 7.
26. Val de Bagnes, Switzerland. Tschopp (1923–4, p. 118). $\gamma-\alpha = 0{\cdot}009$–$0{\cdot}010$.
27. Allalin, Switzerland. Schäfer (1896, p. 111).
28. St. Marcel, Piedmont, Italy. Des Cloizeaux (1884). Analysis 95, Table 7.
29. Val de Chisone, Piedmont, Italy. Des Cloizeaux (1884).
30. Island of Bru, Stavanger, Norway. Goldschmidt (1920, p. 78). $\gamma-\alpha = 0{\cdot}007$.
31. Champion Mine, Michigan, U.S.A. Keller & Lane (1891). Analysis 33, Table 4. $\gamma-\alpha = 0{\cdot}007$.
32. Pregratten, Tirol, Austria. Tschermak & Sipöcz (1879, p. 507). Analysis 39, Table 5.
33. Newport, Rhode Island, U.S.A. Tschermak & Sipöcz (1879, p. 509).
34. Mt. Blia, Sweden. Weibull (1896). Analyses 68, 69, Table 6. $\gamma-\alpha = 0{\cdot}008$.
35. Chesterfield County, South Carolina, U.S.A. Hietanen (1951).
36. Michigamme Lake, Michigan, U.S.A. Hobbs (1895). Analysis 71, Table 6.
37. Ottré, Belgium. de Rauw (1912). Analysis 16, Table 3.
38. Ottré, Belgium. Koch (1935). Analysis 56, Table 6.
39. Berwyn, Pennsylvania, U.S.A. Cloos & Hietanen (1941, p. 143).
40. Saas Valley, Switzerland. Friedlaender (1929). Analysis 27, Table 4.
41. Natick, Rhode Island, U.S.A. Koch (1935). Analysis 31 Table 4.

particularly if variations occur, that any chloritoid crystal in which X or Y lie in (001) is monoclinic with the direction in (001) = b. Rather, it is necessary to show that such a direction coincides with the b-axis. But, if a chloritoid is known to be monoclinic from X-ray or other evidence, and if only one optic direction lies in (001), then this direction must by reason of symmetry coincide with the b-axis.

In view of the preceding statements, it can be shown from the information recorded in previous studies that in Table 19 all except three of the monoclinic chloritoids on which the necessary measurements have been made agree with the results obtained by the writer. The three in disagreement are from Collier Bay, Yampi Sound, Western Australia (20, Table 19); Chesterfield County, South Carolina (35, Table 19); and Dutchess County, New York (1, Table 19).

The optical data for the Collier Bay chloritoid have been obtained from a diagram presented by Simpson (1915). In it, the a- and b-axes have been interchanged as shown by the 120° cleavages. Y is shown in (001). X-ray powder patterns obtained by the writer show that this chloritoid consists of both monoclinic and triclinic polymorphs. The new optical measurements show that in some grains both X and Y are very close to (001). Therefore, without more information it is impossible to say whether Y lies along b or not.

The Chesterfield County chloritoid was studied by Hietanen (1951). She measured a number of lamellae in chloritoid twins, and concluded that some are monoclinic and others are triclinic, and that in the monoclinic polymorphs $Y = b$. A stereogram in her paper shows three lamellae in a twin in which Y lies in (001). Apparently her conclusions regarding the polymorphs observed and the orientation of the optic normal in the monoclinic one are based on whether or not one optic direction lies in (001). As previously stated, this evidence may not be sufficient to distinguish monoclinic from triclinic chloritoid.

Barth & Balk (1934) measured chloritoid from Dutchess County. They found that Y lies in (001) in more than 20 crystals, whereas X and Z vary considerably with respect to (001). From this they concluded that this chloritoid was monoclinic with $Y = b$. This chloritoid seems to be a valid exception to the optic orientation in monoclinic chloritoids measured by the writer.

---

42. Dale of Oddsta, Shetland Islands, Scotland. Guppy & Sabine (1956, pp. 63–64). Analysis 8, Table 2.
43. From sillimanite zone, Kitakami Area, Japan. Seki (1954, p. 230).
44. From biotite zone, Kitakami Area, Japan. Seki (1954, p. 236).
45. From altered lava, Hollinger Mine, Ontario, Canada. Gustafson (1946).

Additional data:

Ardennes, Belgium. Corin (1929). $\perp(001) \wedge X = 73°–76°$. $\perp(001) \wedge Z = 20°$.
Alp de Nadèls, Switzerland. Niggli (1912, p. 24). Analysis 59, Table 6. $\perp(001) \wedge Z = 25°$.
El Cardoso, Spain. Recarte (1951). Analysis 85, Table 7. Optic plane $\parallel(010)$. $2V_Z = 60°$.
Kossoibrod, Ural Mountains, U.S.S.R. Sigg (1918, p. 165). $\gamma - \alpha = 0{\cdot}014$.
Gleinalp, Steiermark, Austria. von Foullon (1883). Analysis 70, Table 6. $\perp(001) \wedge Z = 26°$.
Kalgoorlie, Western Australia. Simpson (1930). Analysis 22 Table 3. $\perp(001) \wedge Z = 4° - 11°$ y.
Tarapaka, Krivoy–Rog, Ukraine, U.S.S.R. Tarasenko (1925). Analysis 46, Table 5. $2V_Z$ variable, $0° - 20°$.
Lainiciu, Rumania. Duparc & Mrazec (1893). Analysis 98, Table 7. $\gamma - \alpha = 0{\cdot}016$. $\perp(001) \wedge Z = 21°$ r, 17° b.
Lakkasandra, Mysore, India. Pichamuthu (1943). $\gamma - \alpha = 0{\cdot}009$–$0{\cdot}010$. $\perp(001) \wedge Z = 9°$.
Eyre Peninsula, South Australia. Tilley (1925). $\gamma - \alpha = 0{\cdot}007$. $\beta = \sim 1{\cdot}73$. Dispersion $r > v$.
Apuane Alps, Italy. D'Achiardi (1886) and Manasse (1906). $\perp(001) \wedge Z = 9° - 38°$. Optic plane $\perp(010)$.
Ernen Power Station, Switzerland. Oberholzer (1955, p. 388). Analysis 28, Table 4. $\alpha = 1{\cdot}732$. $2V_Z = 68° \pm 2°$.

TABLE 20

New optical data on chloritoid

Direction angles between the normal to the (001) cleavage and the nearest optic directions X, Y, and Z, optic angle, and refractive indices. All determinations were made in sodium light

Sample No.:		6	11	12	19*M*	21*a*	42
Figure No.:		7B	7C	7D	7A	7E	7F
$\perp(001) \wedge X$	average*	87°	90°	75°	86°	90°	76°
	range	85°–90°	88°–90°	67°–84°	76°–90°	88°–90°	69°–90°
$\perp(001) \wedge Y$	average	81°	67°	77°	70°	65°	84°
	range	78°–83°	64°–70°	70°–87°	62°–88°	60°–70°	75°–90°
$\perp(001) \wedge Z$	average	9°	23°	20°	20°	25°	15°
	range	6°–11°	20°–26°	17°–24°	2°–30°	21°–30°	6°–22°
$2V_Z$	average	59°	50°	124°	51°	53°	60°
	range	57°–61°	47°–54°	122°–125°	46°–58°	51°–55°	50°–72°
Observed	α'	1·719	1·725	1·725	1·725	1·727	1·726
	β'	1·721	1·727	1·729	1·727	1·729	1·728
Calculated	α	1·719	1·725	1·725	1·725	1·727	1·725
	β	1·720	1·726	1·729	1·726	1·728	1·728
	γ	1·725	1·732	1·730	1·732	1·733	1·735
Polymorph†		M+T	M	T	M+T	M	T

Sample No.:		1		2	13	22	51	
$\perp(001) \wedge X$	average	84°	82°	90°	90°	90°	90°	73°
	range	71°–90°	78°–85°	89°–90°	88°–90°	88°–90°	—	65°–82°
$\perp(001) \wedge Y$	average	80°	74°	71°	80°	85°	70°	90°
	range	67°–89°	71°–79°	65°–75°	75°–84°	81°–88°	66°–73°	—
$\perp(001) \wedge Z$	average	12°	18°	19°	10°	5°	20°	17°
	range	2°–23°	13°–21°	15°–25°	6°–16°	2°–9°	17°–24°	8°–25°
$2V_Z$	average	50°	95°	42°	52°	47°	59°	> 90°
	range	39°–60°	92°–97°	37°–53°	46°–56°	36°–51°	57°–60°	—
Polymorph†		M+T		M	M	M	M+T	

* Average direction angles were obtained from measurements on at least eight grains, and average optic angles on at least five grains in each sample except as noted below.
† Obtained from X-ray data: M, monoclinic; T, triclinic.

1. Collier Bay, Western Australia. Analysis 15, Table 3. Acute optic angles about Z were measured on four grains, and obtuse optic angles on two grains. Direction angles corresponding to the obtuse optic angles were measured on the same two grains.
2. Ile de Groix, France. Muséum National d'Histoire Naturelle, Paris, No. 101.302.
6. Rawlinsville, Pennsylvania, U.S.A. Analysis 1, Table 2.
11. Üstüaçiksarinç, Turkey. Analysis 100, Table 8.
12. Chibougamau, Quebec, Canada. Analysis 101, Table 8.
13. Pregratten, Tirol, Austria. U.S. National Museum, R4496.
19*M*. Salm-Château, Belgium. Analysis 99, Table 8.
21*a*. Natick, Rhode Island, U.S.A. Analysis 102, Table 8.
22. St. Marcel, Piedmont, Italy, U.S .National Museum. R4502.
42. Michipicoten District, Ontario, Canada. Analysis 103. Table 8.
51. Mt. Herrick, Vermont, U.S.A. Analysis 2, Table 2. Acute optic angles abcut Z and direction angles corresponding to the acute optic angles were measured on two grains.

Z is the acute bisectrix in most chloritoids, which are, therefore, optically positive. The Chibougamau chloritoid is negative, however. Some of the chloritoid crystals from Collier Bay and from Mt. Herrick were also found to be optically negative. The optic angles in the optically negative crystals from Mt. Herrick were not measured because no thin section was available to the writer, and only those in which Z is the acute bisectrix could be measured in grain mounts. Optically negative chloritoid has been previously reported from Chesterfield County, South Carolina (Hietanen, 1951). Calculations of the optic angles

from the refractive index measurements in Table 19 indicate that chloritoids from Stonehaven, Scotland; Hollinger Mine, Ontario; and Kitakami Area, Japan (10, 17, 18, 43, 44, 45; Table 19), are also optically negative.

The refractive indices of chloritoid vary as follows: α from 1·713 to 1·730, β from 1·719 to 1·734, and γ from 1·723 to 1·740. Fig. 8 shows some of these variations with increasing magnesium content. Only those analyses in Tables 2,

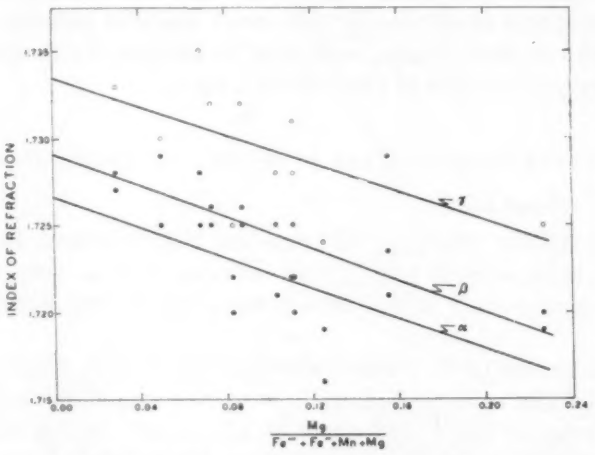

FIG. 8. Variation of indices of refraction with composition of chloritoid: α designated by filled-in circles, β by half filled-in circles, and γ by open circles. The composition is expressed as the ratio of magnesium atoms to the sum of ferric iron, ferrous iron, manganese, and magnesium atoms in the unit cell. The ratios have been calculated from the values given in Tables 2, 3, 5, and 8.

3, 5, and 8 for which refractive index measurements are available have been plotted. The scatter of the points is probably due partly to the number of composition variables and partly to the large changes in $2V$. Fig. 8 shows that increasing magnesium content lowers the refractive indices. This figure should not be used as a determinative chart.

Pleochroism has been omitted from Tables 19 and 20 because the general formula X = green, Y = blue, Z = colourless to yellow, noted by nearly all previous observers, agrees with the observations of the writer. Little is to be gained by listing all the tints previously recorded because their description is so subjective and because they vary considerably in intensity with the thickness of the grains. Different pleochroic formulae have been recorded by Tschermak & Sipöcz (1879, p. 508) and de Rauw (1912). These formulae do not agree with those determined by the writer or others on samples from the same localities.

Other features of chloritoid which can be observed under the polarizing microscope are polysynthetic twinning, the hour-glass structure, and zoning. The twin lamellae are parallel to the (001) cleavage, but were not studied in detail. The recent work on chloritoid twinning has been summarized by Harrison & Brindley (1957). The hour-glass structure is characteristic of chloritoids from

many localities. Commonly, inclusions are concentrated within the hour-glass, thereby giving it prominence, as in Plate 1, fig. D. This structure is also distinctly visible in some chloritoids which are free from inclusions (Plate 1, figs. E, F). It is visible because the part within the hour-glass has a colour different from the rest of the crystal. From this it is concluded that the two parts of the crystal have different optical orientations (see Plate 1, fig. F). Attempts to measure these differences in sodium light were unsuccessful. Observations of the hour-glass structure in chloritoids from many localities indicate that its long axis is parallel to (001). Zoning was noted in sections of chloritoids from St. Gilles, Quebec, cut parallel to (001) (Plate 2, fig. A).

EXPERIMENTS ON THE STABILITY OF CHLORITOID

Previous and related studies

Doelter & Dittler (1912, p. 910) reported that chloritoid from Zermatt, Switzerland, melts at about 1,400° C to a very viscous mass. They obtained only glass after heating for 1 h, but dark-coloured glass with rhombic pyroxene after 12 h.

Lindner & Gruner (1939) treated chloritoid from Natick, Rhode Island, with (1) hydrosulphuric acid, (2) sodium hydrosulphide solution, and (3) sodium sulphide solution at 300° C and about 85 atm in runs lasting about a week. In each run chloritoid was decomposed, the products being (1) pyrite, chlorite, quartz?, nontronite?; (2) pyrite, kaolinite?; (3) magnetite, haematite, kaolinite.

Dr. Loring Coes, Jr., of the Norton Company, Worcester, Massachusetts, performed the first synthesis of chloritoid about 1950 (personal communication, 29 Nov. 1955). He used a reaction mixture consisting of magnesium oxide, hydrated alumina, silica, ferric oxide, and aluminium nitrate. He synthesized chloritoid under the following conditions: 40,000 atm, 700° C; 30,000 atm, 900° C; 25,000 atm, 900° C. The only published reference to this work is by Roy & Tuttle (1956, p. 147).

Bachmann (1956) dehydrated natural chloritoids from Pregratten, Tirol; Lake Superior Iron Region, Michigan; and Natick, Rhode Island. His work shows that when chloritoid is heated in air from room temperature to over 900° C at rates of 4° and 8° C per min, it loses weight between 360° and 700° C. This weight-loss is apparently due to the loss of water and the oxidation of the iron. His work was performed under non-equilibrium conditions for the system FeO–Al_2O_3–SiO_2–H_2O. It is doubtful, from the X-ray diffraction powder data presented and the relatively short experimental time, that the 'dehydrated chloritoid' is a stable phase in the system FeO–Fe_2O_3–Al_2O_3–SiO_2–H_2O at 900° C.

Van der Plas *et al.* (1958) reported the results of both thermogravimetric and differential thermal analyses of chloritoid from Hennensädel, Switzerland. The chloritoid was heated at rates of 2½°, 10°, and 20° C per min. The analyses

showed an endothermic reaction at about 770° C, but all the water was not driven off until 1,050° C.

Schairer & Yagi (1952) investigated the system FeO–Al_2O_3–SiO_2, which includes the anhydrous chloritoid composition. Their work shows that the anhydrous chloritoid composition will crystallize to 44·59 per cent hercynite

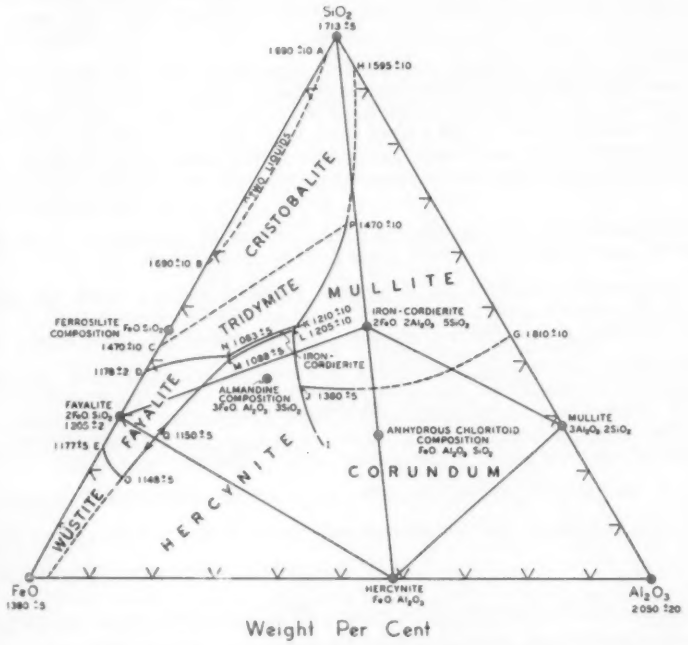

FIG. 9. Equilibrium diagram of the system FeO–Al_2O_3–SiO_2 showing fields of primary crystalline phases, tie lines, and invariant points. After Schairer & Yagi (1952).

and 55·41 per cent iron cordierite by weight below 1,205° ± 10° C, the temperature of the reaction point *L* in Fig. 9. With rising temperature, liquid appears at that point and increases in amount until iron cordierite is consumed. The stable phases are hercynite + mullite + liquid. With increasing temperature, the composition of the liquid follows the boundary curve *LJ* (Fig. 9) to *J*, 1,380° ± 5° C. At this point mullite reacts with liquid to give corundum. When the mullite is consumed the stable phases are hercynite + corundum + liquid. With increasing temperature the composition of the liquid changes along the boundary curve *JI* (Fig. 9) between the fields of hercynite and corundum until a point is reached which lies on the projection of a line connecting the anhydrous chloritoid composition with corundum. Here the hercynite has disappeared and the stable phases are corundum + liquid. Extrapolation from the liquidus isotherms (Fig. 10) indicates that complete melting would be achieved near 1,700° C.

Method of investigation

The starting materials, together with their sources, chemical analyses (if available) and other information, are given in Table 21. Two or three of these materials at a time were weighed out in the proportions of the chloritoid composition, and mixed in lots of about 2 g by grinding them together under acetone

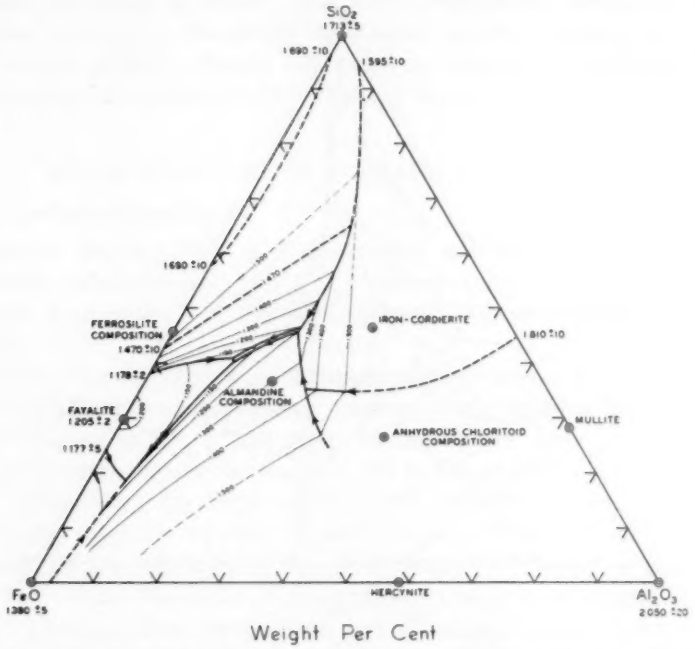

FIG. 10. Equilibrium diagram of the system $FeO–Al_2O_3–SiO_2$ showing isotherms. After Schairer & Yagi (1952).

in a mechanical grinder for about 2 h. Several mixtures were tried at first, in order to determine the reagents yielding the highest rates of reaction and the highest quality of products. Also, if the same products are obtained from several mixtures under the same conditions then the investigator can be more certain of having obtained equilibrium in his experiments. Additional mixtures were prepared when those tried first did not yield chloritoid at pressures up to 2,000 bars. The mixtures found to be most suitable were those containing kaolinite, γ-alumina, and either siderite or ferrous oxalate. The reagents in each mixture are included in Table 22. In addition to these mixtures others which contained andalusite, fayalite, kyanite, pyrophyllite, sillimanite, and staurolite were used in a few experiments. They gave the same results as the other mixtures, but reaction in those containing any one of andalusite, kyanite, sillimanite, or staurolite was very slow.

TABLE 21

Materials used in mixtures

Ferrous oxalate: From Merck Co., S 3547, C 1253. Loss at 1,000° C, determined by the writer, 43·4%.

Powdered iron: Baker's analysed C.P. by hydrogen, lot No. 1·2642. Analysis on label: subst. insol. in H_2SO_4, 0·04%; H_2O sol. subst., 0·024%; N, 0·0067%; S, 0·000%; As, 0·000%.

Siderite: From the Doré Lake Area, Chibougamau, Quebec, Canada, collected by Dr. Gilles Allard. Partial analysis of grab sample by the Quebec Department of Mines: SiO_2, 1·96%; Fe, 41·69%; Mn, 2·22%; CaO, 0·35%; MgO, 2·77%; S, 0·32%; As, 0·00%; P, 0·00%; Cu, 0·34%; loss at 1,000° C, 31·17%. Loss at 1,000° C, determined by the writer, 32·67%. Neither quartz nor copper minerals were detected in X-ray diffraction powder patterns or in grain mounts under the microscope in the siderite actually used.

Fayalite: From Rockport, Massachusetts, U.S.A., analysed by Penfield & Forbes (1896, p. 130): SiO_2, 30·08%; FeO, 68·12%; MnO, 0·72%; H_2O, 0·88%; total, 99·80%.

γ-alumina: Fisher Scientific Company $Al(OH)_3$, E and A tested purity reagent, cat. No. A–581, lot No. 470434 was heated 40 min with a Meeker burner. The X-ray powder pattern was characteristic of γ-alumina. Loss after 5½ h at 1,000° C, 1·65%.

Kaolinite: From Zettlitz, Czechoslovakia, analysed by Ross & Kerr (1930): SiO_2, 46·90%; Al_2O_3, 37·40%; Fe_2O_3, 0·65%; P_2O_5, 0·08%; TiO_2, 0·18%; ZrO_2, 0·007%; MnO, 0·007%; CaO, 0·29%; MgO, 0·27%; BaO, 0·02%; SrO, 0·006%; Cr_2O_3, 0·015%; V_2O_3, 0·002%; K_2O, 0·84%; Na_2O, 0·44%; SO_3, 0·03%; loss at 105°–110° C, 12·95%; total, 100·087%. Loss on ignition determined by the writer, 13·20%.

Andalusite: From Standish, Maine, U.S.A., obtained from Dr. F. C. Kracek.

Kyanite: Supplied by Dr. H. S. Yoder. This material had been treated with aqua regia.

Silica glass: Heraens supplied by Dr. H. S. Yoder.

Experiments were performed in five types of equipment which maintained the mixtures at fixed temperatures and fixed total pressures throughout the length of the runs: (1) unsealed platinum foil crucibles within larger unsealed crucibles containing the same preparation as the charge (Bowen & Tuttle, 1949, p. 441) in a Tuttle press (Van den Heurk, 1953), (2) sealed platinum capsules (Yoder & Eugster, 1954, p. 160) in a cold-seal bomb (Tuttle, 1949), (3) sealed platinum capsules in an internally heated high-pressure apparatus (Yoder, 1950, pp. 827–30),[1] (4) evacuated silica-glass tubes without a pressure vessel, (5) 'simple squeezer' apparatus (Boyd & England, 1956).[2] The numbers in Table 22 under 'Apparatus' refer to these five types of equipment. The products were identified chiefly by their X-ray diffraction powder patterns obtained with a Norelco Geiger-counter diffractometer. Some use was made of the Philips powder camera previously mentioned. The products of all runs were examined in reflected light with a stereomicroscope and in transmitted light with a petrographic microscope.

[1] Runs in the internally heated apparatus were performed with the cooperation of Drs. H. S. Yoder and D. B. Stewart.

[2] Runs in the 'simple squeezer' were performed with the cooperation of Dr. F. R. Boyd, Jr., and Mr. J. L. England.

TABLE 22

Results of hydrothermal treatment of various charges having the composition of chloritoid

Temp. °C	*Pressure in kilobars*	*Time in hours*	*Apparatus*	*Products**
		Triclinic chloritoid, Chibougamau, Quebec, Canada (anal. 101, Table 8)		
530	0	3,192	4†	T-ctd
400	1	429	2	T-ctd
400	1	3,630	2	T-ctd
500	1	429	2	T-ctd
500	1	4,049	2	T-ctd + mul‡
600	1	240	2	T-ctd + her + Fe-cord + *mul*§
600	1	1,688	2	her + Fe-cord + ctd + *mul*
400	2	3,742	2	T-ctd
515	2	165	1	T-ctd
515	2	167	2	T-ctd
550	2	165	1	T-ctd
550	2	999	2	T-ctd + *mul*
550	2	1,534	2	T-ctd + *mul*
575	2	160	1	T-ctd
575	2	403	1	T-ctd
585	2	599	1	T-ctd + mag + Q
585	2	842	2	T-ctd + *mul*
600	2	70	1	T-ctd + *her* + *Fe-cord*
600	2	70	2	T-ctd + *her* + *Fe-cord* + *mul*
600	2	139	1	T-ctd + her + *Q* + *mag*
600	2	165	1	T-ctd + her + *Q* + *mag*
600	2	405	1	T-ctd + mag + *Q* + *mul*
600	2	494	2	T-ctd + Fe-cord + her + mul
600	2	626	2	T-ctd + Fe-cord + her + *mul*
610	2	499	1	her + Fe-cord + ctd
650	2	1	1	T-ctd
650	2	40	1	her + Fe-cord + ctd + *mul*
650	2	117	2	T-ctd + Fe-cord + her + *mul*
650	2	165	1	her + Fe-cord + *ctd* + *mul*
700	2	144	2	her + Fe-cord + mul
850	2	72	2	her + Fe-cord + Q + mul
600	5	204	2	T-ctd + *mul*
550	6	88	3	T-ctd
700	6	16	3	T-ctd + her + Q + *mul*
650	9·2	22	3	T-ctd + Q + mag
600	10	1	5	T-ctd
600	10	6	3	T-ctd
650	10	3	5	T-ctd
675	10	3	5	T-ctd
700	10	1	5	T-ctd + *undetermined incipient decomposition products*
700	10	4	3	T-ctd
725	10	3	5	T-ctd + her + alm + staur + Q
750	10	1	5	T-ctd + her + alm + staur
800	10	1	5	alm + staur + her + Q
800	10	24	3	cor + mag + Q + staur
675	20	3	5	T-ctd
700	20	3	5	T-ctd
725	20	3	5	T-ctd + staur + her
750	20	1	5	staur + alm + her + ctd
800	20	1	5	staur + alm + her
600	30	1	5	T-ctd
675	30	3	5	T-ctd
700	30	1	5	T-ctd
725	30	3	5	T-ctd + alm + staur + her
750	30	3	5	staur + alm + ctd
800	30	1	5	staur + alm + her

TABLE 22 (*cont.*)

Temp. °C	*Pressure in kilobars*	*Time in hours*	*Apparatus*	*Products**
		Monoclinic chloritoid, Üstüaçiksarinç, Turkey (anal. 100, Table 8)		
400	2	3,742	2	M-ctd
550	2	165	2	M-ctd
650	2	165	2	her + Fe-cord + *mul*
700	10	1	5	M-ctd + *undetermined incipient decomposition products*
750	10	1	5	M-ctd + her + alm + staur
800	10	1	5	staur + alm + her + Q
800	20	1	5	staur + alm + her
600	30	1	5	M-ctd
700	30	1	5	M-ctd
750	30	1	5	M-ctd + *staur* + *alm* + *her*
750	30	3	5	M-ctd + staur + alm + her
800	30	1	5	staur + alm + her
		Ferrous oxalate + γ-alumina + silica glass		
500	2	520	2‖	cham + Q + mul
550	2	1	1	cham + *?* + *?*
550	2	24	1	cham + *?* + *?*
550	2	186	1	her + Q
550	2	257	1¶	cham + her
600	2	334	2	her + Q + Fe-cord + *mul*
600	2	494	2	her + Fe-cord + Q + *mul*
650	2	117	2	her + Q + Fe-cord + *mul*
700	2	144	2	Q + her + *mul*
800	2	308	2	cor + her + Q + mul
850	2	72	2	her + Q + mul
		Siderite + γ-alumina + silica glass		
500	2	246	1	cham + *mag* + *Q*
550	2	312	1	cham + her
600	2	406	2	her + Fe-cord + Q
		Ferrous oxalate + γ-alumina + kaolinite		
400	1	429	2	cham + *?*
400	1	3,630	2	cham + *?*
500	1	429	2	cham + *?* + *mul*
500	1	4,049	2	cham + *?* + *mul*
600	1	1,688	2	her + Fe-cord + Q + *mul*
400	2	3,742	2	cham + *?*
450	2	2,216	2	cham + *mul* + *?*
500	2	192	1	cham + *Q*
500	2	1,510	2	cham + Q
550	2	20	2	cham + *?* + *?*
550	2	185	1	cham + *?* + *?*
550	2	280	2	cham + *?* + *?*
550	2	1,534	2	Q + her + *cham*
600	2	10	2	cham + *her* + *?*
600	2	283	2	her + Q + Fe-cord
700	2	144	2	her + Fe-cord + mul
800	2	308	2	her-mag solid solution + cor + Q + mul
600	5	204	2	cham + Q + *her* + *mul*
550	6	88	3	cham + *?*
700	6	16	3	her + Q + *mul*
650	9·2	22	3	ctd + mag + Q + cor
		Siderite + γ-alumina + kaolinite		
400	1	3,630	2	cham
500	1	429	2	cham + *Q* + *?*
500	1	4,049	2	cham + *Q*
600	1	1,688	2	her + Fe-cord + Q + *mul*

TABLE 22 (*cont.*)

Temp. °C	*Pressure in kilobars*	*Time in hours*	*Apparatus*	*Products**
400	2	3,742	2	cham + *?*
450	2	2,215	2	cham + *?* + *?*
500	2	189	1	cham + *?* + *?*
500	2	1,510	2	cham + her + *Q*
550	2	334	1	mag + *?* + *?*
550	2	476	2	cham + *Q*
550	2	1,576	2	cham + Fe-cord + Q + her
600	2	476	2	her + Fe-cord
600	5	204	2	chlorite + Q + *mul*
500	6	107	3	cham + her + *Q*
550	6	88	3	cham + Q + siderite
700	6	16	3	her + Q + *mul*
650	9·2	22	3	ctd + mag + cor + Q
600	10	6	3	ctd + *?*
700	10	4	3	her + alm + staur + Q
800	10	24	3	staur + alm + Q + cor + mag
		Powdered iron + γ-alumina + silica glass		
500	2	191	1	cham + *?* + *?*
550	2	23	2	cham + *?*
550	2	191	1	cham + her + *?*
550	2	280	2	cham + Q
550	2	1,581	2	cham + her + Q + Fe-cord
600	2	19	2	Q + her
600	2	283	2	her + Q + Fe-cord
		Powdered iron + γ-alumina + kaolinite		
500	2	192	1	cham + Q
550	2	143	1	her + Q
550	2	280	2	cham + *?*
550	2	1,534	2	cham + Q + her
600	2	283	2	Fe-cord + her + mul
700	6	16	3	Q + her + mul
		Ferrous oxalate + kyanite		
500	2	192	1	ky + cham + her + *Q*
550	2	192	1	ky + her + cham + mag
550	2	268	2	ky + her + cham + Fe-cord
550	2	1,581	2	ky + her + *Q*
600	2	268	2	ky + her + *Q*
		Siderite + kyanite		
500	2	191	1	ky + cham + her
550	2	194	1	ky + her + cham + Q
550	2	476	2	ky + cham
550	2	1,581	2	ky + chlorite + her
600	2	476	2	ky + her + siderite
700	6	16	3	ky + her + Fe-cord
		Ferrous oxalate + andalusite		
500	2	245	1	and + cham + *mag*
550	2	162	1	and + mag + cham + her
550	2	268	2	and + mag
600	2	268	2	and + mag
		Siderite + andalusite		
500	2	245	1	and + cham + *mag*
500	2	1,510	2	and + cham + *mag*
550	2	23	2	and + siderite + cham
550	2	161	1	and + cham + mag
550	2	268	2	and + mag + cham
600	2	19	2	and + mag
600	2	268	2	and + mag + Fe-cord
		Fayalite + γ-alumina + kaolinite		
650	9·2	22	3	ctd + mag + Q + cor

Experimental data

The experiments performed, and their results, are given in Table 22. Equilibrium was evidently not attained in many of these experiments because, according to the Phase Rule, too many phases were present as products. Phases considered to be metastable formed in some experiments. In order to determine the more stable phases in runs where too many phases were observed, and to obtain information about possible metastable phases, many experiments were repeated under the same conditions of pressure and temperature, only the time being changed.

The stability of chloritoid, $FeO \cdot Al_2O_3 \cdot SiO_2 \cdot H_2O$, is controlled by the temperature, the total pressure, the water pressure, and the oxygen pressure. The experiments listed in Table 22 were carried out under controlled temperatures and total pressures, and with the water pressure equal to the total pressure, although the water pressure may have been less than the total pressure in the 'simple squeezer'. They were performed before buffers were used in attempting to control the oxygen pressure in sealed capsules (Eugster, 1957; 1959, p. 412). Nevertheless, throughout the pressure and temperature ranges of the experiments made in sealed capsules and cold-seal bombs[1] magnetite was found to be the stable iron oxide. The alloy of the bombs is considered to have much the same effect on controlling the oxygen pressures as the buffers described by Eugster, but the oxygen pressures in equilibrium with this alloy and its oxides are known only to be within the range of oxygen pressures in equilibrium with magnetite. The buffers around the closed but unsealed crucibles used in the Tuttle press may have controlled the oxygen pressure at least in the shorter runs. In the experiments made with unsealed crucibles, scaly white quartz was noted between the layers of platinum foil. It indicated some leaching of silica from the charges. The results obtained from both types of experiments agree, however, except that in the unsealed crucibles magnetite formed from the decomposition of chloritoid in long runs. Oxygen pressures were not controlled in experiments carried out in Yoder's internally heated, high-pressure apparatus nor in the 'simple squeezer'. At 10,000 bars, a pressure attainable in both of these two types of equipment, the results agree.

[1] The bombs were composed of Cr, 19–21 per cent; Ni, 9–11 per cent; Co, 46–53 per cent; Fe, 3 per cent max.; W, 14–16 per cent; C, 0·15 per cent max.; Mn, 1–2 per cent; Si, 1 per cent max.; an alloy known as Haynes No. 25, obtainable from Haynes Stellite Company, Kokomo, Indiana.

Notes to Table 22.

* Products are given in order of decreasing abundance and are abbreviated as follows: alm, almandine; and, andalusite; cham, chamosite; cor, corundum; ctd, chloritoid; Fe-cord, iron cordierite; her, hercynite; ky, kyanite; mag, magnetite; M-ctd, monoclinic chloritoid; mul, mullite; Q, quartz; staur, staurolite; T-ctd, triclinic chloritoid; ?, unidentified phase.

† See text (p. 93) for description of apparatus to which numbers refer.

‡ Mullite formed on the surface of the charges only (see text, p. 103).

§ Italicized products were observed only under the microscope and did not show on X-ray diffraction powder patterns; they probably constituted less than 5 per cent of the products.

‖ Zinc and water were used as a buffer in an outer sealed capsule.

¶ Powdered iron was used as a buffer in the outer crucible.

The results of experiments listed in Table 22 indicate that at 2,000 bars and 593°±8° C, chloritoid decomposed to iron cordierite+hercynite+vapour. This decomposition was sluggish: even after almost 4 weeks at 600° C in a sealed capsule less than about 10 per cent of the chloritoid had decomposed. Decomposition was somewhat faster in unsealed crucibles, but in them magnetite formed more readily. At a pressure of 2,000 bars and at temperatures between 600° and 700° C, the mixtures having the composition of chloritoid also reacted to form hercynite and iron cordierite. Generally hercynite and quartz formed first and then reacted to form iron cordierite. At 1,000 bars and 550°±50° C chloritoid also decomposed to hercynite+iron cordierite+vapour. This temperature was not determined more precisely because of the sluggishness of the reaction. The same results were obtained with mixtures of the chloritoid composition. Hercynite and iron cordierite are believed to be stable up to the beginning of melting, a point determined as 1,205° C in nitrogen at atmospheric pressure by Schairer & Yagi (1952). In this temperature range iron cordierite might be expected to undergo one or more inversions similar to those for the magnesium analogue. In two runs at 2,000 bars and 550° C iron cordierite was one of the products of the charges which originally consisted of siderite, γ-alumina, and kaolinite, and ferrous oxalate, and kyanite. As it did not form in other experiments under these conditions, it is probably metastable. Nevertheless, it is possible that chloritoid may decompose even under these conditions if given long enough, and that in the other experiments the crystallization of iron cordierite was inhibited by the metastable crystallization of chamosite (see following section on phases synthesized). In 16-hour runs at 6,000 bars and 700° C, hercynite and iron cordierite formed from a mixture of siderite and kyanite, whereas only hercynite and quartz formed from the decomposition of chloritoid and from a mixture of ferrous oxalate, γ-alumina, and kaolinite. It is believed that in longer runs hercynite and iron cordierite would have formed from both mixtures and from the chloritoid. At any rate, iron cordierite crystallized at 700° C under a water pressure of 6,000 bars. At 10,000 bars water pressure, however, experiments at 700° C have shown other phases to form from the decomposition of chloritoid. Hence iron cordierite is not stable in mixtures having the chloritoid composition at 10,000 bars water pressure and 700° C, but it may be stable at this total pressure with lower water pressures.

At pressures greater than 10,000 bars chloritoid decomposed to staurolite+almandine+hercynite+vapour, at about 700° C. The actual pressures and temperatures of decomposition were: 10,000 bars, 688°±13° C; 20,000 bars, 712°±13° C; 30,000 bars, 713°±13° C. These same products, plus quartz were obtained from a mixture of siderite, γ-alumina, and kaolinite heated at 10,000 bars and 700° C for 4 h. Although natural chloritoid did not decompose in 4 h under these same conditions in Yoder's internally heated, high-pressure apparatus, incipient decomposition was observed at the edges of chloritoid plates held at the same pressure and temperature for 1 h in the 'simple squeezer'.

Therefore, the decomposition temperature of chloritoid at 10,000 bars is placed between 675° and 700° C. In all experiments made in the 'simple squeezer' below 700° C the chloritoid contained some opaque inclusions and did not appear as fresh as when put in, although no other phases showed on X-ray diffraction powder patterns. In some runs in the squeezer, only two of the three

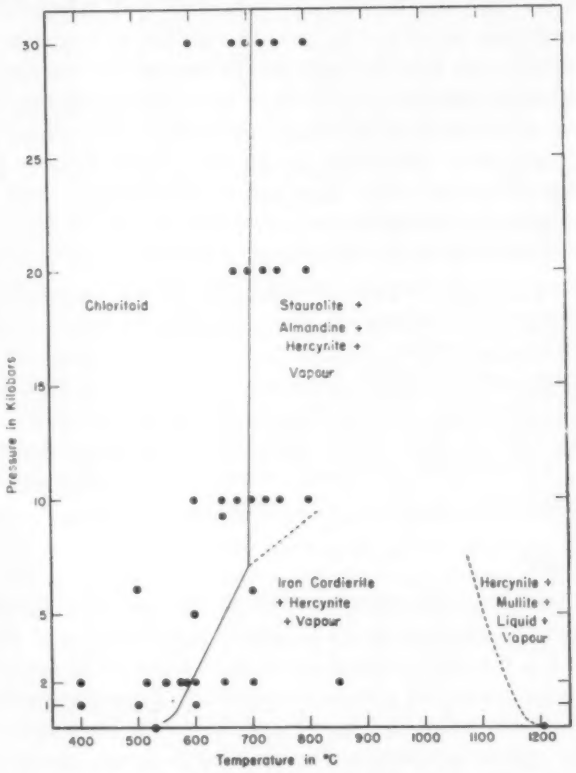

FIG. 11. Preliminary univariant curves for the reactions chloritoid $\rightleftarrows$ iron cordierite+hercynite+vapour, chloritoid $\rightleftarrows$ almandine+staurolite+hercynite+vapour, staurolite+almandine $\rightleftarrows$ iron cordierite+hercynite+vapour, and iron cordierite $\rightleftarrows$ mullite+liquid. The point at 1205° C was determined by Schairer & Yagi (1952).

solid phases were observed in the decomposition runs. For these reasons the results obtained with the squeezer must be regarded with caution. Two of the temperatures at which chloritoid was synthesized by Coes lie above the decomposition curve determined in this study (Fig. 11). His chloritoid may have crystallized metastably at these temperatures or, more likely, was stabilized by the partial substitution of magnesium for ferrous iron.

Chloritoid was synthesized at 9,240 bars and 650° C in 22 h from three mixtures and at 10,000 bars and 600° C in 6 h from one mixture having the composition of chloritoid. In none of these runs was chloritoid alone produced but

was accompanied by magnetite, quartz, and corundum in the 22-h runs and by one or more unidentified phases in the 6-h run. In the longer runs it is probable that chloritoid formed and then, as the oxygen pressure increased, part of it broke down to magnetite, quartz, and corundum.

As natural chloritoid did not decompose on the low-temperature side of the curves drawn through the limiting temperatures and pressures given in the preceding paragraphs (see Fig. 11), even in runs up to 5 months, chloritoid is considered stable in this field although the decomposition reactions were not reversed. Furthermore, chloritoid is known in natural hydrothermal environments (see section on occurrence of chloritoid, pp. 106–7, 117) where the pressures were probably less than 2,000 bars. In the two longest runs at 1,000 bars the chloritoid appeared coarser than when put in. Chamosite, which formed from most of the mixtures at temperatures and pressures in this field, is considered to be metastable and will be discussed later. For those runs, in Table 22, where there were enough chloritoid peaks in the X-ray diffraction powder pattern, the chloritoid polymorph is designated. In no experiment was a change from triclinic to monoclinic chloritoid or from monoclinic to triclinic chloritoid noted.

In several experiments triclinic chloritoid and quartz, mixed in the proportions of iron cordierite, showed no change after 15 weeks at 550° C and 2,000 bars. However, after 17 h at 700° C and 4,060 bars the products were quartz and hercynite. Additional experiments are required to define the conditions of the reaction chloritoid + quartz $\rightleftarrows$ iron cordierite + vapour.

Phases synthesized

Chloritoid. An X-ray diffraction powder photograph of the products from a mixture of siderite, γ-alumina, and kaolinite held at 600° C and 10,000 bars for 6 h is shown in Fig. 6 F. The *d* values are given in Table 23. In addition to chloritoid one or more unidentified phases were present. Lines due to these unidentified phases have been noted in Fig. 6 F and Table 23. They were too small to determine their optical properties. The chloritoid pattern shows a mixture of both monoclinic and triclinic polymorphs. When the platinum capsules in which chloritoid grew were opened, the chloritoid appeared in irregular clear or whitish platy aggregates about 30 μ across. If present with other phases, some of these were included in it. Under the petrographic microscope they had a greenish tint, and very low birefringence. The individual plates composing the aggregates were too small to observe all their optical properties, but they had an index of refraction of about 1·720.

Chamosite. The term chamosite is here restricted to aluminium-bearing iron-rich phases of the chlorite composition which have 7-Å basal spacings in X-ray diffraction patterns in contrast to the better-known polymorphs with 14-Å basal spacings. The conversion of a 7-Å phase into a 14-Å phase was first demonstrated by Yoder (1952, pp. 579–81, 595) and subsequently by Nelson & Roy (1958). In this study, chamosite crystallized from all but one of the investigated mixtures

TABLE 23

Interplanar spacings of synthetic chloritoid and other phases

d	*I*	*d*	*I*	*d*	*I*	*d*	*I*
10·02*	2	3·10*	2	2·225	2 broad	1·481	1
8·25*	3	2·96	4	2·134	7	1·422	1
5·30*	2	2·70	6 broad	2·094	3	1·385	1
4·95*	3	2·64		1·865	2	1·363	7
4·74	3	2·55*	2	1·831	2	1·254	1
4·45	10	2·49	7 broad	1·750	1	1·184	1
4·14*	8	2·45		1·580	8	1·112	1
3·98*	1	2·37	4	1·558	5	1·033	1
3·34*	1	2·33	1	1·495	1	1·019*	1
3·25	2	2·30	3				

* Spacings so marked are due to unidentified phases mixed with the chloritoid.

at temperatures below 600° C. It formed in as short a time as 1 h and persisted for as long as 5½ months, although in some of these long runs it was not as abundant as before, its place being taken by quartz, hercynite, or iron cordierite. At 600° C it formed in a few runs but never persisted longer than about 3 weeks, and then only in very small amounts. For these reasons it is regarded as metastable. It probably crystallized during the time the charges were being brought up to the temperature of the runs.

It formed pale green to brownish-green platy aggregates from a few to a few tens of microns across. In these the individual plates were less than 10 μ, but were seldom isolated. The flakes had an interference colour of first-order grey, and an index of refraction of about 1·69. This index of refraction is higher than 1·68, the index assigned by Hey (1954) to the high-aluminium end of the ferrous iron chlorite solid solution series, probably because of some oxidation of the iron. The X-ray diffraction powder pattern contained only a few peaks as follows:

d	*I*	*d*	*I*
7·06	10	2·47	1
3·53	8	2·41	1
2·89	3	1·558	3

The basal spacing of 7·06 Å indicates a composition near the high aluminium end of the chamosite solid solution series, according to Nelson & Roy (1958). It is concluded that the chamosites made in this study had compositions close to pseudothuringite, $2FeO \cdot Al_2O_3 \cdot SiO_2 \cdot 2H_2O$.

In some runs chamosite was the only phase observed and identified, and in others it was accompanied by one or more of hercynite, iron cordierite, quartz, magnetite, an unidentified phase, or by unreacted minerals in the starting mixtures. This unidentified phase was present in some runs as a few flakes about 5 μ or less across and with an index of refraction lower than that of the chamosite.

As no peaks belonging to such a phase were apparent on the X-ray diffraction powder patterns, it is concluded that this phase was present in amounts too small to show on the patterns, was amorphous or too fine-grained to be resolved by X-rays, or its peaks coincided with those of chamosite. A distinct possibility for this phase is kaolinite. It may well have been entirely hidden by the chamosite in some runs. Thus where chamosite is shown as the chief or only aluminous product in Table 22, it probably is hiding another phase and, hence, has a composition different from chloritoid.

Chlorite. In two runs, both at 2,000 bars but one at 550° C and the other at 600° C, a mineral resembling chamosite, but having a 14-Å basal spacing was noted as one of the products. It probably inverted from a chamosite. As the peak corresponding to the 14-Å basal spacing in iron-rich chlorites is not strong, it may not have been recorded on some of the diffractometer patterns. Thus it is possible that some of the products identified as chamosite are actually chlorite.

Hercynite and magnetite. Hercynite was one of the products in many of the experiments. It crystallized readily at 600° C and above, but was less common below 600° C. It grew in green isotropic grains of varying size from octahedra several tens of microns in size to crystals only a few microns across and too small to determine their habit. Its index of refraction was about 1·83. The peaks on its X-ray diffraction powder pattern yielded a unit cell edge of 8·175 Å, which corresponds to a solid solution between magnetite and hercynite containing 91 per cent hercynite, according to Turnock & Eugster (1958*a*). Magnetite crystallized along with corundum and quartz in several experiments at 650° and 800° C. Its growth in these runs is attributed to the decomposition of ferrous aluminium silicates by increasing oxygen pressures. Its cell edge was 8·36 Å. Magnetite also crystallized in some of the longer runs made in unsealed crucibles, probably for the same reason. In other experiments when the aluminium silicate of the starting mixture scarcely reacted at all, magnetite was one of the products. It also had a cell edge of 8·36 Å. Its growth in such experiments probably results from the decomposition of the ferrous iron compound of the starting mixture, and little or no subsequent reaction with the aluminium silicate. When magnetite and hercynite were not present in sufficient quantity to show on X-ray diffraction powder patterns, an optical distinction between them was made: hercynite is translucent, and magnetite is opaque. Such a distinction, however, is not entirely satisfactory between grains only a few microns in size.

In some experiments some peaks on the X-ray diffraction patterns corresponding to the general spinel pattern lay at 2θ angles between those of the magnetite and those of the hercynite previously described. Measurements were not made on all patterns with such peaks but some of these spinels had cell edges of 8·233 Å equivalent to 70 per cent hercynite in a magnetite–hercynite solid solution. Such phases have been designated magnetite–hercynite solid solution in Table 22.

Iron cordierite. The compound $2FeO \cdot 2Al_2O_3 \cdot 5SiO_2$ crystallized as one of the

products from mixtures having the composition of chloritoid and from the decomposition of natural chloritoids at pressures up to 6,000 bars. It even grew in two runs below what is believed to be the decomposition temperature of chloritoid. It was accompanied by quartz and hercynite in many of the runs where it was noted. As it increased in amount at their expense in longer runs it is believed to have formed by reaction between quartz and hercynite in those charges which consisted of mixtures. It seemed to form directly from the decomposition of chloritoid. The size and number of the crystals varied from run to run and could not be predicted. The largest crystals came from a mixture of powdered iron, γ-alumina, and kaolinite held at 2,000 bars and 600° C for 283 h. They were clear, hexagonal, and barrel-shaped, and measured 200 by 50 μ. They had parallel extinction and indices of refraction of $\alpha' = 1{\cdot}560$ and $\gamma' = 1{\cdot}569$. In other runs the crystals were smaller, but had similar properties. The X-ray diffraction powder pattern of the iron cordierite formed in these experiments was similar to that of the iron cordierite produced by Schairer & Yagi (1952, p. 499).

Almandine. Almandine was identified by means of its X-ray diffraction powder pattern. It occurred as greenish equant grains up to about 15 μ across as one of the products from the decomposition of chloritoid at pressures of 10,000 bars and greater, and from a mixture of siderite, γ-alumina, and kaolinite at 700° C and 10,000 bars. Optically it was not easily distinguished from hercynite, both having an index of refraction of about 1·83.

Staurolite. Greenish rod-like crystals up to about 30 μ long formed at pressures of 10,000 bars and greater as one of the products from the decomposition of chloritoid and from a mixture of siderite, γ-alumina, and kaolinite at 700° C and 10,000 bars. These crystals had parallel extinction and an index of refraction normal to their length of $1{\cdot}740 \pm 0{\cdot}003$. Their optical properties and X-ray diffraction powder pattern are similar to those of a natural staurolite from Epworth, Georgia.

Corundum. Pale bluish-green crystals up to about 20 μ across, with refractive indices of about 1·76, were formed as one of the products in some runs at 650° and 800° C at several different pressures. They were identified as corundum by means of their X-ray diffraction powder patterns.

Quartz. Quartz crystallized readily in many of the experiments in crystals of varying size. It was identified by its X-ray diffraction powder pattern and optically by its indices of refraction, which are lower than those of other phases obtained in these experiments.

Mullite. In many of the experiments carried out in sealed capsules and in some of the unsealed foil crucibles white needles 10 to 20 μ long grew around the charge adjacent to the platinum walls. They were more plentiful in some of the longer experiments and in those conducted at temperatures above about 700° C. Only a few were observed in short runs at low temperatures. They were mixed with smaller amounts of quartz crystals which in some experiments were

terminated by hexagonal pyramids. The platinum of the containers in which these needles were numerous was tarnished and brittle. The needles had indices of refraction of about 1·65 but their size prevented more precise measurements. They were weakly birefringent and had parallel extinction. X-ray diffraction powder patterns indicated that they were mullite or sillimanite, but the presence of quartz in the material X-rayed made distinctions between the two difficult. The 2θ angles equivalent to interplanar spacings of 1·79 to 1·54 Å, the range with the greatest differences in the patterns of mullite and sillimanite, were scanned slowly on the diffractometer. The patterns obtained suggested the presence of mullite rather than sillimanite but were not conclusive. These observations suggest that the iron in the charge adjacent to the walls went into solid solution with the platinum of the container leaving a shell of material having the composition $Al_2O_3 \cdot SiO_2$ around the charge. This material consisted of SiO_2 as quartz and another phase which must have contained less SiO_2 than that given by a one-to-one ratio of alumina to silica. This other phase is probably mullite. The needles characteristic of mullite were observed in runs held at pressures up to 6,000 bars and at temperatures up to 800° C.

OCCURRENCE OF CHLORITOID

Previous theories

Chloritoid is thought by some geologists to be a rare mineral and was considered to form only under stress conditions in rocks of a restricted chemical composition. It has, however, been described from more than a hundred localities and from several geological environments in rocks containing a relatively high content of alumina but otherwise having a wide range of chemical composition. The concept that shearing stress or non-hydrostatic stress plays an important part in the stability of minerals was proposed by Harker (1918; 1928; 1932, pp. 147–51). He distinguished between stress minerals and anti-stress minerals. Stress minerals are those whose field of stability on a pressure-temperature diagram increases with increasing shearing stress, whereas the field of stability of anti-stress minerals decreases with increasing shearing stress. Harker also recognized a neutral class whose field of stability is not notably affected by shearing stress. He considered chloritoid to be a stress mineral. Not all petrologists, however, attribute the presence of chloritoid to the action of stress, but they are generally agreed that it is a low-temperature mineral. The various theories regarding the conditions under which chloritoid grows will be presented by reviewing selected studies of chloritoid-bearing rocks.

The best-known chloritoid occurrences are in the schists and phyllites of the Belgian Ardennes. Van Werveke (1885) noted chloritoid crystals oriented across the schistosity in these rocks and concluded that the chloritoid had formed prior to the schistosity. Gosselet (1888) decided that these rocks were already schists before the chloritoid developed, and that later movements tended to orient

the chloritoid plates parallel to the schistosity and also to fracture some of the previously formed chloritoid crystals. He concluded that the chloritoid in some schists was developed by dynamometamorphism adjacent to faults, whereas in other schists it formed in beds of the proper composition—a phenomenon termed stratic metamorphism. Some schists gave no direct evidence of its origin. De Dorlodot (1909–10) found it difficult to explain the randomly oriented chloritoid crystals in a rock whose texture had arisen by 'écoulement sous l'influence de la pression'. He thought that the chloritoid crystallized before the schistosity, and disagreed with Gosselet that faults played any role in the formation of the chloritoid. Anten (1923) found no special relationship between the faults and the metamorphism. Corin (1930–1) summarized the conflicting views as he saw them by quoting Fourmarier: 'Le problème du métamorphisme des terrains anciens de l'Ardenne n'a pas encore reçu de solution définitive; les géologues belges se sont partagés sur le point de savoir si les transformations subies par ces roches doivent être attribuées à la seule influence de la profondeur ou s'il faut admettre l'intervention des minéralisateurs dégagés d'un magma situé à faible distance sous la surface actuelle du sol.' Corin thought that the Vielsalm area possesses all the characteristics of epizonal dynamometamorphism. Furthermore, he thought that the quartz veins in the area were of magmatic origin and had produced thermal effects on the adjacent rocks. De Dycker (1938–9) and Michot (1954–5) clearly showed that new chloritoid formed in the contact aureoles of quartz veins. Its formation was accompanied by a change in colour from wine to green due to the reduction of haematite to magnetite, and a gradual obliteration of the schistosity as the vein is approached.

Other important occurrences of chloritoid are in the Transvaal in South Africa. Götz (1886) presented the petrographic details of a suite of rocks including some containing chloritoid and andalusite from the Mt. Maré area. According to him the chloritoid crystals are randomly oriented with respect to the schistosity and their attitude has not been influenced by it. They are younger than the schistosity but some have been broken by later movements. He noted the similarity of these rocks to those normally found in contact aureoles, but as he knew of no igneous intrusion in the vicinity he concluded that both chloritoid and andalusite were formed in a regionally metamorphosed terrain. Hatch (1905) and Hall (1910*b*, 1918), however, found granitic intrusions in the area and concluded that this chloritoid was formed under contact metamorphic conditions. Hall (1910*a*) also noted that chloritoid and andalusite schists are confined to definite horizons. Read (1951, p. 18) observed both chloritoid and andalusite in hornfelses of the contact aureole of the Bushveld complex. He also saw chloritoid slates in the gold-bearing rocks of the Rand. These occurrences, coupled with his previous experience with chloritoid-bearing rocks in the Shetland Islands (Read, 1932, 1934, 1937), led him to conclude that the division of metamorphic minerals into stress and anti-stress types has no foundation in the field. Graton (1930, p. 170) noted that the greatest amount of chloritoid was

developed in the shale immediately under the Main Reef Leader at the Rand, close to channelways of hydrothermal action. He thought that the chloritoid was formed by the same action as the pyrite, sericite, and chlorite.

Niggli (1912) described chloritoid-bearing schists from the northern edge of the Gotthard massive in Switzerland. He observed (op. cit., pp. 59–62) the apparently random orientation of chloritoid crystals in these schists and concluded that this orientation was a result of the external forces on the chloritoid, its power of crystallization, and its rate of growth. He thought that they were being rotated to positions parallel to each other. He considered (op. cit., pp. 66–73) the univariant curves about an invariant point in a pressure-temperature diagram and showed how the different mineral associations, which he had previously noted in rocks of almost the same chemical compositions, could be explained by different pressures and temperatures. He remarked (op. cit., p. 82) that chloritoid is characteristic of relatively low temperature and very considerable stress (pressure). At higher temperatures its place is taken by staurolite and cordierite. He noted (op. cit., p. 51) the wide variations in the SiO_2 contents, the high contents of Al_2O_3 and Fe_2O_3+FeO, and the lower contents of alkalis as shown by chemical analyses of these rocks.

At Kalgoorlie, Western Australia, Simpson & Gibson (1912, pp. 63–64) noted the occurrence of chloritoid in schistose gold-bearing greenstones. They believed that it was related to the development of carbonate in these rocks, and concluded that both minerals were due to the 'ore-depositing action'. Later Prider (1947) expressed the opinion that the chloritoid at Kalgoorlie formed in hydrothermally metasomatized basic igneous rocks as the result of stress during low-grade dynamothermal metamorphism subsequent to the main shearing movements.

Tilley (1925) described chloritoid rocks from Eyre Peninsula, South Australia, and from the Tintagel Area, north Cornwall. At Eyre Peninsula, both chloritoid and andalusite have grown in a schist within the contact aureole of a granite mass under conditions which Tilley termed piezocontact metamorphic. He believed that the chloritoid formed subsequent to the andalusite at a period of increased shearing stress and falling temperature. At Tintagel, Tilley concluded that the chloritoid was formed under conditions prevailing during regional metamorphism. Further, Tilley recognized the wide range in chemical composition of chloritoid-bearing rocks in general, but noted the characteristically high Al_2O_3 and low CaO. He thought that high contents of CaO inhibit the formation of chloritoid, zoisite and epidote developing instead. Tilley pointed out that chloritoid may start growing at a very early stage of progressive metamorphism and persist through higher zones until it gives place to staurolite. Under the highest temperatures of thermal metamorphism, its equivalents are cordierite and spinel. In a subsequent paper, Tilley (1926, pp. 44–45) showed that chloritoid schists contain fewer alkalis and, in part, higher alumina and iron oxide than pelitic mica schists.

Stuckey (1926) suggested that the chloritoid occurring in the wall rocks of the

Womble pyrophyllite deposit, North Carolina, had formed in the same way as the pyrophyllite, namely, by hydrothermal replacement under conditions of intermediate temperature and pressure, but that its formation was influenced by an iron-rich breccia.

Barth (1936, p. 815), in a study of the metamorphic rocks of Dutchess County, New York, suggested that chloritoid was not stable in typical argillaceous schists, and that its formation requires abnormal temperature–pressure conditions acting locally. Subsequently, Barth (1952, p. 336) stated that chloritoid is unable to form in magnesia-rich rocks.

Hietanen (Cloos & Hietanen, 1941) studied the genesis of chloritoid in the Wissahickon and Marburg schists of southern Pennsylvania. She found that chloritoid occurs throughout a wide range of metamorphic conditions, from low-grade slates to staurolite-bearing rocks, but only in certain beds. Generally she favoured the action of stress for its formation. At Rawlinsville, however (Hietanen, 1951), the largest flakes are adjacent to a quartz vein where they clearly crystallized after the shearing movements which caused microfolding of the micas. Hietanen (Cloos & Hietanen, 1941, p. 119) realized that chloritoid schists are characteristically high in alumina and iron but had alkali contents similar to those of ordinary slates. She also thought that the absence of CaO favoured the growth of chloritoid.

Gustafson (1946) ascribed the chloritoid in the highly sericitized and ankeritized gold-bearing volcanic rocks at the Hollinger Mine, Ontario, to hydrothermal processes.

Williamson (1953) described chloritoid-bearing rocks in the vicinity of porphyry intrusions north of Stonehaven, Kincardineshire. Farther north, chloritoid gives way to staurolite. He compared several chemical analyses of chloritoid schists and noted the following characteristics: wide variation in silica, high potash, and low lime and magnesia. He noted that the ratios Fe_2O_3[1]:SiO_2 and Al_2O_3:SiO_2 are of little importance in determining the iron aluminosilicate that can appear. The presence of staurolite, however, requires a ratio of Fe_2O_3:Al_2O_3 of about 0·40. If this ratio exceeds about 0·50, biotite will form instead of staurolite. In chloritoid rocks this ratio can have a wider range of values.

Seki (1954) studied chloritoid-bearing rocks from the Kitakami area in Japan. He discussed the chemical composition of chloritoid rocks in general and stated that they are characterized by: (1) richness in Al_2O_3, FeO, Fe_2O_3, and H_2O; (2) poverty in CaO, Na_2O, K_2O, and MgO; (3) wide range of SiO_2 contents from 40 to 90 per cent. Furthermore, he thought that stress was not the controlling feature in the formation of chloritoid, but that the development of schistosity facilitates the entry of hydrothermal solutions which could effect the chemical changes necessary for the growth of chloritoid in rocks not originally of the right composition. He favoured low temperatures and high pressures for the

[1] Total iron calculated as Fe_2O_3.

growth of chloritoid. Subsequently Seki (1957, pp. 348–50) wrote: 'the formation and decomposition of chloritoid were chiefly controlled by variations not of pressure but of temperature (and/or chemical composition) in metamorphism, for probably the pressure did not vary so markedly as the temperature during the contact metamorphism.'

Atkinson (1956) noted chloritoid adjacent to overthrusts in some beds at Spitzbergen and concluded that it formed under the influence of stress in rocks of the right composition.

Marmo (1958) described chloritoid schists from central Sierra Leone. There they are present in an area characterized by dislocations and shear zones, but not in the most sheared or mylonitized parts. The chloritoid grew after the schistosity and is not arranged parallel to it. Marmo concluded that it grew under non-stress conditions. He noted it in rocks of different mineralogical compositions, but found it less abundant in quartz-rich rocks.

Influence of stress

Harker's division between stress and anti-stress minerals is not theoretically valid as the fields of stability of *all* minerals should decrease with increasing shearing stress. This thermodynamic effect of non-hydrostatic stress on solids has recently been emphasized by MacDonald (1957, p. 272); 'The non-hydrostatically stressed phase will *always* be unstable relative to a phase under a hydrostatic pressure equal to the least of the principal pressures acting on the non-hydrostatically stressed solid. It is thus theoretically impossible for a phase to be stable only under conditions of non-hydrostatic stress.' As chloritoid has been described from several geologic environments including regionally metamorphosed terrains, contact metamorphic aureoles, as a gangue mineral in some hydrothermal ore deposits such as of copper and gold, and from emery deposits, its presence cannot alone be taken as evidence of stress conditions. Even in some regionally metamorphosed terrains some petrologists have pointed out that its growth was apparently controlled by proximity to quartz veins, or that it grew both during and after the shearing stress which produced the schistosity. The experiments on the stability of chloritoid also support the view that the action of stress at any particular temperature and composition has little or no effect on the mineral associations in metamorphic rocks. Differences in mineralogy between regionally metamorphosed rocks and those formed in contact aureoles may be the result of different pressures prevailing in the two environments. Thus in quartz-bearing rocks containing chloritoid the reaction chloritoid + quartz $\rightleftarrows$ iron cordierite + vapour might be expected under the lower pressures of some contact metamorphism and the reaction chloritoid + quartz $\rightleftarrows$ almandine + staurolite + vapour under the higher pressures of some regional metamorphism. Localities for assemblages of these minerals are recorded in Table 24. At intermediate pressures the association staurolite–cordierite might be expected. Such associations are known from the Lizard, Cornwall (Tilley, 1937, p. 307), and

from the contact aureole of the Bushveld complex in South Africa (Hall, 1909, p. 127). It is concluded that stress has little or no influence on the stability of chloritoid in most rocks, but that the shearing of rock along planes of schistosity or faults facilitates entry of the chemical constituents necessary for the growth of chloritoid if they were not present originally. Stress may also increase rates of reaction by faulting or shearing the rock, thereby producing channels along which water has easy access, and increasing the surface areas of reactants in contact.

In many chloritoid schists, the chloritoid grows in single porphyroblasts which are randomly oriented (Plate 2, fig. B). In others, chloritoid crystals are intergrown in aggregates (Plate 2, fig. E) which are similar to the rosettes observed in a hydrothermally altered rock (Plate 2, fig. D). In some schists the chloritoid has evidently been fractured along the planes of schistosity and then rotated by the shearing stress (Plate 2, fig. C). In other schists it is parallel or almost parallel to the schistosity (Plate 2, fig. F). It is concluded that shearing stress has no general effect on the orientation of chloritoid crystals.

Chemical composition of chloritoid-bearing rocks

According to the conclusions reached by previous investigators, chloritoid forms only in rocks of a restricted chemical composition (see section on previous theories, pp. 106–7). In order to examine and precisely define these restrictions, 210 chemical analyses of chloritoid-bearing rocks from more than 25 widely separated localities have been collected (Halferdahl, 1959). These chemical analyses show wide variations in the percentages of many components, but the ratios between some of those components fall within narrow ranges. Some of these variations and restrictions are shown in five histograms (Fig. 12), and a triangular diagram (Fig. 13).

The percentage of silica in these analyses varies widely (see Fig. 12 A). The three modes in the histogram are probably related to the common occurrence of chloritoid in three types of rocks: emery, pelitic schists, and impure quartzites. The range of ratios of Al_2O_3:Fe_2O_3+FeO+MnO+MgO is shown in Fig. 12B. In about three-quarters of the analysed rocks alumina is from 1 to 3 times as abundant as the sum of the mafic constituents. Both are much more abundant than potash+soda+lime, as shown by the cluster of points near the Al_2O_3—Fe_2O_3+FeO+MnO+MgO side of the triangle in Fig. 13. When they are reduced to mol per cents most of the chemical analyses indicate that chloritoid-bearing rocks contain more alumina than of any other non-volatile constituent except silica. When (1) all the K_2O is calculated as muscovite or biotite; (2) all the Na_2O is calculated as paragonite or albite; and (3) all the excess CaO after allowing for calcite, apatite, and sphene is calculated as margarite or epidote; then for most of the analyses considerable alumina remains. In such calculations, ideal compositions for the micas were used as the actual compositions of the coexisting micas are not known. The restrictions on the ratios of FeO+MnO:MgO and FeO+Mno+Fe_2O_3:MgO are shown in Fig. 12 C, E.

None is less than one-tenth; and more than two-thirds of both ratios are in the range 1–10. The ratios of $FeO+MnO:Fe_2O_3$ (Fig. 12 D) provide a clue to the amount of oxidation in chloritoid-bearing rocks. No ratio is less than two-tenths and about 70 per cent lie between 1 and 10. As one might expect from the low

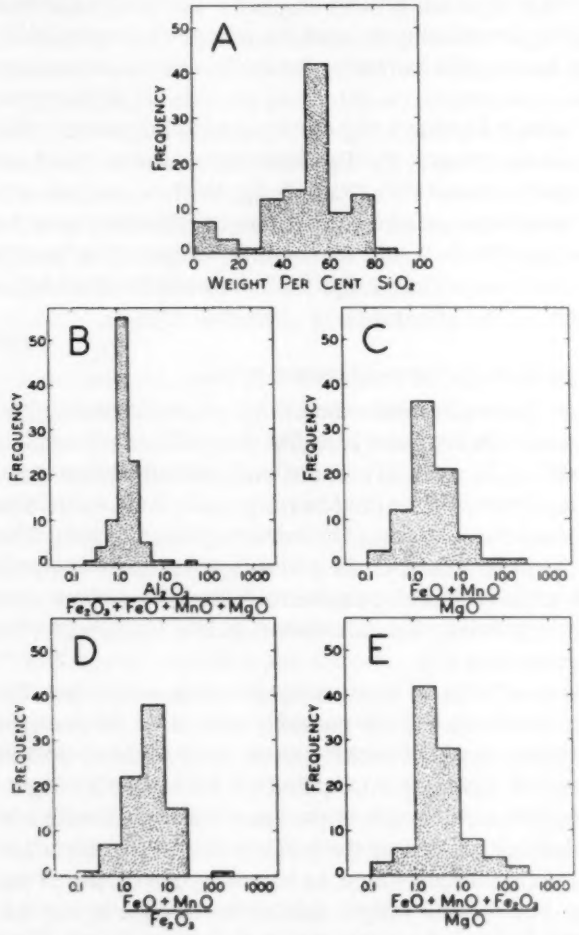

FIG. 12. Histograms showing variations and restrictions in the chemical composition of chloritoid-bearing rocks, obtained from chemical analyses tabulated by Halferdahl (1959). A, weight per cent SiO_2. B, mol ratios of $Al_2O_3:Fe_2O_3+FeO+MnO+MgO$. C, mol ratios of $FeO+MnO:MgO$. D, mol ratios of $FeO+MnO:Fe_2O_3$. E, mol ratios of $FeO+MnO+Fe_2O_3:MgO$.

ratios, magnetite and haematite are associated with chloritoid in some rocks. On the other hand, chloritoid is associated with carbonaceous material in rocks with a high ratio of $FeO+MnO:Fe_2O_3$. In general, rocks containing chloritoid are characterized by (1) a wide range of silica contents; (2) slightly more alumina than total mafic constituents; (3) excess alumina after K_2O, Na_2O, and CaO

are calculated as muscovite or biotite, paragonite or albite, and margarite or epidote, respectively; (4) more FeO+MnO than MgO; and (5) more FeO+MnO than Fe_2O_3.

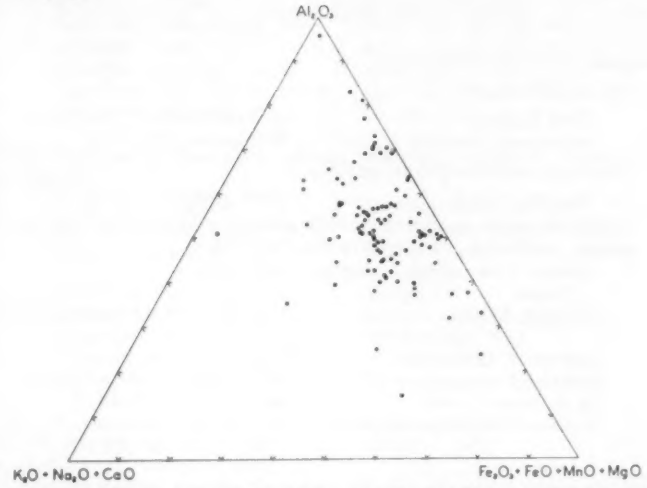

FIG. 13. Variation of K_2O+Na_2O+CaO, Al_2O_3, and $Fe_2O_3+FeO+MnO+MgO$ in chloritoid-bearing rocks, obtained from chemical analyses tabulated by Halferdahl (1959).

Minerals associated with chloritoid

The mineral assemblages previously reported in chloritoid-bearing rocks have been tabulated (Halferdahl, 1959) and summarized here in Table 24. Unfortunately, many published petrographic descriptions do not record all the minerals in individual rocks, but merely list the minerals in a suite of rocks. Although an attempt was made to list only those minerals actually associated with chloritoid, others may have been included in Table 24. In Table 25 are listed the minerals associated with chloritoid in rocks studied by the writer. These minerals were observed under the microscope in thin sections, and their identifications confirmed by X-ray diffraction powder patterns of various fractions of the crushed rocks. Such fractions were obtained by means of heavy liquids and a magnetic separator.

In many localities listed in Tables 24 and 25 chloritoid was observed to be actually in contact with one or more of the following minerals: quartz, chlorite, muscovite, paragonite, magnetite, haematite, ilmenite, rutile, almandine, staurolite, kyanite, andalusite, cordierite, biotite, pyrophyllite, kaolinite, corundum, diaspore, glaucophane, albite, anorthite, epidote, margarite, calcite, and siderite. Hence it is considered to have been in equilibrium with each of them under certain conditions even though the minerals now in the rock may be a disequilibrium assemblage. The most common mineral assemblage in low-grade chloritoid schists is chloritoid–quartz–chlorite–muscovite–rutile–iron oxide, the iron oxide being one or more of magnetite, haematite, ilmenite. In higher grade

TABLE 24

Mineral assemblages in chloritoid-bearing rocks, from the geological literature

1. *Low-grade schists and similar rocks*

Chloritoid–kaolinite	
Ottré, Belgium	de Rauw, 1912
Stonehaven, Scotland	Williamson, 1953
Chloritoid–kaolinite–gibbsite–goethite	
Anatolia, Turkey	Önay, 1949, pp. 390–447
Chloritoid–quartz–muscovite*–chlorite–magnetite–ilmenite† (haematite, rutile, epidote, carbonates, manganese oxides, carpholite)‡	
Eastern Townships, Quebec, Canada	Hunt, 1861
Pyrénées, France	Damour, 1879; Manasse, 1911; Zwart, 1959
Röhrsdorf, Germany	Kalkowsky, 1882
Steiermark, Austria	von Foullon, 1883, pp. 228–34
Île de Groix, France	Barrois, 1884*b*, pp. 34–45
Ardennes, Belgium, and France	van Werveke, 1885, pp. 229–34; Gosselet, 1888, pp. 186–93, 302–12; De Dycker, 1938–9, pp. M29–38, M60–62; Michot, 1954–5, pp. M11–21
Apuane Alps, Italy	D'Achiardi, 1886; Manasse, 1910, pp. 130–7
Transvaal, South Africa	Götz, 1886, pp. 143–56; Hall, 1918; Nel, 1927, pp. 81–83
Grossarl, Austria	Cathrein, 1887
Tintagel, England	Hutchings, 1889; Phillips, 1928*b*
São Paulo, Brazil	Hussak, 1890
Rhode Island, U.S.A.	Wolff, 1890, p. 161
Samos, Greece	Chelussi, 1893, pp. 36–37
Lainiciu, Rumania	Duparc & Mrazec, 1893
Mt. Blia, Sweden	Igelström, 1896*b*, p. 603
Piedmont, Italy	Rosati, 1907
Southern Jenissei, Siberia, U.S.S.R.	Meister, 1910
Skiddaw, England	Rastall, 1910, pp. 126–7
Fasortastein, Switzerland	Blumenthal, 1911, p. 13
Monte Fenouillet, France	Manasse, 1911
Gotthard Area, Switzerland	Niggli, 1912, pp. 23–34; Friedlaender, 1929
Collier Bay, Western Australia	Simpson, 1915
Harz Mts., Germany	Mügge, 1918
Krivoy-Rog, Ukraine, U.S.S.R.	Tarasenko, 1925; Tschirwinsky, 1929; Istshenko, 1957, pp. 288–9
Blackbird District, Idaho, U.S.A.	Shannon, 1926
Ural Mts., U.S.S.R.	Tschirwinsky, 1929
North-east China	Lin, 1932
Shetland Islands, Scotland	Read, 1932, pp. 317–22; Guppy & Sabine, 1956, pp. 46–49
Upper Michigan, U.S.A.	Lamey, 1935, p. 1145
Mt. Magnet Mines, Western Australia	Simpson, 1937
Fhurni, Greece	Köhne, 1938, p. 23
Lakkasandra, India	Pichamuthu, 1943, p. 332
South-eastern Pennsylvania and Maryland, U.S.A.	Stose & Stose, 1944, p. 40; Agron, 1950, pp. 1273–6

TABLE 24 (*cont.*)

Central Bohemia	Jelínek, 1948
El Cardoso, Spain	Recarte, 1951, p. 71
Troy, New York, U.S.A.	Balk, 1953, pp. 824, 843
Kitakami, Japan	Seki, 1954, pp. 229–44
Castleton, Vermont, U.S.A.	Zen, 1955
Red Rock, New Mexico, U.S.A.	Heinrich, 1956, p. 146
Central Sierra Leone	Marmo, 1958, pp. 109–10

Chloritoid–biotite–muscovite (quartz, chlorite, magnetite, ilmenite, rutile, epidote)‡

Ile de Groix, France	Barrois, 1884*b*, pp. 34–45
Ardennes, Belgium, and France	van Werveke, 1885, pp. 229–34
Upper Michigan, U.S.A.	Keller & Lane, 1891; Hobbs, 1895; Rominger, 1895
Harz Mts., Germany	Mügge, 1918
Broken Hill, Australia	Browne, 1922, pp. 304–5
Steiermark, Austria	Machatschki, 1923
Panamint Mts., California, U.S.A.	Murphy, 1932
Santa Monica Mts., California, U.S.A.	Neuerburg, 1951, pp. 33–34
Stonehaven, Scotland	Williamson, 1953
Spitzbergen	Atkinson, 1956

Chloritoid–garnet (quartz, muscovite, chlorite, magnetite, haematite, ilmenite, rutile, carbonates, zoisite)‡

Piedmont, Italy	Delesse, 1843, p. 388; 1846*a*, p. 232
Shetland Islands, Scotland	Heddle, 1879, pp. 27–29
Ile de Groix, France	Barrois, 1884*b*, pp. 34–45
Ardennes, Belgium, and France	Renard, 1882–4, p. 250; van Werveke, 1885, pp. 229–34; Gosselet, 1888, pp. 186–93; Corin, 1927–8; Michot, 1954–5, pp. M11–21
Abukuma, Japan	Koto, 1893, p. 271
Tintagel, England	Hutchings, 1889; Phillips, 1928*b*
Wallis, Switzerland	Woyno, 1912, p. 186; Tschopp, 1923–4, pp. 118–30
Tessin, Switzerland	Bossard, 1929, p. 140 and chart
Western Hills, Peiping, China	Ho, 1936, pp. 55–60
Stonehaven, Scotland	Williamson, 1953
Upper Michigan, U.S.A.	Villar, personal communication

Chloritoid–garnet–biotite (quartz, muscovite, chlorite, plagioclase, ilmenite, magnetite, haematite, zoisite)‡

Rhode Island, U.S.A.	Emerson & Perry, 1907
Val Piora, Switzerland	Krige, 1917, pp. 610–11
Stavanger, Norway	Goldschmidt, 1920, pp. 78–81
Steiermark, Austria	Machatschki, 1923
Stonehaven, Scotland	Williamson, 1953
Rockville, Connecticut, U.S.A.	Aitken, 1955, pp. 7–8, 49
Krivoy-Rog, Ukraine, U.S.S.R.	Istshenko, 1957, pp. 288–9
Blackbird District, Idaho, U.S.A.	Roedder, personal communication

Chloritoid–paragonite–quartz–rutile (chlorite, zoisite, calcite)‡

Curaglia, Switzerland	Schmidt, 1891, pp. 20–21
Castleton, Vermont, U.S.A.	Zen, 1955

Chloritoid–paragonite–albite–garnet–muscovite–quartz–zoisite

Po Valley, Italy	Harder, 1956, pp. 250–1

TABLE 24 (*cont.*)

Chloritoid–albite or sodic plagioclase–muscovite (quartz, chlorite, garnet, epidote, magnetite, ilmenite, rutile, haematite, carbonates, orthoclase)‡

Chalcidice, Greece	Becke, 1878, p. 270
Taunus Mts., Germany	von der Marck, 1878, p. 258
Ile de Groix, France	Barrois, 1884*b*, pp. 34–45
Tuscany, Italy	D'Archiardi, 1886
Hoosac Mts., New England, U.S.A.	Wolff, 1890, pp. 164–5
Vals and Furlt, Switzerland	Schmidt, 1891, p. 40
Krokets, Sweden	Törnebohm, 1892, p. 139
Samos, Greece	Chelussi, 1893, pp. 36–37
Peloponesus, Greece	Lepsius, 1893, pp. 129–31
Apuane Alps, Italy	Lepsius, 1893, p. 166; Manasse, 1910, pp. 130–7
Stonehaven, Scotland	Barrow, 1898
Potaro River, British Guiana	Harrison, 1908, pp. 59–61
Central Provinces, India	Fermor, 1909, pp. 199–200, 314
Kossoibrod, U.S.S.R.	Sigg, 1918, p. 165
Stavanger, Norway	Goldschmidt, 1920, pp. 78–81
Crestlianderstobel, Switzerland	Friedlaender, 1929
Barão de Guaicuhy, Brazil	Schneiderhöhn, 1936, p. 183
South-eastern Pennsylvania, U.S.A.	Cloos & Hietanen, 1941, pp. 119–23
Anatoki Valley, New Zealand	Hutton, 1950, p. 659
Rawlinsville, Pennsylvania, U.S.A.	Hietanen, 1951
Mesquite Canyon, California, U.S.A.	Dibblee & Gay, 1952
Kitakami, Japan	Seki, 1954, pp. 229–44
Ernen Power Station, Switzerland	Oberholzer, 1955, p. 387

Chloritoid–glaucophane (paragonite, albite, quartz, muscovite, chlorite, garnet, epidote, carbonate, magnetite, rutile)‡

Ile de Groix, France	von Lasaulx, 1883, p. 270
Zermatt, Switzerland	Des Cloizeaux, 1884
Peloponesus, Greece	Lepsius, 1893, pp. 129–31
Cyclade Islands, Greece	Ktenas, 1907
Val de Bagnes, Switzerland	Tschopp, 1923–4, pp. 118–30; Harder, 1956, pp. 249–51
South-east Celebes	de Roever, 1956

Chloritoid–anorthite–biotite–muscovite–quartz–hornblende–magnetite

Hitachi District, Japan	Seki, 1955

Chloritoid–actinolite or hornblende (biotite, chlorite, garnet, epidote, feldspar, talc, muscovite, calcite, ilmenite, magnetite, rutile)‡

Taunus Mts., Germany	von der Marck, 1878, pp. 261–2
Peloponesus, Greece	Lepsius, 1893, pp. 129–31
Allalin, Switzerland	Schäfer, 1896, pp. 110–11
Upper Michigan, U.S.A.	Clements & Smyth, 1899, pp. 442–4
Valaissian Alps, Switzerland	Duparc & Loup, 1903

Chloritoid–pyrophyllite–quartz (muscovite, chlorite, calcite, ilmenite, rutile)‡

Chatham County, North Carolina, U.S.A.	Genth, 1873, p. 399
Steiermark, Austria	Machatschki, 1923
Rand, South Africa	Liebenberg, 1955, p. 12

TABLE 24 (*cont.*)

2. *High-grade schists and similar rocks*

Chloritoid–kyanite (quartz, muscovite, biotite, garnet, chlorite, epidote, carbonates, magnetite, haematite, rutile)‡

Shetland Islands, Scotland	Heddle, 1879, pp. 27–29; Read, 1932, pp. 317–22
Mt. Blia, Sweden	Weibull, 1896, p. 518
Vredefort Dome, South Africa	Nel, 1927, pp. 66–76, 81–83
Anatolia, Turkey	Önay, 1949, pp. 390–447
Pregratten, Austria	Bachmann, 1956, p. 146
Hennensädel, Switzerland	van der Plas *et al.*, 1958, p. 238

Chloritoid–kyanite–staurolite (quartz, muscovite, biotite, chlorite, magnetite)‡

Shetland Islands, Scotland	Read, 1934, pp. 648–62
Mayurbhanj, India	Naha, 1955*b*

Chloritoid–kyanite–staurolite–garnet–quartz–muscovite (biotite, chlorite, magnetite, ilmenite, rutile, haematite, zoisite, plagioclase, hornblende)‡

Val Piora, Switzerland	Krige, 1917, pp. 615, 630
Tessin, Switzerland	Bossard, 1929, chart
Shetland Islands, Scotland	Read, 1932, pp. 317–22; 1934, pp. 648–62

Chloritoid–staurolite–garnet–biotite (quartz, muscovite, magnetite, ilmenite, rutile, haematite, carbonate, zoisite, chlorite, sillimanite, feldspar)‡

New England, U.S.A.	Hobbs, 1893, pp. 176–7
Val Piora, Switzerland	Krige, 1917, pp. 582, 605–6, 609, 629
Steiermark, Austria	Machatschki, 1923
Tessin, Switzerland	Bossard, 1929, pp. 151–2
Dutchess County, New York, U.S.A.	Barth & Balk, 1934

Chloritoid–staurolite (biotite, muscovite, quartz, plagioclase, magnetite, ilmenite, rutile)‡

Val Piora, Switzerland	Krige, 1917, p. 631
Tessin, Switzerland	Bossard, 1929, chart
Shetland Islands, Scotland	Read, 1932, pp. 317–22
Congo	Thoreau, 1936
Stonehaven, Scotland	Williamson, 1953

Chloritoid–garnet–sillimanite–muscovite–chlorite–biotite–magnetite

Mt. Monadnock, New Hampshire, U.S.A.	Fowler-Billings, 1949, p. 1259

Chloritoid–staurolite–andalusite–quartz–muscovite–chlorite–magnetite

Shetland Islands, Scotland	Guppy & Sabine, 1956, pp. 46–49

Chloritoid–kyanite–andalusite–muscovite

Vredefort Dome, South Africa	Nel, 1927, pp. 81–83
Shetland Islands, Scotland	Read, 1934, pp. 648–62

3. *Rocks of contact aureoles and similar environments*

Chloritoid–andalusite (quartz, muscovite, chlorite, biotite, garnet, magnetite, haematite, ilmenite, rutile, sillimanite)‡

Transvaal, South Africa	Götz, 1886, pp. 143–56; Hall, 1918
St. Barthélemy, France	de la Durandière, 1895
Skiddaw, England	Rastall, 1910, pp. 126–7
Broken Hill, Australia	Browne, 1922 pp. 304–5

TABLE 24 (*cont.*)

Eyre Peninsula, South Australia	Tilley, 1925
Vredefort Dome, South Africa	Nel, 1927, pp. 81–83
Shetland Islands, Scotland	Phillips, 1928*a*, pp. 503–4
Western Hills, Peiping, China	Ho, 1936, pp. 55–60; de Chardin, 1949
South-eastern Pennsylvania, U.S.A.	Agron, 1950, p. 1276
Kitakami, Japan	Seki, 1954, pp. 229–44
Central Sierra Leone	Marmo, 1958, pp. 109–10

Chloritoid–andalusite–pyrophyllite (quartz, muscovite, kyanite, rutile)‡

Ottré, Belgium	de Rauw, 1912
Worcester, South Africa	Potgieter, 1950, pp. 233–5

Chloritoid–andalusite–cordierite–garnet

Vredefort Dome, South Africa	Nel, 1927, pp. 81–83

Chloritoid–cordierite–biotite–quartz (muscovite)‡

Vredefort Dome, South Africa	Hall & Molengraaff, 1925, p. 118
Santa Monica Mts., California, U.S.A.	Neuerburg, 1951, pp. 33–34

Chloritoid–cordierite–anthophyllite–almandine–quartz–muscovite–biotite–chlorite

Kitakami, Japan	Seki, 1954, pp. 229–44

Chloritoid–anthophyllite–biotite–quartz–plagioclase–actinolite–magnetite–rutile

Vredefort Dome, South Africa	Nel, 1927, p. 31

Chloritoid–cordierite–staurolite–andalusite–muscovite

Rand, South Africa	du Toit, 1939, p. 175

4. *Emery*

Chloritoid–corundum or diaspore (magnetite, rutile, margarite, ilmenite, haematite, muscovite, carbonate, epidote)‡

Kossoibrod, Urals, U.S.S.R.	Fiedler, 1832, p. 327; Rose, 1837, p. 252; Hermann, 1851, pp. 13–16
Naxos, Greece	Tschermak, 1895, p. 326; Papavasiliou, 1913, p. 77; Önay, 1949, pp. 478–9
Chester, Massachusetts, U.S.A.	Emerson, 1898, p. 127
Samos, Greece	de Lapparent, 1937, pp. 16–18
Anatolia, Turkey	Önay, 1949, pp. 390–447

Chloritoid–kyanite–corundum–muscovite (paragonite, margarite, andalusite)‡

Bull Mt., Virginia, U.S.A.	Genth, 1890

Chloritoid–staurolite–corundum–margarite–magnetite

Naxos, Greece	Tschermak, 1895

Chloritoid–sillimanite–corundum–magnetite–rutile

Naxos, Greece	Papavasiliou, 1913, pp. 82–83

Chloritoid–diaspore–kaolinite–muscovite–magnetite–haematite–rutile

Samos, Greece	de Lapparent, 1937, pp. 16–18

TABLE 24 (*cont.*)

5. *Hydrothermal veins, hydrothermally altered rocks, and other mineralized rocks*

Chloritoid–quartz (chlorite, muscovite, calcite, ankerite, siderite, epidote, albite or plagioclase, pyrophyllite, garnet, magnetite, haematite, ilmenite, rutile, chalcopyrite, gold, pyrite, arsenopyrite, sphalerite, galena)‡

Silesia	Websky, 1853, p. 435
Rand, South Africa	Young, 1914, p. 32; 1917, pp. 19–20, 91; Lagrange, personal communication
Michipicoten, Ontario, Canada	Collins *et al.*, 1926
Womble Mine, North Carolina, U.S.A.	Stuckey, 1926
Kalgoorlie, Western Australia	Simpson, 1930, pp. 27–30; Prider, 1947
Hollinger Mine, Ontario, Canada	Gustafson, 1946
Harvey Hill Mine, Quebec, Canada	Milne, 1949
Barvue Mine, Quebec, Canada	Cornwall, 1955
Chibougamau, Quebec, Canada	Allard, 1956, p. 141

* Throughout this table minerals reported as sericite or white mica have been listed as muscovite.
† In some localities one or more of these minerals is absent.
‡ Minerals enclosed in parentheses have been reported from the listed localities, but all or any are not present in any one assemblage. Those at the end of the list are less common. Accessory minerals such as tourmaline, zircon, apatite, graphite, and sphene have been omitted.

schists almandine, staurolite, and kyanite are common associates. Cordierite is present with chloritoid in a few contact metamorphic aureoles. An assemblage of chloritoid–quartz–chlorite–muscovite–ilmenite or magnetite with or without calcite or siderite is known in several hydrothermal veins or in hydrothermally altered rocks. Chloritoid in emery deposits is commonly found with corundum or diaspore, margarite, magnetite, rutile, and calcite. Some of the mineral associations in chloritoid-bearing rocks and the reactions giving rise to them will be examined in the light of the Phase Rule and available experimental data. These include data on the ternary systems: FeO–SiO_2–H_2O (Flaschen & Osborn, 1952 and 1957), Al_2O_3–SiO_2–H_2O (Roy & Osborn, 1954), FeO–Al_2O_3–SiO_2 (Schairer & Yagi, 1952); and on individual minerals: almandine (Yoder, 1955, p. 520), chamosite (Brindley & Youell, 1953), iron-rich chlorites (Turnock & Eugster, 1958*b*).

First, however, it is convenient to consider the minerals whose compositions can be expressed in terms of the oxides FeO, Al_2O_3, SiO_2, H_2O (Fig. 14). Most of these minerals are well known, but some raise questions. The montmorillonite group is composed of many solid solution series. The limits of these series, at least in the FeO–Al_2O_3–SiO_2–H_2O system, are not known. Therefore, for simplicity only an aluminium end-member of the group is shown. The ferrous iron montmorillonite, $Fe_2^{2+}Si_5O_{20}(OH)_4 \cdot nH_2O$, as well as bayerite, endellite, halloysite, nacrite, and dickite have been omitted as little or no reliable data on their stabilities exist.

Minerals of the chlorite composition exist in two known polymorphs: those with 14-Å basal spacings and those with 7-Å basal spacings. The ferrous iron 7-Å polymorphs constitute a solid solution series from $3FeO \cdot 2SiO_2 \cdot 2H_2O$ to

TABLE 25. *Chloritoid localities and the minerals present in chloritoid-bearing rocks investigated in this study*

Locality	*Type of occurrence*	*Mineral assemblage*	*Source of specimen*
Ile de Groix, France	schist	M chloritoid, quartz, chlorite, magnetite, 2M muscovite, almandine, rutile	Muséum National d'Histoire Naturelle, No. 101·302
Üstüaçiksarinç, Turkey	emery	M chloritoid, calcite, haematite, kaolinite	Prof. H. P. Eugster
Pregratten, Tirol, Austria	—	M chloritoid, quartz, calcite	U.S. National Museum, R4496
Gumuchdagh, Turkey	emery	M chloritoid, chlorite, diaspore, ilmenite, haematite	U.S. National Museum, 79909
Natick, Rhode Island, U.S.A.	schist	M chloritoid, chlorite, 2M muscovite, ilmenite, biotite, almandine	U.S. National Museum, 93568
Natick, Rhode Island, U.S.A.	schist	M chloritoid, chlorite, 2M muscovite, ilmenite, biotite, almandine	The Johns Hopkins University
St. Marcel, Piedmont, Italy	—	M chloritoid, chlorite	U.S. National Museum, R4502
Leoben, Austria	schist	M chloritoid, quartz, chlorite, 2M muscovite, ilmenite, haematite	U.S. National Museum, R4495
Winnemucca, Nevada, U.S.A.	schist	M chloritoid, quartz, chlorite, 2M muscovite, ilmenite	Dr. R. R. Compton, No. 17–19–9
Mesquite Canyon, Kern Co., Calif., U.S.A.	schist	M chloritoid, quartz, chlorite, magnetite, 2M muscovite	Mr. C. W. Chesterman
Summit of Mt. Leconte, Tennessee, U.S.A.	schist	M chloritoid, quartz, chlorite, 2M muscovite, paragonite, ilmenite	Prof. C. A. Hopson
Ellijay, Georgia, U.S.A.	schist	M chloritoid, quartz, chlorite, 2M muscovite, ilmenite	Dr. V. J. Hurst
Ottré, Belgium	schist	T chloritoid, quartz, chlorite, 2M muscovite	U.S. National Museum, 47022
Ottré, Belgium	schist	T chloritoid, quartz, chlorite, 2M muscovite, pyrophyllite, rutile	The Johns Hopkins University
Womble Mine, North Carolina, U.S.A.	hydrothermally altered rocks	T chloritoid, quartz, chlorite, leucoxene T chloritoid, quartz, pyrophyllite, leucoxene	Dr. J. L. Stuckey
Crestlianderstobel, Switzerland	schist	T chloritoid, quartz, chlorite, haematite	Prof. C. Burri
Chibougamau, Quebec, Canada	hydrothermally altered rocks	T chloritoid, chlorite, 2M muscovite, ilmenite, plagioclase T chloritoid, quartz, 2M muscovite, siderite, rutile T chloritoid, quartz, ilmenite, magnetite, siderite T chloritoid, quartz, 2M muscovite, siderite, ilmenite, rutile	Dr. Gilles Allard
Salm-Château, Belgium	schist	T chloritoid, quartz, 2M muscovite, haematite, chlorite	Dr. Jean Michot
Vielsalm, Belgium	schist	T chloritoid, quartz, 2M muscovite, chlorite, haematite	U.S. National Museum, R4498
St. Gilles, Quebec, Canada	schist	T chloritoid, quartz, chlorite, 2M muscovite, ilmenite	U.S. National Museum, 79008
Lebanon, Massachusetts, U.S.A.	schist	T chloritoid, quartz, chlorite, 2M muscovite, haematite	U.S. National Museum, 79007
Mt. Blia, Sweden	schist	T chloritoid, quartz, chlorite, 2M muscovite, haematite	U.S. National Museum, R4508
Kalgoorlie, Western Australia	hydrothermally altered rocks	T chloritoid, quartz, 2M muscovite, ankerite	Prof. R. T. Prider
Michipicoten District, Ontario, Canada	hydrothermally altered rocks	T chloritoid, quartz, magnetite, 2M muscovite, siderite	Dr. W. A. Jarvis

TABLE 25 (*cont.*)

Locality	*Type of occurrence*	*Mineral assemblage*	*Source of specimen*
Yukizawa, Kitakami Area, Japan	hornfels	T chloritoid, quartz, chlorite, 2M muscovite, andalusite	Dr. Yôtarô Seki, No. YS 53081502
Hollinger Mine, Ontario, Canada	hydrothermally altered lavas	T chloritoid, quartz, chlorite, ankerite, paragonite, pyrite	Dr. W. A. Jones
Barvue Mine, Quebec, Canada	hydrothermally altered lavas	T chloritoid, quartz, chlorite, 2M muscovite, siderite, haematite, sphalerite	Dr. R. Assad
Collier Bay, Western Australia	schist	M and T chloritoids, quartz, chlorite, magnetite, 2M muscovite, rutile	Government Chemical Laboratory, Western Australia
Rawlinsville, Pennsylvania, U.S.A.	schist	M and T chloritoids, quartz, chlorite, 2M muscovite, haematite	Collected by writer
Harvey Hill Mine, Quebec, Canada	schist	M and T chloritoids, quartz, chlorite, 2M muscovite	Dr. Paul E. Grenier
Vénasque, France	schist	M and T chloritoids, quartz, chlorite, 2M muscovite	U.S. National Museum, R4506
Ernen Power Station, Switzerland	schist	M and T chloritoids, quartz, chlorite, 2M muscovite	Prof. C. Burri
Newfound Gap, Swain County, North Carolina, U.S.A.	schist	M and T chloritoids, quartz, chlorite, 2M muscovite, almandine, kyanite, staurolite, carbonaceous material	Dr. J. B. Hadley
Lemhi County, Idaho, U.S.A.	schist	chloritoid,* quartz, almandine, biotite, rutile	Dr. E. Roedder
North Adams Quadrangle, Massachusetts, U.S.A.	schist	chloritoid, 2M muscovite, chlorite, ilmenite, rutile, tourmaline chloritoid, 2M muscovite, chlorite, quartz, magnetite	Dr. N. Herz
Lisbon, New Hampshire, U.S.A.	schist	chloritoid, quartz, chlorite, 2M muscovite, biotite, almandine, ilmenite, staurolite	U.S. National Museum, R4504
Mt. Maré, South Africa	schist	chloritoid, quartz, 2M muscovite, andalusite	Dr. L. O. Nicolaysen
Merced, California, U.S.A.	slate	chloritoid, quartz, chlorite, 2M muscovite, opaques	Prof. C. Durrell
Rand, South Africa	quartzite	chloritoid, quartz, pyrophyllite, ilmenite, rutile	Dr. A. O. Fuller
Vredefort Area, South Africa	hornfels	chloritoid, cordierite, biotite, 2M muscovite, quartz, opaque	Dr. L. O. Nicolaysen
Humboldt, Michigan, U.S.A.	schist	chloritoid, quartz, 2M muscovite, magnetite chloritoid, quartz, chlorite, ilmenite chloritoid, quartz, 2M muscovite, chlorite, almandine, magnetite	Mr. J. Villar

* Where the chloritoid polymorph is not specified, not enough pure chloritoid could be separated from the rock to make a distinction.

$2FeO \cdot Al_2O_3 \cdot SiO_2 \cdot 2H_2O$. The aluminium-bearing iron-rich 7-Å polymorphs are here termed chamosites. The aluminium-free 7-Å polymorphs are greenalite and ferroantigorite corresponding to chrysotile and antigorite, the analogous magnesium minerals. The extent of the 14-Å chlorite solid solution toward the aluminium-free end is not known. Nelson & Roy (1958) considered that a minimum content of alumina is necessary in the 14-Å magnesium chlorites. Only one analysis plotted by Hey (1954) has less alumina than pennine.

Ferrostilpnomelane can be obtained from minnesotaite by substituting 2Al for $Fe^{2+}Si$ per formula of $Fe_6Si_8O_{20}(OH)_4$ according to Yoder (1957, p. 236).

The assemblage minnesotaite–stilpnomelane (Gruner, 1946, p. 27 and pl. IV) suggests that complete solid solution between the two does not exist under all conditions.

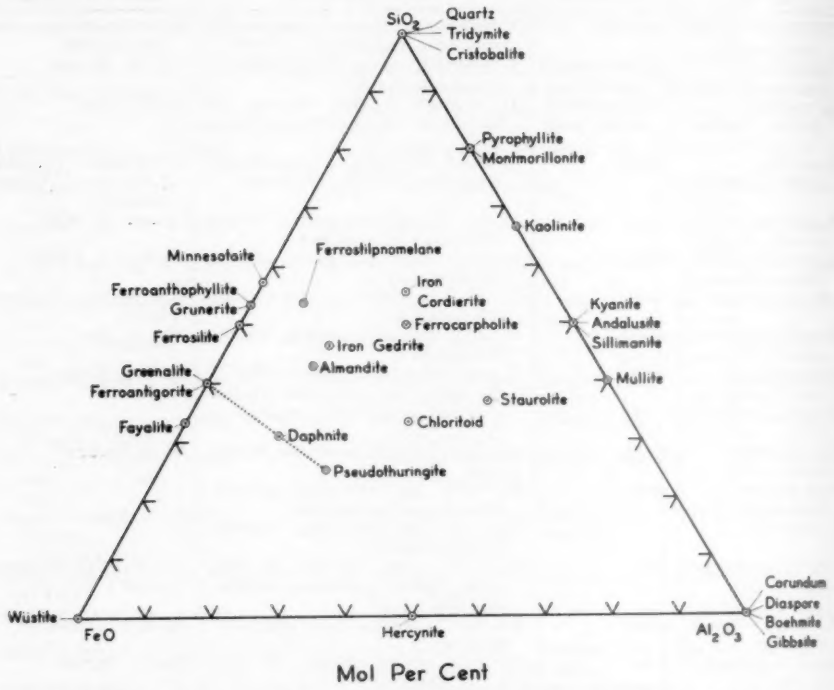

FIG. 14. Minerals in the system $FeO–Al_2O_3–SiO_2–H_2O$ projected onto the $FeO–Al_2O_3–SiO_2$ plane.

The amphibole end-members ferroanthophyllite and iron gedrite may not exist, according to the analyses listed by Rabbitt (1948). Nevertheless, a more recent analysis (Seitsaari, 1956) indicates the existence of an amphibole very close to gedrite in composition and having a mol ratio of MgO:FeO of less than 0·25.

The formula of staurolite is not known with certainty. The position of staurolite plotted in Fig. 14 has been obtained from the analyses made by Juurinen (1956), but differs slightly from that of his proposed formula $H_4Fe_4Al_{18}Si_8O_{48}$ which, as noted by Yoder (1957, p. 237), does not balance electrostatically. It is close to $HFe_2Al_9Si_4O_{24}$, the formula recently used by Náray–Szabó & Sasvári (1958), in a revision of the structure of staurolite.

Ferrocarpholite, $FeO \cdot Al_2O_3 \cdot 2SiO_2 \cdot 2H_2O$, has been recorded by de Roever (1951) in low-grade metamorphic phyllites and quartzitic rocks from eastern central Celebes, in association with quartz, sericite, biotite, chlorite, haematite, leucoxene, tourmaline, rutile, and zircon. Except for these data, nothing is known of its stability, and hence it will not be considered further.

In the application of the Phase Rule and experimental data to the mineral assemblages in chloritoid-bearing rocks, a sequence of probable reactions during progressive metamorphism in quartz-bearing pelitic and lateritic sediments and in iron formations will be presented. First, these sediments will be restricted to those whose composition can be expressed in terms of FeO, Al_2O_3, SiO_2, and H_2O. Then some of the effects of components such as MgO, K_2O, Na_2O, CaO, Fe_2O_3, will be mentioned. The water content of shales and residual clays ranges from 2 to more than 10 per cent (Pettijohn, 1949, pp. 271, 283, 285). Therefore, throughout progressive metamorphism water will be given off, and one phase will be vapour consisting mostly of H_2O. As the experimental data which will be used have been determined with the H_2O pressure equal to the total pressure, only this case will be considered here. This and other cases in which the H_2O pressure is less than the total pressure have been considered by Yoder (1952, 1955) and more generally by Thompson (1955).

In a four-component system the pressure-temperature conditions of divariant equilibrium permit the coexistence of a maximum of four phases. If one of these four components is mobile and the system is open to that component, then the number of phases will be reduced by one (Thompson, 1955). However, in the case under discussion the pressure on all phases, including the mobile component, H_2O, is the same. Thus the system can be considered closed, and all phase assemblages will contain essentially pure water or water vapour as one phase. If the four components are represented by a tetrahedron, then any four-phase assemblage forms a subsidiary tetrahedron within the larger one. This subsidiary tetrahedron encloses all the compositions for which the four phases can coexist under the conditions specified. If one of the phases is an intermediate member of a binary solid solution series, the equilibrium remains divariant; however, only three phases may coexist. In this case the subsidiary tetrahedron degenerates into a triangle. In the four-component system under consideration it is convenient to place H_2O at the apex of the tetrahedron. Then many of the subsidiary four-phase tetrahedra in which H_2O is a phase have bases which slope up into the larger tetrahedron.

In Fig. 15 are given some of the various assemblages which are believed to coexist at various temperatures and pressures up to and including the breakdown of chloritoid in the system FeO–Al_2O_3–SiO_2–H_2O. Each assemblage includes a vapour consisting essentially of H_2O. Localities for many of these assemblages are recorded in Tables 24 and 25. The alumina-poor, chloritoid-free assemblages are not included; many have been described by Gruner (1946). The reactions from which the assemblages arise are given in Table 26. Each reaction can be visualized as breaking through one or more of the sloping planes which form the bases of the subsidiary tetrahedra. Actually, each reaction permits drawing another triangle similar to those in Fig. 15 and showing other assemblages. Such additional triangles, however, are not warranted from the data presently available. The sequence of reactions has been deduced from

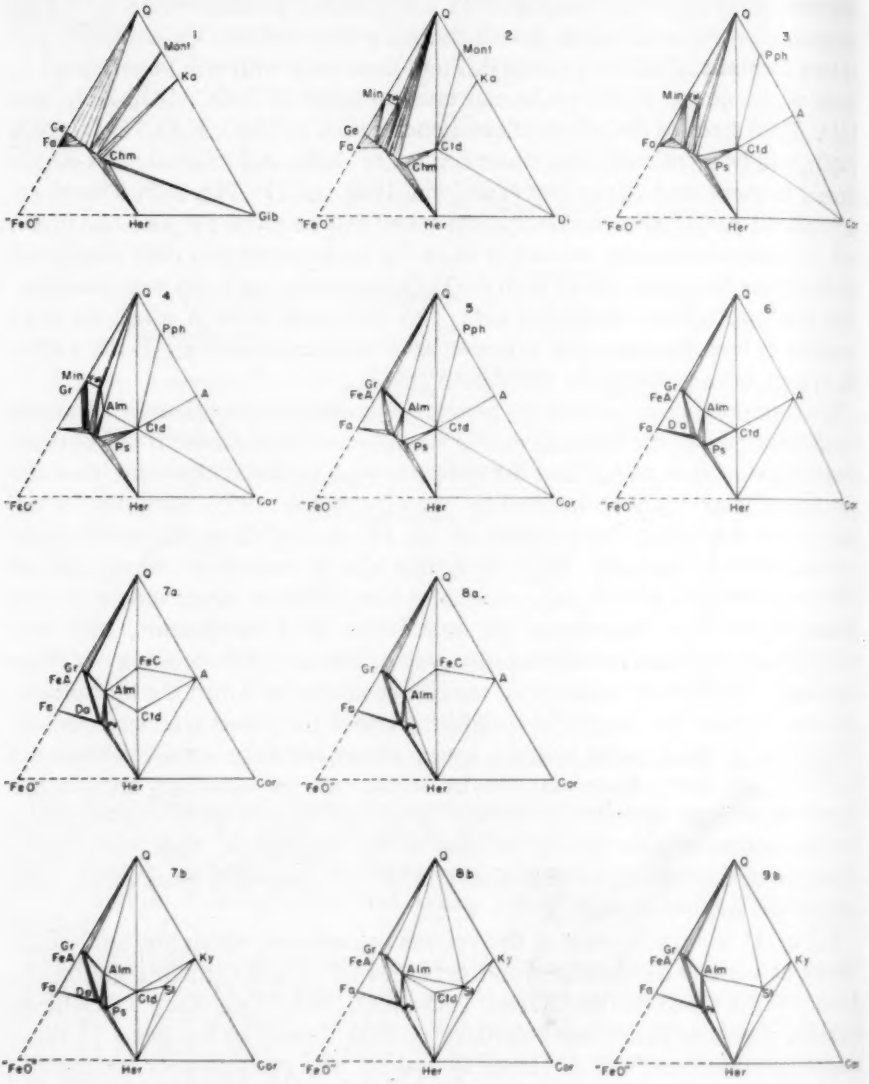

FIG. 15. Mineral assemblages in the system $FeO–Al_2O_3–SiO_2–H_2O$ from sedimentary conditions up to the breakdown of chloritoid. Symbols used are: A, andalusite; Alm, almandine; Chm, chamosite; Cor, corundum; Ctd, chloritoid; Di, diaspore; Da, daphnite; Fa, fayalite; FeA, ferroanthophyllite; FeC, iron cordierite; Fst, ferrostilpnomelane; Ge, greenalite; Gib, gibbsite; Gr, grunerite; Her, hercynite; Ky, kyanite; Min, minnesotaite; Mont, montmorillonite; Pph, pyrophyllite; Ps, pseudothuringite; Q, quartz; St, staurolite.

TABLE 26

Sequence of reactions in the system $FeO–Al_2O_3–SiO_2–H_2O$ *from sedimentary conditions up to the breakdown of chloritoid*

Triangle No. in Fig. 15	*Probable conditions*		*Reaction*	
	Temperature (° *C*)	*Pressure* (*bars*)		
1	Sedimentary		kaolinite + gibbsite + chamosite ⇄ chloritoid + vapour	1
			diaspore + chamosite ⇄ chloritoid + hercynite + vapour	2*a*
			kaolinite + chamosite ⇄ chloritoid + montmorillonite + vapour	2*b*
			montmorillonite + chamosite ⇄ chloritoid + quartz + vapour	3
			gibbsite ⇄ boehmite + vapour ⇄ diaspore + vapour	4
			greenalite + quartz ⇄ minnesotaite + vapour	5
			chamosite + quartz ⇄ ferrostilpnomelane + vapour	6
2	~ 400	1,000–2,000	diaspore ⇄ corundum + vapour	1
			kaolinite ⇄ montmorillonite + andalusite + vapour	2
			montmorillonite ⇄ pyrophyllite + vapour	3
			greenalite ⇄ minnesotaite + fayalite + vapour	4
			chamosites ⇄ iron chlorites	5
3	~ 485	1,000–2,000	minnesotaite + fayalite ⇄ grunerite + vapour	1
			iron chlorite + quartz ⇄ almandine + vapour	2
4	~ 500	1,000–2,000	minnesotaite + iron chlorite ⇄ grunerite + ferrostilpnomelane + vapour	1
			minnesotaite ⇄ grunerite + quartz + vapour	2
			ferrostilpnomelane + iron chlorite ⇄ grunerite + almandine + vapour	3
			ferrostilpnomelane ⇄ grunerite + almandine + quartz + vapour	4
5	< 575	1,000–2,000	pyrophyllite ⇄ andalusite + quartz + vapour	1
			chloritoid + corundum ⇄ andalusite + hercynite + vapour	2
6	575–600	1,000–2,000	chloritoid + quartz ⇄ iron cordierite + vapour	1
			chloritoid + pseudothuringite ⇄ almandine + hercynite + vapour	2
7*a*	< 600	1,000–2,000	chloritoid ⇄ iron cordierite + hercynite + vapour	
8*a*	~ 600	1,000–2,000		
6	575–675	~ 9,000	chloritoid + kyanite + hercynite ⇄ staurolite + vapour	
7*b*	< 675	~ 9,000	chloritoid + kyanite ⇄ staurolite + quartz + vapour	1
			chloritoid + pseudothuringite ⇄ almandine + hercynite + vapour	2
			chloritoid + quartz ⇄ almandine + staurolite + vapour	3
8*b*	< 675	~ 9,000	chloritoid ⇄ staurolite + almandine + hercynite + vapour	
9*b*	~ 700	~ 9,000	staurolite + quartz ⇄ almandine + kyanite + vapour	

experimental data, natural assemblages, and geometrical considerations. Deductions from these sources do not yet permit this sequence to be fixed in every detail. The interpretation of the order of some of the reactions and of the nature of some of the reactions themselves will undoubtedly be changed as further experimental data become available.

In Fig. 15, triangles 1–6, 7*a*, and 8*a* show some of the various assemblages stable during increasing temperatures at 1,000–2,000 bars water pressure. Triangles 1–6, 7*b*, 8*b*, and 9*b* are believed to show some of the various assemblages stable during increasing temperatures at pressures greater than about 9,000 bars. At these pressures, andalusite should be replaced by kyanite in triangles 3–6. Triangle 1 shows the phases believed to be stable under sedimentary conditions. The assemblage chamosite–kaolinite–gibbsite has been reported from County Antrim, Ireland (Dunham, Eyles, & Taylor, 1951). The composition FeO is represented by iron plus magnetite below 570° C. The dashed lines indicate that here Fig. 15 no longer represents a quarternary system: all the phases can coexist with magnetite. It must be emphasized that the compositions of the iron chlorites, and chamosites and other solid solution series shown in Fig. 15, are only estimates as no data are available.

That iron chlorites persist to higher temperatures than does chloritoid, has been hesitantly assumed. Brindley & Youell (1953, pp. 66–68) found that ferrous chamosite was stable up to 650° C in steam at 1 atm pressure. Turnock & Eugster (1958*b*) found that daphnite is stable from 525° to 650° C depending on the partial pressure of oxygen. Yoder (1952) found that clinochlore, the magnesium analogue of daphnite, decomposed at 680° C and 2,000 bars. Until more experimental data are accumulated on chamosites and ferrous chlorites no firm conclusions can be drawn.

According to the reactions listed in Table 26, the sequence of new minerals to appear during progressive metamorphism of quartz-bearing pelitic sediments containing only FeO, Al_2O_3, SiO_2, and H_2O, is chloritoid, andalusite, pyrophyllite, almandine, iron cordierite at moderate pressures, and chloritoid, kyanite, pyrophyllite, almandine, staurolite at high pressures. The sequence of new minerals to appear during progressive metamorphism of reduced lateritic sediments is chloritoid, boehmite, diaspore, corundum, andalusite or kyanite, staurolite. Chloritoid is not found in alumina-poor iron formations.

For chloritoid to appear during progressive metamorphism a source of alumina as well as ferrous oxide and silica is required. In sediments, gibbsite, boehmite, and diaspore are the only minerals containing alumina without another metallic oxide. Therefore, for chloritoid to crystallize during the earliest stages of progressive metamorphism, the alumina must be supplied by one of these minerals. Ferrous oxide can be supplied by chamosite as indicated in Table 26, or by siderite, magnetite, or ilmenite. The common association, chloritoid–rutile, suggests that ilmenite may have supplied much of the ferrous oxide for chloritoid. Silica can come from quartz or a clay mineral.

According to the Phase Rule, the addition of another component to a four-component system permits the coexistence of five phases. Therefore, because Mg can replace Fe^{2+} in almost all the phases shown in Fig. 15, to some extent at least, the addition of MgO to the system means that assemblages can coexist in which one pair of joins intersect. For example, the assemblages chloritoid–quartz–almandine–chlorite, chloritoid–almandine–anthophyllite–quartz, chloritoid–staurolite–quartz–almandine are thereby permitted.

FIG. 16. Projection of some minerals onto the plane $K_2O \cdot Al_2O_3 + Na_2O \cdot Al_2O_3 - Al_2O_3 + Fe_2O_3 - FeO + MgO + TiO_2$. Higher grade minerals are in smaller type.

The addition of K_2O to the system also permits the coexistence of another phase. In many rocks this phase is muscovite. Another possible potash-bearing phase is glauconite (Fig. 16). Glauconite, however, has not been recorded with chloritoid, probably because it disappears before chloritoid appears. Where potash is present chloritoid–biotite assemblages can arise by several means. The relations can be visualized by reference to Fig. 16. In low-grade rocks chloritoid–biotite assemblages are not common, probably because most chloritoid-bearing rocks are too high in alumina for biotite to form; the assemblage is chloritoid–quartz–muscovite–chlorite. Where biotite is present with chloritoid in low-grade rocks, it has probably formed by reactions which do not involve chloritoid, such as glauconite + daphnite (or any chlorite or chamosite)

$\rightleftarrows$ muscovite + biotite + vapour.[1] Most of the recorded chloritoid–biotite assemblages are in higher grade rocks where biotite has formed probably by the reaction muscovite + daphnite (or any chlorite) $\rightleftarrows$ biotite + cordierite (or staurolite, kyanite, andalusite, sillimanite) + vapour. Almandine in place of one of these five minerals can even form by this reaction if the reacting chlorite is not too high in alumina. Chloritoid may finally disappear by the reaction chloritoid + muscovite $\rightleftarrows$ biotite + staurolite (or kyanite, andalusite, sillimanite) + vapour. Even though chloritoid–orthoclase assemblages were recorded many years ago from a few localities (Table 24) it is doubtful if the potash feldspar is actually in contact with the chloritoid and that this assemblage actually exists.

The additional component Na_2O may give rise to paragonite or albite. Both chloritoid–paragonite–chlorite and chloritoid–albite–chlorite assemblages are known from several localities. Hence from Fig. 16 one is led to postulate the reaction chlorite + paragonite + quartz $\rightleftarrows$ chloritoid + albite + vapour as a possible one for the formation of chloritoid. Another soda-bearing mineral which is associated with chloritoid in some places is glaucophane.

If CaO is added, phases such as epidote, zoisite, margarite, and anorthite appear in assemblages with chloritoid. Highly calcareous rocks apparently do not contain a high enough proportion of alumina for the formation of chloritoid.

At higher pressures of oxygen Fe_2O_3 appears as a component. Chloritoid–magnetite and even chloritoid–haematite–magnetite assemblages are known, but as chloritoid is essentially a ferrous aluminium silicate it cannot be expected to persist much, if any, beyond the oxygen pressures corresponding to the equilibrium between haematite and magnetite, though ilmenite may take the place of magnetite in some natural assemblages. The presence of Fe^{3+} or Mn or both in natural chloritoids may, possibly, permit the assemblage chloritoid–haematite. The following reactions are some of those most likely to occur: chloritoid + oxygen + vapour $\rightarrow$ kaolinite + goethite + diaspore and chloritoid + oxygen $\rightarrow$ magnetite (or haematite) + kyanite (or andalusite) + vapour.

CONCLUSIONS

The simple chemical composition of chloritoid is $H_2FeAl_2SiO_7$; in naturally occurring chloritoids magnesium and, to a lesser extent, manganese replace some of the ferrous iron, and ferric iron replaces even less of the aluminium. Those analyses which show lime, alkalis, and excess silica were made on impure samples of chloritoid or are in error. Chloritoid crystallizes in both monoclinic and triclinic polymorphs; the triclinic cell is equal to one-half the monoclinic cell and contains $H_8Fe_4Al_8Si_4O_{28}$. In many monoclinic chloritoids the optic plane is normal to (010), while in many triclinic chloritoids it is almost parallel to (010). Some of the optical properties of both polymorphs vary in different crystals from the same sample. Additional optical studies in conjunction with complete

[1] In equations involving chlorite or biotite, quartz will have to be added to one side or the other, depending on the composition of the chlorite or biotite.

chemical analyses and, if possible, knowledge of the crystallization history might reveal the reasons for these variations.

Above certain temperatures chloritoid decomposes at high pressures to almandine, staurolite, hercynite, and vapour, and at low pressures to iron cordierite, hercynite, and vapour. Precise determination of the conditions for these decompositions requires control of the partial pressure of oxygen and very long runs at low pressures. The use of very finely ground reaction mixtures might permit the attainment of equilibrium more rapidly at low pressures. Below the decomposition temperatures chloritoid is stable in both stress and stress-free environments in rocks having a high content of alumina relative to lime, alkalis, and mafic constituents, and with more iron than magnesium. The conditions under which one of the chloritoid polymorphs will form in preference to the other are uncertain. Natural occurrences suggest that the monoclinic polymorph forms more readily than the triclinic under severe conditions of pressure and temperature, or under more moderate conditions prevailing for a long time. Chloritoid is present in some rocks which have undergone both regional and contact metamorphism and in some hydrothermal veins and hydrothermally altered rocks. It is more common than was previously thought. Careful work on the chemical composition and physical properties of the minerals naturally coexisting with chloritoid, and quantitative experimental data on reactions involving it, will undoubtedly provide useful new isograds for the metamorphic petrologist.

ACKNOWLEDGEMENTS

This work was carried out at the Geophysical Laboratory during the tenure of a fellowship awarded jointly by the Carnegie Institution of Washington and The Johns Hopkins University. The writer is grateful to Dr. P. H. Abelson, Director of the Geophysical Laboratory, for the opportunity to work there. The writer expresses his sincere gratitude to Dr. H. S. Yoder, Jr., under whose guidance the work was carried out. The writer is also indebted to other staff members and fellows of the Geophysical Laboratory, particularly Drs. F. Chayes, G. Donnay, G. L. Davis, F. R. Boyd, and J. R. Smith, and to Professors J. D. H. Donnay and A. C. Waters of The Johns Hopkins University. To the many mineralogists and geologists who supplied specimens, or through whom specimens were obtained, the writer expresses his thanks.

REFERENCES

ACHIARDI, A. D', 1886. Rocce ottrelitiche delle Alpi Apuane. *Mem. Soc. tosc. Sci. nat.*, **8**, 442–54.

AGRON, S. L., 1950. Structure and petrology of the Peach Bottom slate, Pennsylvania and Maryland, and its environment. *Bull. geol. Soc. Amer.* **61**, 1265–306.

AITKEN, J. M., 1955. Bedrock geology of the Rockville quadrangle. *St. geol. Nat. Hist. Surv. Conn. Quad. Rep.* **6**, 55 pp.

ALLARD, G. O., 1956. The geology of a portion of McKenzie township, Chibougamau District, Quebec. Unpublished thesis for Ph.D. degree. The Johns Hopkins Univ., Baltimore.

ANTEN, J., 1923. Le Salmien métamorphique du sud du massif de Stavelot. *Mém. Acad. R. Belg. Cl. Sci.*, 2e sér., T.V., **3**, 1–34.

ATKINSON, D. J., 1956. The occurrence of chloritoid in the Hecla Hoek formation of Prince Charles Foreland, Spitzbergen. *Geol. Mag. Lond.* **93,** 63–71.

BACHMANN, H. G., 1956. Dehydration von Chloritoiden. *Z. Kristallogr.* **108,** 145–56.

BALK, R., 1953. Structure of graywacke areas and Taconic Range, east of Troy, New York. *Bull. geol. Soc. Amer.* **64,** 811–64.

BARROIS, C., 1884*a*. Note sur le chloritoïde du Morbihan. *Bull. Soc. minéral. France* **7,** 37–43.

—— 1884*b*. Sur les schistes métamorphiques de l'île de Groix. *Ann. Soc. géol. Nord* **11,** 18–71.

BARROW, G., 1898. On the occurrence of chloritoid in Kincardineshire. *Quart. J. geol. Soc. Lond.* **54,** 149–56.

BARTH, T. F. W., 1936. Structural and petrologic studies in Dutchess County, New York, part II. *Bull. geol. Soc. Amer.* **47,** 795, 815.

—— 1952. *Theoretical petrology*. New York: John Wiley & Sons. 387 pp.

—— & BALK, R., 1934. Chloritoid from Duchess County, New York. *Amer. Min.* **19,** 345–50.

BECKE, F., 1878. Gesteine der Halbinsel Chalcidice. *Miner. petrogr. Mitt.*, N.F., **1,** 242–74.

BLUMENTHAL, M., 1911. Geologie der Ringel-Segnesgruppe. *Beitr. geol. Karte Schweiz*, N.F., 33, 1–71, Lief.

BOSSARD, L., 1929. Petrographie der mesozoischen Gesteine im Gebiete der Tessiner Kulmination. *Schweiz. min. petrogr. Mitt.* **9,** 107–59.

BOUBÉE, N., 1857. Bains et courses de Luchon. Cited by Damour, 1879.

BOWEN, N. L., & TUTTLE, O. F., 1949. The system MgO–SiO_2–H_2O. *Bull. geol. Soc. Amer.* **60,** 439–60.

BOYD, F. R., & ENGLAND, J. L., 1956. Phase equilibria at high pressure. *Carnegie Inst. Washington Year Book*, **55,** 154–7.

BREZINA, A., 1876. Ein Mineral aus den manganreichen Fundstellen von S. Marcel, Piemont. *Anz. Akad. Wiss., Wien,* **13,** 101–3.

BRINDLEY, G. W., & HARRISON, F. W., 1952. The structure of chloritoid. *Acta Cryst., Camb.* **5,** 698–9.

—— & YOUELL, R. F., 1953. Ferrous chamosite and ferric chamosite. *Miner. Mag.* **30,** 57–70.

BROWNE, W. R., 1922. Report on the petrology of the Broken Hill region, excluding the great lode and its immediate vicinity, Appendix I. pp. 295–353, in *The geology of the Broken Hill district*, by E. C. Andrews. *Mem. Geol. Surv. N.S.W.*, **8.**

BUTTGENBACH, H., 1947. *Les minéraux de Belgique et du Congo Belge*. Paris: Dunod; or Liége: Vaillant-Carmanne.

CATHREIN, A., 1887. Über Chloritoidschiefer von Grossarl. *Miner. petrogr. Mitt.*, N.F., **8,** 331–7.

CHARDIN, T. DE, 1949. Les chloritoïdes des Western Hills près Pékin. *Ann. Hébert et Haug* **7,** 381–7.

CHELUSSI, I., 1893. Alcune rocce dell' isola di Samos studio microscopico. *G. Mineral. Crist. Pet.* **4,** 33–38.

CLEMENTS, J. M., & SMYTH, H. L., 1899. The Crystal Falls iron-bearing district, Michigan. *Mem. U.S. geol. Surv. Mon.* **36,** 442–5.

CLOIZEAUX, A. DES, 1862. *Manuel de minéralogie*, vol. 1. Paris: Dunod. 572 pp.

—— 1884. Sur la forme cristalline et les caractères optiques de la sismondine. *Bull. Soc. minéral. France* **7,** 80–85.

—— & DAMOUR, M. A., 1842. De l'ottrélite, nouvelle espèce minérale. *Ann. Min. Paris*, 4e sér., **2,** 357–61.

CLOOS, E., & HIETANEN, A., 1941. Geology of the 'Martic Overthrust' and the Glenarm series in Pennsylvania and Maryland. *Spec. Pap. geol. Soc. Amer.* **35,** 207 pp.

COLLINS, W. H., QUIRKE, T. T., & THOMSON, E., 1926. Michipicoten iron ranges. *Mem. geol. Surv. Can.* **147,** 29–30.

CORIN, F., 1927–8. Sur quelques roches aimantifères, ottrélitifères et spessartinifères du Salmien à l'est de Vielsalm. *Ann. Soc. géol. Belg.* **51,** B67–69.

—— 1929. Contribution à l'étude des chloritoïdes. *Bull. Sci. Acad. roy. Belg.* **15,** 928–31.

—— 1930–1. Le métamorphisme de l'Ardenne. *Ann. Soc. géol. Belg.* **54,** B99–115.

CORNWALL, F., 1955. Unpublished thesis for Ph.D. degree, McGill Univ., Montreal.

DAMOUR, M. A., 1879. Note sur la vénasquite. *Bull. Soc. minéral. France* **2,** 167–8.

DANA, E. S., 1892. *The system of mineralogy of James Dwight Dana, descriptive mineralogy*. New York: John Wiley & Sons. 6th ed., 1134 pp.; and First Appendix, 1899, 75 pp.; Second Appendix, 1909, 114 pp.; Third Appendix, 1915, 87 pp.

DANA, J. D., 1868. *A system of mineralogy, descriptive mineralogy*. New York: John Wiley & Sons. 5th ed., 827 pp.

DAVREAUX, C. J., 1833. Essai sur la constitution géognostique de la province de Liège. *Mém. journ. Acad. roy. Sci. Belles-Lettres* **9,** 1–297.

DELESSE, A., 1843. Analyse de quelques minéraux. *Ann. Chim.* (*Phys.*), 3e sér., **9,** 385–99.

—— 1846*a*. Sur la sismondine. *Ann. Min., Paris*, 4th sér., **10,** 232–6.

—— 1846*b*. Sismondine. *C.R. Acad. Sci.* **22,** 595–6.

DETHIER, 1819. Le guide des curieux qui visitent les eaux de Spa. Liége, 14. Cited by Buttgenbach, 1947.
DIBBLEE, T. W., & GAY, T. E., 1952. Geology of the Saltdale quadrangle, California, and mineral deposits of Saltdale quadrangle. *Bull. Calif. Dept. Nat. Res. Div. Mines*, **160**, 14.
DOELTER, C., & DITTLER, E., 1912. Über einige Mineralsynthesen. *S. B. Akad. Wiss. Wien*, **121**, Abt. I, 897–914.
DONNAY, J. D. H., NOWACKI, W., & DONNAY, G., 1954. Crystal data. *Mem. geol. Soc. Amer.* **60**, 138.
DORLODOT, L. DE, 1909–10. Contribution à l'étude du métamorphisme du massif Cambrien de Stavelot. *Ann. Soc. géol. Belg.* **37**, M145–94.
DUNHAM, K. C., EYLES, V. A., & TAYLOR, J. H., 1951. Appendix to the crystal structure of some chamosite minerals. *Miner. Mag.* **29**, 522–5.
DUPARC, L., & LOUP, L., 1903. Sur des euphotides à chloritoïde, trouvées dans l'erratique des environs de Genève. *C. R. Acad. Sci.* **136**, 258–60.
—— & MRAZEC, L., 1893. Sur un schiste à chloritoïde des Carpathes. Ibid. **116**, 601–3.
DURANDIÈRE, DE LA, 1895. Note sur un gisement d'ottrélite à Saint Barthélemy (Orne). *Bull. Soc. minéral. France* **18**, 398–9.
DYCKER, R. DE, 1938–9. Recherches sur la nature et les causes du métamorphisme des terrains manganésifères du Cambrien supérieur, dans la partie sud-occidentale du massif de Stavelot. *Ann. Soc. géol. Belg.* **62**, M1–M102.
EMERSON, B. K., 1898. Geology of old Hampshire County, Massachusetts. *Mem. U.S. geol. Surv. Mon.* **29**, 127.
—— & PERRY, J. H., 1907. The green schists and associated granites and porphyries of Rhode Island. *Bull. U.S. geol. Surv.* **311**, 42–44.
EMMONS, R. C., *et al.*, 1953. Selected petrogenic relationships of plagioclase. *Mem. geol. Soc. Amer.* **52**, 142 pp.
ERDMANN, O. L., 1835. Analyse des sogenannten Chloritspathes. *J. prakt. Chem.* **6**, 89–92.
—— 1845. Chemische Notizen (2). Zusammensetzung des Chloritspathes (Chloritoïd). *J. prakt. Chem.* **34**, 454–6.
EUGSTER, H. P., 1957. Heterogeneous reactions involving oxidation and reduction at high pressures and temperatures. *J. chem. Phys.* **26**, 1760–1.
—— 1959. Reduction and oxidation in metamorphism. pp. 397–426 in *Researches in geochemistry*, editor P. H. Abelson, New York: John Wiley & Sons. 511 pp.
FERMOR, L. L., 1909. The manganese-ore deposits of India. *Mem. geol. Surv. India* **37**, 199–200, 314.
FIEDLER, K. G., 1832. Lagerstätten des Diaspor, Chloritspath, Pyrophyllit und Monazite, aufgefunden im Ural. *Ann. Phys. Chem. Poggendorff*, **25**, 322–33.
FLASCHEN, S. S., & OSBORN, E. F., 1952. A hydrothermal study of the system FeO–SiO_2–H_2O. *School Mineral Ind., Penn. State College, 7th Tech. Rep.*, 54 pp.
—— 1957. Studies of the system iron oxide–silica–water at low oxygen partial pressures. *Econ. Geol.* **52**, 923–43.
FOULLON, H. VON, 1883. Ueber die petrographische Beschaffenheit der krystallinischen Schiefer der untercarbonischen Schichten und einiger älterer Gesteine aus der Gegend von Kaisersberg bei St. Michael ob Leoben und krystallinischer Schiefer aus dem Palten- und oberen Ennsthale in Obersteiermark. *Jb. geol. Reichsanst.* **33**, 207–52.
FOWLER-BILLINGS, K., 1949. Geology of the Monadnock region of New Hampshire. *Bull. geol. Soc. Amer.* **60**, 1249–80.
FRANKEL, J. J., 1944. On silicates and dusts from the Witwatersrand gold mines (some preliminary notes). *J. chem. Soc. S. Afr.* **44**, 169–77.
FRIEDLAENDER, C., 1929. Der Chloritoid vom Crestlianderstobel. *Schweiz. min. petrogr. Mitt.* **9**, 247–64.
GENTH, F. A., 1873. Corundum, its alterations and associated minerals. *Proc. Amer. phil. Soc.* **13**, 361–406.
—— 1890. On a new occurrence of corundum in Patrick County, Virginia. *Amer. J. Sci.*, 3rd ser., **39**, 47–50.
GLOCKER, E. F., 1839. Grundr. 570. Cited by Dana, 1892.
GOLDSCHMIDT, V. M., 1920. Geologisch-petrographische Studien im Hochgebirge des südlichen Norwegens. V. Die Injektionsmetamorphose im Stavanger-Gebiete. *Skr. Vidensk. Selsk., Christ.*, **10**, 1–142.
GOSSELET, J., 1888. L'ottrélite dans le Salmien supérieur. *Ann. Soc. géol. Nord* **15**, 185–215, 261–318.
GÖTZ, J., 1886. Untersuchungen einer Gesteinsuite aus der Gegend der Goldfelder von Marabastad im nördlichen Transvaal, Süd-Afrika. *Neues Jb. Min. Geol. Paläont.*, **4**, B.B., 110–77.
GRATON, L. C., 1930. Hydrothermal origin of Rand gold deposits. *Econ. Geol.* **25**, supplement, 170.
GRUNER, J. W., 1946. *Mineralogy and geology of the Mesabi Range*. Office Comm., Iron Range Res. Rehab., Saint Paul, Minnesota. 127 pp.

GUPPY, E. M., & SABINE, P. A., 1956. Chemical analyses of igneous rocks, metamorphic rocks and minerals, 1931–1954, compiled from the records of the Geological Survey. *Mem. geol. Surv. Gt. Britain*, 46–49, 63–64.

GUSTAFSON, J. K., 1946. Two occurrences of chloritoid as a hydrothermal mineral in igneous rocks. *Amer. Min.* **31**, 313–16.

HALFERDAHL, L. B., 1959. Chloritoid: its chemical composition, X-ray and optical properties, stability, and occurrence. Unpublished thesis for Ph.D. degree, Baltimore: The Johns Hopkins Univ., Baltimore. 232 pp.

HALL, A. L., 1909. Über die Kontaktmetamorphose an dem Transvaalsystem im östlichen und zentralen Transvaal. *Miner. petrogr. Mitt.*, N.F., **28**, 115–52.

—— 1910*a*. Geology of Mount Maré, near Pietersburg, and its connection with that of Moodies, near Barberton. *Trans. geol. Soc. S. Afr.* **12**, 32–53.

—— 1910*b*. On contact metamorphism in the Western Transvaal. Ibid., 119–38.

—— 1918. The geology of the Barberton gold mining district. *Mem. geol. Surv. S. Afr.* **9**, 143–9, 188.

—— & MOLENGRAAFF, G. A. F., 1925. The Vredefort Mountain land in the southern Transvaal and the northern Orange Free State. *Verh. Akad. Wet. Amst.*, 2nd sec. **24**, No. 3, 183 pp.

HARDER, H., 1956. Untersuchungen an Paragoniten und an natriumhaltigen Muskoviten. *Heidelberg. Beitr. Min.* **5**, 227–71.

HARKER, A., 1918. Metamorphism in rock-masses. *Quart. J. geol. Soc. Lond.* **74**, lxiii–lxxx.

—— 1928. Normal regional metamorphism. *Fennia* **50**, Sederholm Volume, No. 36, 8 pp.

—— 1932. *Metamorphism*. London: Methuen. 360 pp.

HARRISON, F. W., & BRINDLEY, G. W., 1957. The crystal structure of chloritoid. *Acta Cryst., Camb.* **10**, 77–82.

HARRISON, J. B., 1908. *Geology of the goldfields of British Guiana*. London: Dulau. 320 pp.

HATCH, F. H., 1905. The oldest sedimentary rocks of the Transvaal. *Trans. geol. Soc. S. Afr.* **7**, 148.

HAÜY, R. J., 1822. *Traité de minéralogie*, 2. Paris: Bachelier. 2nd ed., 612 pp.

HEDDLE, M. F., 1879. The geognosy and mineralogy of Scotland. *Miner. Mag.* **3**, 18–56.

HEINRICH, E. W., 1956. *Microscopic petrography*. New York: McGraw-Hill. 296 pp.

HERMANN, R., 1851. Untersuchungen über die Glimmer und Cordierite, besonders über: Monazite, Chloritoïd, Perlglimmer, Kammererit, Rhodochrom, Baltimorit, und Chromchlorit. *J. prakt. Chem.* **53**, 1–30.

HEURK, VAN DEN J., 1953. Improved hydrothermal quenching apparatus. *Bull. geol. Soc. Amer.* **54**, 993–6.

HEY, M. H., 1954. A new review of the chlorites. *Miner. Mag.* **30**, 277–92.

HIETANEN, A., 1951. Chloritoid from Rawlinsville, Lancaster County, Pennsylvania. *Amer. Min.* **36**, 859–68.

HINTZE, C., 1897. *Handbuch der Mineralogie. 2. Silicate und Titanate*. Leipzig: Veit. 1841 pp.

HO, T. L., 1936. The granitic intrusions of the Western Hills, Peiping. *Contr. nat. Res. Inst. Geol. Acad. Sinica*, No. **5**, 43–73.

HOBBS, W. H., 1893. Phases in the metamorphism of the schists of Southern Berkshire. *Bull. geol. Soc. Amer.* **4**, 167–78.

—— 1895. Chloritoid from blocks on the south shore of Michigamme Lake, Michigamme, Michigan. *Amer. J. Sci.*, 3rd ser., **50**, 125–7.

—— 1896. Chloritoid from Michigan—a correction. Ibid. 4th ser., **2**, 87.

HUNT, T. S., 1861. Note on chloritoid from Canada. Ibid., 2nd ser., **31**, 442–3.

HUSSAK, E., 1890. Contribuições mineralógicas e petrográficas. V. Phyllites com ottrelita e com magnetita do Estado de São-Paulo. *Bol. Serv. met. S. Paulo* **7**, 28–35.

HUTCHINGS, W. M., 1889. On the occurrence of ottrelite in the phyllites of North Cornwall. *Geol. Mag. Lond.* **26**, 214–20.

HUTTON, C. O., 1950. Studies of heavy detrital minerals. *Bull. geol. Soc. Amer.* **61**, 635–710.

IGELSTRÖM, L. J., 1896*a*. Mineralogiska meddelanden, Bliabergsit och Ransätit, tvenne nya mineral från Bliaberget i Ransäters socken, Vermland. *Geol. Fören. Stockh. Förh.* **18**, 41–44.

—— 1896*b*. Munkforssit, Bliabergit und Ransätit, drei neue Mineralien vom Kirchspiel, Ransäter, Gouvernement Wermland, Schweden. *Z. Kristallogr.* **27**, 601–4.

ISTSHENKO, D. I., 1957. O khloritoide v porodakh Krivogo Roga. *Mineral. Sbornik, Lvov. Geol. Obstshestvo*, No. **11**, 288–94.

ITO, T., 1950. *X-ray studies on polymorphism*. Tokyo: Maruzen. 231 pp.

JACKSON, C. T., 1840. *Report on the geological and agricultural survey of the State of Rhode Island*, 88.

JELÍNEK, J., 1948. Occurrence of chloritoid (ottrelite) schists southeast of Zvánovice in Central Bohemia. *Věstn. geol. Úst. čsl.* **23**, 293–303 (from *Chem. Abstr.*).

JUURINEN, A., 1956. Composition and properties of staurolite. *Ann. Acad. Sci. fenn.*, ser. A, III Geol.-Geogr., **47**, 53 pp.

KALKOWSKY, E., 1882. Einige Beobachtungen im sächsischen Granulitgebirge. *Neues Jb. Min. Geol. Paläont.*, **1**, 231–3.

KELLER, H. F., & LANE, A. C., 1891. Chloritoid von Champion, Michigan, U.S.A. *Z. Kristallogr.* **19**, 383–5.

KOBELL, F. VON, 1853. Ueber den Sismondin, Chloritoid und Masonit, und über die Mischung dieser und ähnlicher Silikate (Disterrit, Xanthophyllit, Clintonit, Chlorit, Ripidolith) aus dem Gesichtspunkte der Polymerie betrachtet. *J. prakt. Chem.* **58**, 39–44.

—— 1854. Ueber Chloritoïd von Bregratten in Tirol und Klinochlor von Markt Leugast im Bayreuthischen, und über die Scheidung von Eisenoxyd und Eisenoxydul bei diesen und ähnlichen Silikaten. *Ann. Chemie Pharm.* **90**, 244–51.

KOCH, G., 1935. Chemische und physikalisch-optische Zusammenhänge innerhalb der Sprödglimmergruppe. *Chem. d. Erde* **9**, 453–63.

KÖHNE, F., 1938. Petrographie und Geologie der Phurni-Inseln bei Samos. *Neues Jb. Min. Geol. Paläont.*, **73**, B.B., Abt. A, 1–78.

KOTO, B., 1893. The Archean formation of the Abukuma plateau. *J. Coll. Sci. Tokyo* **5**, 197–293.

KRIGE, L. J., 1917. Petrographische Untersuchungen im Val Piora und Umgebung. *Ecl. geol. Helv.* **14**, 519–654.

KTENAS, K. A., 1907. Die Einlagerungen im krystallinen Gebirge der Kykladen auf Syra und Sifnos. *Miner. Petrogr. Mitt.*, N.F., **26**, 257–320.

LACROIX, A., 1886. Propriétés optiques du chloritoïde, son identité avec la sismondine, masonite, ottrélite, vénasquite et phyllite. *Bull. Soc. minéral. France* **9**, 42–46.

—— 1893–1913. *Minéralogie de la France et de ses colonies*, 1, Paris: Librairie Polytechnique, Baudry 723 pp. 4, Paris: Ch. Béranger. 923 pp. 5, 2nd supplément, 501 pp.

LAMEY, C. A., 1935. The Palmer gneiss. *Bull. geol. Soc. Amer.* **46**, 1137–63.

LANE, A. C., & KELLER, H. F., 1891. Notes on Michigan minerals. I. Chloritoid. *Amer. J. Sci.*, 3rd ser., **42**, 499–505.

LAPPARENT, J. DE, 1937. L'émeri de Samos. *Miner. petrogr. Mitt.*, N.F., **49**, 1–30.

LASAULX, VON, 1883. Ueber Glaukophan von der Insel Groix (Bretagne). *Verh. naturh. Ver. preuß. Rheinl.* **40**, 263–76.

LEONHARD, K. C. VON, 1821. *Handbuch der Oryktogonosie*. Heidelberg. Cited by Haüy, 1822.

LEPSIUS, R., 1893. *Geologie von Attika*. Berlin: Dietrich Reimer. 196 pp.

LIEBENBERG, W. R., 1955. The occurrence and origin of gold and radioactive minerals in the Witwatersrand system, the Dominion Reef, the Ventersdorp Contact Reef and the Black Reef. *Trans. geol. Soc. S. Afr.*, **58**, 100–254.

LIN, L. S., 1932. Étude sur quelques schistes à ottrélite de Chine. *C.R. Acad. Sci.* **195**, 444–5.

LINDNER, J. L., & GRUNER, J. W., 1939. Action of alkali sulphide solutions on minerals at elevated temperatures. *Econ. Geol.* **34**, 537–60.

MACDONALD, G. J. F., 1957. Thermodynamics of solids under non-hydrostatic stress with geologic applications. *Amer. J. Sci.* **255**, 266–81.

MACHATSCHKI, F., 1923. Steirische Chloritoidschiefer. *Geol. Arch.* **2**, 188–206.

—— & MUSSGNUG, F., 1942. Über die Kristallstruktur des Chloritoids. *Naturwissen.* **30**, 106.

MANASSE, E., 1906. Contribuzioni alla mineralogia della Toscana. Cloritoide di Strettoia (Alpi Apuane). *P.V. soc. tosc. Sci. nat.* **15**, 26–29.

—— 1910. Cloritoide (ottrelite) delle Alpi Apuane. *Mem. Soc. tosc. Sci. nat.* **26**, 121–42.

—— 1911. Sulla composizione chimica di alcuni minerali del gruppo del cloritoide. *P.V. Soc. tosc. Sci. nat.* **20**, 29–42.

MARCK, W. VON DER, 1878. Chemische Untersuchungen westfälischer und rheinischer Gebirgsarten und Mineralien. *Verh. naturh. Ver. preuß. Rheinl.* **35**, 237–71.

MARMO, V., 1958. Chloritoid schists of central Sierra Leone. *Bull. Comm. géol. Finl.* **180**, 105–12.

MEISTER, A., 1910. Die Gesteine und die Bedingungen der Goldhaltigkeit im südlichen Teile des Jenissei-Distriktes. *Geol. Untersuch. in goldführenden Gebieten Sibiriens, Jenissei-Distr.* **34**, 668.

MÉLON, J., 1938. Description des chlorites et clintonites belges, 4e partie, clintonites: salmite et ottrélite. *Mém. Acad. roy. Belg. Cl. Sci.* **17**, fasc. 4, 63–72.

MICHOT, J., 1954–5. Genèse du chloritoïde en milieu statique. *Mém. Ann. Soc. géol. Belg.* **78**, M 3–54.

MILNE, I. H., 1949. Chloritoid from Megantic County, Quebec. *Amer. Min.* **34**, 422–34.

MÜGGE, O., 1918. Ottrelith- und Karpholithschiefer aus dem Harz. *Neues Jb. Min. Geol. Paläont.*, 75–98.

—— 1927. *Rosenbusch's mikroskopische Physiographie der Mineralien und Gesteine*, I, 2. Stuttgart: E. Schweizerbart. 814 pp.

MURPHY, F. M., 1932. Geology of a part of the Panamint Range, California. *Calif. Div. Mines, 28th Rep. St. Mineral.* 345–7.

NAHA, K. M., 1955*a*. Triclinic chloritoid from NE. Mayurbhanj and its optical characters. *Proc. Indian Sci. Congr.*, 42nd Sess., Baroda, pt. III, 183–4 (abstr.).

NAHA, K. M., 1955*b*. Kyanite–chloritoid–schists from north-eastern Mayurbhanj. *Proc. Indian Sci. Congr.*, 42nd Sess., Baroda, pt. III, 190–1 (abstr.).

NÁRAY-SZABÓ, I., & SASVÁRI K., 1958. On the structure of staurolite. $HFe_2Al_9Si_4O_{21}$. *Acta. Crys. Camb.* **11**, 862–5.

NAUMANN, C. F., & ZIRKEL, F., 1901. *Elemente der Mineralogie*. Leipzig: Wilhelm Engelmann. 807 pp.

NEL, L. T., 1927. Geology of the country around Vredefort. *Mem. geol. Surv. S. Afr.*

NELSON, B. W., & ROY, R., 1958. Synthesis of the chlorites and their structural and chemical constitution. *Amer. Min.* **43**, 707–25.

NEUERBURG, G. J., 1951. Petrology of the Pre-Cretaceous rocks of the Santa Monica Mountains, California. Unpublished thesis for Ph.D. degree, Univ. Calif., Los Angeles. 180 pp.

NIGGLI, P., 1912. Die Chloritoidschiefer und die sedimentäre Zone am Nordostrande des Gotthardmassivs. *Beitr. geol. Karte Schweiz*, N.F., **36**, Lief.

OBERHOLZER, W., 1955. Geologie und Petrographie des westlichen Gotthardmassivs. *Schweiz. min. petrogr. Mitt.* **35**, 320–409.

ÖNAY, T. S., 1949. Über die Smirgelgesteine SW-Anatoliens. Ibid. **29**, 357–491.

PAPAVASILIOU, S. A., 1913. Die Smirgellagerstätten von Naxos nebst denjenigen von Iraklia und Sikinos. *Z. Dtsch. geol. Ges.* **65**, 1–123.

PEACOCK, M. A., 1935. On wollastonite and parawollastonite. *Amer. J. Sci.*, 5th ser., **29**, 495–529.

PENFIELD, S. L., & FORBES, E. H., 1896. Fayalite from Rockport, Massachusetts, and on the optical properties of the chrysolite-fayalite group and of monticellite. Ibid., 4th ser., **1**, 129–35.

PETTIJOHN, F. J., 1949. *Sedimentary rocks*. New York: Harper & Brothers. 526 pp.

PHILLIPS, F. C., 1928*a*. Petrographic notes on three rock-types from the Shetland Islands. *Geol. Mag. Lond.* **65**, 500–7.

—— 1928*b*. Metamorphism in the Upper Devonian of North Cornwall. Ibid. **65**, 541–56.

PICHAMUTHU, C. S., 1943. A note on the occurrence of chloritoid in Tumkur district, Mysore State. *Curr. Sci.* **12**, 332.

PLAS, L. VAN DER, HUGI, T., MLADECK, M. H., & NIGGLI, E., 1958. Chloritoid vom Hennensädel südlich Vals (nördliche Aduladecke). *Schweiz. min. petrogr. Mitt.* **38**, 237–46.

POTGIETER, C. T., 1950. The South African pyrophyllite deposits. *Ann. Univ. Stellenbosch*, **26**, sec. A, 223–65.

PRIDER, R. T., 1947. Chloritoid at Kalgoorlie. *Amer. Min.* **32**, 471–4.

PROST, E., 1883–4. Sur la salmite de Dumont, chloritoïde manganésifère. *Mém. Ann. Soc. géol. Belg.* **11**, 93–97.

QUIROGA, F., 1879. Diaspore de El Cardoso. *Anales* (*Mus.*) *Hist. Nat.* **8**. Cited by Recarte, 1951.

RABBITT, J. C., 1948. A new study of the anthophyllite series. *Amer. Min.* **33**, 263–323.

RASTALL, R. H., 1910. The Skiddaw granite and its metamorphism. *Quart. J. geol. Soc. Lond.* **66**, 116–41.

RAUW, H. DE, 1912. Note sur la salmite, le rutile et la tourmaline d'Ottré. *Ann. Soc. géol. Belg.* **38**, B209–14.

READ, H. H., 1932. On quartz–kyanite rocks in Unst, Shetland Islands, and their bearing on metamorphic differentiation. *Miner. Mag.* **23**, 317–28.

—— 1934. The metamorphic geology of Unst in the Shetland Islands. *Quart. J. geol. Soc. Lond.* **90**, 637–88.

—— 1937. Metamorphic correlation in the polymetamorphic rocks of the Valla Field Block, Unst, Shetland Islands. *Trans. roy. Soc. Edinb.* **59**, pt. I, 195–221.

—— 1951. Metamorphism and granitisation. *Trans. geol. Soc. S. Afr.*, **54** annexure, 18.

RECARTE, A. B., 1951. Nota acerca del mineral clasificado como 'diasporo' de el Cardoso (Somasierra), Guadalajara. *Notas Inst. geol. Esp.* **23**, 65–72.

RENARD, A., 1882. Les roches grenatifères et amphiboliques de la région de Bastogne, appendix. *Bull. Mus. Hist. nat. Belg.* **1**, 43–47.

—— 1882–4. Recherches sur la composition et la structure des phyllades Ardennais. Ibid., **1**, 215–49; **2**, 127–49; **3**, 231–68.

—— & DE LA VALLÉE POUSSIN, CH., 1879. Note sur l'ottrélite. *Mém. Ann. Soc. géol. Belg.*, **6**, 51–68.

ROEVER, W. P. DE, 1951. Ferrocarpholite, the hitherto unknown ferrous iron analogue of carpholite proper. *Amer. Min.* **36**, 736–45.

—— 1956. Some additional data on the crystalline schists of the Rumbia and Mendoke Mountains, South East Celebes. *Verh. Akad. Wet. Genoot.* **16**, 385–93.

ROMINGER, C., 1895. Geological report on the upper peninsula of Michigan: iron and copper regions. *Geol. Surv. Michigan* **5**, 30–31.

ROSATI, A., 1907. Ottrelite schist and sodic amphibolite of the valley of Monfieis near Demonte. *Mem. Accad. Lincei* **16**, I, 343–7 (from *Chem. Abstr.* **1**, 1907).

ROSE, G., 1837. *Mineralogisch-geognostische Reise nach dem Ural, dem Altai und dem Kaspischen Meere*, I. Berlin: Sandersche Buchhandlung (C. W. Eichhoff). 641 pp.

ROSENBUSCH, H., 1889. *Microscopical physiography of the rock-making minerals*. Translated and abridged by J. P. Iddings. New York: John Wiley & Sons. 2nd ed., 333 pp. The ottrelite group, 266–9.

ROSS, C. S., & KERR, P. F., 1930. The kaolin minerals. *Prof. Pap. U.S. geol. Surv.* **165-E**, 164.

ROY, R., & OSBORN, E. F., 1954. The system Al_2O_3–SiO_2–H_2O. *Amer. Min.* **39**, 853–85.

—— & TUTTLE, O. F., 1956. Investigations under hydrothermal conditions. pp. 138–80 in *Physics and chemistry of the earth*, **1**, editors L. H. Ahrens *et al.*, New York: McGraw-Hill. 317 pp.

SCHÄFER, R. W., 1896. Ueber die metamorphen Gabbrogesteine des Allalingebietes im Wallis zwischen Zermatt- und Saasthal. *Miner. petrogr. Mitt.*, N.F., **15**, 91–134.

SCHAIRER, J. F., & YAGI, K., 1952. The system FeO–Al_2O_3–SiO_2. *Amer. J. Sci.*, Bowen Vol., 471–512.

SCHMIDT, C., 1891. Beiträge zur Kenntniss der im Gebiete von Blatt XIV der geolog. Karte der Schweiz. *Beitr. geol. Karte Schweiz*, pp. 20–21, 40, 55.

SCHNEIDERHÖHN, P., 1936. Brasilianische Gesteine. *Neues Jb. Min. Geol. Paläont.*, **70**, B.B., Abt. A, 151–201.

SCHRÖDER, M., 1884. Chloritoidphyllit in sächsischen Vogtlande. *Z. Naturwiss.* **57**, 481–3.

SEITSAARI, J., 1956. A ferroan-aluminian anthophyllite from Kemiö, Finland. *Bull. Comm. géol. Finl.* **172**, 77–83.

SEKI, Y., 1954. On chloritoid rocks in the Kitakami median metamorphic zone, north-eastern Japan. *Sci. Rep. Univ. Saitama*, ser. B, **1**, 223–63.

—— 1955. On calcic plagioclases associated with chloritoid schists in the Hitachi District, Ibaragi Prefecture, Japan. Ibid., **2**, 115–31.

—— 1957. Petrological study of hornfelses in the central part of the median zone of Kitakami Mountain land, Iwate Prefecture. Ibid., **2**, 307–61.

SHANNON, E. V., 1926. The minerals of Idaho. *Bull. U.S. nat. Mus.* **131**, 377–8.

SHEPARD, C. U., 1852. *Treatise on mineralogy*. New Haven: Yale College. 3rd ed., p. 161.

SIGG, H., 1918. Quelques roches et minéraux de la Sysserskaya-Datcha dans l'Oural. *Bull. Soc. Sci. nat. Vaudoise* **52**, 161–81.

SIMPSON, E. S., 1915. On chloritoid and its congeners. *Bull. geol. Surv. W. Aust.*, **64**, 64–78.

—— 1930. Contributions to the mineralogy of Western Australia. (4) Chloritoid, Kalgoorlie, Cen. Div. *J. roy. Soc. W. Aust.* **16**, 27–30.

—— 1937. Contributions to the mineralogy of Western Australia. Series X (4) Chloritoid, Mt. Magnet, Mur. Ibid. **23**, 22–23.

—— & GIBSON, C. G., 1912. Contributions to the study of the geology and ore deposits of Kalgoorlie, East Coolgardie Goldfield. Part I. *Bull. geol. Surv. W. Austr.*, **42**.

SMITH, J. L., 1851. Memoir on emery. Part 2. On the minerals associated with emery: corundum, hydrargillite, diaspore, zinc spinel, pholerite, ephesite (a new species), emerylite (a new species), muscovite, chloritoid (a new variety), black tourmaline, chlorite, magnetic oxyd of iron, oligiste iron, hydrated oxyd of iron, iron pyrites, rutile, ilmenite and titaniferous iron. *Amer. J. Sci.*, 2nd ser., **11**, 53–66.

SNELLING, N. J., 1957. A contribution to the mineralogy of chloritoid. *Miner. Mag.* **31**, 469–75.

SOUZA-BRANDÃO, V., 1914. Orientação optica do chloritoide das phyllites de Alcapedrinka (Arada, Districto de Aveiro). *Commun. Comm. geol. Portug.* **10**, 144–58.

STEVENS, R. E., 1942. A system for calculating analyses of micas and related to minerals to end members. *Bull. U.S. geol. Surv.* **950**, 101–19.

STOSE, A. J., & STOSE, G. W., 1944. Geology of the Hanover–York District, Pennsylvania. *Prof. Pap. U.S. geol. Surv.* **204**, 84 pp.

STUCKEY, J. L., 1926. Chloritoid from the Deep River region, North Carolina. *Amer. Min.* **11**, 186–8.

TARASENKO, V. E., 1925. On some crystalline schists in the Krivoi-Rog ore-bearing district. *Acta Univ. Voronegiensis* (olim Jurievensis–Dorpatensis), Voronezh, **1**, 265–89 (in Russian, from *Miner. Abstr.*).

THOMPSON, J. B., 1955. The thermodynamic basis for the mineral facies concept. *Amer. J. Sci.* **253**, 65–103.

THOMSON, T., 1828. Chemical examination of some minerals, chiefly from America, with notes by John Torrey. *Ann. Lyceum Nat. Hist. New York*, **3**, 9–86.

THOREAU, J., 1936. Matériaux pour l'étude du métamorphisme et des intrusions magmatiques dans le Ruanda-Urundi. *Mém. Inst. géol. Univ. Louvain* **10**, 437.

TILLEY, C. E., 1925. Petrographical notes on some chloritoid rocks. *Geol. Mag. Lond.* **62**, 309–19.

—— 1926. Some mineralogical transformations in crystalline schists. *Miner. Mag.* **21**, 34–46.

—— 1937. Anthophyllite–cordierite–granulites of the Lizard. *Geol. Mag. Lond.* **74**, 300–9.

TOIT, A. L. DU, 1939. *The geology of South Africa.* Edinburgh: Oliver & Boyd. 2nd ed., 539 pp.
TÖRNEBOHM, A. E., 1892. Om kloritoid och bergbeck i ett qvartsbrott på Kolmården. *Geol. Fören. Stockh. Förh.* **14,** 137–47.
TSCHERMAK, G., 1895. Ueber den Smirgel von Naxos. *Miner. petrogr. Mitt.*, N.F., **14,** 311–42.
—— & SIPÖCZ, L., 1879. Die Clintonitgruppe. *Z. Kristallogr.* **3,** 496–515.
TSCHIRWINSKY, P., 1929. Beiträge zur Mineralogie Rußlands, III Teil. Ibid. **70,** 271–3.
TSCHOPP, H., 1923–4. Die Casannaschiefer des oberen Val de Bagnes (Wallis). *Ecl. geol. Helv.* **18,** 77–206.
TURNOCK, A. C., & EUGSTER, H. P., 1958*a*. Magnetite–hercynite relations. *Carnegie Inst. Washington Year Book*, **57,** 209.
—— —— 1958*b*. Iron-rich chlorites. Ibid. 191–2.
TUTTLE, O. F., 1949. Two pressure vessels for silicate-water studies. *Bull. geol. Soc. Amer.* **60,** 1727–9.
U.S. Geological Survey, 1893. *Bull. U.S. geol. Surv.* **113.**
WEBSKY, 1853. Ueber die geognostischen Verhältnisse der Erzlagerstätten von Kupferberg und Rudelstadt in Schlesien. *Z. Dtsch. geol. Ges.* **5,** 373–438.
WEIBULL, M., 1896. Om bliabergsitens plats i mineralsystemet. *Geol. Fören. Stockh. Förh.* **18,** 515–22.
WERVEKE, L. VAN, 1885. Ueber Ottrelithgesteine von Ottré und Viel-Salm. *Neues Jb. Min. Geol. Paläont.* **1,** 227–35.
WHITNEY, J. D., 1849. On the composition of chloritoid or chlorite-spar, and masonite. *Proc. Boston Soc. nat. Hist.* **3,** 100–2.
WILLIAMSON, D. H., 1953. Petrology of chloritoid and staurolite rocks north of Stonehaven, Kincardineshire. *Geol. Mag. Lond.*, **90,** 353–61.
WOLFF, J. E., 1890. On some occurrences of ottrelite and ilmenite schist in New England. *Bull. Mus. Comp. Zool., Harv.* **16,** 159–65.
WOYNO, T. J., 1912. Petrographische Untersuchung der Casannaschiefer des mittleren Bagnetales (Wallis). *Neues Jb. Min. Geol. Paläont.*, **33,** B.B., 136–207.
YODER, H. S., 1950. High-low quartz inversion up to 10,000 bars. *Trans. Amer. geophys. Un.* **31,** 827–35.
—— 1952. The MgO–Al_2O_3–SiO_2–H_2O system and the related metamorphic facies. *Amer. J. Sci.*, Bowen Vol., 569–627.
—— 1955. Role of water in metamorphism. *Spec. Pap. geol. Soc. Amer.* **62,** 505–24.
—— 1957. Isograd problems in metamorphosed iron-rich sediments. *Carnegie Inst. Washington Year Book*, **56,** 232–7.
—— & EUGSTER, H. P., 1954. Phlogopite synthesis and stability range. *Geochim. et Cosmoch. Acta* **6,** 157–85.
YOUNG, R. B., 1914. Metasomatism in Banket. *Trans. geol. Soc. S. Afr.* **17,** 31–38.
—— 1917. *The Banket, a study of the auriferous conglomerates of the Witwatersrand and the associated rocks.* London: Gurney & Jackson. pp. 19–20, 43–44, 83, 91.
ZEN, E., 1955. Metamorphism of sedimentary rocks in the Castleton area, Vermont. Unpublished thesis for Ph.D. degree, Harvard Univ., Cambridge, U.S.A.
ZWART, H. J., 1959. On the occurrence of chloritoid in the Pyrénées. *Geol. en Mijnb.*, NW. ser., **21,** 119–22.

EXPLANATION OF PLATES

PLATE 1

FIG. A. Part of a chloritoid crystal with inclusions of quartz (low relief) and carbonate (*C*) from the Michipicoten District, Ontario, Canada. Transmitted plane polarized light.

FIG. B. Chloritoid crystals (laths) in a groundmass of quartz (low relief) and chlorite (higher relief) from the Womble Mine, North Carolina, U.S.A. The black material is leucoxene. Transmitted plane polarized light.

FIG. C. Chloritoid crystals (*Ctd*) in a groundmass of carbonate (high relief) and muscovite (low relief) from Kalgoorlie, Western Australia. The inclusions in the chloritoid are mostly carbonate. *P*, plagioclase; black material, leucoxene. Transmitted plane polarized light.

FIG. D. Hour-glass structure in a chloritoid crystal from Salm-Château, Belgium. Inclusions of quartz and haematite are concentrated within the hour-glass. The groundmass consists of quartz, muscovite, chlorite, and haematite. Transmitted plane polarized light.

FIG. E. Hour-glass structure in a chloritoid crystal from Chibougamau, Quebec, Canada. The hour-glass structure is clearly visible even without inclusions. The groundmass consists of muscovite and chlorite. The black material is leucoxene. Transmitted plane polarized light.

FIG. F. Same as fig. E but with crossed nicols.

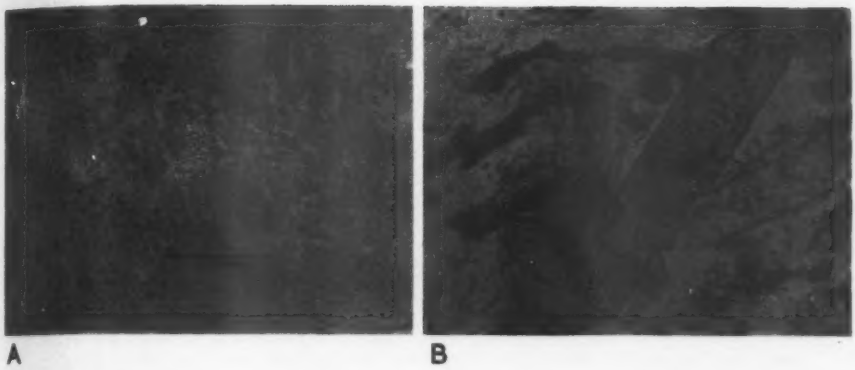

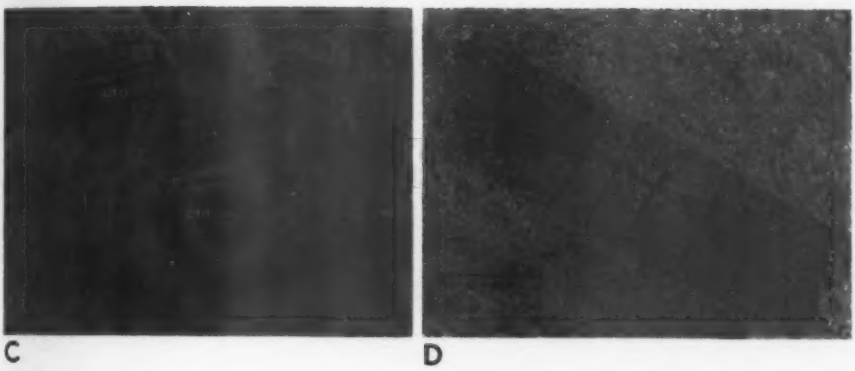

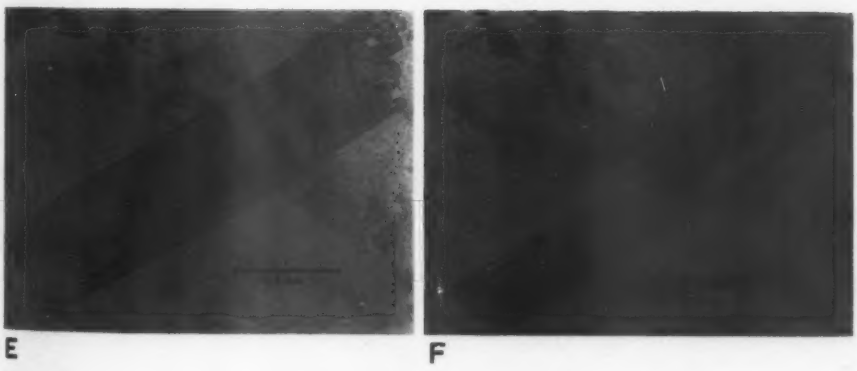

L. B. HALFERDAHL

Plate 1

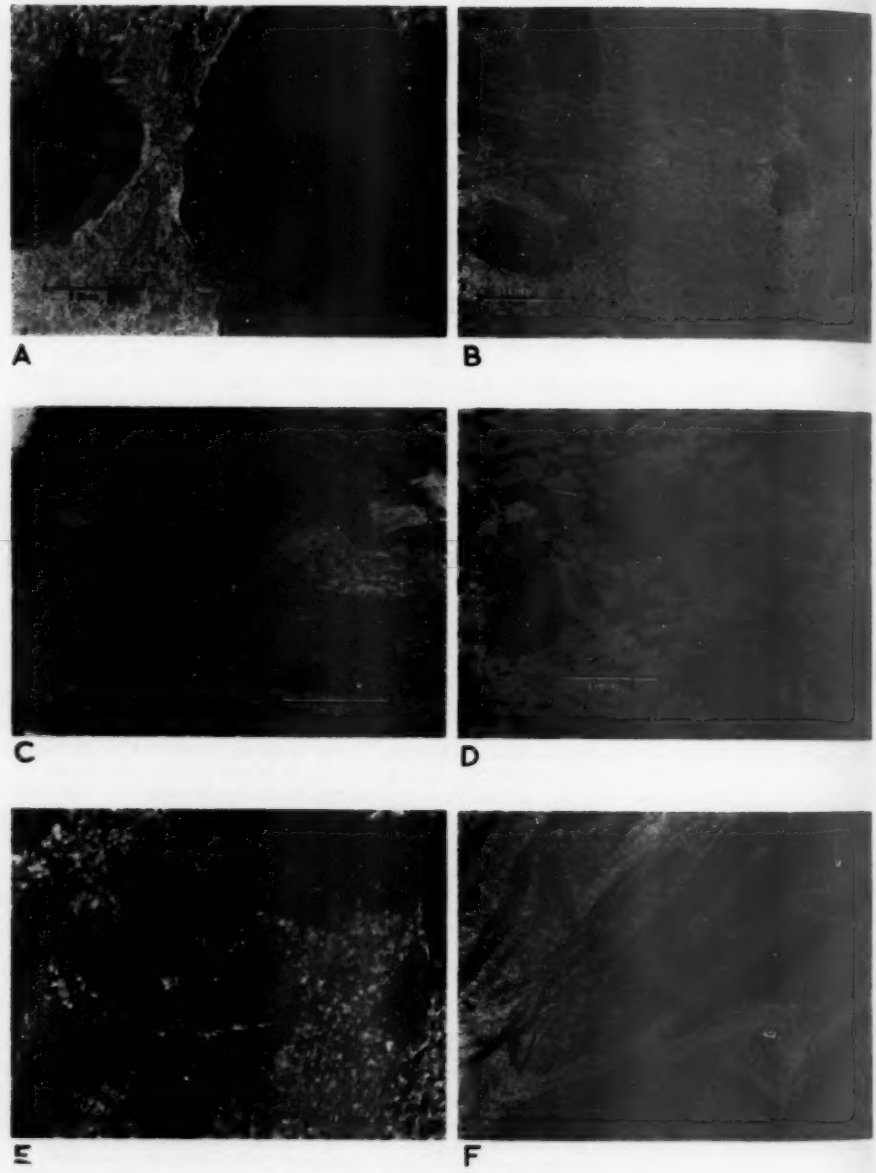

L. B. HALFERDAHL

Plate 2

PLATE 2

FIG. A. Zoning in chloritoid crystals from St. Gilles, Quebec, Canada (U.S. National Museum, 79008). The groundmass consists of lath-shaped muscovite, chlorite, minor quartz, and leucoxene. Transmitted plane polarized light.

FIG. B. Randomly oriented chloritoid porphyroblasts in a schist from Ellijay, Georgia, U.S.A. The matrix consists of quartz, muscovite, chlorite, calcite, and leucoxene. Transmitted plane polarized light.

FIG. C. Rotated chloritoid porphyroblast in a schist from the Harvey Hill Mine, Quebec, Canada. The parallel cracks in the chloritoid were probably parallel to the schistosity before rotation which has caused distortion of the schistosity around the crystal. The matrix consists of quartz, chlorite, and muscovite. Transmitted plane polarized light.

FIG. D. Rosettes of chloritoid in a mass of quartz and pyrophyllite, from a breccia adjacent to the Womble pyrophyllite deposit, North Carolina, U.S.A. The black material is leucoxene. Transmitted plane polarized light.

FIG. E. Intergrown chloritoid porphyroblasts in a schist from Weaver Hill, Vermont, U.S.A. The matrix is quartz and leucoxene (fine black grains). Crossed nicols.

FIG. F. Chloritoid porphyroblasts parallel to the schistosity whose planes have been folded. The schist is from Winnemucca, Nevada, U.S.A. The orientation of some of the chloritoid crystals has apparently been changed by the folding. The matrix consists of quartz, chlorite, muscovite, and ilmenite.

Obituary Notice

DR. A. B. EDWARDS, a member of the Honorary Advisory Board, died suddenly in Rome on 8 October 1960.

He was born on 15 August 1909. After graduating in geology at the University of Melbourne he was awarded an 1851 Royal Exhibition which enabled him to spend the years 1932–4 on research at Imperial College, London, where he was awarded the degree of Ph.D. In 1934 he was appointed Assistant Geological Research Officer to the Australian Council for Scientific and Industrial Research, where he later combined the duties of Senior Research Officer in the Mineragraphic Section with those of Lecturer in Mining Geology at the University of Melbourne. Subsequently, he was appointed Officer-in-Charge of the Mineragraphic Section of the Commonwealth Scientific and Industrial Research Organization, Melbourne.

During his twenty-six years at Melbourne he published a series of contributions on the mineralogy and geology of Australian ore deposits, the majority of the papers involving the use of mineragraphic techniques. The results of much of this work are brought together in his textbook, *Textures of the Ore Minerals*. He was also responsible for valuable petrological work on the Tertiary igneous rocks of southern Australia and Victoria. He was, at the time of his death, on a private tour of Europe arranged in order to learn more about the origin of lead-zinc ores and the effects of regional metamorphism on the textures of sulphide ores.